2012

Integration of Transcriptomic and Metabolomic Profiling to Identify Mechanisms and Biomarkers of Statin-Induced Myopathy

Jeffrey David Vassallo
Lehigh University

Integration of Transcriptomic and Metabolomic Profiling to Identify Mechanisms and Biomarkers of Statin-Induced Myopathy

by

JEFFREY D. VASSALLO

A Dissertation

Presented to the Graduate and Research Committee

of Lehigh University in Candidacy for the Degree of

Doctor of Philosophy

In

Department of Biological Sciences

Lehigh University

May 2012

Approved and recommended for acceptance as a dissertation in partial fulfillment of the requirements for the degree of Doctor of Philosophy

Integration of Transcriptomic and Metabolomic Profiling to Identify Mechanisms and Biomarkers of Statin-Induced Myopathy
Jeffrey D. Vassallo

_____
Defense Date

_____
Linda Lowe-Krentz, Ph.D.
Dissertation Advisor

_____
Approved Date

Committee Members:

_____
Michael Kuchka, Ph.D.

_____
Kathy Iovine, Ph.D.

_____
Lois Lehman-McKeeman, Ph.D.

Acknowledgments

I would like to express my gratitude to Dr. Lois Lehman-McKeeman for her mentoring, patience and time while supporting my pursuit of a Ph.D. I would also like to thank Bristol-Myers Squibb, and specifically Discovery Toxicology, for providing me with the opportunity and the financial support for this pursuit. Furthermore, I would like to thank my friends and colleagues at Bristol-Myers Squibb who were very supportive during this time. This work would not have been possible without the significant time and resource commitments made by many to help me achieve this goal. Specifically, I would like to acknowledge Dr. Nelly Aranibar for help with the metabolomic investigations; Dr. Petia Shipkova for help with the MS investigations; Dr. Bill Foster, Vasanthi Bhaskaran and soon-to-be Dr. David Nelson for their guidance on transcriptional profiling; Dr. Evan Janovitz for teaching me muscle histopathology; Steve Stryker and Brenda Lehman for training me on skeletal muscle isolation; and Dr. Gina Ravenscroft for guidance on primary myofiber isolation. Additionally, I would like to thank Dr. Don Robertson, Dr. James Sidaway, Dr. John Rathmacher and Lloyd Lecureux for their thoughtful scientific discussions.

I would like to express my gratitude to Dr. Linda Lowe-Krentz for her mentoring, patience and time while supporting my pursuit of a Ph.D. I would also like to thank Lehigh University, and specifically the Department of Biological Sciences, for providing me with the opportunity to pursue this goal. Furthermore, I want to thank my graduate committee members Dr. Michael Kuchka and Dr. Kathy Iovine for their time and guidance. Additionally, I would like to thank my friends and colleagues, including Dr.

Christina Godfried Sie and soon-to-be Dr. Michael Kearse at Lehigh University for their support in helping me achieve this goal.

I am especially grateful for my family, including my parents and brother, and also my friends for their unending support and encouragement. Lastly, my greatest thanks is reserved for my wife, Melissa, and our three children, Tara, Joshua and Ava who have made huge sacrifices in order for me to complete this Ph.D. I greatly appreciate your love, support and patience.

Table of Contents

List of Figures

List of Tables

List of Abbreviations

ALT	Alanine aminotransferase
AMP	Adenosine monophosphate
ATP	Adenosine triphosphate
ANOVA	Analysis of Variance
AST	Aspartate Aminotransferase
Atrogin-1	Muscle Atrophy F-box
CH25H	Cholesterol 25-hydroxylase
CHD	Coronary heart disease
CK	Creatine kinase
Cmax	Maximum concentration of a drug in plasma
Dia	Diaphragm
DHT	Dihydrotestosterone
ER	Endoplasmic reticulum
ERα/β	Estrogen receptor α/β
FPP	Farnesyl pyrophosphate
FG	Fast-twitch glycolytic muscle
FOG	Fast-twitch oxidative muscle
Fabp3	Fatty acid binding protein 3
FDB	Flexor digitorum brevis
FoxO3	Forkhead box protein O3
Gastroc	Gastrocnemius
GC-MS	Gas chromatography-mass spectroscopy
GGPP	Geranylgeranyl pyrophosphate
GTPase	G protein
GDF8	Growth and differentiation factor 8 (GDF8; myostatin)
HMQC	Heteronuclear Multiple Quantum Correlation
HMBC	Heteronuclear Multiple Bond Correlation
HPLC	High Performance Liquid Chromatography
HSkMC	Human myoblast cell line
HMG-CoA	3-Hydroxy-3-methylglutaryl coenzyme A

INSIG	Insulin induced gene
IGF-1	Insulin-like growth factor-1
IP	Intraperitoneal injection
IUPAC	International Union of Pure and Applied Chemistry
LOD	Limit of detection
LC_{50}	Lethal concentration causing 50% death
LDL-C	Low density lipoprotein cholesterol
Ldlr	Low density lipoprotein receptor
1-MH	1-Methylhistidine
3-MH	3-Methylhistidine
C2C12	Mouse myoblast cell line
M1	Macrophages involved with proinflammatory response
M2	Macrophages involved with anti-inflammatory response
Myl3	Myosin light chain 3
MTBSTFA	N-methyl-N-(t-butyldimethylsilyl)-trifluoroacetamide
MRF	Muscle regulatory factor
MAFbx	Muscle Atrophy F-box
MuRF1	Muscle RING Finger 1
MyoD	Myogenic determination factor 1
NAD^+	Nicotinamide adenine dinucleotide (oxidized)
NADH	Nicotinamide adenine dinucleotide (reduced)
NADPH	Nicotinamide adenine dinucleotide phosphate (reduced)
^1H NMR	Nuclear Magnetic Resonance
PPAR	Peroxisome proliferator-activated receptor
PGC-1α	Peroxisome proliferative activated receptor, gamma, coactivator 1 alpha
PCA	Principal Component Analysis
PDK4	Pyruvate dehydrogenase kinase 4
Quad	Quadriceps
L6	Rat myoblast cell line
ROS	Reactive oxygen species
RT-PCR	Real time Polymerase chain reaction

SERCA	Sarcoplasmic reticulum Ca^{2+}-ATPase
sTnI	Skeletal muscle troponin I
SO	Slow-twitch oxidative muscle
SCAP	Sterol-sensing domain SREBP cleavage-activating protein
SREBP	Sterol regulatory element binding protein
SSD	Sterol-sensing domain
TMS	Tetramethylsilane
TSP	Trimethylsilyl-2,2,3,3-tetradeuteropropionic acid
Ub	Ubiquitin
E1	Ub-activating enzyme
E2	Ub-conjugating enzyme
E3	Ub-ligase enzyme
UPP	Ubiquitin proteasome pathway

Abstract

Despite extensive research efforts indicating statin-induced myopathy is an on-target effect mediated by HMG-CoA reductase inhibition, the underlying pathophysiology remains unknown. The purpose of this dissertation was to use transcriptomic and metabolomic profiling to identify mechanisms and biomarkers of statin-induced myopathy. Investigative studies were conducted with cerivastatin (0.5 and 1 mg/kg; 14 days) in the rat because this species is predictive of the clinical response. Integration of transcriptomic and metabolomic profiles of skeletal muscles revealed alterations in cholesterol homeostasis and energy metabolism associated with myopathy in fast-twitch muscles, whereas slow-twitch muscles showed evidence of altered energy metabolism without myotoxicity. To further investigate these potential mechanisms of myopathy, a time course study was conducted with cerivastatin (1 mg/kg; 1, 6, 8, 10, and 14 days) in female rats which indicated that alterations in cholesterol homeostasis, and specifically upregulation of the 25-hydroxycholesterol pathway is likely mediated by pathology, removal of excess cholesterol and regeneration. This time course study also indicated an early and sustained transcriptional induction of pyruvate dehydrogenase kinase 4 in fast-twitch muscles, suggesting a metabolic switch in energy metabolism which precedes induction of PGC-1α resulting in a more oxidative phenotype. However, evidence of myofibrillar protein degradation and myopathy ensued indicating impaired energy metabolism may be causally related to myopathy. In contrast, this transcriptional profile was not observed in slow-twitch muscles. Similar time course experiments were also conducted in primary fast-twitch myofibers. However, the in vivo findings were not always recapitulated in this model despite dose- and time-dependent cerivastatin-induced

toxicity which was prevented with mevalonate supplementation. Accordingly, the value and limitations of the in vitro model for investigating mechanisms of toxicity was demonstrated in this work. To identify biomarkers of myopathy, metabolomic profiling was conducted on urine from cerivastatin treated rats which revealed an increase in 1- and 3-methylhistidine (MH) with myopathy. These metabolites were most abundant in skeletal muscle and originated from the dipeptide anserine (1-MH) and myofibrillar proteins (3-MH: actin and myosin). Experimental paradigms resulting in myofibrillar protein catabolism indicated transcriptional induction of the muscle specific ubiquitin ligases (atrogin-1 and MuRF-1) were generally correlated with increased serum 3-MH. Furthermore, serum 3-MH was more sensitive than urine 3-MH, and traditional biomarkers of myopathy, including creatine kinase (CK) and aspartate aminotransferase (AST), suggesting it may be a useful preclinical biomarker of myopathy in non-fasted rats. In contrast, urine 3-MH provides an advantage over CK and AST as it detects skeletal muscle atrophy and hypertrophy. Collectively, this dissertation represents a body of work demonstrating the utility of transcriptomic and metabolomic profiling in identifying potential mechanisms and biomarkers of statin-induced myopathy.

Chapter 1

Introduction

1.1. Historical perspective: HMG-CoA reductase, cholesterol and coronary heart disease

High serum cholesterol is a condition associated with atherosclerosis and coronary heart disease (CHD), the most common cause of mortality in developed countries (Vaklavas et al., 2009). A variety of risk factors have been identified for CHD including tobacco smoking, high blood pressure, obesity, sedentary lifestyle and age (Dent, 2010). However, low-density lipoprotein cholesterol (LDL-C) is one of the most important risk factors for developing atherosclerosis, and the 3-hydroxy-3-methylglutaryl coenzyme A (HMG-CoA) reductase inhibitors, otherwise known as statins, represent a class of drugs used to modulate LDL-C levels by competitively inhibiting the rate-limiting step in cholesterol biosynthesis (Figure 1.1) (Coresh and Kwiterovich, 1996; Fielding and Fielding, 1996; Goldstein and Brown, 1990; Knopp et al., 1994; Vaklavas et al., 2009). The causal relationship between high cholesterol and CHD was initially proposed over 50 years ago and since that time numerous studies have confirmed that lowering LDL-C in patients with hypercholesterolemia can reduce the incidence of CHD (Anderson et al., 1987; Castelli et al., 1986; Keys, 1997; Pekkanen et al., 1990; Shepherd et al., 1995; Scandinavian Simvastatin Survival Study Group, 1994; Stamler et al., 1986). In 2005, over 150 million prescriptions were written for statins making this therapeutic class the

world's most widely prescribed class of drugs with sales in the billions of dollars (Bhardwaj and Chalasani, 2007; Buettner and Lecker, 2008; Fernandez et al., 2011; Kidd et al., 2006; Law and Rudnicka, 2006). Based on recent findings, the patient population indicated to receive long-term statins is likely to expand as it was confirmed that statin treatment causes a significant reduction of cardiovascular events in patients without pre-existing hypercholesterolemia and statin therapy in children with familial hypercholesterolemia might prevent atherosclerosis in adolescence (Alegret and Silvestre, 2006; Rodenburg et al., 2007). Although statin therapy targets reduction in LDL-C some studies have also shown a marginal reduction in triglyceride levels and increased anti-atherogenic high-density lipoproteins (HDL) (Ginsberg et al., 1987; Vega et al., 1998; Bakker-Arkema et al., 1996; Grundy, 1998; Brown et al., 1998; Brown and Goldstein, 1986, 2004).

1.2. HMG-CoA reductase structure, function and regulation

HMG-CoA reductase is highly conserved across species and is composed of a single polypeptide (887-888 amino acids depending on species) which is separated into hydrophobic membrane and hydrophilic catalytic domains (Figure 1.2; DeBose-Boyd, 2008). The membrane domain consists of three functional portions. Specifically, the N-terminal membrane domain is comprised of 339 amino acids in the endoplasmic reticulum, with eight membrane spanning segments, and the linker region which connects to the soluble 548 amino acid C-terminal domain which represents the catalytic portion of HMG-CoA reductase (Figure 1.2; DeBose-Boyd, 2008; Istvan and Deisenhofer, 2000; Istvan et al., 2000). This protein is composed of two monomers in a dimer and two

dimers in a tetramer which catalyzes the 4-electron oxidoreduction of HMG-CoA into CoA and mevalonate with oxidation of two molecules of NADPH (Figures 1.1 and 1.2; Friesen and Rodwell, 2004). The HMG-like moieties of statins occupy the HMG-binding pocket in the active site of the enzyme through hydrogen bonding and ion pairing resulting in a conformational change preventing it from achieving its functional structure (Alegret and Silvestre, 2006). Although the tight binding is reversible the affinity of statins for the active site is in the nanomolar range whereas it is in the micromolar range for HMG-CoA (Alegret and Silvestre, 2006).

HMG-CoA reductase is a highly regulated enzyme, subjected to diurnal variation, short and long term regulation as well as transcriptional and translational regulation (Clarke et al., 1984; Xu and Simoni, 2003). In the rat liver, HMG-CoA reductase mRNA and activity shows diurnal variation with the peak levels occurring during the daily 12 hour dark cycle and the nadir at the middle of the 12 hour light cycle (Clarke et al., 1984). Short-term regulation is mediated by phosphorylation and dephosphorylation by AMP activated kinase and protein phosphatase 2A, respectively (Gaussin et al., 1997; Hardie, 1992). Long-term regulation involves modulation of HMG-CoA reductase protein level by several factors. Inhibition of HMG-CoA reductase leads to a reduction in mevalonate synthesis and sterol levels resulting in activation of the endoplasmic reticulum sterol regulatory element binding protein (SREBP) and HMG-CoA reductase through the intramembrane sequence called the sterol-sensing domain (SSD) (Figure 1.3; DeBose-Boyd, 2008; Ikonen, 2008). SREBP cleavage-activating protein (SCAP) contains an SSD which binds and escorts SREBP proteins, which are membrane bound transcription

factors, from the ER to the Golgi by vesicle coated COPII proteins where they undergo two sequential preoteolytic cleavages including a serine protease (S1P) and a zinc metalloprotease (S2P) (Figure 1.3; Brown and Goldstein, 1997, 1999; Horton et al., 2002; Ikonen, 2008). Following proteolytic cleavage, these transcriptional factors translocate to the nucleus where they bind the sterol regulatory element (SRE) and induce expression of sterol-regulated genes including the LDL-C receptor and cholesterol metabolism genes with up to 200-fold induction of HMG-CoA reductase enzyme levels (Figure 1.3; Brown and Goldstein, 1997; Goldstein et al., 2006; Horton and Shimomura, 1999; Ikonen, 2008). Consequently, hepatic inhibition of HMG-CoA reductase with statin therapy results in reduced cholesterol biosynthesis, decreased intracellular levels of cholesterol, upregulation of LDL-C surface receptors, and increased LDL-C uptake with a concomitant decrease in serum LDL-C (Goldstein and Brown, 1990).

In sterol deprived cells, SCAP binds to SREBPs and is escorted from the ER to the Golgi where SREBPs are proteolytically processed to yield fragments that enter the nucleus and induce expression of sterol-regulated genes (Figure 1.3; Brown and Goldstein, 1999; Ikonen, 2008). In contrast, high intracellular cholesterol leads to fatty acid esterification and storage of these more hydrophobic sterols (Ikonen, 2008). Additionally, when ER membrane cholesterol levels increase the SCAP/SREBP complex fails to exit the ER, the proteolytic processing of SREBPs is abolished and the transcription of sterol-regulated genes is reduced (Ikonen, 2008). ER retention of SCAP/SREBP is mediated by sterol-dependent binding to an insulin induced gene (INSIG), an ER resident protein which induces a conformational change (Figure 1.3; Yang et al., 2002; Ikonen, 2008).

Intracellular accumulation of lanosterol induces HMG-CoA reductase to bind INSIG, promoting ubiquitination and proteasomal degradation (Figure 1.3; Sever et al., 2003; Ikonen, 2008). Furthermore, intracellular accumulation of cholesterol results in enzymatic conversion to oxysterols, which are typically present in minor amounts (approximately 1:1000 compared to cholesterol) (Ikonen, 2008). Oxysterols, like 25-hydroxycholesterol are more hydrophilic and play a role in cholesterol regulation, and at high levels they function as membrane solubilizers leading to reverse cholesterol transport from extrahepatic tissues and hepatic bile acid formation (Ikonen, 2008). Specifically, this regulation is mediated by cholesterol binding to SCAP and 25-hydroxycholesterol binding to INSIG which promotes these chaperones to bind each other rendering a signal in SCAP which is not accessible to the COPII complex thereby preventing ER to Golgi vesicle transport (Figure 1.3; Ikonen, 2008).

Mevastatin was the first compound in the class of HMG-CoA reductase inhibitors identified in 1976 following isolation from the fungus Penicillium citrinum and lovastatin was subsequently isolated from Aspergillus terreus and was the first statin approved by the Food and Drug Administration in 1987 (Figure 1.4; Endo et al., 1976, 1977; Endo and Kuroda, 1976, Tobert, 1987, 2003). Chemical modulation of fungal and microbial products led to the development and marketing of simvastatin in 1988 and pravastatin in 1989, respectively (Figure 1.4; Tobert, 2003). Several compounds with completely different chemical structures were subsequently synthesized and approved for marketing including fluvastatin in 1994, atorvastatin in 1997, cerivastatin in 1998, rosuvastatin in 2003 and pitavastatin 2003 (Figure 1.4; Alegret and Silvestre, 2006; Tolbert, 2003). The naturally occurring statins posses a common naphthalene ring and a β-hydroxylactone

structure along with different side chains. Mevastatin, lovastatin and simvastatin are considered prodrugs because they contain an inactive closed β-hydroxylactone ring which is activated by esterase in the liver to the open lactone form whereas the other statins are administered as the active acid form (Shitara and Sugiyama, 2006). Although the HMG-CoA like moiety is common to all statins the synthetic compounds are structurally dissimilar and this contributes to unique physicochemical and pharmacokinetic properties (Figure 1.4) (Shitara and Sugiyama, 2006). Importantly, there are pharmacokinetic differences in absorption, distribution, metabolism and excretion which affects the safety of these compounds (Garcia et al., 2003; Shitara and Sugiyama, 2006).

1.3. Pleiotropic effects of statins

Statins have a variety of pleiotropic effects representing clinical benefits other than the pharmacological action of reducing LDL-C (Alegret and Silvestre, 2006). Mevalonate is the precursor for several biological intermediates, including isoprenoids farnesyl pyrophosphate (FPP) and geranylgeranyl pyrophosphate (GGPP), and the pleiotropic effects are mediated by the ability of statins to inhibit the synthesis of these isoprenoid products (Figure 1.5; Alegret and Silvestre, 2006). Isoprenoids, including farnesyl and geranylgeranyl residues are covalently attached post-translationally to proteins involved with cellular signaling. This process, termed isoprenylation results in the addition of a hydrophobic isoprenoid moiety which permits anchoring of these prenylated proteins to cellular membranes and facilitates interactions with other membrane bound proteins (Grosshans et al., 2006; Leung et al., 2006; McTaggart et al., 2006). There are numerous prenylated compounds including ubiquinone, dolichol, Heme-a and nuclear lamins, however GTP-binding proteins, including Ras, Rho, Rab and Rac appear to be the most

important in mediating the pleiotropic effects of statins (Figure 1.5; Alegret and Silvestre, 2006). GTPases cycle between a GDP-bound inactive and GTP-bound active state. In the GTP-bound state, these proteins activate a variety of effector proteins until GTP hydrolysis renders them inactive. To bind GTP, the GTPases must translocate from the cytoplasm to the plasma membrane and this process is dependent on isoprenylation and appropriate membrane attachment. GTPases are involved with a variety of cellular functions, including signaling, differentiation, proliferation, and cytoskeleton dynamics (Bellosta et al., 2000; Chan et al., 2003). Therefore, statin mediated depletion of isoprenoids has the potential to modulate a variety of cellular processes. Specifically, the pleiotropic effects of statins are mediated by several mechanisms including modulation of nitric oxide, inflammation, immunomodulation, coagulation and cell proliferation which stabilize atherosclerotic plaques, reduce platelet aggregation, improve endothelial function and reduce inflammation (Alegret and Silvestre, 2006; Bellosta et al., 2000; Buhaescu and Izzedine, 2007; Chan et al., 2003). In fact, the extensive therapeutic benefit of statins has led to these drugs being considered the "new aspirin" (Veillard and Mach, 2002).

1.4. Adverse effects associated with statin therapy

Statins are generally well tolerated and have a good safety profile. However, a variety of adverse effects have been observed in humans (Armitage, 2007). Hepatotoxicity, characterized by a non-asymptomatic elevation of liver enzymes, namely AST and ALT has been observed with an incidence of 1%, and usually occurs within 6 months of initiating statin therapy, and typically resolves with statin withdrawal or time (Bhardwaj

and Chalasani, 2007). Scattered case reports of peripheral neuropathy with statin treatment are rare and the risk is considered very low as this adverse effect has not been confirmed in randomized trials (Armitage, 2007). Gastrointestinal effects have also been reported with statin therapy but again the risk is considered minimal (Armitage, 2007). More recently, statin therapy has been associated with a modest increased risk of diabetes (Preiss and Sattar, 2012). However, the most commonly reported adverse effects of statins are various forms of myotoxicity ranging from myalgia to frank rhabdomyolysis (Table 1.1) (Buettner and Lecker, 2008; Rosenson et al., 2004; Sirvent et al., 2008).

Statin-induced rhabdomyolysis is rare. However, clinical evidence indicates that myalgia may progress to life threatening rhabdomyolysis (Radcliffe and Campbell, 2008). First reported approximately 20 years ago, muscle-related complications did not receive significant attention until 2001 following the withdrawal of cerivastatin (Baycol®) from the market after more than 100 rhabdomyolysis-related deaths were associated with the drug (Thompson et al., 2003). Depending on the study, up to 20% of patients may experience statin-related muscle side effects which interfere with activities of daily living and this has contributed to the fact that fewer than 50% of statin users adhere to the therapy after 1 year (Buettner and Lecker, 2008). The incidence of statin myopathy in clinical practice is significantly greater than what was initially observed in randomized clinical trials evaluating statin efficacy (Fernandez et al., 2011; Kashani et al., 2006). There are several potential causes of this disparity including characteristics of patients in both groups as well as inconsistency in collection of adverse data (Buettner and Lecker, 2008). Compared to typical patients, clinical trial participants were generally younger,

healthier and using fewer medications (Buettner and Lecker, 2008). Furthermore, up to half of all study participants screened were excluded because of various comorbities like renal or hepatic insufficiency, a history of muscular complaints, and patients already taking drugs which could increase systemic exposure of the statins (Fernandez et al., 2011). Additionally, clinical trials with statins were designed to assess efficacy and adverse effects like rhabdomyolysis but not minor muscle discomfort which is often common in older patients (Fernandez et al., 2011). While clinical trials clearly demonstrated the therapeutic benefits of statin therapy these studies greatly underestimated the incidence of statin-induced myopathy which has been observed in clinical practice (Fernandez et al., 2011). In fact, the high incidence of adverse muscle effects, and the perceived risk of myopathy associated with these drugs, has limited the potential clinical benefit of statin therapy that otherwise could be achieved (Fernandez et al., 2011). Despite 20 years of use, both the etiology and mechanism of statin-induced rhabdomyolysis remain obscure. Therefore, elucidating the mechanism of myopathy may enable clinicians to fully harness the therapeutic potential of these drugs while minimizing the risk of this untoward effect.

1.5. Rhabdomyolysis

Rhabdomyolysis is the most severe form of myopathy and occurs in up to 0.5% of patients on statin therapy (Buettner and Lecker, 2008). Rhabdomyolysis is a life-threatening syndrome first reported several thousand years ago by the Israelites following abundant consumption of quail which fed on hemlock during Spring migration (Billis et al., 1971; Rizzi et al., 1991; Rutecki et al., 1998). It is now recognized that eating quail

meat after they have consumed large amounts of hemlock causes rhabdomyolysis through a mechanism which may be directly related to the presence of toxic alkaloids including coniine in Hemlock which paralyzes muscles by blocking the nicotinic receptor on the post-synaptic membrane of the neuromuscular junction (Billis et al., 1971; Rizzi et al., 1991; Rutecki et al., 1998). More recently, crush syndrome, characterized by crushing injury of skeletal muscle was reported during the 1908 Sicilian earthquake and in the German military medical literature during World War I in which soldiers were buried in trenches (Bywaters and Beall, 1941). Today, a variety of different causes have been associated with rhabdomyolysis including use of HMG-CoA reductase inhibitors, cyclosporine, fibrates, corticosteroids, alcohol, cocaine and amphetamines (Sauret et al., 2002; Singh et al., 2005). Other significant causes of rhabdomyolysis include trauma (e.g. third degree burns, crush injury, electric shock), heat-related causes (e.g. heatstroke and malignant hyperthermia), ischemic limb injury and physical overexertion (e.g. marathon runners) (Sauret et al., 2002; Singh et al., 2005). Additionally, rhabdomyolysis has been associated with infections, inflammation, electrolyte imbalance, metabolic and endocrinologic causes and genetic disorders in lipid, carbohydrate and purine metabolism (Sauret et al., 2002; Singh et al., 2005). Importantly, the incidence of statin-induced myopathy is most prevalent in patients with underlying disorders associated with rhabdomyolysis including carnitine palmityl transferase, myophosphorylase and myoadenylate deficiencies (Phillips and Haas, 2008). Regardless of the mechanism of muscle injury, rhabdomyolysis is initiated by a pathologic cascade of events including leakage of extracellular calcium into the intracellular space, followed by a pathologic interaction with actin and myosin leading to overcontraction of the contractile apparatus,

and ultimately muscle destruction and fiber necrosis (Singh et al., 2005; Vanholder et al., 2000). Muscle damage results in the leakage of large quantities of muscular cell constituents (e.g. potassium, phosphate, and myoglobin) into the circulation. These constituents are then filtered by the kidneys causing myoglobin to precipitate in the renal filtrate, and leading to renal tubular obstruction and damage, acute renal failure, multiorgan failure and death (Singh et al., 2005; Vanholder et al., 2000). The importance of rhabdomyolysis is not limited to the clinic as the incidence of skeletal muscle injury during the drug discovery process has become increasingly more prevalent in preclinical animals following investigative studies on new therapeutic targets (Scatena et al.., 2004; Vassallo et al., 2009).

1.6. Muscle biology, physiology and biochemistry

1.6.1. Skeletal muscle

Skeletal muscle comprises approximately 40-55% of body mass in mammals and plays a vital role in posture, movement, heat production and more than 50% of over-all-whole body metabolism (Riechman et al., 2009; Zierath et al., 2004). Accordingly, skeletal muscle plays a major role impacting health and disease mediated by caloric, glucose, fat and cholesterol intake (Riechman et al., 2009). Specifically, skeletal muscle is the major site of glucose disposal and becomes insulin resistant with inactivity (Riechman et al., 2009). In contrast, skeletal muscle contraction can directly stimulate growth and maintenance to prevent or treat the loss of muscle mass with various debilitating conditions associated with ageing and disease (Riechman et al., 2009). Skeletal muscle activity also contributes to cardiovascular health by accelerating metabolism, weight

control, increased vascularization, cholesterol regulation and anti-inflammatory effects (Riechman et al., 2009).

Skeletal muscles are by volume the largest animal cell composed of post-mitotic myofibers (Guyton and Hall, 2006). Myofibers represent a unique cell type in that they are multinucleated, with more than 100 peripherally located nuclei per myofiber (Figure 1.8; Bruusgaard et al., 2003; Newlands et al., 1998). Each of the nuclei is responsible for maintaining a defined area of the sarcoplasm and this has been described as the nuclear / cytoplasmic ratio (Gundersen and Bruusgaard, 2008). In fact, multinucleated skeletal muscle cells employ a unique mechanism of gene regulation. While all myonuclei are capable of transcription, the number of nuclei expressing a specific gene is a dynamic process, as the proportion of transcriptionally active nuclei decreases during fiber growth, with the frequency of active loci within these nuclei reflecting the degree of fiber differentiation (Newlands et al., 1998).

Myofibers are established during embryogenesis by fusion of spindle-shaped myogenic stem cells known as myoblasts or satellite cells which form primary multinucleated myotubes (Figure 1.6; Gundersen and Bruusgaard, 2008; Yablonka-Reuveni et al., 2008). During postnatal development, myogenic cells proliferate, differentiate and fuse with the enlarging myofibers (Figure 1.6). In differentiated muscles, satellite cells reside beneath the basal lamina and are typically quiescent. However, following muscle damage, regeneration of the myofibers is initiated when myogenic stem cells proliferate into myotubes and repair the tissue by fusing with existing myofibers (Yablonka-Reuveni et

al., 2008). Accordingly, satellite cells are required throughout the life of a myofiber and specific regulation is needed to control quiescence, proliferation, differentiation and renewal. Satellite cell myogenesis depends on a highly orchestrated genetic program which controls transcription of specific genes in accordance with cell-cycle progression and differentiation (Figure 1.6; Yablonka-Reuveni et al., 2008). Myogenesis of satellite cells is regulated by a family of muscle-specific transcription factors known as muscle regulatory factors (MRF) (Figure 1.6). These muscle regulatory factors are expressed in a temporal ordered manner and include myogenic determination factor 1 (MyoD), myogenic factor 5 (Myf5), myogenin and myogenic regulatory factor 4 (MRF4) (Figure 1.6). In normal mature muscle, satellite cells are mitotically quiescent but express a number of genes including paired-homeobox transcription factors (Pax3 and Pax7), CD34 and Myf5 which are considered molecular markers of this phenotype (Zammit et al., 2006). When satellite cells are activated, identified as the proliferative stage, they rapidly initiate MyoD expression, undergo CD34 isoform switch and continue expressing Pax7 and Myf5 while proliferating to produce myoblasts (Zammit et al., 2006). The onset of early myogenic differentiation is marked by myogenin expression along with other regulatory and structural genes associated with differentiated skeletal muscle cells (Zammit et al., 2006). As they elongate, myoblasts align with each other, guided in this by mutual membrane recognition followed by cell fusion and formation of long striated multinucleated myotubes which differentiate into mature myofibers (Mermelstein et al., 2007).

Regulation of skeletal muscle regeneration following damage is also dependent on the immune response. Following acute skeletal muscle injury, neutrophils are recruited and increase in number within 2 hours and typically peak in concentration between 6 and 24 hours post-injury and then decline rapidly (Tidball and Villalta, 2010). Following neutrophil invasion, phagocytic macrophages are recruited reaching peak levels about 24 hours post-injury and continue to increase in concentration for about 2 days post-injury and then begin to decrease in number (Tidball and Villalta, 2010). A population of nonphagocytic macrophages invades the muscle and peaks in concentration at about 4 days post-injury and remain elevated for several days (Tidball and Villalta, 2010). Coincident with the invasion of myeloid cells in skeletal muscle following acute injury the myogenic cells transition through the regeneration process described above (Figure 1.7). In fact, in vitro and in vivo studies have demonstrated that factors released by the monocyte/macrophage lineage promote satellite cell proliferation and differentiation (Tidball and Villalta, 2010).

Initiation of the inflammatory response occurs in injured skeletal muscle within a few hours and is believed to occur via membrane damage and release of stored chemoattractants. Several candidate proteins have been identified, including desmin which activates the complement system, chemokines (CXCL1 and CXCL5) and interleukin-6 which recruit neutrophils and mediate the Th1 inflammatory response (Tidball and Villalta, 2010). Additional chemokines, including CCL3, CCL4, CCL2 are also highly expressed following muscle injury suggesting these small molecules play an important role in the inflammatory and regeneration response (Tidball and Villalta,

2010). As with other tissues, damaged skeletal muscle responds with an innate immune response driven by Th1 cytokines including interferon-γ and TNF-α which promotes activation of macrophages to an M1 phenotype, which express the $CD68^+$ (ED1) marker, and propagates a pro-inflammatory response (Tidball and Villalta, 2010). $CD68^+$ is a receptor for oxidized-LDL and following ligand binding phagocytosis is activated by the M1 macrophages (Tidball and Villalta, 2010). Oxidized-LDL results from neutrophil release of myeloperoxidase which damages the skeletal muscle membrane and is considered an important step in regulating the process of tissue regeneration (Tidball and Villalta, 2010). M2 macrophages are activated by Th2 cytokines including interleukin-4,10 and 13 as well as immune complexes and Toll-like receptors and attenuate the inflammatory process and promote tissue repair (Tidball and Villalta, 2010). The M2a and M2c macrophages express CD206 whereas M2c macrophages also express CD163. These CD antigens play an important function determining macrophage phenotype and regulating their specific activity (Tidball and Villalta, 2010). CD163 is a macrophage specific receptor for complexes of hemoglobin and haptoglobin, which following internalization and degradation, returns the extracellular levels to normal, thereby reducing additional cellular damage. This process inhibits the neutrophil and M1 macrophage mediated extracellular formation of Fe^{3+} catalyzed free radicals (Tidball and Villalta, 2010). Furthermore, CD206 is a mannose receptor that binds and internalizes sugar moieties and myeloperoxidase present at high levels in damaged tissues and thus reduces inflammation and ongoing cytotoxicity (Tidball and Villalta, 2010). Although attenuation of the inflammatory response mediates skeletal muscle regeneration, inhibitors (e.g. non-steroidal anti-inflammatory drugs) of cycloxygenase-2 impair this

process by preventing metabolism of arachidonic acid necessary for prostaglandin synthesis which affects skeletal muscle proliferation, differentiation, fusion and muscle fiber growth (Tidball and Villalta, 2010). Accordingly, a very specific cascade of events in the inflammatory response is critical in skeletal muscle regeneration.

Myofibers are densely packed with hundreds to thousands of myofibrils which represent more than 60% of total muscle proteins (Guyton and Hall, 2006; Munoz et al., 1994). Specifically, each myofibril contains about 1500 myosin (thick) filaments and 3000 actin (thin) filaments which are aligned adjacent to each other and responsible for muscle contraction (Figure 1.8). For illustrative purposes, a general overview of the skeletal muscle cell and function are described in Figure 1.9 and the histological appearance is shown in Figure 1.10.

Energy required for muscle contraction is provided by ATP hydrolysis which is normally maintained by creatine kinase, adenylate kinase and myoadenylate deaminase. The concentration of ATP in muscles is approximately 4 mM and is sufficient to maintain full contraction for 1 to 2 seconds (Figure 1.11). The first source of energy that is used to reconstitute ATP is phosphocreatine, which carries a higher amount of free energy than ATP. However, the total amount of phosphocreatine in the muscle is also low, representing about 5-times as much as ATP. Therefore, the combined energy of ATP and phosphocreatine is sufficent to maintain maximal contraction for 5 to 8 seconds (Guyton and Hall, 2006). The second source of energy used to reconstitute ATP and phosphocreatine is glycolysis which utilizes glucose from stored muscle glycogen

(Guyton and Hall, 2006). The rapid degradation of glycogen to pyruvate and lactate liberates energy which is used to form ATP. Glycolysis is important because the reactions can occur in the absence of oxygen so muscle contraction can be maintained even when blood flow is diminished. Moreover, the glycolytic process is about 2.5-times more rapid than ATP generation from cellular oxidation of lipids (Guyton and Hall, 2006). However, because several end products accumulate in the muscle, glycolysis loses its ability to sustain maximum muscle contraction after about 1 minute (Guyton and Hall, 2006). The third source of energy is oxidative metabolism in which products of glycolysis as well as fatty acids and proteins are oxidized to liberate ATP (Guyton et al., 2006). More than 95% of all energy used for sustained, long-term contraction is derived from this source.

To meet the various functional needs, skeletal muscle is comprised of a heterogeneous spectrum of fiber types that differ in their contractile, metabolic and morphologic properties (Table 1.2**;** Guyton and Hall, 2006; Owczarek et al., 2005; Zierath et al., 2004). Skeletal muscles were originally classified by color (red or white) and rate of contraction (slow or fast) in 1873 (Ranvier, 1873). At that time, skeletal muscles were classified based on the contraction speed which correlated with their morphology; fast-twitch appeared white in color whereas slow-twitch fibers appeared red in color. However, it took another 53 years before the red color of skeletal muscle was found to be related to myoglobin content and capillary density (Needham, 1926). Between 1962 and 1970, histochemical staining was developed which identified various myosin ATPase activities which generally correlated with the speed of contraction and fatigue properties and led to the functional classification of muscle fibers: slow-twitch oxidative (type I),

fast-twitch glycolytic oxidative (type IIA) and fast-twitch glycolytic (type IIB) (Pette et al., 1999). However, the relationship between fiber composition and athletic performance was not discovered until 1976 when endurance athletes were found to have a higher proportion of slow-twitch muscles and sprinters were found to contain predominately fast-twitch muscles (Costill et al., 1976).

Currently, muscle fibers are classified with three different methods, including histochemical staining for myosin ATPase, myosin heavy chain isoforms by immunohistochemistry and biochemical differences in energy metabolism (Pette et al., 1999; Scott et al., 2001). These methods led to the recent identification of an additional fast-twitch fiber called IID or IIX which is typically designated as IID(X), corresponding to the MHCIId(x) isoform (Pette et al., 1999). MHCIIb is very similar to MHCIId(x) and these isoforms have often been categorized together. However, humans only express MHCIId(x) whereas small mammals express both MHCIId(x) and MHCIIb (Scott et al., 2001). Despite this species difference, the nomenclature for humans has not changed and MHCIIb is often used to represent MHCIId(x) (Pette et al., 1999; Scott et al., 2001). Together, these results indicate a total of four pure fiber types containing one MHC, including three fast (types IIA, IIB, IID(X) and one slow (type I) which correspond to MHCIIa, MHCIIb, MHCd(x) and MHCI. Additional studies have demonstrated the existence of hybrid fibers which contain two or more MHC isoforms and exhibit a heterogeneous phenotype (Pette et al., 1999; Scott et al., 2001). It should also be noted that myosin light chain, tropomyosin, α-actinin and troponin proteins have various isoforms which are expressed in a fiber specific manner (Scott et al., 2001). While these

proteins are not typically used for assessing muscle fiber types their expression can be confirmatory. Furthermore, it is important to mention that muscle fiber distribution varies between skeletal muscles within a species and between similar muscles of different species (Pette et al., 1999). Specifically, when comparing the same muscle across species the relative amount of MHCIIb is inversely related to the size of the animal (Pette et al., 1999). In the mouse and rat, the psoas consists of predominately IIB fibers whereas in rabbits the same muscle contains a predominance of II(D)X fibers (Pette et al., 1999).

Biochemical classification of skeletal muscle is also based on differences in energy metabolism and this approach leads to three different fiber types, including slow-twitch oxidative (SO), fast-twitch oxidative (FOG) and fast-twitch glycolytic (FG) (Table 1.2; Guyton and Hall, 2006; Owczarek et al., 2005; Zierath et al., 2004). Specifically, slow-twitch oxidative muscle fibers are predominately involved with continuous activity requiring endurance (e.g. marathon running). To meet this long-term energy demand, this muscle type is more suited for the generation of aerobic energy, and as such contains more mitochondria compared to fast-twitch muscle fibers (Table 1.2; Guyton and Hall, 2006; Zierath et al., 2004). Fast-twitch glycolytic fibers are used for phasic activity requiring maximal power during short periods of time (e.g. weightlifting). To achieve this short burst of energy requirement, these muscle fibers contain greater enzyme activity involved with rapidly releasing energy from phosphocreatine-creatine system, glycolysis and glycogen degradation compared to slow-twitch oxidative muscle fibers (Table 1.2; Guyton and Hall, 2006; Zierath et al., 2004). Furthermore, fast-twitch muscles have a significantly higher level of creatine phosphate (Pette et al., 1999). Fast-twitch oxidative

fibers have characteristics which are intermediate between the other two muscles (Table 1.2).

1.6.2. Cardiac and smooth muscle

Although the emphasis of this dissertation is on cerivastatin-induced skeletal muscle toxicity it is important to note that cardiac and smooth muscle are functionally and morphologically unique. Each of these muscles have diverse phenotypic properties, functional roles and morphology which may contribute to differences in sensitivity and selectivity to drug-induced toxicity. Cardiac myofibers (cardiomyocytes) contain a single centrally located nucleus, are branched and interlock with adjacent myofibers through intercalated discs, which enable the heart to contract in a synchronous manner (Guyton and Hall, 2006). However, dysregulation of this synchronous cardiac cycle can damage the heart muscle thereby disrupting the synchronous waves resulting in random fiber contraction known as fibrillation, which can lead to cardiomyocyte death. Similar to slow-twitch muscles, the heart contains a rich supply of mitochondria which reflects its dependence on oxidative metabolism of fatty acids and to a lesser extent glucose for ATP (Guyton and Hall, 2006). Accordingly, drugs like isoproterenol specifically target the heart and slow-twitch muscles but not fast-twitch muscles (Ng et al., 2002). However, while cardiac muscle shares similarities with slow-twitch muscles, there are functional and morphological differences, and these properties likely contribute to the fact that some compounds like adriamycin selectively target the heart (Zhang et al., 2009).

Smooth muscle consists of single nucleated, spindle-shaped cells which contain no visual striations, representing the arrangement of actin and myosin in the sarcomere as well as the troponin complex involved with contraction. Although smooth muscle contraction is mediated by calcium ions and ATP major differences exist in the duration and quantity of energy required for contraction compared to striated muscles (Guyton and Hall, 2006). Specifically, skeletal muscle contraction is rapid whereas smooth muscle contraction is prolonged, lasting hours or days and this difference is attributed to the fact that significantly less energy is required to maintain contraction in smooth compared to skeletal muscle (Guyton and Hall, 2006).

1.7. Skeletal muscle as a target organ of drug toxicity

1.7.1. Fiber differences in skeletal muscle degeneration

Numerous drugs have been shown to cause skeletal muscle toxicity, and in many cases these effects occur in a fiber specific manner (Owczarek et al., 2005; Sardao et al., 2008). Fibrates (PPAR-α agonists), β-adrenergic agonists, chloroquine (used for malaria treatment) and bupivacaine (anaesthetic) preferentially cause a slow twitch myopathy (De Souza et al., 2006; Irwin et al., 2002; Ng et al., 2002; Velasco et al., 1995), whereas HMG-CoA reductase inhibitors and alcohol primarily target fast-twitch muscles (Adachi et al., 2003; Preedy et al., 2001; Westwood et al., 2005). Additionally, some compounds like glucocorticoids, adriamycin (cancer chemotherapeutic), carbofuran (pesticide), and pyridostigmine bromide (cholinesterase inhibitor) do not discriminate, causing toxicity in both fiber types (Braunstein and De Girolami, 1981; Dirks-Naylor and Griffiths, 2009; Doroshow et al., 1985; Hudson et al., 1985; Lee et al., 2005; Milatovic et al., 2005). In a similar manner, myopathy associated with several diseases, including diabetes,

sarcopenia, cachexia, sepsis and starvation predominately target fast-twitch muscle fibers (Gribmy, 1995; Lexell, 1995; Narici and Maffulli, 2010; Tomlinson and Irving, 1977). However, a more generalized skeletal muscle degeneration can also occur with strenuous exercise, inherited diseases (e.g. muscular dystrophy and metabolic myopathies) and myotonic dystrophy (Ashizawa and Sarkar, 2011; Vanholder et al., 2000). The mechanistic basis of fiber specific toxicity remains unknown but is believed to be associated with differences in contractile, metabolic and morphologic properties of the skeletal muscle (Vanholder et al., 2000). Specifically, the low oxidative capacity of fast glycolytic fibers has been proposed to predispose this fiber type to injury through depletion of high-energy phosphates (Gupta and Goad, 2000). Additionally, slow-twitch muscles contain higher levels of certain cytoskeletal proteins that may provide structural support for the sarcomeres and cell membrane which may help to maintain the integrity of these structures in the face of injury.

In contrast to fiber specific degeneration, the specific fiber composition of skeletal muscle also contributes directly to the risk of developing various diseases. Specifically, individuals with a greater fast-twitch fiber composition are more likely to have chronic metabolic syndromes like insulin resistance, type 2 diabetes, obesity, and a blood lipid profile associated with an increased risk of cardiovascular diseases (Campbell et al., 2001; Zierath et al., 2004). In contrast, having a greater proportion of slow-twitch muscle fibers increases insulin-stimulated glucose uptake and metabolism. However, with aging and physical inactivity, a slow- to fast-twitch fiber conversion occurs which increases the risks of metabolic diseases (Zierath et al., 2004).

1.7.2. Sex differences in skeletal muscle degeneration

Skeletal muscle degeneration also occurs in a sex specific manner in humans, with females showing a greater sensitivity to HMG-CoA reductase inhibitors, fibromyalgia, temporomandibular disorder (masticatory muscle pain), and repetitive motion muscle disorders whereas men are more likely to develop sporadic inclusion body myositis (a muscle-specific autoimmune disease) (Bartels et al., 2009; Hart et al., 1998; Needham and Mastaglia, 2008; Warren and Fried, 2001). In contrast, the incidence of diseases like Duchene Muscular Dystrophy show no sex difference (Moser, 1984). The mechanistic basis for sex specific muscle degeneration is unclear. However, it is generally believed that sex hormones including testosterone and estradiol play an important role in modulating a variety of biochemical pathways affecting skeletal muscle energetics, metabolism, growth, maintenance of muscle mass and inflammation related to damaged tissue repair however the exact mechansims of action in skeletal muscle remain largely unknown (Sheffield-Moore and Urban, 2004; Tiidus et al., 2008). These broad effects are not surprising given that skeletal muscle is one of the most metabolically active tissues responsible for 75% of the insulin-induced glucose uptake in the body, has a large substrate storage capacity, and supplies precursors for glucose via gluconeogenesis and a repository of protein and amino acids (Barros and Gustafsson, 2011). Accordingly, the homeostatic balance of these biochemical pathways in skeletal muscle undergoes a continuous remodeling during growth, health, disease and ageing which is hormonally regulated in a sex-dependent manner (Sheffield-Moore and Urban, 2004).

Androgens like testosterone are converted to the bioactive metabolite dihydrotestosterone (DHT) by 5α-reductase or to estradiol by aromatase and target both reproductive and non-reproductive tissues such as skeletal muscle (Chen et al., 2005). In general, sex steroids are secreted by the ovary, testis and adrenal cortex. However, skeletal muscle is also capable of locally synthesizing sex steroid hormones from circulating testosterone, and acute exercise enhances the local bioactive androgen metabolism in skeletal muscle of both sexes (Aizawa et al., 2007, 2010). Given that skeletal muscle also contains both androgen and estrogen (ERα and ERβ) receptors these sex steroid hormones may exert an autocrine and/or paracrine action in skeletal muscle (Aizawa et al., 2007). In skeletal muscle, testosterone and DHT are known to promote protein synthesis, cell signaling, myoblast cell proliferation, glucose metabolism-related signaling, ATP production and reduce protein degradation (Haren et al., 2011; Pires-Oliveira et al., 2010; Yoshioka et al., 2006). Specifically, a net increase in protein anabolism is mediated in part by suppression of the skeletal muscle specific ubiquitin ligases atrogin-1 and MuRF-1 in the ubiquitin proteasome pathway which reduces myofibrillar protein degradation (Pires-Oliveira et al., 2010; Sato et al., 2008; Ustunel et al., 2003; Zhao et al., 2008b).

Most research on androgens has been directed towards hypogonadal men or those suffering wasting diseases causing profound skeletal muscle loss since these effects show a strong correlation with reduced circulating androgen levels (Sheffield-Moore and Urban, 2004). In hypogonadism patients, the therapeutic use of anabolic agents increases skeletal muscle mass and strength resulting from a net increase in muscle protein synthesis (Sheffield-Moore and Urban, 2004). Furthermore, testosterone does not affect

the relative proportions of fast- and slow-twitch myofibers in young and old men but rather increases the muscle fiber cross-sectional area and volume of both fiber types in a dose-dependent manner (Sinha-Hikim et al., 2002; 2006). Consistent with a role in energy metabolism, reduced serum testosterone levels in aging men correlates with an increased incidence of metabolic disorders like type 2 diabetes (Salehzadeh et al., 2011). Based on these effects, testosterone and selective androgen receptor modulators are being pursued as anabolic therapies for various catabolic skeletal muscle conditions like sarcopenia as frailty and old age are major public health problems which impact mobility and quality of life (Bhasin et al., 2006). Given the focus of this dissertation it is important to note that HMG-CoA reductase inhibition with statin therapy does not affect circulating levels of androgens in men (Hall et al., 2007).

Similar to androgens, estradiol is considered an important regulator of metabolic homeostasis, including glucose and lipid metabolism (Foryst-Ludwig and Kintscher, 2010). Although the exact mechanism is unclear, estradiol plays an important role in modulating glucose disposal in skeletal muscle through action on several proteins in the insulin signaling pathway (Barros and Gustafsson, 2011). Accordingly, physiological levels of estradiol are beneficial for insulin sensitivity and homeostatic metabolic regulation in skeletal muscle (Barros and Gustafsson, 2011; Livingstone and Collison, 2002). In contrast, dysregulation of estradiol or the estrogen receptors (ERα and β), have specific metabolic actions in various tissues, including skeletal muscle. Specifically, these effects play a pivotal role in the development and progression of the metabolic syndrome, through modulation of carbohydrate and lipid metabolic homeostasis in

skeletal muscle (Barros and Gustafsson, 2011; Foryst-Ludwig and Kintscher, 2010; Ropero et al., 2008). Although the mechanism of these changes has yet to be completely elucidated, ERα along with the peroxisome proliferator-activated receptor γ coactivator 1α (PGC1α) have been shown to coactivate pyruvate dehydrogenase kinase 4 and thus directly regulate glucose metabolism (Wende et al., 2005; Zhang et al., 2006).

Estradiol also has a direct action on the hypothalamus mediated by ERα and β in which higher levels are associated with the estrus and menstrual cycles and pregnancy, and associated with reduced food intake. In contrast, ovarictomy, antiestrogen treatment and menopause result in increased food intake, body weight and abdominal fat accumulates which is mitigated with estradiol replacement (Barros and Gustafsson, 2011). Moreover, estradiol regulates peripheral feedback hormones that affect food consumption through actions on the central nervous system. Leptin, which is a potent catabolic hormone released by adipose cells reduces food intake and increases energy expenditure and it has been shown that estradiol modulates the leptin receptor and increases hypothalamic sensitivity to leptin, altering peripheral fat distribution (Barros and Gustafsson, 2011). Another important peptide (ghrelin) is produced in the stomach, regulated by estradiol and acts on growth hormone receptors which are potent stimulators of food intake through an unknown mechanism (Barros and Gustafsson, 2011).

Given the biological effects of testosterone and estradiol it is not surprising that sex specific transcriptional regulation exists in skeletal muscle (Roth et al., 2002; Salehzadeh et al., 2011; Yoshioka et al., 2007). In fact, in vivo as well as in vitro studies have

demonstrated transcriptional differences related to cytoskeletal/contractile apparatus, mitochondrial processes, glucose, lipid, protein and amino acid metabolism (Yoshioka et al., 2007). However, the most abundant transcripts are similar in female and male rats indicating that the population of various fiber-types is not sex-dependent (Yoshioka et al., 2007). Collectively, these data indicate that both testosterone and estradiol modulate skeletal muscle energy homeostasis and may be important mediators of sex-specific skeletal muscle toxicity. However, the role, if any, for these hormones in mediating statin-induced myopathy has yet to be investigated despite the observation that females are more sensitive than males.

1.7.3. Adaptive characteristics of skeletal muscle to altered physiology and pathology

Skeletal muscle demonstrates a remarkable plasticity which enables functional, morphological and metabolic adaptation to the ever changing physiological stimuli like exercise, environmental conditions and substrate availability as well as pathological conditions. In particular, weight lifting and aerobic exercise cause adaptations consisting of increased blood flow, increased muscle mass, satellite cell proliferation and evidence of new myofiber formation (Appell et al., 1988; McCormick and Thomas, 1992). These external stimuli activate various signaling pathways which modulate gene expression resulting in phenotypic changes in muscle fiber type, diameter, length and vascular supply. The fiber-type profile of different muscles is initially established during development and independent of neural influence. However, nerve activity plays a significant role in maintenance and modulation of the fiber phenotype during postnatal

development, in adults and during muscle regeneration (Schiaffino et al., 2007). Skeletal muscle fiber-type transformation occurs when either a slow- or fast-twitch fiber develops phenotypic properties of the other fiber type. Several independent signaling pathways including Ras/mitogen-activated protein kinase, NFAT, calcineurin, calcium/calmodulin-dependent protein kinase IV, PPARs and the peroxisome proliferator γ coactivator (PGC-1) are known to regulate this process (Schiaffino et al., 2007; Zierath et al., 2004).

Skeletal muscle can also adapt to various physiological conditions by modulating mass. An increase in muscle mass is called hypertrophy whereas a decrease in muscle mass is called atrophy. The mass of skeletal muscle is governed by regulatory processes that modulate the rate of protein synthesis and degradation (Murton et al., 2008). These adaptations result in alteration in the mass and metabolic properties of the muscle fibers, with physiological capabilities that match the new functional demands. The multinucleated nature of skeletal muscle provides this tissue with a unique mechanism enabling it to adapt to such physiological changes. Specifically, each myonuclei regulates a local cytoplasmic domain in the vicinity of the nucleus, called the myonuclear domain (Gundersen and Bruusgaard, 2008). It is currently believed that regulation of muscle fiber mass during atrophy results in loss of nuclei by apoptosis whereas with hypertrophy new nuclei from muscle satellite cells fuse with the myofiber (Dupont-Versteegden, 2006; Gundersen and Brusgaard, 2008; Tews, 2005). In most cells, apoptosis leads to destruction of the nucleus and cell death however multinucleated muscle cells are able to harness this process to remodel the myofiber by eliminating specific myonuclei and reducing fiber size (Allen et al., 1999). It is unknown whether the number of nuclei is the

causative factor in regulating muscle mass or a consequence, but regardless the myonuclear domain is maintained during this processes (Allen et al., 1999; Gundersen and Bruusgaard, 2008).

Muscle hypertrophy is associated with a net increase in protein synthesis, reduction in protein degradation or both resulting in increased number of contractile proteins, mitochondria, enzymes involved with energy metabolism and nuclei to maintain a constant ratio of nuclei to cytoplasmic volume (Boonyarom and Inui, 2006; Otto and Patel, 2010). Furthermore, and perhaps more importantly, an anabolic response in skeletal muscle is associated with increased muscle strength and function. Muscle hypertrophy results from a variety of factors including increased muscle activity associated with exercise and anabolic agents like testosterone, growth hormone (peptide released by hypothalamus) and β-adrenergic agonists (e.g. epinephrine), as well as insulin, insulin-like growth factor-1 (IGF-1) and growth and differentiation factor 8 (GDF8; myostatin) (Murton et al., 2008). However the anabolic actions of various hormones on skeletal muscle vary based on a variety of factors including age, sex, and duration of exposure (Sheffield-Moore and Urban, 2004). At the molecular level, skeletal muscle mass is controlled by two major signaling pathways that are regulated by either IGF-1 or myostatin. IGF-1 has a major effect on skeletal muscle size by increasing stem cell proliferation, protein synthesis, fusion of new myonuclei into myofibers, and myoblast differentiations (Figure 1.12). IGF-1 signals through the IGF-1 receptor via direct interaction with IGF-1 binding proteins and activation of several pathways with each culminating into different phenotypic changes in the muscle leading to an increase

and maintenance of muscle mass (Figure 1.12; Otto et al., 2010). Additionally, anabolic effects (e.g. testosterone) negatively regulate the myogenic atrophy pathways thereby maintaining existing skeletal muscle mass through prevention of muscle protein degradation and wasting (Otto and Patel, 2010).

Myostatin is expressed specifically in developing and adult skeletal muscle and is regarded as a negative regulator of muscle mass (Lee, 2004). During development, myostatin expression limits the muscle size in concert with other factors that develop the limbs in relation to skeletal, vascular and ectodermal patterns of growth. In myogenic cells, myostatin downregulates expression of myogenic cell proliferation markers (Pax-3 and Myf-5) and the muscle differentiation marker Myo-D (Rodino-Klapac et al., 2009). Targeted disruption of myostatin results in muscle hypertrophy and hyperplasia with muscle mass increases of up to 3-fold (Rodino-Klapac et al., 2009). Thus, myostatin modulates the number of muscle fibers that are ultimately formed by regulating proliferation and differentiation of myoblasts during development and second it regulates muscle fiber growth postnatally through hypertrophy and hyperplasia (Lee., 2004; Otto and Patel, 2010).

Muscle atrophy is associated with a net increase in protein degradation resulting in reduction in number of contractile proteins, mitochondria, enzymes involved with energy metabolism and nuclei to maintain a constant ratio of nuclei to cytoplasmic volume (Boonyarom and Inui, 2006; Sandri, 2010). Induction of muscle atrophy is associated with a variety of conditions including neuromuscular diseases, diabetes mellitus, cancer

cachexia, disuse, immobilization, denervation, sarcopenia, wasting, fasting, starvation and drugs like glucocorticoids, and chloroquine (Murton et al., 2008). At the cellular level, the hallmark change associated with muscle atrophy is a reduction in the myofibrillar proteins resulting in dissolution of the sarcomeres (Boonyarom and Inui, 2006). Although intracellular proteins are continuously hydrolyzed to their constituent amino acids and replaced by synthesis of new proteins, degradation occurs at widely differing rates, varying from minutes for some regulatory enzymes to weeks for myofibrillar proteins like actin and myosin (Lecker et al., 2006; Munoz et al., 1994). To ensure continual protein degradation is highly selective, cells contain several specific proteolytic systems maintained by complex regulatory mechanisms (Murton et al., 2008; Sandri, 2010).

The cytosolic Ca^{2+}-activated (ATP-independent) pathway consists of calpains which are cysteine proteases activated when cells are injured and cytosolic Ca^{2+} increases (Costelli et al., 2005). These proteases are thought to play an important role in tissue injury, necrosis and autolysis (Costelli et al., 2005; Lecker et al., 2006). Caspases are cytosolic proteases which cleave proteins after aspartic acid residues and are critical in destroying cell constituents during apoptosis (Lecker et al., 2006). Both the calpain and caspase pathways perform a limited proteolysis due to restricted specificity (Costelli et al., 2005). In contrast, two proteolytic systems; the autophagy-lysosome pathway and ubiqutin-proteasome pathway (UPP) are responsible for degrading most proteins to their constituent amino acids during basal and catabolic-induced adaptive physiological responses (Sandri, 2010). These two pathways serve distinct yet coordinately regulated

functions through forkhead box protein O3 (FoxO3) transcriptional factor to preserve the appropriate composition and distribution of proteins and organelles in atrophying muscle which enables cells to respond to environmental and nutrient changes (Bursch et al., 2008; Sandri, 2010; Zhao et al., 2008a). Additionally, these pathways are involved with diverse physiological responses such as biosynthesis, regulation of metabolism through elimination of specific enzymes, morphogenesis, cellular differentiation, tissue remodeling, aging, cellular defense, survival against injury, programmed cell death and ultimately as a fundamental survival strategy serving as a homeostatic mechanism at the subcellular level (Bursch et al., 2008).

The autophagy-lysosome pathway constitutes a major adaptive survival response which degrades long-lived proteins and organelles whereas the UPP degrades myofibrillar and most soluble short-lived proteins (Sandri, 2010). In normal physiology, these pathways maintain homeostasis of skeletal muscle mass by tightly regulating protein degradation. During catabolic conditions, skeletal muscle is considered a protein reservoir which is mobilized by autophagy and the UPP to maintain gluconeogenesis in liver, to maintain protein synthesis, and to provide alternative energy substrates for preservation of critical organ function, including skeletal muscle (Figure 1.13) (Lecker et al., 2006; Rabinowitz and White, 2010; Sandri, 2010). Paradoxically, dysregulation representing inhibition or excessive skeletal muscle protein degradation can exacerbate other catabolic conditions and lead to pathogenic mechanisms, myofiber degeneration, morbidity and mortality (Masiero and Sandri, 2010; Motojima et al., 2002; Motojima and Seto, 2003; Nishida et al., 2009; Sandri, 2010).

In the autophagy pathway, double membrane vesicles or vacuoles engulf a portion of the cytoplasm including mitochondria, ribosomes, peroxisomes, ER, ribosomes, lipid droplets, cytosolic proteins, glycogen and protein aggregates that are released into the cytoplasm for reutilization in biosynthetic pathways (Figure 1.14) (Rabinowitz and White, 2010; Sandri, 2010). However, a massive quantity of autophagic vacuoles often forms before the manifestation of cell death and this is considered a hallmark reflecting the cells effort to survive a life-threatening insult (Bursch et al., 2008). These autophagic vacuoles or autophagosomes are delivered to lysosomes and the contents are degraded by the acidic proteases cathepsin B, D and H as well as other hydrolases. In the autophagy system, small ubiquitin-like molecules including LC3, GABARAP, GATE16 and Atg12 are transferred from the conjugation system to membranes targeted for lysosomal degradation (Lecker et al., 2006; Sandri, 2010). Expression of the transcription factor FoxO3 is sufficient and required to activate the lysosomal-dependent protein degradation and this pathway is activated by the lack of insulin or essential amino acids (Lecker et al., 2006; Sandri, 2010).

A substantial body of evidence has accumulated implicating the UPP as the major regulator of myofibrillar protein degradation leading to skeletal muscle atrophy (Murton et al., 2008). However the UPP is unable to degrade intact myofibrils therefore initial disruption of the intact sarcomeric proteins is catalyzed by calpains and to a lesser extent caspases which targets proteins (nebulin, titin and desmin) involved in the correct assembly of the myofilaments to the sarcolemma (Costelli et al., 2005). Following calpain degradation of the sarcomere structure, the contractile proteins are released and

available for UPP protein degradation (Figure 1.15) (Costelli et al., 2005; Jackman and Kandarian, 2004; Murton et al., 2008). The UPP is an ATP dependent proteolytic system involving degradation of target proteins with substrates identified for degradation by the addition of ubiqutin (Ub) molecules. Ub is first bound to the Ub-activating enzyme (E1) via high-energy thioester bond. Ub is subsequently transferred to the Ub-conjugating enzyme (E2) and then conjugated to the target protein by an Ub-ligase enzyme (E3). This process is repeated until a minimum of four Ub monomers are covalently attached via lysine residue to the target protein at which time the 26S proteasome recognizes the protein and degrades it into short peptides via chymotrypsin-like, trypsin-like and caspase-like activities (Murton et al., 2008). Degradation of the protein fragments into individual amino acids is then completed by tripeptidyl-peptidase II and exopeptidases (Figure 1.15; Murton et al., 2008).

The UPP is constantly degrading damaged proteins to maintain normal cellular function. Target specificity of this system is established through hundreds of Ub-ligases (Murton et al., 2008). Muscle RING Finger 1 (MuRF-1) and Muscle Atrophy F-box (MAFbx/atrogin-1) represent two skeletal muscle specific Ub-ligases which are regulated by forkhead box proteins as well as other transcriptional factors and responsible for the UPP mediated myofibrillar protein degradation associated with atrophy (Figure 1.16) (Otto and Patel, 2010). In all catabolic conditions evaluated, there is a common transcriptional induction of MuRF1 and atrogin-1 as well as other components of the proteasome (Figure 1.13) (Lecker et al., 2006; Sandri et al., 2010). Importantly, these ubiqutin ligases are the rate-limiting step in the ubiquitination reaction and increased

expression is sufficient to enhance protein degradation via UPP (Lecker et al., 2006; Sandri et al., 2010). Although there is strong evidence indicating a role for MuRF-1 and MAFbx in muscle atrophy the specific protein targets are still under investigation. MaFbx targets myogenic transcription factors (myogenin and MyoD) and the elongation initiation factor 3 subunit 5 which suggests a role in affecting muscle growth and protein synthesis (Figure 1.16) (Foletta et al., 2011). In contrast, MuRF-1 preferentially interacts with structural proteins including myosin heavy chain, myosin binding protein C, myosin light chains, titin and creatine kinase (Figure 1.16) (Foletta et al., 2011). MuRF-1 has also been reported to interact with glucose production and glycogen metabolism, however it is unknown whether proteins in these pathways are degraded (Figure 1.16) (Foletta et al., 2011). Thus, MuRF-1 may act to control protein degradation and muscle energy metabolism. Collectively, transcriptional induction of the UPP typically leads to increased protein degradation along with a reduction in protein synthesis.

As described above, the multinucleated nature and plasticity of myofibers enables this cell type to adapt to a variety of catabolic signals, including environmental and nutrient changes as well as toxic insults, by reducing muscle mass through processes like autophagy, atrophy and apoptosis. While these normal physiological processes represent adaptive cellular survival responses initiated to maintain cellular homeostasis, chronic stimulation or dysregulation of these pathways leads to excessive protein degradation and myofiber degeneration (Masiero and Sandri, 2010; Motojima et al., 2002; 2003; Nishida et al., 2009; Sandri et al., 2010). Additionally, if there is impairment in ATP synthesis, preventing myofibers from adapting to the toxic insult, these survival pathways will fail

and necrosis will ensue (Orrenius et al., 2011; Zong and Thompson, 2006). Therefore, a variety of factors including type of exposure and duration of a toxic insult as well as whether pathways involved with energetics are affected ultimately dictates the cellular fate of myofibers.

Apoptosis is characterized morphologically by pyknosis, nuclear fragmentation and formation of condensed bodies. This ordered morphology depends on the ability of the dying cell to invoke ATP-dependent processes required for self degradation (Zong and Thompson, 2006). In contrast, necrosis is defined morphologically by electron-lucent cytoplasm, swelling of organelles, collapse of internal homeostasis which occurs when a cells is unable to produce sufficient ATP causing bioenergetic failure and rapid loss of plasma membrane integrity (Bursch et al., 2008; Zong and Thompson, 2006). Apoptosis is widely regarded as an active or programmed form of cell death whereas necrosis is considered uncontrolled or pathological. Despite the notion that necrosis is uncontrolled, accumulating evidence suggests this may not be completely accurate (Zong and Thompson, 2006). Instead it appears that necrosis can also regulate events that contribute to maintenance of tissue homeostasis (Zong and Thompson, 2006). Necrosis may in fact provide cells with an adaptive advantage over apoptosis because it enables an active recruitment of a proinflammatory defensive response and an activation of a satellite cell reparative process to damaged tissue which may otherwise compromise the integrity of the organism as a whole. In fact, similar to apoptosis, a myonuclear domain within a myofiber may undergo necrosis while the remaining portion of the cell remains viable. It is now believed that in response to a specific toxic insult a continuum of pathological

changes occurs with processes like atrophy, autophagy and apoptosis prevailing at low doses and necrosis at high doses, and features of both may also coexist within the same myofiber (Orrenius et al., 2011; Zong and Thompson, 2006). Similarly, it is believed that chronic stimulation of these pathways, characterized by excessive protein degradation may lead to myofiber degeneration (Masiero and Sandri, 2010; Motojima et al., 2002; Motojima and Seto, 2003; Nishida et al., 2009; Sandri et al., 2010). Regardless of the toxic insult, several common pathways including increased mitochondrial reactive oxygen species production, channel-mediated calcium uptake, activation of non-apoptotic proteases and rapid loss of cellular membrane potential lead to energetic failure which triggers necrosis (Zong and Thompson, 2006). Often times, these necrotic mediators are induced in the dying cell simultaneously and potentiate each other's ability to initiate necrosis.

1.8. Role of HMG-CoA reductase in skeletal muscle cholesterol homeostasis

All nucleated cells can synthesize cholesterol from acetyl-CoA through the mevalonate pathway. However the rate of cholesterol biosynthesis in rat skeletal muscle is less than 1% of the liver, and significantly less than other major organs (Spady and Dietschy, 1983). Furthermore, skeletal muscle shows the lowest uptake of LDL-C compared to other major organs and the rate of cholesterol synthesis in skeletal muscle does not respond to fluctuations in plasma LDL-C levels like other organs (Stange and Dietschy, 1984; Turley et al., 1981). The mechanistic basis for this unique tissue-specific regulation of cholesterol is unknown but may be related to the fact that skeletal muscle is predominately comprised of post-mitotic cells which have a theoretical lifespan equal to

the organism. Accordingly, under normal physiological conditions differentiated adult myofibers may have a reduced need for synthesizing cholesterol compared to other tissues. The liver regulates cholesterol levels in the blood and would therefore be expected to show greater flux in this pathway compared to skeletal muscle. Furthermore, tissues undergoing a high cellular turnover rate would have a greater cholesterol need for membrane synthesis compared to skeletal muscle. In contrast, adult myofibers would only be expected to have an increased need for cholesterol during development and differentiation, hypertrophy or repair from injury since these processes require membrane synthesis. Evidence to support this hypothesis is based on the observation that HMG-CoA reductase activity is critical for myogenesis and it has been demonstrated that inhibition of this enzyme results in a decrease in myogenin and myosin heavy chain proteins, considered early and late markers, respectively of myoblast differentiation and also prevents myoblast fusion into multinucleated syncitia (Martini et al., 2009). HMG-CoA reductase is upregulated at an early stage of myogenesis and downregulated at the later stage of differentiation (Martini et al., 2009). At the early stage, the increase in HMG-CoA reductase protein levels are related to transcriptional induction and decreased enzyme degradation whereas the subsequent decrease is mediated by a reduction in transcription and increased protein degradation (Trapani et al., 2010).

There is a strong correlation between cholesterol absorption and synthesis, and increases in skeletal muscle mass associated with resistance training (Riechman et al., 2009; Vinagre et al., 2007). This increase in cholesterol is important in membrane biosynthesis during the recovery and adaptation resulting in skeletal muscle hypertrophy (Riechman et

al., 2009). Furthermore, skeletal muscle damage resulting from various diseases like Muscular Dystrophy and Inclusion Body Myositis as well as statin-induced myopathy are associated with increases in skeletal muscle cholesterol or transcriptional induction of HMG-CoA reductase and the LDL receptor, suggesting this pathway is involved with repair of the damaged tissue (Jaworska-Wilczynska et al., 2002; Kuhn et al., 1990; Morikawa et al., 2005; Paiva et al., 2005; Riechman et al., 2009; Sidaway et al., 2009; Totsuka and Watanabe, 1982; Yokoyama et al., 2007). Together, these studies demonstrate that skeletal muscle regulation of cholesterol synthesis and uptake is different from other tissues like the liver. Furthermore, in skeletal muscle, cholesterol synthesis and uptake is most important during processes like development and differentiation, hypertrophy and repair from injury which require an increase in membrane synthesis.

1.9. Proposed mechanisms of statin-induced myopathy

Despite extensive research efforts, the underlying pathophysiology of statin myopathy remains unknown, but suggested mechanisms include decreased production of prenylated proteins, ubiquinone, and cholesterol, increased skeletal muscle uptake of cholesterol or phytosterols, mitochondrial dysfunction, changes in energy metabolism, catabolism of muscle proteins via UPP, disruption of calcium metabolism, and vitamin D deficiency (Buettner and Lecker, 2008; Draeger et al., 2006; Guis et al., 2006; Gupta and Thompson, 2011; Hanai et al., 2007; Marcoff and Thompson, 2007; Mallinson et al., 2009; Schaars and Stalenhoef, 2008; Paiva et al., 2005; Phillips et al., 2002; Phillips and Haas, 2008; Thompson et al., 2003; Urso et al., 2005; Vaklavas et al., 2009; Yokoyama et al., 2007).

Given the biochemical relationship between these processes it is likely that many of these events contribute to or potentiate the underlying mechanism of statin myopathy. However, identifying the exact cascade of events initiating myotoxicity from the published literature is difficult because of conflicting results from in vivo and in vitro studies, conducted with a variety of different skeletal muscle cell lines lacking a fiber specific phenotype, and with drug concentrations that are often not biologically relevant. Furthermore, data favoring one etiology over another are largely based on cell culture experiments or acute studies in rodents given a toxicological dose which may not reflect the mechanism in humans with a chronic pharmacological statin dose (Antons et al., 2006).

The most compelling evidence suggests that statin myopathy is directly related to HMG-CoA reductase inhibition as mevalonate supplementation prevents in vivo and in vitro myotoxicity (Flint et al., 1997a; Johnson et al., 2004; Nishimoto et al., 2003; Westwood et al., 2005). Further evidence that a mevalonate pathway deficiency may be responsible for muscle injury is based on the observation that an inborn error of metabolism resulting in mevalonate kinase deficiency causes myopathy (Buettner and Lecker, 2008). More specifically, statin-induced mevalonate deficiency is believed to cause depletion of isoprenoids and in vitro studies have demonstrated that statin-induced myotoxicity is ameliorated by supplementation with the isoprenoid geranylgeranyl (Cao et al., 2009; Flint et al., 1997a; Johnson et al., 2004; Sakamoto et al., 2007, 2011; Tanaka et al., 2010). In vitro studies conducted with a variety of cell types, including muscle, indicate that inhibition of protein isoprenylation with either selective inhibitors or depletion of

isoprenoids leads to an accumulation of unprocessed intracellular proteins and apoptosis (Flint et al., 1997a; Johnson et al., 2004; Matzno et al., 2005; Nakagawa et al., 1998; Ostrowski et al., 2007; Repko and Maltese., 1989; Sakamoto et al., 2007; Xu et al., 2005).

Despite some compelling evidence from cultured myotubes, the link between isoprenoid depletion and statin-induced apoptosis has not been empirically demonstrated in vivo. Furthermore, in both clinical and preclinical studies, statins induce vacuoles and degenerated organelles followed by necrosis (Bergman et al., 2003; Chucrallah et al., 1992; Waclawik et al., 1993; Westwood et al., 2005). Accordingly, there is a discrepancy between the in vitro (apoptosis) and in vivo (necrosis) pathophysiology. To reconcile these differences, Sakamoto et al (2007) conducted experiments with isolated rat skeletal fast-twitch myofibers. In these terminally differentiated muscle cells, statins caused a time- and concentration-dependent toxicity which was prevented with the co-application of geranylgeranylpyrophosphate (GGPP). The ultrastructural changes with statins were similar to those described for clinical and preclinical studies, with vacuole formation lining the sarcolemma and in the perinuclear region and swelling of organelles (Sakamoto et al., 2007). These results suggest that primary myofibers may be the most appropriate in vitro model for investigating statin myotoxicity.

Given that Rabs play an important role in intracellular membrane transport and are prenylated by GGPP, Sakamoto et al (2007) hypothesized that Rab GTPase inhibition may cause statin-induced vacuolation similar to the in vivo findings (Grosshans et al.,

2006; Leung et al., 2006). To test this hypothesis, primary rat skeletal fast-twitch myofibers were treated with the Rab geranylgernayl transferase inhibitor perillyl alcohol. Treatment related myofiber vacuolation developed similar to the in vivo findings, suggesting that inactivation of Rab GTPases resulting from isoprenoid depletion may be involved with statin-induced vacuolation and toxicity. More recently, Sakamoto et al., (2011) demonstrated that suppression of Rab1 GTPase function and subsequent inhibition of ER-to-Golgi traffic are involved in statin-induced myotoxicity. While the exact relationship between geranylgeranyl depletion and myopathy has yet to be established the isoprenoids are important in GTPase function and intracellular vesicular transport therefore these processes represent potential targets.

Geranylgeranylation is also required for ubiquinone synthesis and its reduction following statin treatment led to the ubiquinone depletion hypothesis of myopathy proposed in the 1990s (Folkers et al., 1990; Willis et al., 1990). While statins decrease serum ubiquinone, muscle levels are unchanged and mitochondrial respiration is unaffected both in vitro and in vivo (Hargreaves et al., 2005; Johnson et al., 2004; Laaksonen et al., 1995; Marcoff et al., 2007; Nakahara et al., 1998: Phillips et al., 2010; Schaefer et al., 2004; Yamazaki et al., 2006). Moreover, ubiquinone supplementation has no effect on the risk of statin-induced myopathy, thereby casting doubt on the role of ubiquinone in mediating statin-induced myopathy (Levy and Kohlhaas, 2006). Additional geranylgeranylated products are important for skeletal muscle function and inhibition of any of these modifications by statins could underlie the mechanism of myotoxicity. Specifically, N-linked glycosylated proteins, like α-dystroglycan play a central role in the dystrophin-glycoprotein complex

which requires polyprenylated dolichol for its modification (Buettner and Lecker, 2008). Despite these theoretical mechanisms of toxicity, no studies have been performed which directly determine the involvement of these modifications in statin myopathy.

Cholesterol modulates membrane fluidity and changes in the ratio of cholesterol and phospholipids can significantly alter membrane properties, including ionic channels like sodium, potassium, chloride and membrane excitability (Sirvent et al., 2008). The mechanism of statin-induced myopathy was initially thought to involve depletion of cholesterol in skeletal muscle membranes (London et al., 1991). However, in vitro studies conducted with myoblasts from various species indicate that myotoxicity is likely unrelated to decreased cholesterol synthesis because neither squalane synthase nor squalane epoxidase inhibitors induce myotoxicity and statin-induced toxicity is unaffected by squalane supplementation (Flint et al., 1997b; Johnson et al., 2004; Nishimoto et al., 2003). Furthermore, while cholesterol synthesis is reduced, the actual levels of cholesterol are not decreased in skeletal muscle following statin therapy, thereby casting doubt on this mechanism (Draeger et al., 2006; Masters et al., 1995; Morikawa et al., 2005; Phillips et al., 2010; Trapani et al., 2011). However, this does not preclude differences in cholesterol content in some subcellular organelles, like the T-tubules that might be especially vulnerable to cholesterol depletion (Draeger et al., 2006). In contrast to statin-induced reduction in cholesterol, several in vivo studies have demonstrated that statin treatment actually increases the LDL-C receptor, cholesterol, plant sterols and lipid vacuoles in skeletal muscle and these changes precede myopathy (Paiva et al., 2005; Phillips et al., 2002; Phillips et al., 2010; Sakamoto et al., 2007; Trapani et al., 2011;

Waclawik et al., 1993; Westwood et al., 1993; Yokoyama et al., 2007). Skeletal muscle from statin treated patients with myalgia and normal CK have been described histologically as containing extensive lipid-filled vacuoles within the myofibers (Phillips et al., 2002). Similar vacuoles accumulate between myofibrils in statin treated rats and mice and this effect precedes myopathy (Sakamoto et al., 2007; Waclawik et al., 1993; Westwood et al., 2005; Yokoyama et al, 2007). It is unclear whether these changes are causally related to myopathy or simply a reflection of the hyperabsorption of sterols associated with statin use. The accumulation and abnormal localization of free cholesterol adversely effects cellular functions and can lead to cell death (Cui et al., 2002; Ikonon, 2006, 2008; Ridgway et al., 1999; Warner et al., 1995). More specifically, fiber-specific perturbations in lipid and sterol metabolism have been demonstrated as part of the pathophysiology of muscle related disorders (Bruno and DiMauro, 2008; Hegarty et al., 2003; Jaworska-Wilczynska et al., 2002; Sher et al., 2006; Sprott et al., 2000).

Mitochondrial toxicity has been suggested as a mechanism of statin-induced myotoxicity. In patients treated with statins, the lactate/pyruvate ratio is increased suggesting impaired mitochondrial function (De Pinieux et al., 1996). Furthermore, a reduction in mitochondria, respiration, ATP and impaired mitochondrial function has been reported with statin treatment (Hubal et al., 2011; Kaufmann et al., 2006; Nishimoto et al., 2003; Phillips and Haas, 2008; Sirvent et al., 2008). Additionally, many patients with statin myopathy show an increase in urinary 3-methyglutaconic acid which is associated with mitochondrial disorders deficient in oxidative metabolism (Phillips and Haas, 2008).

However, whether these changes are initiating events or simply a biomarker of effects remains unknown.

Several lines of evidence indicate mitochondrial deficiency may result from changes in impaired muscle energetics with statin treatment (Phillips and Haas, 2008). Recently, it was demonstrated that creatine supplementation prevents statin-myopathy in patients (Shewmon and Craig, 2010). Creatine is a kinetically limiting acceptor that controls mitochondrial respiration. Therefore, decreased intramuscular creatine could be involved with statin-induced mitochondrial deficiency. While muscle creatine levels have not been evaluated, urinary levels are markedly increased with statin treatment which is consistent with the notion that intramuscular creatine may be reduced (Aranibar et al., 2011). While the exact target of altered energy metabolism with statins is unknown these drugs have been shown to reduce fatty acid oxidation in skeletal muscle, and muscle biopsies often have deficiencies in carnitine palmityl transferase, respiratory chain enzymes or carnitine which would impair fatty acid oxidation (Fisher et al., 2007; Phillips and Haas, 2008; Phillips et al., 2009). Impaired carbohydrate oxidation is also associated with statin myopathy (Mallinson et al., 2009; Motojima and Seto, 2003; Phillips and Haas, 2008). Specifically, muscle glycogen content increases with statin treatment indicating glycogen oxidation is suppressed (Mallinson et al., 2009). Moreover, statin treatment causes an increase in skeletal muscle pyruvate dehydrogenase kinase 2 and 4 which indicates suppression of glycolysis and shunting of energy metabolism from glucose to an alternative source (Mallinson et al., 2009; Motojima and Seto, 2003). Consistent with an impairment in glycolysis and fatty acid oxidation, statin therapy upregulates the muscle

atrophy program including atrogin-1, MuRF1 and autophagy, with an increase in protein degradation and reduction in protein synthesis (Araki and Motojima, 2008; Aranibar et al., 2011; Hanai et al., 2007; Mallinson et al., 2009; Tuckow et al., 2011; Urso et al., 2005; Vassallo et al., 2011). While transcriptional induction of the muscle atrophy program is dependent on geranylgeranyl depletion it is unknown whether this is a direct effect or an epiphenomenon reflecting impaired substrate (glucose and fatty acid) oxidation similar to fasting (Cao et al., 2009; Jagoe et al., 2002; Phillips and Haas, 2008).

In addition to an adaptive response involving muscle atrophy, statin treatment leads to fiber switching from a fast- to a slow-twitch phenotype (Hanai et al., 2007; Trapani et al., 2011). PPARγ coactivator 1α (PGC-1α) functions as a metabolic sensor initiating an adaptive response characterized by mitochondrial biogenesis and transformation of fast-twitch muscle into a more oxidative phenotype (Lin et al., 2002). PGC-1α is transcriptionally induced with statin treatment, and overexpression in rodents protects against statin myopathy (Hanai et al., 2007; Vassallo et al., 2011). Consistent with this transformation, skeletal muscle from statin treated rats demonstrates a shift in myosin heavy chain isoform expression toward a slower phenotype (Trapani et al., 2011). Collectively, these investigative studies demonstrate that fast-twitch muscles are uniquely sensitive to statin-induced myopathy, and this effect may be related to fiber differences in mitochondrial content and energetics (Phillips and Haas, 2008). However, it is important to note that muscle toxicity, secondary to lipid-lowering, is not exclusive to statins. Rhabdomyolysis has been described with fibrates, niacin and ezetimibe and patients sensitive with one lipid lowering agent show myotoxicity with the other agents (Phillips

and Haas, 2008). Therefore, the most plausible mechanism to explain why such diverse therapies cause a similar myotoxicity is that lipid lowering is toxic to muscle energetics in some patients (Phillips and Haas, 2008).

Statin-induced calcium dysregulation has also been proposed as a potential mechanism of myopathy (Dirks and Jones, 2006; Sirvent et al., 2008). In L6 myoblasts and primary human skeletal muscle cells, statins cause an increase in cytosolic calcium and apoptosis (Sacher et al., 2005). Altered calcium homeostasis has also been observed in rat muscle following statin treatment (Liantonio et al., 2007). It is believed that an alteration in isoprenoid synthesis is responsible for a cytosolic increase in calcium levels which activates calpains and mitochondrial-mediated apoptosis however this has never been empirically demonstrated (Dirks et al., 2006; Sirvent et al., 2008).

Bioactive vitamin D or calcitriol is a steroid hormone that plays an important role in regulating body levels of calcium and phosphorus (Gupta and Thompson, 2011). In skeletal muscle, vitamin D regulates several processes, including calcium uptake which controls contraction and relaxation and phosphate uptake which regulates energy metabolism and causes a mitogenic effect in proliferating myoblasts (Gupta and Thompson, 2011). While the human body can synthesize vitamin D in the skin from sun exposure, it is still considered a vitamin since many people do not synthesize sufficient vitamin D and thus requires an exogenous source (Gupta and Thompson, 2011). Cholesterol is synthesized to 7-dehydrocholesterol (7-DHC) endogenously which is then converted to vitamin D3 in the skin by ultraviolet B light. Dietary sources are in the form

of vitamin D2 from plants and vitamin D3 from animals and these two forms are considered equivalent and interchangeable (Gupta and Thompson, 2011). Vitamin D2 and D3 are converted to the major circulating forms by CYP3A4 hepatic 25-hydroxylase activity (Gupta and Thompson, 2011).

Vitamin D deficiency causes myopathy in fast-twitch muscles and supplementation ameliorates these effects (Ceglia, 2008; Gupta and Thompson, 2011). Several clinical studies have linked vitamin D deficiency with statin myopathy and a resolution of this effect with supplementation (Ahmed et al., 2009; Duell and Connor, 2008; Glueck et al., 2011; Gupta and Thompson, 2011). While these studies indicate vitamin D deficiency potentiates statin-induced myalgia in a subset of patients, a causal association has not been demonstrated. Several mechanisms have been proposed regarding the role of vitamin D deficiency as causal in statin myopathy (Gupta and Thompson, 2011). Specifically, a deficiency may reduce vitamin D receptors resulting in altered calcium and phosphate regulation in skeletal muscle. Additionally, CYP3A4 metabolizes vitamin D as well as statins (Gupta et al., 2004). Therefore, vitamin D deficiency may shunt CYP3A4 25-hydroxylase activity to increase circulating vitamin D levels thereby reducing metabolism of statins causing higher exposure levels (Gupta and Thompson, 2011).

1.10. Predisposing factors of statin-induced myopathy

While the mechanism of statin-induced myopathy remains unknown, a variety of endogenous and exogenous factors have been identified which predispose patients to this

adverse effect (Table 1.3) (Buettner and Lecker, 2008; Fernandez et al., 2011; Phillips and Haas, 2008). Patients with a variety of disorders affecting energy metabolism including muscle myophosphorylase deficiency, carnitine palmityl transferase deficiency and myoadenylate deaminase deficiency are prone to rhabdomyolysis which occurs when the energy metabolism demands of the muscle exceed flux through the compromised metabolic pathway (Phillips and Haas, 2008).

The risk of myopathy also increases with drug concentration and a variety of physicochemical and pharmacokinetic factors are known to contribute to the systemic exposure level of statins (Table 1.3) (Fernandez et al., 2011; Rosenson, 2004). In general, the pharmacokinetics of statins are associated with their physicochemical properties (Table 1.4). HMG-CoA reductase inhibitors are administered as either a prodrug, with a lactone ring or as the biologically active open acid hydrophilic form (Shitara and Sugiyama, 2006). The intestinal absorption and hepatic uptake of lipophilic and hydrophilic statins are predominately mediated by passive diffusion and transporters, respectively (Shitara and Sugyama, 2006). While lipophilicity enables efficient hepatic uptake, this property also allows the drug to permeate the plasma membrane, and this effect is considered an important determinant of skeletal muscle injury (Shitara and Sugyama, 2006). However, since the distribution of a lipophilic statin is 500-times greater in the liver compared to skeletal muscle it is likely that other factors contribute to myotoxicity (Seachrist et al., 2005; Sidaway et al., 2009; Steinke et al., 1996). The hydrophilic statins are unable to passively diffuse into the liver or skeletal muscle. However, a variety of organic anion-transporting polypeptides (OATP) mediate statin

uptake in the liver and skeletal muscle, and OATP1B1 polymorphisms have been identified which are strongly associated with an increased risk of statin-induced myopathy (Kivisto et al., 2007; Sakamoto et al., 2008; Shitara and Sugiyama, 2006; The SEARCH Collaborative Group, 2008).

The metabolism of statins occurs by the cytochrome P450 (CYP) isozymes 3A and 2C (Table 1.4; Shitara and Sugyama, 2006). As such, co-administered drugs which are metabolized by these enzymes may serve as competing substrates for statins, thereby increasing the systemic exposure, and risk of myopathy (Shitara and Sugiyama, 2006). Approximately 60% of lipophilic statin-induced rhabdomyolysis cases are related to interaction with drugs known to inhibit CYP3A4 which increase the systemic exposure of the statin (Table 1.4; Law et al., 2006). Many of the hydroxyl acid forms of statins are glucuronidated and agents which inhibit glucuronidation may also increase the concentration of these drugs and the potential risk of myopathy (Rosenson, 2004). Additionally, since the acid and lactone structures interconvert, the extrahepatic cellular processes affecting the equilibrium of these two forms may be an important determinant in mediating skeletal muscle injury (Blankenberg Skottheim et al., 2008).

In general, statins are rapidly eliminated (Table 1.4; half-life of 2-3 hours) with fecal and urinary excretion representing the major and minor excretion routes, respectively (Bischoff et al., 1998; Shitara and Sugiyama, 2006). As such, disorders affecting renal function or biliary excretion can increase the circulating concentration of these drugs and the potential for myopathy (Rosenson, 2004; Smith et al., 1991). Several efflux

transporters have been shown to transport statins and their expression is modulated during therapy with these drugs (Shitara and Sugiyama, 2006; Wong et al., 2008*)*. Furthermore, nutritional status has also been shown to influence the adverse effects of statins by increasing systemic exposure through modification of transporters involved with hepatic uptake and elimination (Sugatani et al., 2010).

Cerivastatin is often used as a model compound for investigating the mechanism of statin-induced myopathy because it showed the highest incidence of rhabdomyolysis compared to other drugs in this class (Table 1.5; Cziraky et al., 2006). As discussed above, several factors are important in contributing to statin-induced myopathy and co-administration of cerivastatin with the fibrate gemfibrozil highlights the importance of systemic exposure (Kaspera et al., 2010; Noe et al., 2007). Cerivastatin is unique from the other statins in that it is primarily metabolized by CYP2C8 instead of CYP3A4 (Table 1.4). Furthermore, cerivastatin is glucuronidated by UDP-glucuronosyl transferase (Kaspera et al., 2010). Gemfibrozil inhibits CYP2C8 and UGT-mediated glucuronidation, and its glucuronide (gemfibrozil glucuronide) is a mechanism based inhibitor of CYP2C8 (Kaspera et al., 2010). Moreover, liver uptake of statins occurs by OATP1B1 which is inhibited by gemfibrozil (Noe et al., 2007). Accordingly, these factors are considered partially responsible for the increased systemic exposure and incidence of rhabdomyolysis associated with co-administration of cerivastatin and gemfibrozil (Kaspera et al., 2010; Noe et al., 2007).

Although the mechanism of statin-induced myopathy remains to be determined, there is substantial evidence indicating this is an on-target effect in which fast-twitch muscles are most sensitive. However, the fact that most patients do not experience skeletal muscle toxicity with statin therapy suggests HMG-CoA reductase inhibition is necessary but not sufficient for the development of toxicity. Accordingly, predisposing factors, like being female, increasing age and underlying metabolic muscle disorders affecting energy metabolism have been identified. Together, these risk factors indicate that statin-induced myopathy may be mediated in part by alterations in skeletal muscle energy metabolism, which is regulated in a fiber-, sex- and age-dependent manner. Collectively, these data demonstrate a variety of factors can increase the risk of developing statin-induced myopathy, with increased systemic exposure representing one of the most important. However, cerivastatin is an unusual statin because it had the highest incidence of rhabdomyolysis which eventually led to its removal from the market (Table 1.5; Cziraky et al., 2006).

1.11. Experimental models used for investigating mechanisms of myopathy

The rat is an ideal model for investigating mechanisms of statin myopathy because the dosing paradigm and time course for the development of injury are well defined, reproducible and considered predictive of the human response (Schaefer et al., 2004; Seachrist et al., 2005; Westwood et al., 2005). In the rat, simvastatin and cerivastatin, representative hydrophilic and lipophilic statins, cause a dose-dependent myopathy after 10 days of dosing in fast-twitch muscle fibers whereas slow-twitch fibers are unaffected (Figure 1.17) (Schaefer et al., 2004; Seachrist et al., 2005; Westwood et al., 2005). The

rat is also considered an ideal model for studying mechanisms of fiber specific toxicity because individual skeletal muscles are homogenous, with the psoas consisting of 91% fast-twitch fibers and the soleus consisting of 84% slow-twitch fibers (Hamalainen et al., 1993; Koerker et al., 1990). While it is believed that statins also preferentially target fast-twitch muscles in humans the individual muscles are more heterogeneous in fiber composition than the rat (Zierath et al., 2004). Similar to humans, sex specific muscle injury is also observed in the rat, with females showing a greater incidence than males (Vassallo et al., 2009). Fiber- and sex-dependent myotoxicity in the rat is unrelated to differences in exposure or accumulation of statin in the muscle (Seachrist et al., 2005; Sidaway et al., 2009; Reinoso et al., 2002; Steinke et al., 1996). Therefore, the mechanism is likely dependent on biochemical and physiological properties of the female fast-twitch muscle and statin pharmacology as mevalonate supplementation prevents myopathy (Westwood et al., 2005).

In general the rat is a useful model for studying mechanisms of statin-induced myopathy. However statins do not cause a hypocholesterolemic effect in this species (Fujioka et al., 1995). Instead, with repeated dosing, hepatic HMG-CoA reductase is markedly induced and this compensatory effect results in increased serum cholesterol (Fujioka et al., 1995). Similarly, in the rat skeletal muscle, statin-induced myopathy causes a transcriptional induction of HMG-CoA reductase however this is not associated with increased enzyme activity since the IC_{50} (1-2 nM) is significantly less compared to the concentration (30 nM) of cerivastatin (0.5 mg/kg) in the rat gastrocnemius (fast-twitch muscle) (Mullen et

al., 2010; Schaefer et al., 2004; Seachrist et al., 2005; Sidaway et al., 2009; Trapani et al., 2011; Westwood et al., 2005).

Several in vitro models, including rat derived L6, mouse derived C2C12 and human derived HSkMC skeletal muscle cells have also been used for studying mechanisms of statin-induced myopathy (Allen et al., 2005; Flint et al., 1997a, 1997b; Johnson et al., 2004; Masters et al., 1995; Mullen et al., 2010; Nishimoto et al., 2003; Sacher et al., 2005; Yamazaki et al., 2006). These cells are undifferentiated myoblasts which retain the ability in vitro to divide and differentiate into more specialized multinucleated myotubes expressing myofibrillar proteins representing a mixed fast- and slow-twitch phenotype (Allen et al., 2005; Ravenscroft et al., 2007). Conversion of myoblasts to myotubes (myogenesis) in vitro parallels the process observed in vivo following skeletal muscle damage in which the normally quiescent satellite cells begin proliferating, differentiating and fusing into multinucleated myotubes which replace the damaged muscle. While conversion of myoblast to myotubes is similar to the in vivo condition these cells never become fully differentiated myofibers. Therefore, while these in vitro models may be useful for studying mechanisms of toxicity it may be difficult to extrapolate mechanistic findings in vivo.

A more relevant in vitro model has also been used in which fast- and slow-twitch muscles have been isolated from adult mice and rats and used for studying aspects of basic muscle physiology and pathophysiology of diseases (Bekoff and Betz 1977; Ravenscroft et al., 2007; Sakamoto et al., 2008; Shefer and Yablonka-Reuveni, 2005). These post-mitotic

differentiated multinucleated myofibers maintain phenotypic characteristics of mature fast-twitch skeletal muscle cells for up to 10 days in culture (Ravenscroft et al., 2007). In contrast, other undifferentiated cell lines like the C2C12 myotubes are comprised predominately of proteins representing fetal isoforms (Ravenscroft et al., 2007). Recent efforts by Sakamoto et al (2008) have demonstrated the value in using this approach for investigating statin myopathy. Specifically, Sakamoto et al (2008) demonstrated that differentiated myofibers have functional Oatp1a4 and 2b1 transporters whereas these proteins are deficient in L6 myoblast. The LC50 value of fluvastatin myotoxicity in myofibers was 0.3 µM whereas it was 8.3 µM in L6 myoblast, an effect directly related to transporter expression in this differentiated phenotype (Sakamoto et al., 2008).

1.12. Assessment of drug-induced myopathy

Since drug-induced rhabdomyolysis is a life threatening condition it is important to have biomarkers which can rapidly and accurately assess myopathy. Clinically, the diagnosis of drug-induced skeletal muscle injury is challenging because direct methods are invasive (biopsy) or difficult to interpret (e.g. magnetic resonance imaging), and indirect methods such as muscle soreness are subjective and commonly observed clinically with aging. Historically, several serological biomarkers including creatine kinase (CK) and aspartate aminotransferase (AST) have been used routinely to assess clinical and preclinical skeletal muscle injury (Bohlmeyer et al., 1994; Sorichter et al., 1999). However, these biomarkers have poor sensitivity, lack skeletal muscle specificity and are of limited diagnostic value (Bohlmyer et al., 1994; Sorichter et al., 1999; Vassallo et al., 2009). The ongoing need for reliable biomarkers of drug-induced skeletal muscle injury is

highlighted by the Critical Path Initiative's effort to identify new biomarkers which are skeletal muscle specific, sensitive to minimal injury and reflect reversibility during recovery from toxicity (Goodsaid et al., 2008). Ideal biomarkers should also be easily measurable, have a large dynamic range, long half-life and be translated to the clinic. Based on investigational studies, several potential skeletal muscle specific proteins including skeletal muscle troponin I (sTnI), myosin light chain 3 (Myl3), fatty acid binding protein 3 (FABP3), parvalbumin (Parva) and myoglobin (MB) meet these criteria and are currently under evaluation by the Critical Path Initiative (Table 1.5) (Arif, 2009; Berchtold et al., 1984; Berna et al., 2007; Bohlmeyer et al., 1994; Celio and Heizmann, 1982; Dare et al., 2002; Lee and Vasan, 2005; Pritt et al., 2008; Schmitt and Pette, 1991; Simpson et al., 2005; Singh et al., 2005; Vanholder et al., 2000; Vassallo et al., 2009; Wilkinson and Grand, 1978). While these new biomarkers may enhance detection of drug-induced myotoxicity, there remains an ongoing interest to identify additional biomarkers which are more sensitive and specific than CK and AST. The life-threatening potential of statin-induced rhabdomyolysis provides an excellent example of where more sensitive and specific biomarkers would fulfill an unmet clinical need.

1.13. Tools used for investigating mechanisms and biomarkers of myopathy

Recent advances in investigative toxicology enable assessment of transcriptional and metabolic differences in fast- and slow-twitch muscles which may be important in the mechanism of statin-induced myopathy (Collings and Vaidya, 2008; Robertson et al., 2011; Gatzidou et al., 2007; Xu et al., 2011). Transcriptomics is the quantitative evaluation of mRNA expression using microarrays which provides a genome-wide

perspective on the transcriptional effects associated with pathophysiological changes (Gatzidou et al., 2007). Metabolomics is a systems approach for studying in vivo metabolic profiles representing the total metabolite pool in biofluids or tissue extracts (Nicholson et al., 2002). This approach combines analytical technologies like nuclear magnetic resonance spectrometry (NMR) with statistics to provide a quantitative assessment of the metabolic response to pathophysiological changes (Gatzidou et al., 2007; Nicholson et al., 2002). Together, these technologies provide an unbiased, comprehensive and ideally synergistic assessment of cellular perturbations in biochemical pathways which may be causally associated with a potential mechanism of toxicity. Furthermore, these tools have been useful in identifying new biomarkers of toxicity (Collings and Vaidya, 2008).

1.14. Research objectives

The major objective of this dissertation was to identify molecular and biochemical targets which are causally associated with the mechanism of cerivastatin-induced myopathy in the rat. To determine transcriptional and metabolite changes, global gene expression analysis and metabolomic profiling, respectively were conducted on skeletal muscles from rats in a cerivastatin dose response. Furthermore, gene expression analysis and metabolomic profiling were also conducted on naïve rats to define the fiber- and sex-specific differences in skeletal muscles which may contribute to myopathy. Integration of these results led to the identification of a variety of changes, some of which were associated with the pathology, whereas others appeared causally related to the mechanism of toxicity. Therefore, based on these findings, specific hypotheses regarding modes of

toxicity were developed and investigated in a time course of cerivastatin-induced myopathy. Furthermore, a method for isolating and culturing primary rat fast-twitch differentiated myofibers was developed and used to further probe specific pathways causally related to the mechanism of cerivastatin-induced myopathy. An additional objective of this work was to identify biomarkers of drug-induced myopathy. To identify potential biomarkers, metabolomic profiling was conducted on urine collected from rats in the cerivastatin dose response study. These results led to the identification of two new potential biomarkers of drug-induced myopathy. To further determine the utility of these potential biomarkers in urine and serum investigative studies were conducted. Specific hypotheses for this research are described below.

Hypothesis 1: Cerivastatin-induced myopathy in rats occurs in a fiber- and sex-dependent manner which is recapitulated in isolated rat fast-twitch differentiated myofibers (Chapter 2).

Hypothesis 2: Transcriptional profiles of skeletal muscles from rats are useful for identifying molecular targets causally related to the mechanism of cerivastatin-induced myotoxicity (Chapter 3).

Hypothesis 3: Metabolomic profiles of skeletal muscles from rats are useful for identifying metabolic changes causally related to the mechanism of cerivastatin-induced myotoxicity (Chapter 4).

Hypothesis 4: Cerivastatin-induced myopathy is causally related to alterations in cholesterol homeostasis (Chapter 5).

Hypothesis 5: Cerivastatin-induced myopathy is causally related to alterations in energy metabolism (Chapter 6).

Hypothesis 6: Metabolomic profiling of urine is useful for identifying biomarkers of cerivastatin-induced myopathy (Chapter 7).

Hypothesis 7: 3-Methylhistidine is a preclinical biomarker of drug-induced myopathy (Chapter 8).

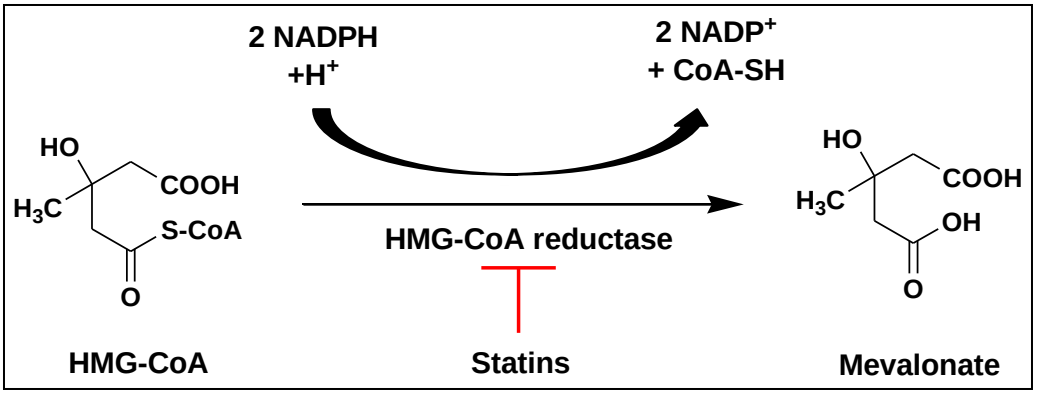

Figure 1.1. HMG-CoA reductase inhibition by statins (Voet and Voet, 2005). HMG-CoA reductase is the rate limiting step in cholesterol biosynthesis. The HMG-like moiety of statins occupies the HMG-binding pocket in the active site of the enzyme which competitively inhibits enzyme activity.

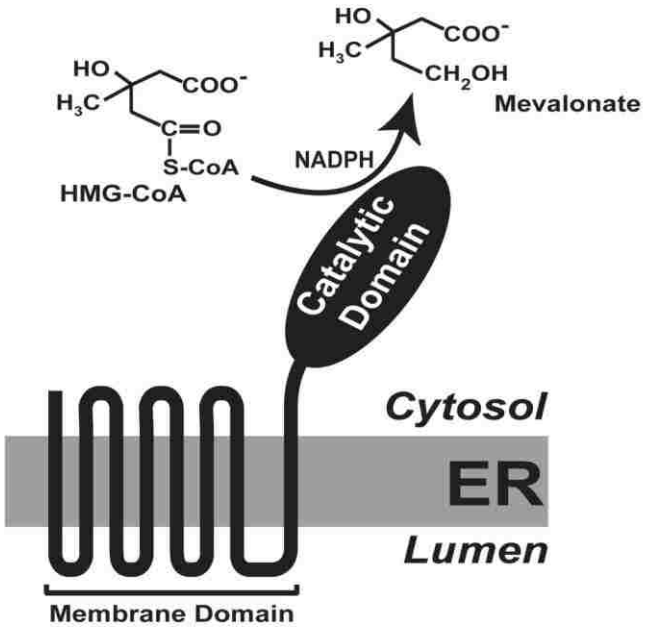

Figure 1.2. Domain structure of HMG-CoA reductase (DeBose-Boyd, 2008). HMG-CoA reductase is composed of two distinct domains represented by an N-terminal hydrophobic membrane domain containing eight membrane spanning segments anchoring the protein to the endoplasmic reticulum and a C-terminal hydrophilic catalytic domain projecting into the cytosol.

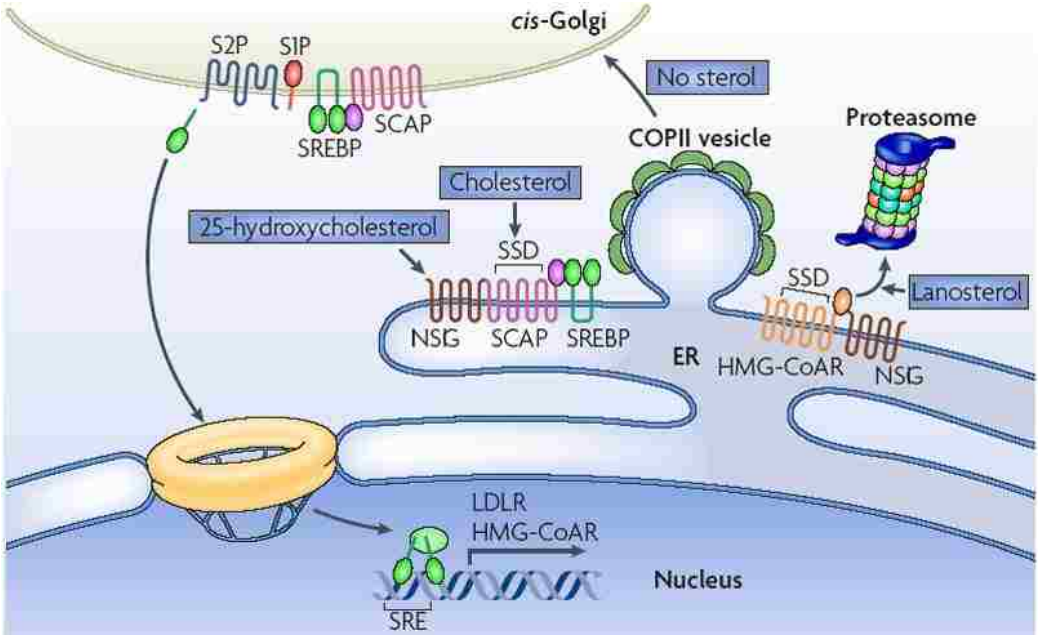

Figure 1.3. Regulation of cholesterol metabolism (Ikonen, 2008). Intracellular accumulation of cholesterol leads to retention of the INSIG protein in the endoplasmic reticulum (ER) thereby preventing SREBP-SCAP transport to the Golgi by COPII-coated vesicles. In contrast, cholesterol deficiency results in transport of SREBP to the Golgi where it is cleaved by two proteases (S1P and S2P) and the transcription factor is transported to the nucleus where it binds the sterol-regulatory element (SRE) and induces sterol-regulated genes (e.g. HMG-CoA reductase and LDL-C receptor). HMG-CoA reductase is also post-transcriptionally regulated by sterols like lanosterol and 25-hydroxycholesterol which causes proteasome degradation or ER retention, respectively.

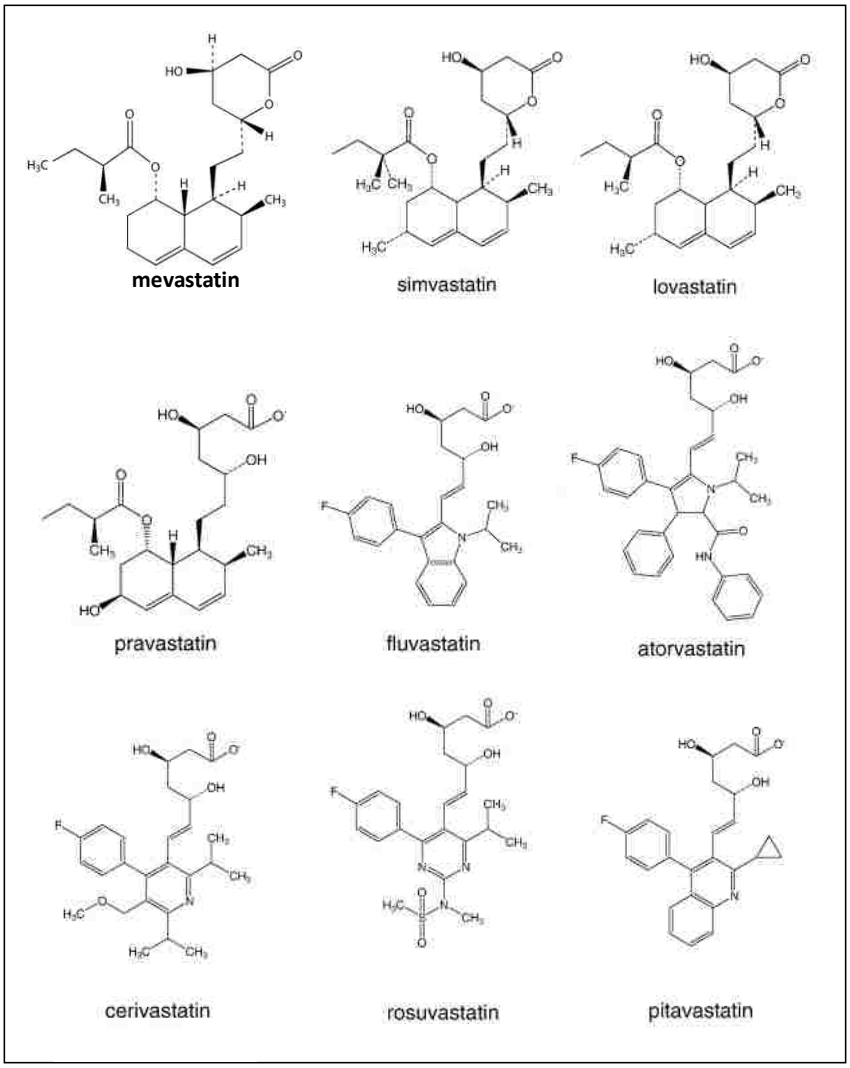

Figure 1.4. Chemical structures of statins (Alegret and Silvestre, 2006; Shitara and Sugiyama, 2006; Sirtori, 1993). The HMG-CoA like moiety is common among all statins. However, both simvastatin and lovastatin are prodrugs as they contain an inactive close ring lactone whereas the other statins are administered as the active acid form. Structural differences in the statins contribute to their unique physicochemical and pharmacokinetic properties.

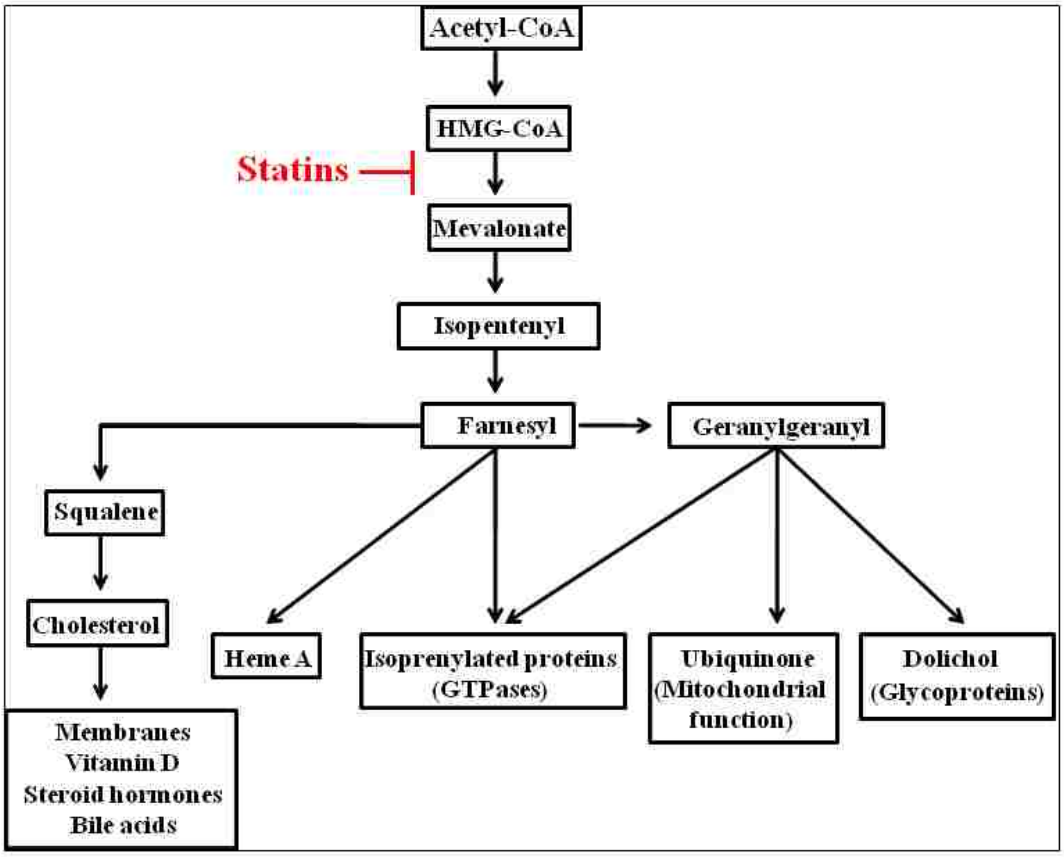

Figure 1.5. Products of the mevalonate pathway. Mevalonate is the precursor for numerous biologically relevant intermediates and statin-induced myopathy as well as the pleiotropic effects of these drugs have been associated with both farnesyl and geranylgeranyl depletion.

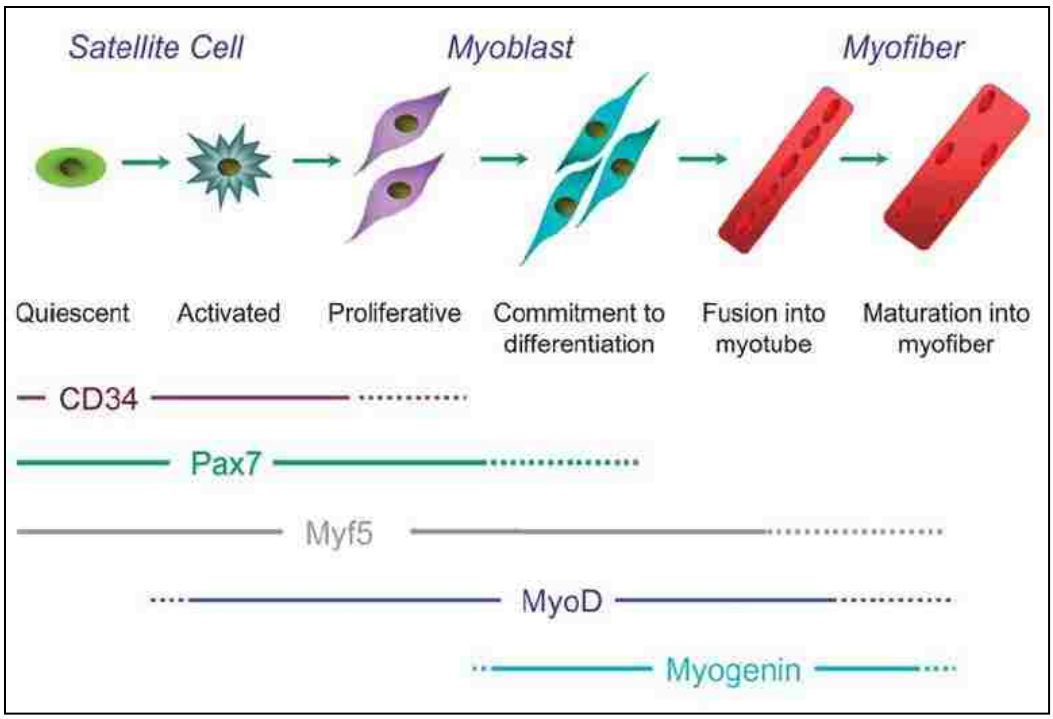

Figure 1.6. Satellite cell myogenesis following skeletal muscle damage (Zammit et al., 2006). Following skeletal muscle damage myogenic satellite cells initiate a genetic program to proliferate and differentiate into myotubes which repair the tissue by fusing with existing multinucleated myofibers.

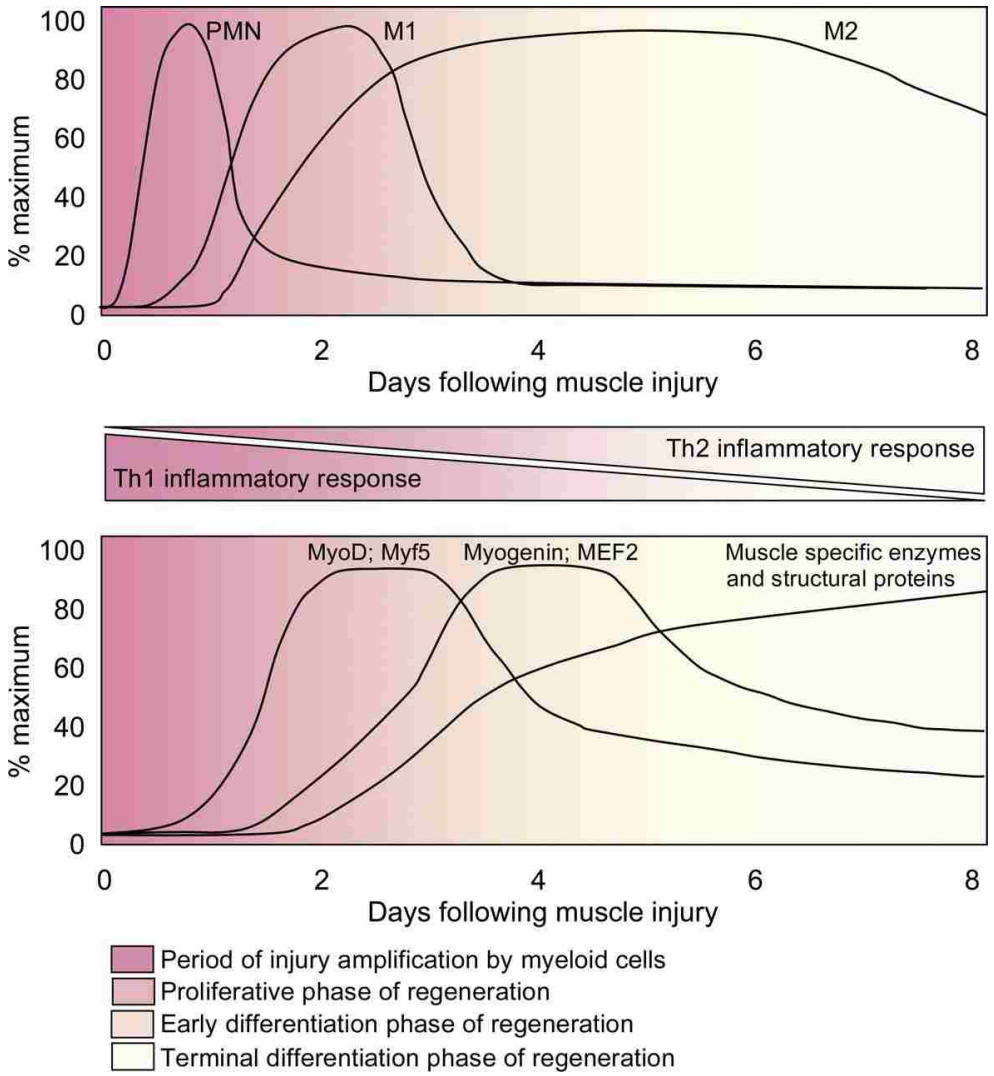

Figure 1.7. Time course of changes in myeloid cell population (top) and expression of transcription factors involved with skeletal muscle regeneration (bottom; Tidball and Villalta, 2010). Following acute skeletal muscle injury, polymorphonuclear neutrophils (PMN) are recruited and then decline rapidly followed by invasion of M1 phagocytic macrophages (Th1 response) and a gradual increase in nonphagocytic macrophages (Th2 response). Coincident with the invasion of myeloid cells, regeneration of skeletal muscle is initiated and dependent on the inflammatory response.

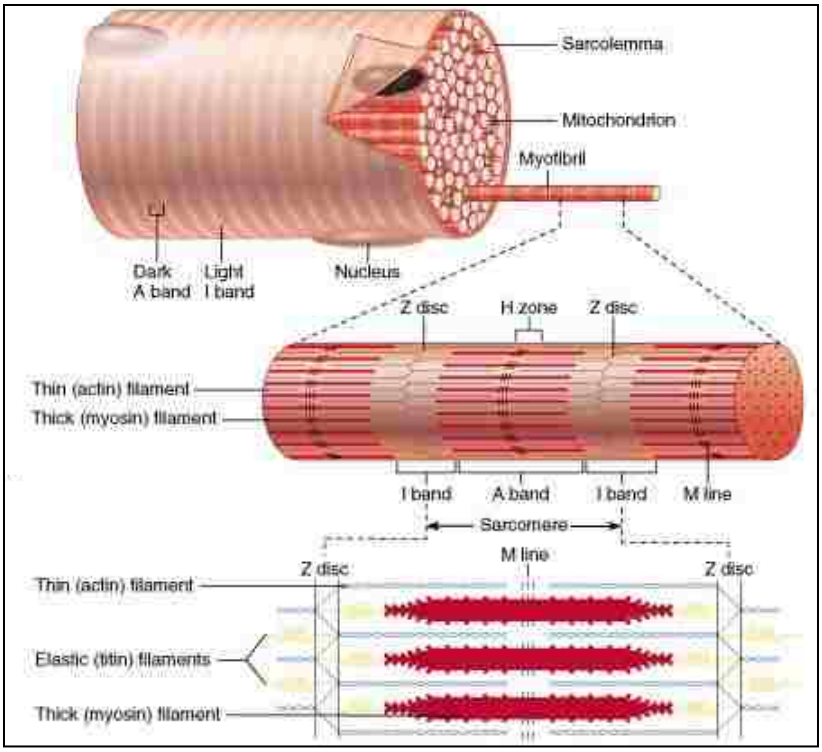

Figure 1.8. Skeletal muscle sarcomere (Marieb, 2000). The sarcomere is the functional unit of skeletal muscle which is responsible for transduction of chemical energy into mechanical work during muscle contraction. The sarcomere is composed of thick (myosin) and thin (actin) myofibrils held together by titin which provides a framework holding the contractile machinery in place. Calcium-mediated contraction is regulated by the concentration of calcium and dependent on troponin which is a loosely bound complex of three protein subunits (I, T and C) attached to tropomyosin in the thin filament. In a relaxed state, contraction is prevented because troponin T and I are bound to tropomyosin which blocks the attachments site for the myosin crossbridge. When the muscle is stimulated to contract by an action potential, the sarcoplasmic reticulum releases calcium which attaches to troponin C, causing a conformation change and exposing the site for myosin on the actin filament. When ATP is hydrolyzed, the actin filament bridges with and slides along myosin, contracting the sarcomere.

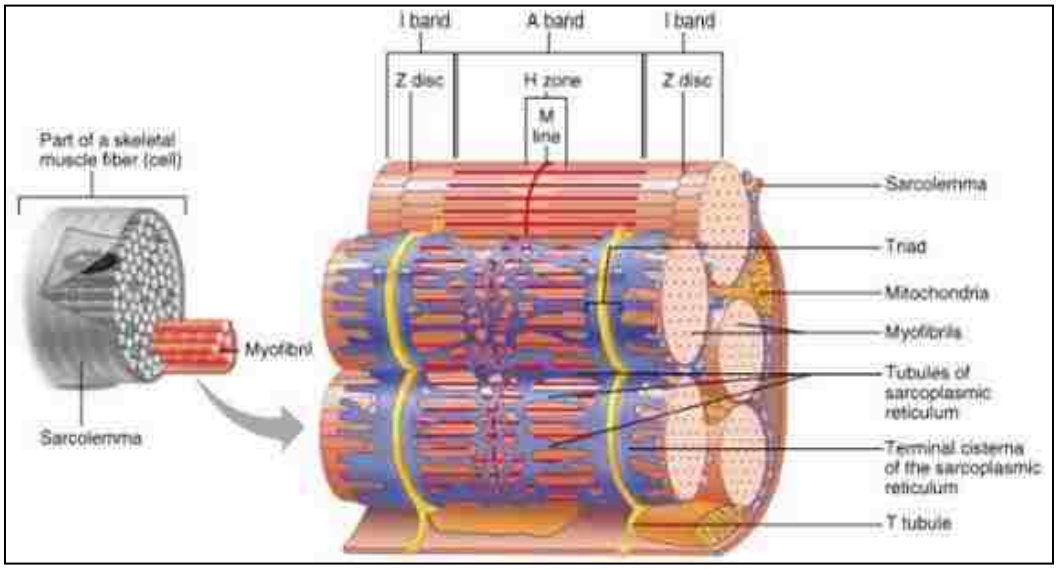

Figure 1.9. Organization of a skeletal muscle cell (Marieb, 2000). A skeletal muscle cell is surrounded by a plasma membrane (sarcolemma) and the cytoplasm (sarcoplasm) fills the space between the densely pack myofibrils. The mitochondria lie parallel to the myofibrils and provide ATP necessary for muscle contraction. The endoplasmic reticulum (sarcoplasmic reticulum) stores calcium which is released and sequestered when muscles are stimulated to contract and relax, respectively. The transverse tubule (T tubule) is an invagination in the sarcolemma containing L-type calcium channels which represent the major site for the coupling of excitation and contraction. The L-type calcium channels in T tubules activate in response to electrical stimulation and allow calcium to flow down the electrochemical gradient and into the cell.

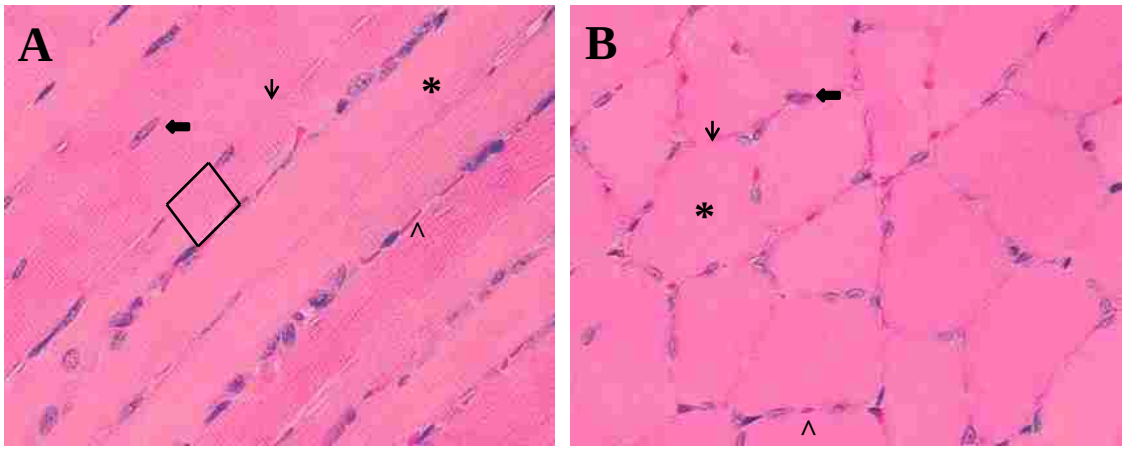

Figure 1.10. Photomicrographs of skeletal muscle. Longitudinal (A) and cross-section (B) of skeletal muscle illustrating the sarcoplasm (*), sarcolemma (↓), nuclei (▬), red blood cells (^) and alternating pattern of dark myosin (A) and light actin (I) bands (box).

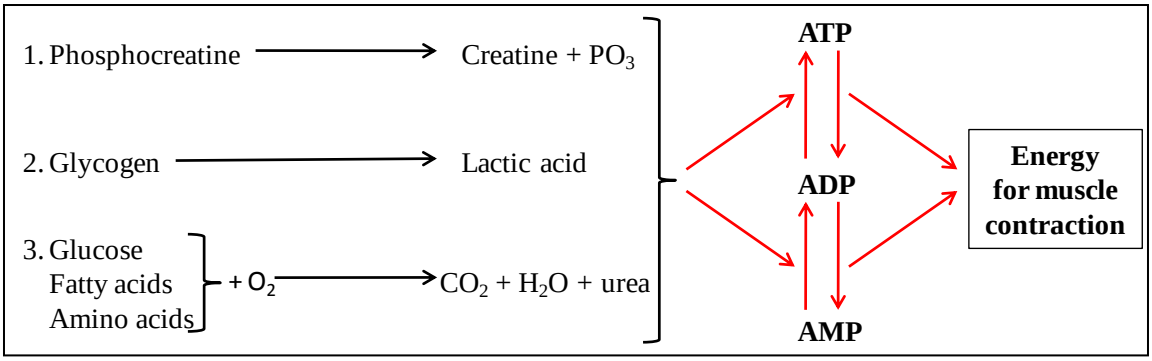

Figure 1.11. Metabolic pathways that supply energy for muscle contraction. Energy required for muscle contraction is supplied by ATP hydrolysis. Phosphocreatine represents the first source of energy to reconstitute ATP as it has a higher amount of free energy. However, once phosphocreatine is depleted the muscle relies on intermediary metabolism including glycolysis which utilizes glucose from stored glycogen. Oxidative metabolism including products of glycolysis, fatty acids and amino acids are considered the last source of energy but most important for sustained, long-term contraction.

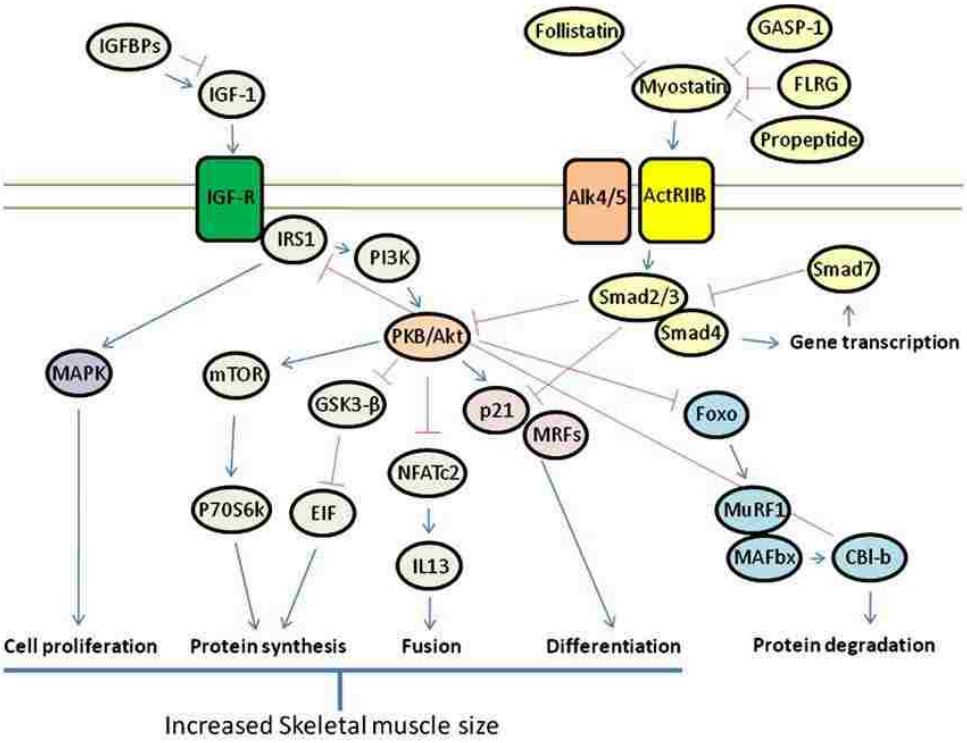

Figure 1.12. Signaling pathways involved with skeletal muscle hypertrophy and atrophy (Otto and Patel, 2010). Skeletal muscle has a remarkable plasticity which enables it to adapt functionally, morphologically and metabolically to the ever changing stimuli like exercise, environmental conditions and substrate availability. Muscle hypertrophy (anabolism) and atrophy (catabolism) represent two mechanisms by which the myofiber can adapt. Although many signaling pathways are involved in these processes, regulation of protein synthesis and degradation are considered the most important.

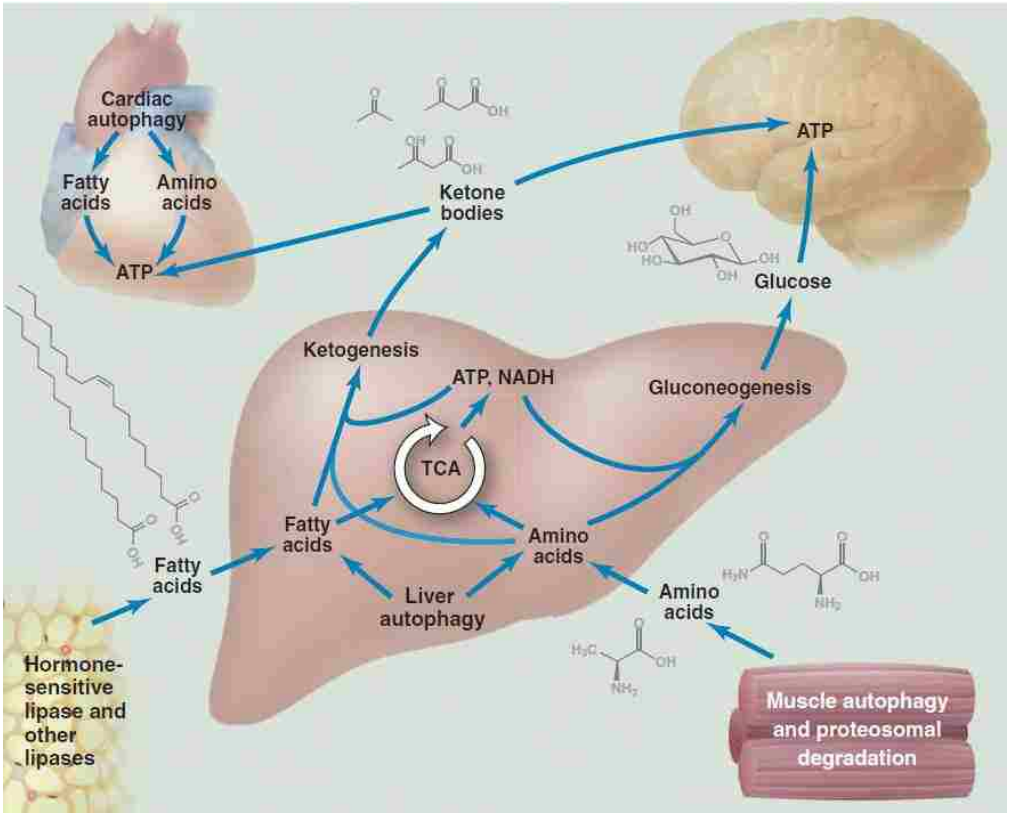

Figure 1.13. Role of autophagy and UPP in muscle atrophy during catabolic conditions like fasting (Rabinowitz and White, 2010). During normal physiology, skeletal muscle mass is maintained by tightly regulating protein degradation. However, during catabolic conditions, skeletal muscle is considered a protein reservoir which is mobilized to maintain gluconeogenesis, protein synthesis, and to provide alternative energy substrates for preservation of critical organ function, including skeletal muscle. This adaptive survival response is mediated by the autophagy-lysosome pathway which degrades long-lived proteins and organelles whereas the UPP degrades myofibrillar and most soluble short-lived proteins. Paradoxically, dysregulation representing inhibition or excessive skeletal muscle protein degradation can exacerbate other catabolic conditions and lead to pathogenic mechanisms, myofiber degeneration, morbidity and mortality.

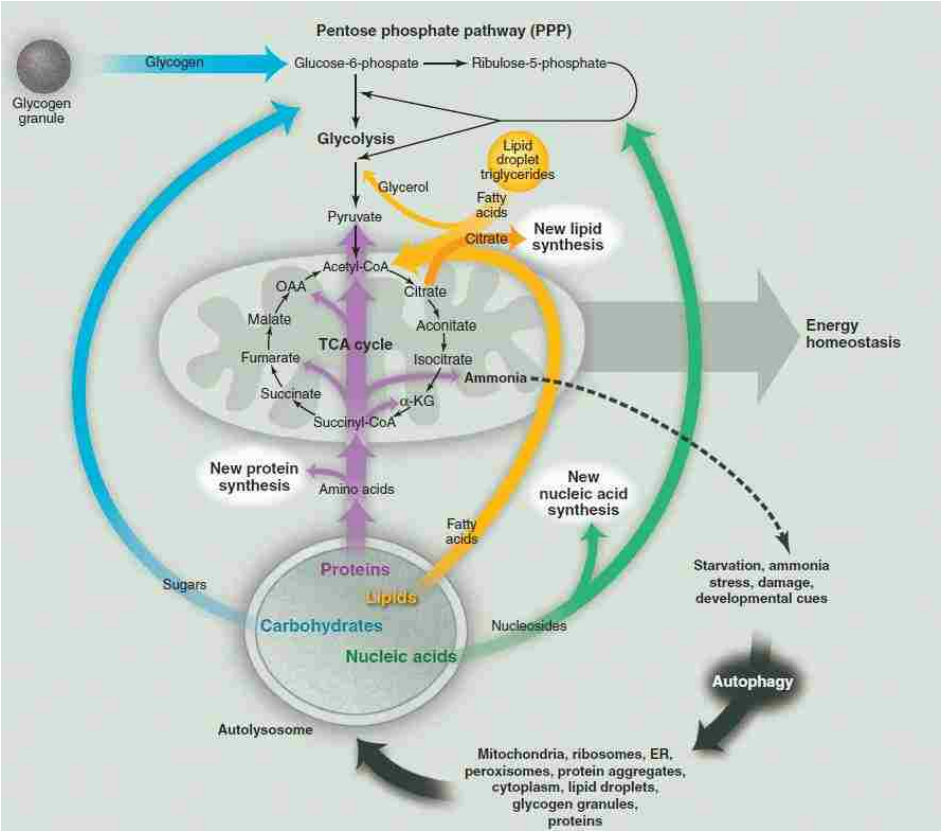

Figure 1.14. Autophagy and reutilization of products in biosynthetic pathways (Rabinowitz and White, 2010). During autophagy, mitochondria, ribosomes, peroxisomes, ER, ribosomes, lipid droplets, cytosolic proteins, glycogen and protein aggregates are engulfed into the autolysosome, degraded, and released into the cytoplasm for reutilization in biosynthetic pathways.

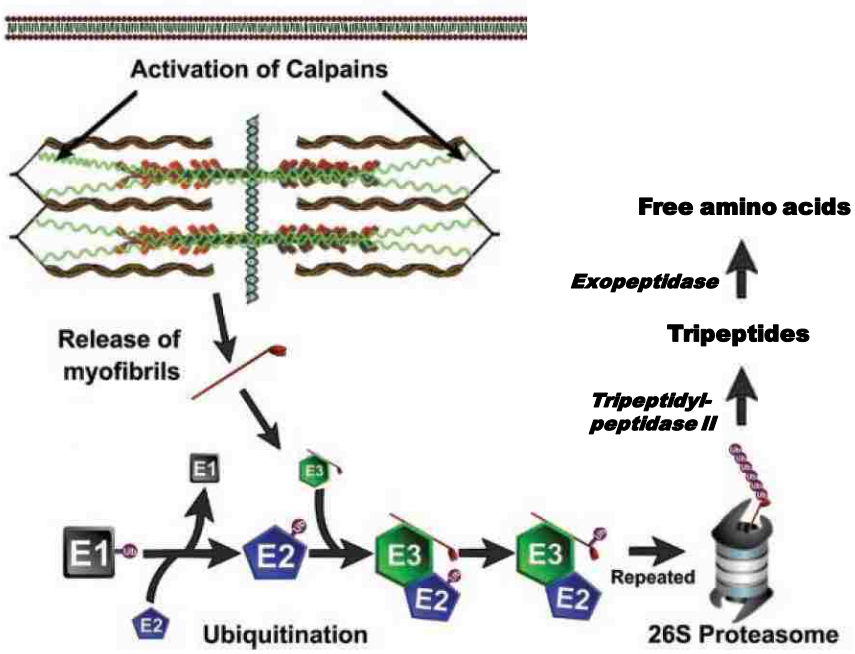

Figure 1.15. Degradation of sarcomere myofibrils by calpain and the UPP (Jackman and Kandarian, 2004). Calpains cause the release of myofibrils by degrading several proteins including nebulin, titin and desmin which are involved with sarcomeric assembly. The UPP degrades target proteins like the myofibrils with substrates identified by the addition of ubiqutin (Ub) molecules. Ub is first bound to the Ub-activating enzyme (E1) via high-energy thioester bond and is subsequently transferred to the Ub-conjugating enzyme (E2) where it is conjugated to the target protein by an Ub-ligase enzyme (E3). This process is repeated until a minimum of four Ub monomers are covalently attached via lysine residue to the target protein at which time the 26S proteasome recognizes the protein and degrades it into short peptides via chymotrypsin-like, trypsin-like and caspase-like activities (Murton et al., 2008). Degradation of the protein fragments into individual amino acids is then completed by tripeptidyl-peptidase II and exopeptidases.

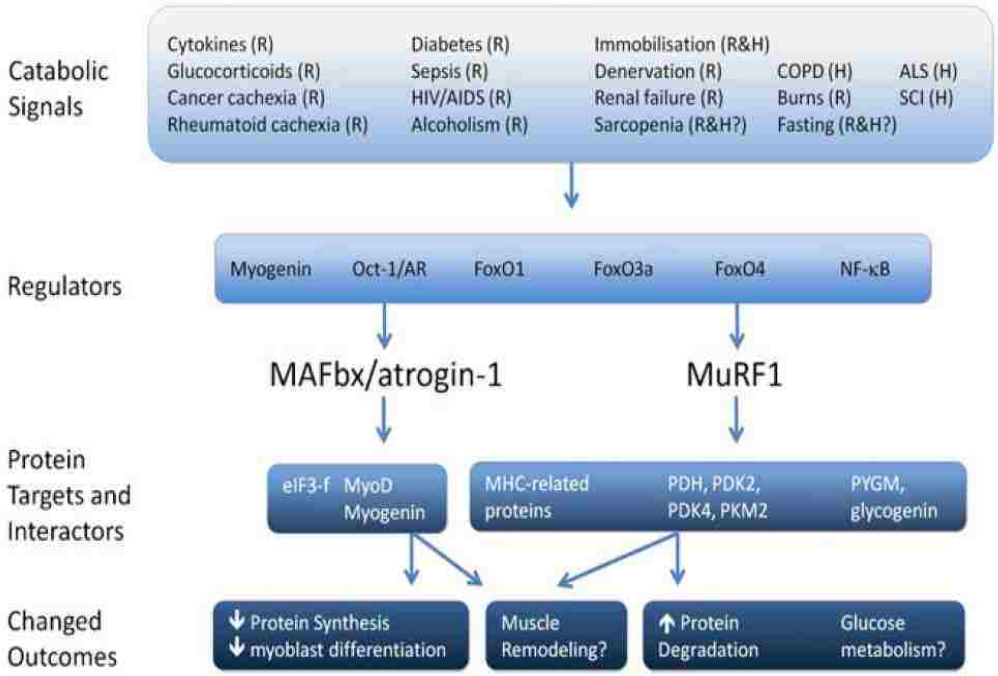

Figure 1.16. Catabolic signaling pathways involved in atrogin-1 and MuRF-1 regulation (Foletta et al., 2011). The catabolic signals and proposed physiological outcomes of the skeletal muscle specific ubiquitin ligases (atrogin-1 and MuRF-1) are shown (rodent, R; human, H). A variety of diseases and injuries function as catabolic signals to regulate gene expression of atrogin-1 and MuRF-1 via several transcription factors resulting in skeletal muscle myofibrillar protein degradation, decreased protein synthesis, altered glucose metabolism and muscle remodeling.

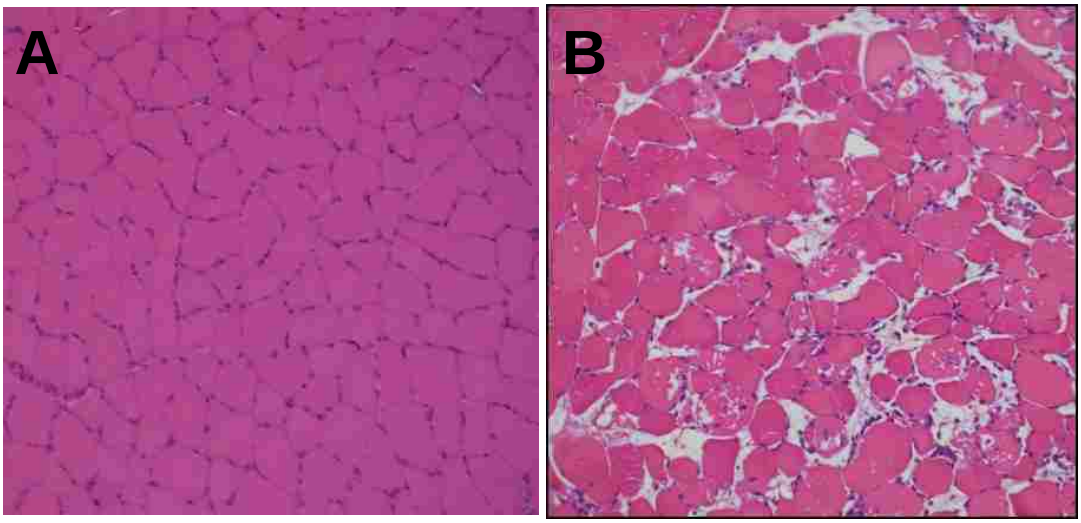

Figure 1.17. Histopathology of skeletal muscle from a cerivastatin treated rat. Histopathology of a fast-twitch muscle from (A) control and (B) cerivastatin (1 mg/kg; 14 days) treated rat showing severe myopathy characterized by myofibril lysis, hyalinization and cellular infiltration.

Table 1.1. Clinical characteristics of statin myopathy[a]	
Term	**Clinical description**
Myopathy	Any muscle disease
Myalgia	Muscle symptoms characterized by weakness, soreness, stiffness, cramping, aching either at rest or with exertion without elevated creatine kinase
Myositis	Muscle symptoms with an elevation in creatine kinase less than 10-times the upper limit of normal.
Rhabdomyolysis	Muscle symptoms with an increase in creatine kinase level 10-times the upper limit of normal or higher.

[a]Tomaszewski et al., 2011; Vaklavas et al., 2009

Table 1.2. Characteristics of skeletal muscle fiber types[ab]			
Characteristic	**Slow-twitch Oxidative (Type I)**	**Fast-twitch Oxidative (Type IIA)**	**Fast-twitch Glycolytic (Type IIB or IIX/D[b])**
Contractile characteristics			
Time to peak tension	1.0	0.4	0.4
Ca2+ myosin ATPase	1.0	3.0	3.0
Mg2+ actomyosin ATPase	1.0	2.8	2.8
Maximum duration of use	Hours	<30 min	<1 to 5 min
Fatigue resistance	High	Fairly high	Low
Enzyme activities			
Creatine phosphokinase	1.0	1.3	1.3
Phosphofructokinase	1.0	1.5	2.1
Glycogen phosphorylase	1.0	2.1	3.1
Citrate synthase	1.0	0.8	0.6
Morphological characteristics			
Size of motor neuron	Small	Medium	Large
Capillary density	1.0	0.8	0.6
Mitochondrial density	1.0	0.7	0.4
Metabolic properties			
Oxidative potential	1.0	0.7	0.2
Glycolytic potential	1.0	1.5	2.0
Phosphocreatine	1.0	1.2	1.2
Glycogen	1.0	1.3	1.5
Triacylglycerol	1.0	0.4	0.2
Myosin heave chain (MYH)	MYH7	MYH2	MYH4 – IIb MYH1 – IIx/d

[a]Zierath et al., 2004

[b]Type IIB and IIX/D were used interchangeably in the early literature because of species differences and inconsistent nomenclature. However, humans only express IIX/D even though these are generally referred to as IIB fibers (Scott et al., 2001). In contrast, both IIB and IIX/D are expressed in rodents (Scott et al., 2001). Type IIX/D have intermediate characteristics between IIB and IIA fibers (Scott et al., 2001).

Table 1.3. Risk factors for statin myopathy[a]	
Endogenous risks	**Exogenous risks**
Advanced age (>80 years)	Alcohol consumption
Low body mass index and frailty	Heavy exercise
Female sex	Surgery with severe metabolic demands
Renal and hepatic dysfunction	Drugs inhibiting CYP3A4
Thyroid disorders	Cyclosporine
Hypertriglyceridemia	Fibrates
Diet	Nicotinic acid
Diabetes	Calcium channel blockers (e.g. verapamil)
Carnitine palmityl transferase II deficiency	Amiodarone
McArdle disease (myophosphorylase deficiency)	Azole antifungals
Myoadenylate deaminase deficiency	Colchine
Family history of muscle symptoms	Digoxin
Personal history of elevated CK or muscle symptoms	HIV protease inhibitors
Statin properties	Warfarin
High systemic exposure	Macrolide antibiotics
Lipophilicity	Corticosteroids
High bioavailability and limited protein binding	Consuming > 1 L of grapefruit per day

[a]Antons et al., 2006; Chatzizisis et al., 2010

Table 1.4. Pharmacologic and pharmacokinetic properties of statins in humans[a]

Variable	Atorvastatin	Cerivastatin	Fluvastatin	Lovastatin	Pravastatin	Rosuvastatin	Simvastatin
LDL cholesterol reduction (dose range, mg)	38-54% (10-80)	25-44% (0.2-0.8)	17-33% (20-80)	29-48% (20-80)	19-48% (20-80)	52-63% (10-40)	29-48% (10-80)
IC_{50} purified human HMG-CoA reductase	8	10	28	NA	44	5	11
Elimination half-life (h)	15-30	2.1-3.1	0.5-2.3	2.9	1.3-2.8	19	2.3
Bioavailability (%)	12	60	19-29	5	18	20	5
Protein binding (%)	80-90	>99	>99	>95	43-55	88	94-98
Solubility	Lipophilic	Lipophilic	Lipophilic	Lipophilic	Hydrophilic	Hydrophilic	Lipophilic
Cytochrome P450 metabolism	3A4	3A4, 2C8	2C9	3A4	-	2C9	3A4, 3A5

[a]Alegret and Silvestre, 2006; Shitara and Sugiyama, 2006

Table 1.5. Incidence of rhabdomyolysis with all statins[a]

Managed care claims database, 42 month follow-up, 6 month minimal statin use, 473,343 patients

Drug	Patient-Years	Incidence Rates (per 10,000 person-years)* (95% CI)
Atorvastatin	261,567	2.4 (1.9-3.1)
Fluvastatin	12,635	1.6 (0.2-5.7)
Lovastatin	26,122	2.3 (0.8-4.5)
Pravastatin	64,254	3.4 (2.1-5.2)
Rosuvastatin	8,213	2.4 (0.3-8.8)
Simvastatin	54,394	3.5 (2.1-5.6)
Cerivastatin	4,719	10.6 (3.4-24.7)

[a]**Cziraky et al., 2006**

Table 1.6. Biomarkers of skeletal muscle toxicity		
Biomarker	**Tissue specificity**	**Matrix**
Creatine kinase[a]	Skeletal and cardiac muscle	Serum
Aldolase[b]	Skeletal muscle and liver	Serum
Aspartate aminotransferase[c]	Skeletal muscle and liver	Serum
Skeletal muscle troponin I[d]	Fast-twitch muscle	Serum
Myosin light chain 3[e]	Slow-twitch muscle	Serum
Fatty acid binding protein 3[f]	Slow-twitch and cardiac muscle	Serum
Parvalbumin[g]	Fast-twitch muscle	Serum
Myoglobin[h]	Skeletal and cardiac muscle	Urine

[a]Apple et al., 1984; Pritt et al., 2008; [b] Lebherz and Rutter, 1969; [c]Pritt et al., 2008; [d]Mullen and Barton, 2000; Vassallo et al., 2009; [e]Berna et al., 2007; [f]Pritt et al., 2008; [g]Arif, 2009; Schmitt and Pette, 1991; [h]Weber et al., 2007

Chapter 2

Characterization of experimental models of cerivastatin-induced myopathy

2.1. Introduction

Investigative studies of statin-induced myopathy have been frequently conducted in the rat because the effects in this species are considered predictive of the human toxicity. The development of statin myotoxicity in rats occurs in a time- and dose-dependent manner with female rats and fast-twitch muscles showing the greatest sensitivity (Seachrist et al., 2005; Vassallo et al., 2009; Westwood, et al., 2005). In general, the dosing paradigm necessary to induce statin myopathy is reproducible across rat studies. However the study duration and dose necessary to achieve this effect vary and are dependent on the specific statin and the strain of rat. Likewise, mechanistic in vitro studies have been routinely conducted in undifferentiated rat myoblasts and myotubes as well as in differentiated myofibers. However, similar to the in vivo studies the concentration and time necessary to achieve statin myotoxicity vary.

The goal of this work was to establish the dosing paradigm which causes statin myopathy in Sprague-Dawley rats and in isolated differentiated fast-twitch myofibers. Primary fast-twitch rat myofibers were used for the current in vitro work because these cells maintain a differentiated state in culture and express statin transporters, including Oatp1a4 and Oatp2b1, whereas myoblasts and myotubes are undifferentiated and lack expression of

these transporters (Ravenscroft et al., 2007; Sakamoto et al., 2008). For this work, the dose response, time course, sex- and fiber-specific toxicity were investigated with cerivastatin, a compound which has been commonly used for investigative studies because it is considered the most toxic statin which was withdrawn from the market because of rhabodmyolysis-related deaths (Thompson et al., 2003).

2.2. Methods

Chemicals. Cerivastatin (Na salt) was purchased from Sequoia Research Products (Pangbourne, United Kingdom). Methylcellulose A15C premium (cerivastatin vehicle) was purchased from the Dow Chemical Company (West Point, PA).

Animals. Male (250-300 g) and female (175-225 g) Sprague-Dawley rats (8-9 weeks old; Charles River Laboratories, Portage, MI) were individually housed in temperature and humidity controlled rooms with a 12-h light/dark cycle. Animals were allowed free access to water and a standard lab diet (Harlan Teklad 2018C, Madison, WI) and acclimated for one week prior to dosing. The conduct of all animal studies was approved by the Bristol-Myers Squibb Animal Care and Use Committee.

In vivo studies. Study 1*:* Female and male rats were randomized by weight and dosed by oral gavage with cerivastatin (0.5 and 1 mg/kg; 5 ml/kg) (n = 6 - 9 animals per group) or vehicle (0.5% methylcellulose) for 14 days. These dosages were selected based on the literature in which 0.5 and 1 mg/kg caused a minimal and severe myopathy, respectively in female rats (Westwood et al., 2005).

Study 2*:* Female rats were randomized by weight and treated with cerivastatin (1 mg/kg) for 1, 6, 8, 10 or 14 days of dosing. Dosing times were selected based on the literature indicating that the development of myopathy requires a minimum of 8 doses followed by a time-dependent increase in severity and incidence of myotoxicity with up to 14 doses (Westwood et al., 2005). Female rats were used for this study because this sex was more

sensitive to cerivastatin-induced myopathy (Vassallo et al., 2009). At necropsy, rats were anesthetized by ip injection with sodium pentobarbital (150 mg/kg) (*study 1*) or with inhalation exposure with isoflurane (*study 2*) prior to exsanguination approximately 24 hours after the last dose. Blood was collected for serum separation and tissues were harvested as described below.

Histopathology. For both studies, skeletal muscles representing a slow-twitch (soleus), fast-twitch (quadriceps femoris, gastrocnemius and psoas) and a mixed (diaphragm) fiber type composition from the left side of the rat, the left coronal section of the heart and left lateral lobe of the liver were collected for histopathologic evaluation (Table 2.1) (Armstrong and Phelps, 1984; Hamalainen and Pette, 1993; Koerker et al., 1990). Tissues were fixed in 10% neutral buffered formalin and processed for hematoxylin and eosin staining. Histopathologic evaluation of tissues was conducted without knowledge of treatment group by light microscopy (magnification ×40). The severity of myotoxicity was graded based on an arbitrary scale of 1 – 3 (*study 1*) and 1 – 4 (*study 2*), representing a minimal (1) to severe myopathy (4). For *study 2*, a scale of 1 – 4 was used for histopathology to provide a greater range for assessing the severity of myopathy. However, regardless of the scale used, a designation of 3 in *study 1* was equivalent to a designation of 4 in *study 2* and both represented severe myopathy.

In vitro studies with isolated myofibers. Laminin covered plates were prepared by diluting laminin solution (Sigma) 20-times with DMEM and transferring 0.1 ml to each well on a 96-well clear bottom plate (Corning catalog # 3903) and incubating at 37˚C for a minimum of 2 hours or overnight. The laminin solution was removed from the 96-well

plate and reused up to 3-times. The wells were washed twice with phosphate buffered saline (PBS) and allowed to dry. Maintenance medium (70 µl), containing DMEM (Invitrogen), 1% penicillin-G / streptomycin (Gibco), 200 mM glutamine (Gibco) and 20% controlled serum replacement-2 (Sigma) was transferred to each well and incubated at 37˚C for 2 hours prior to the addition of myofibers.

Myofibers from the rat flexor digitorum brevis (FDB) fast-twitch muscle were isolated and cultured based on the published literature (Figure 2.1; Ravenscroft et al., 2007; Sakamoto et al., 2011). Female and male Sprague-Dawley rats (8-9-weeks old) were anesthetized with isoflurane and exsanguinated. The FDB muscles were isolated, connective tissue removed and the muscles were incubated at 37˚C for 3 hours in a 15 ml conicle with 5 ml of pre-warmed (37˚C) isolation medium containing DMEM, 10% fetal bovine serum (FBS; Gibco) and 1% penicillin-G / streptomycin with 0.3% collagenase (Sigma). After incubation, the isolation medium was discarded and 6 ml of pre-warmed proliferation medium containing DMEM, 10% FBS, 1% penicillin-G / streptomycin, and 200 mM glutamine was immediately added to the muscles. The muscles were gently triturated approximately 25 times with a transfer pipette. The myofibers were incubated at 37˚C for 30 minutes to allow the cells to settle by gravity sedimentation. After incubation, the isolation medium was discarded and 6 ml of fresh maintenance medium was added to the myofibers. The muscles were triturated approximately 25 times with a transfer pipette. The myofibers were incubated at 37˚C for 30 minutes. After incubation, the maintenance medium was discarded and 6 ml of fresh pre-warmed maintenance medium was added. The muscles were triturated approximately 25 times and incubated at

37˚C for 30 minutes. This process was repeated until all of the clumps of cells were reduced to individual myofibers. The myofibers were resuspended in a final volume of 8 ml of maintenance medium. For each myofiber suspension, 50 µl (approximately 50 myofibers) was transferred to each well on a laminin covered 96-well plate containing 70 µl of pre-warmed maintenance medium. Myofibers were incubated overnight which allowed them to attach to the laminin covered plates and then treated with cerivastatin or vehicle (maintenance media) the following morning.

A concentration response of myotoxicity was determined by incubating myofibers with 1, 3, 10, 30, 100, 300 and 1000 nM of cerivastatin or vehicle (maintenance) for 5 days. The time-dependent development of myotoxicity was determined by incubating myofibers with 300 nM for 1, 2, 3, 4, 5, 6 days. This concentration was selected because a toxic dose of cerivastatin in female rats is associated with a maximum plasma concentration (Cmax) of 221 nM (Reinoso et al., 2002; Steinke et al., 1996). Therefore, for the current work a slightly higher concentration was selected for testing. Morphological characteristics of myofibers treated with cerivastatin (1 µM) were determined daily for up to 5 days by light microscopy. To determine whether myotoxicity was dependent on HMG-CoA reductase inhibition, cerivastatin (1 µM) was incubated with and without mevalonate (100 µM) for 5 days. This concentration of mevalonate was selected based on the literature indicating 100 µM prevents statin-induced myotoxicity in vitro (Mullen et al., 2010).

For all in vitro myofiber experiments, cerivastatin stock solutions were prepared in phosphate buffered saline, diluted in maintenance medium and 30 µl of the appropriate concentration was added to each well containing approximately 50 myofibers for a final volume of 150 µl. Myotoxicity was determined by removing 50 µl of myofiber medium and diluting it with 50 µl of PBS. Viability was assessed by either trypan blue (Mediatech, Inc.) exclusion or measuring ATP in the myofibers according to the manufacturer's instructions (Promega CellTiter-Glo Luminescent Cell Viability Assay). CK and ATP results represent mean values ± SE of 3 - 4 separate experiments in which 4 (time course) – 12 (concentration response) wells containing approximately 50 myofibers / well were used for each treatment or time point.

Clinical chemistry analysis. Serum samples and cell culture medium were stored at -80°C immediately after collection and analyzed for CK, AST and ALT on a Seimens Advia 1800 chemistry autoanalyzer (Seimens Healthcare Diagnostics, Tarrytown, NY). Skeletal muscle troponin I (sTnI) was quantified by ELISA (Life Diagnostics, Inc., West Chester, PA) for *study 1* and by electrochemiluminescence (Meso Scale Diagnostics, Maryland) for *study 2*.

Data analysis. The mean concentration ± SE of CK, sTnI, AST, ALT and ATP were determined for each treatment group. Group means of treated rats were compared to their respective experimental control with a student's t-test or ANOVA ($p < 0.05$). Concentration response curves and LC_{50} values were determined in Graphpad Prism (Graphpad Software, Inc., California).

2.3. Results

In vivo studies

Cerivastatin caused a dose dependent, fast-twitch specific myofiber degeneration in female rats after 14 days of dosing (Figure 2.2, panel B; Table 2.2). In female rats, a mild to severe myopathy was observed in all fast-twitch muscles evaluated whereas the slow-twitch fibers of the soleus were unaffected (Table 2.2). Histopathologic changes noted in the fast-twitch muscles included myofibril lysis and hyalinization along with the presence of cellular infiltrates and nuclear rowing indicating myofiber regeneration. At 0.5 mg/kg, mild muscle toxicity was observed and increased levels of sTnI, CK and AST were noted. At 1 mg/kg, a mild to severe muscle toxicity was observed and increased levels of sTnI, CK and AST were noted. Muscle toxicity was also observed in male rats but the incidence and severity were much less than female rats (Table 2.2). With cerivastatin treatment, cardiac myofiber degeneration was also noted in the left ventricle, predominately in female rats (Figure 2.2, panel D; Table 2.2). Histopathologic changes noted in the heart include myofiber vacuolization, hyalinization and atrophy with interstitial cellular infiltrates.

Cerivastatin caused a time dependent, fast-twitch specific myofiber degeneration in female rats (Figure 2.3; Table 2.3). Histopathologic changes noted in fast-twitch muscles included myofibril lysis, hyalinization and cellular infiltration whereas the slow-twitch (soleus) muscle was unaffected (Figure 2.3). These changes were first noted in 25% of the animals after 8 days of cerivastatin treatment and the incidence of myopathy increased to 75% and 100% of the animals after 10 and 14 days, respectively (Table 2.3).

The severity of cerivastatin-induced myotoxicity also increased with time from a minimal injury after 8 days (Figure 2.3, panel B) to a severe myopathy after 14 days of cerivastatin treatment (Figure 2.3, panel D). In contrast to the histopathology, sTnI, CK and AST were only increased after 10 and 14 days of treatment. Cardiac myofiber necrosis was also observed after 10 and 14 days of cerivastatin and was characterized by myofiber vacuolization, hyalinization, atrophy and interstitial cell infiltration.

In vitro studies

Several different FDB myofiber isolation procedures were evaluated because initial experiments, using published protocol conditions, resulted in numerous broken cells. Myofibers damaged in the course of the isolation procedure do not survive and are easily distinguished from intact myofibers because they typically hypercontract. Follow up experiments indicated that several key steps within the harvesting and processing of the myofibers were important to obtain healthy viable myofibers which attach to the laminin covered plates. Specifically, the FDB muscles must be gently removed from the animal as stretching and cutting the tendon too close to the myofibers increases the number of damaged cells. The collagenase concentration and incubation time are important factors which should be controlled. Trituration of the muscles after collagenase treatment releases the individual myofibers, however if the muscles are forced into the pipette this will result in a significant increase in the number of damaged fibers. Therefore, patience and finesse are absolutely critical when triturating the muscles. The type and size of the laminin covered plates are also important variables. Initial experiments were conducted with 12 and 24 well plates and various volumes of medium. In all cases, the myofibers

did not attach to the laminin covered plate but instead remained in suspension. Commercially available laminin covered plates were also evaluated but again the myofibers remained in suspension. Final conditions, including 120 µl of medium as well as laminin covered plates prepared the day before isolation were identified as important factors needed to maximize the number of viable myofibers attached to the plate. The number of myofibers transferred to the laminin covered plate is also important because too many cells results in tangling which leads to the cells breaking. Furthermore, myofibers which are not fully triturated into individual cells end up as clumps on the plate and after several days in culture these muscle fibers began to fibrillate. Therefore, to minimize these unwanted conditions special care was taken to completely triturate the muscles into individual myofibers and approximately 50 cells were added to each well on a 96 well plate.

FDB muscles were chosen for cell culture because these myofibers are short (approximately 1 µm long) whereas myofibers from muscles like the soleus are 8-times longer and are more susceptible to breaking (Bekoff and Betz, 1977; Calderon et al., 2009; Shefer and Yablonka-Reuveni, 2005). Longer myofibers from several sources including extensor digitorum longus (EDL), tibialis anterior and the soleus were isolated and plated on 96 well laminin covered plates. Several isolation experiments were conducted and in all cases when the myofibers were evaluated by light microscopy on the 96 well plate the cells were broken and hypercontracted. However, viable soleus myofibers, which attached to the laminin covered plates, were finally obtained with meticulous care and when only a 1 – 2 myofibers were placed in a well.

The concentration response of cerivastatin was determined in female and male rat FDB myofibers after 5 days of treatment (Figure 2.4). The LC_{50} for cerivastatin in female rats was determined to be 106 nM with a 95% confidence interval of 62-167 nM. To determine if sex differences in sensitivity to cerivastatin toxicity is maintained in vitro male rat myofibers were isolated and treated under the same conditions. The LC_{50} for cerivastatin in male rats was determined to be 32 nM with a 95% confidence interval of 23-46 nM.

The time-dependent myotoxicity was determined in female rat FDB myofibers treated with cerivastatin (300 nM) for up to 6 days. Daily evaluation of ATP levels indicated that a steady decline in viability was initiated on day 3 and continued until day 6 (Figure 2.5, panel A). Similarly, daily evaluation of CK in the medium indicated a significant increase after 3 days which increased on day 4 followed by a sharp decrease on days 5 and 6 (Figure 2.5, panel B). Despite a general correlation between ATP and CK changes on days 3 and 4 the level of CK was highly variable and decreased on days 5 and 6, suggesting it was degraded and thus may not be a reliable marker.

The morphology of female rat myofibers was evaluated by light microscopy immediately after the cells attached to the laminin covered plates and daily for up to 6 days. Myofibers looked similar across the time course and were characterized by cross striations and peripherally located nuclei which are indicative of differentiated viable myofibers (Figure 2.6; Table 2.4). In contrast, cerivastatin (1 μM) treated female rat myofibers exhibited 3 distinct morphological stages. Stage 1 was represented by days 1 – 2 in which the

morphology of the treated myofibers was similar to control. Stage 2 occurred between days 3 – 4 in which several myofibers began developing blebs or vacuoles on the plasma membrane and the cells appeared swollen. Stage 3 was characterized by an increase in the number of blebs and the myofibers appeared dark in color, without striations and many of the cells were detached from the laminin covered plate (Figure 2.6; Table 2.4).

To determine whether myotoxicity was dependent on HMG-CoA reductase inhibition cerivastatin (1 μM) was incubated with and without mevalonate for 5 days. Consistent with previous in vitro and in vivo experiments, cerivastatin caused a marked decrease in myofiber viability whereas mevalonate supplementation prevented toxicity (Figure 2.7). These results demonstrate that mevalonate supplementation prevents myotoxicity, and suggests that decreased levels of one or more downstream products likely contributes to toxicity.

2.4. Discussion

The goal of this work was to establish the dosing paradigm which causes myopathy in Sprague-Dawley rats and in isolated differentiated fast-twitch rat myofibers using cerivastatin as a model compound. The in vivo studies confirmed that cerivastatin-induced myopathy is a fast-twitch muscle specific effect in which female rats are more sensitive than males. Furthermore, the development of myopathy occurred in a dose-dependent manner with 1 mg/kg showing the most severe toxicity. The cerivastatin (1 mg/kg) time course study indicated that the development of myopathy requires a minimum of 8 daily doses with increased incidence and severity following longer dosing duration. Together, the dose response and time course for cerivastatin-induced myopathy in Sprague-Dawley rats was consistent with previously published results in Wistar Hannover rats (Westwood et al., 2005). Furthermore, this is the first report of cerivastatin-induced cardiotoxicity. Given that the focus of this dissertation is on cerivastatin-induced skeletal muscle toxicity the mechanism of cardiomyopathy was not pursued. However, this was an unexpected finding given that slow-twitch muscles were resistant to cerivastatin-induced toxicity and this fiber type and cardiac muscle are similar in regards to energy metabolism.

Although most in vitro research on mechanisms of statin-induced myopathy has involved undifferentiated myoblasts and myotubes recent evidence indicates that differentiated myofibers may be more appropriate and representative of the in vivo pathophysiology (Ravenscroft et al., 2007; Sakamoto et al., 2007, 2008). Therefore, a method for harvesting and culturing differentiated fast-twitch myofibers from the rat FDB muscle was developed and conditions associated with cerivastatin-induced myotoxicity were

determined. Importantly, these results demonstrate that cerivastatin-induced toxicity in isolated FDB myofibers recapitulates the in vivo myopathy at relevant concentrations, and mevalonate supplementation prevents the toxicity. Specifically, the development of toxicity in FDB myofibers was time-dependent, with an LC_{50} between 30 – 100 nM, depending on sex which is consistent with the in vivo concentration of cerivastatin (30 and 200 nM) reported in skeletal muscles and plasma, respectively in female rats showing evidence of myopathy (Seachrist et al., 2005; Sidaway et al., 2009; Westwood et al., 2005). Despite this correlation, a lower LC_{50} for male compared to female rat myofibers was observed in vitro which is opposite of what was observed in vivo. While the mechanism of this sex specific sensitivity to statin myopathy is unknown these results suggest that in vivo factors may be important in the pathophysiology. It has been proposed that statin myopathy is the result of transcriptional induction of the muscle specific ubiquitin ligases, including atrogin-1 and MuRF-1 with subsequent and excessive myofibrillar protein degradation (Hanai et al., 2007). Testosterone has been shown to suppress transcriptional induction of these ubiquitin ligases (Foletta et al., 2011). However, these myofibers were cultured in the absence of serum and thus testosterone. Therefore, it is possible that testosterone plays a role in mediating in vivo sex differences in statin-induced myopathy. However, this mode of action was not pursued further. Recently, differential gene expression of whole mouse skeletal muscles was compared to isolated differentiated mouse myofibers (Chemello et al., 2011). Genes highly expressed in non-muscle cells were downregulated, and based on their functional role were derived from blood cells, endothelial cells or Schwann cells (Chemello et al.,

2011). Accordingly, sex differences in statin-induced myopathy may also be related to specific in vivo conditions which were not recapitulated in vitro.

Cerivastatin-induced myofiber effects were evaluated by measuring viability and toxicity with ATP and CK, respectively. ATP values were highly reproducible across experiments whereas CK was more variable and showed a marked decrease at later time points, presumably due to protease degradation. These results are consistent with the fact that the preclinical utility of CK is limited because of its marked variability (Bohlmeyer et al., 1994). Unexpectedly, CK was significantly increased on day 3 whereas ATP was not significantly reduced until day 4 in vitro. However, it is likely that CK was released from viable or stressed, but not necrotic cells. The formation of blebs or vacuoles which was first noted on day 3 may represent one mechanism by which the stressed myofibers release cytoplasmic contents, including CK prior to a significant reduction in ATP. Such a mechanism has been described for cardiac myocytes under ischemic conditions in which the cells produce blebs on the surface of the plasma membrane and release cytoplasmic contents, including enzymes, without undergoing necrosis (Brancaccio et al., 2010). During re-oxygenation these blebs can be reabsorbed or shed into the circulation. In contrast, when ischemia is protracted, the blebs grow, collapse and cell necrosis ensues (Brancaccio et al., 2010). Therefore, changes in CK and ATP provide information on two different biochemical and pathophysiological processes in the myofibers. The early increase in CK is likely related to myofiber stress whereas a decrease in ATP, representing a late response indicates the cells were not able to adapt and necrosis ensued.

Myofibers have been isolated and cultured from a variety of limb muscles including extensor digitorum longus, tibialis anterior and the soleus (Shefer and Yablonka-Reuveni, 2005). However, myofibers from these sources are significantly longer (e.g. soleus is 8-times longer than the FDB muscle), tend to tangle and break and this was observed in the current study. However, after several experiments and meticulous care, myofibers from the soleus attached to the lamin covered plate when only 1 - 2 cells were transferred to a well. Given the emphasis of this work on fast-twitch myotoxicity additional experiments in the slow-twitch myofibers were not pursued.

In summary, the current work demonstrates that cerivastatin-induced myopathy occurs in a dose- and time-dependent manner with fast-twitch muscles from female rats showing the greatest sensitivity. Furthermore, an in vitro culture system was established for the evaluation of fast-twitch muscle fiber toxicity. These results demonstrate that cerivastatin-induced toxicity in isolated myofibers recapitulates the in vivo effects at relevant drug concentrations and mevalonate supplementation prevents the toxicity. Collectively, these results provide an in vivo and in vitro dosing paradigm which can be used to investigate mechanisms of toxicity.

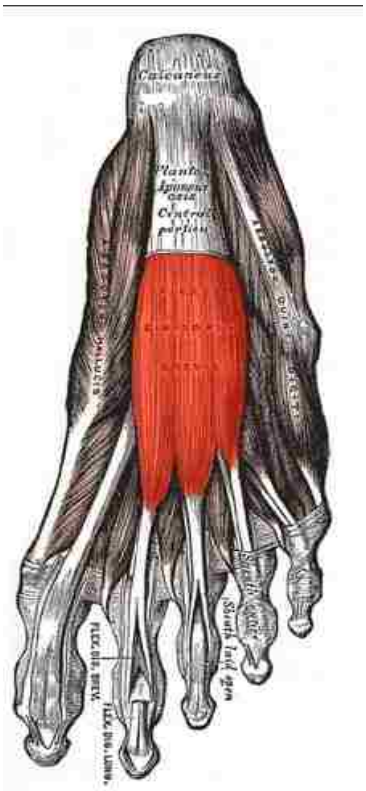

Figure 2.1. Anatomical location and function of the flexor digitorum brevis muscle. The FDB muscle divides into four tendons which insert into the lateral four phalanges of the foot where it functions as a flexor.

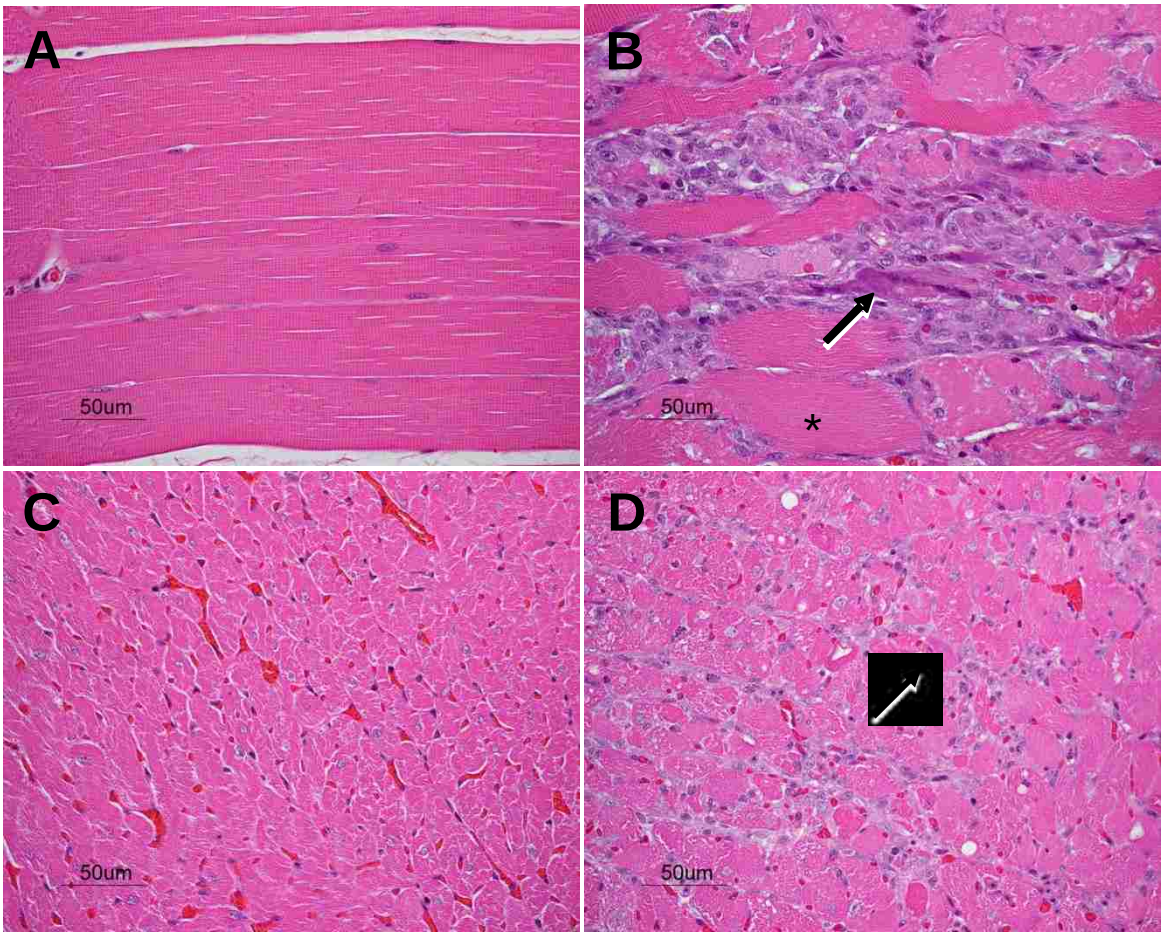

Figure 2.2. Muscle histopathology of female rats treated with cerivastatin (Vassallo et al., 2009). Quadriceps femoris muscle from control (A) and cerivastatin-treated rat (female; 1 mg/kg; B) illustrates severe skeletal myofiber degeneration and necrosis including myofibril lysis and hyalinization (*), cellular infiltration, and nuclear rowing, indicative of myofiber regeneration (arrow). Myocardium of left ventricle from control (C) and cerivastatin-treated rat (female; 1 mg/kg; D) illustrates cardiac myofiber degeneration. Histopathologic changes observed with cerivastatin were characterized by myofiber vacuolization, hyalinization and atrophy with interstitial cellular infiltration.

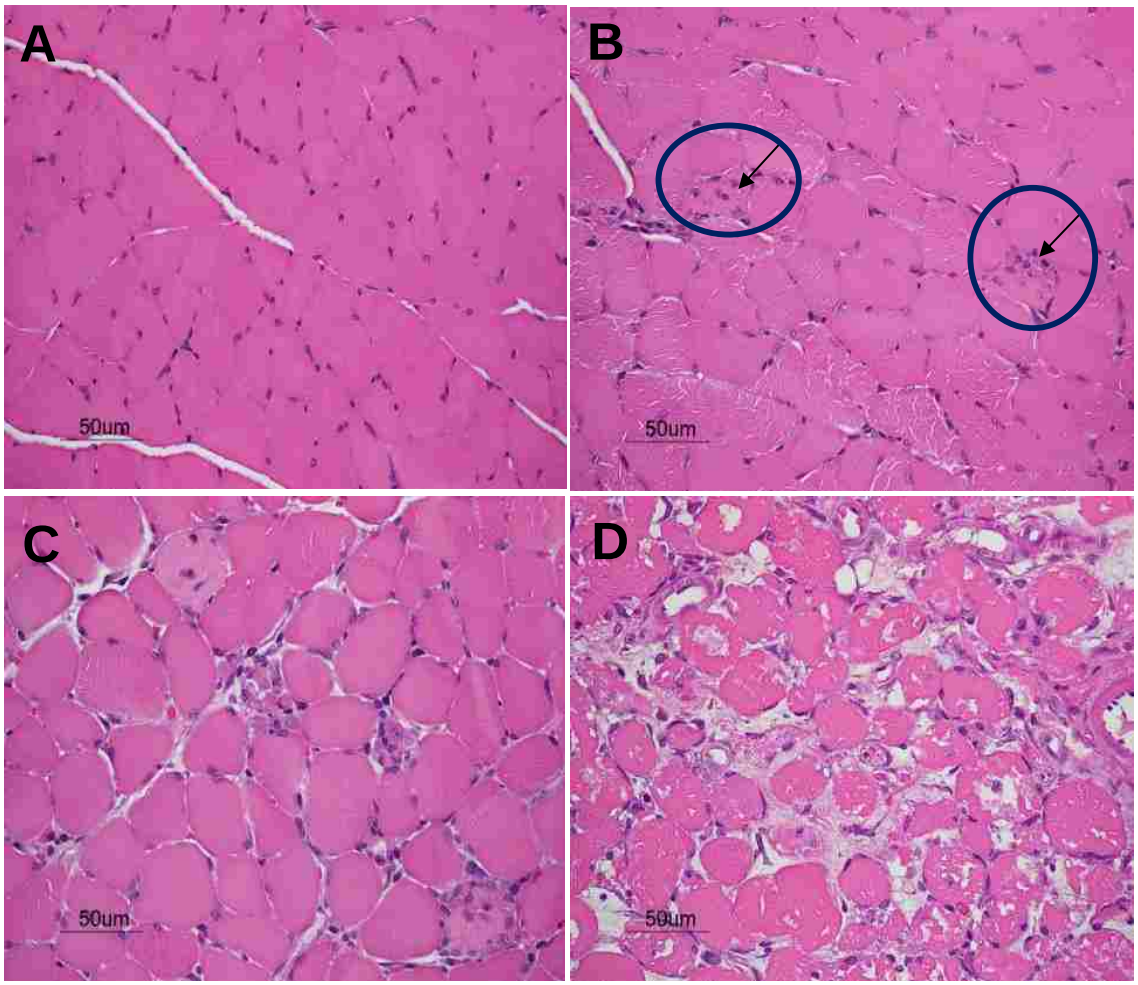

Figure 2.3. Time course of cerivastatin-induced myotoxicity in female rats. Representative fast-twitch muscles from control (A) and cerivastatin-treated female rat (1 mg/kg) showing two necrotic myofibers (arrows) illustrating a minimal grade 1 injury (B; Day 9), a mild grade 2 injury (C; Day 11), and a severe grade 4 myopathy showing degeneration and necrosis characterized by myofibril lysis, hyalinization and cellular infiltration (D; Day 15).

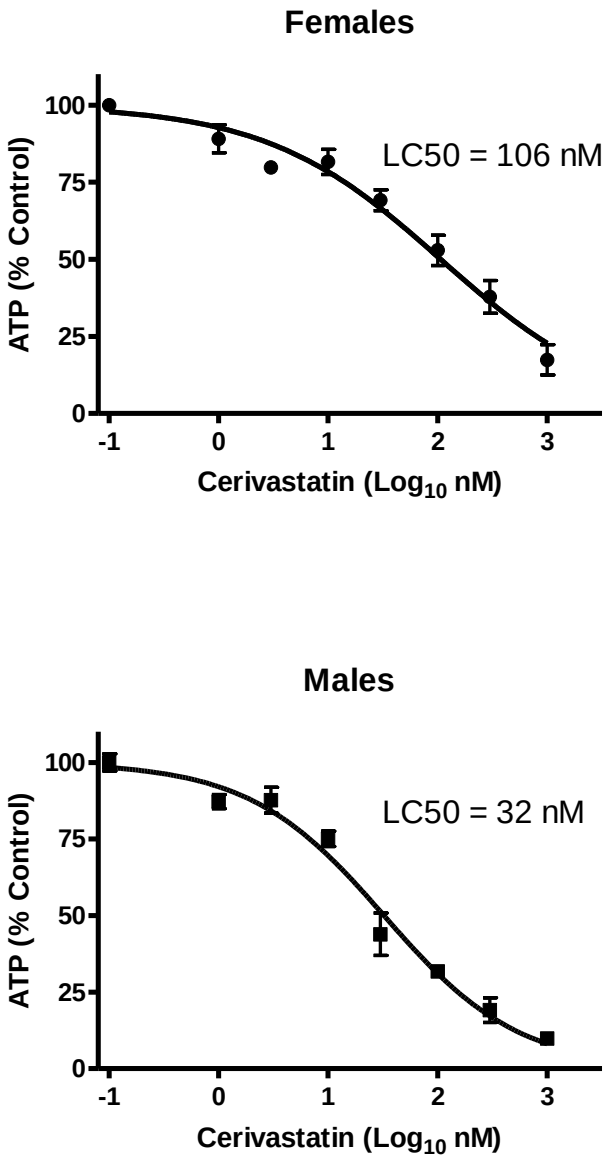

Figure 2.4. Concentration response of cerivastatin-induced toxicity in female and male rat myofibers. Myofibers were treated with cerivastatin (0, 1, 3, 10, 30, 100, 300 and 1000 nM) for five consecutive days at which time ATP was determined in 12 wells containing approximately 50 myofibers per well. The 95% confidence interval for female and male rats was 62-167 nM and 23-46 nM, respectively. Results represent the mean ± SE of three separate experiments.

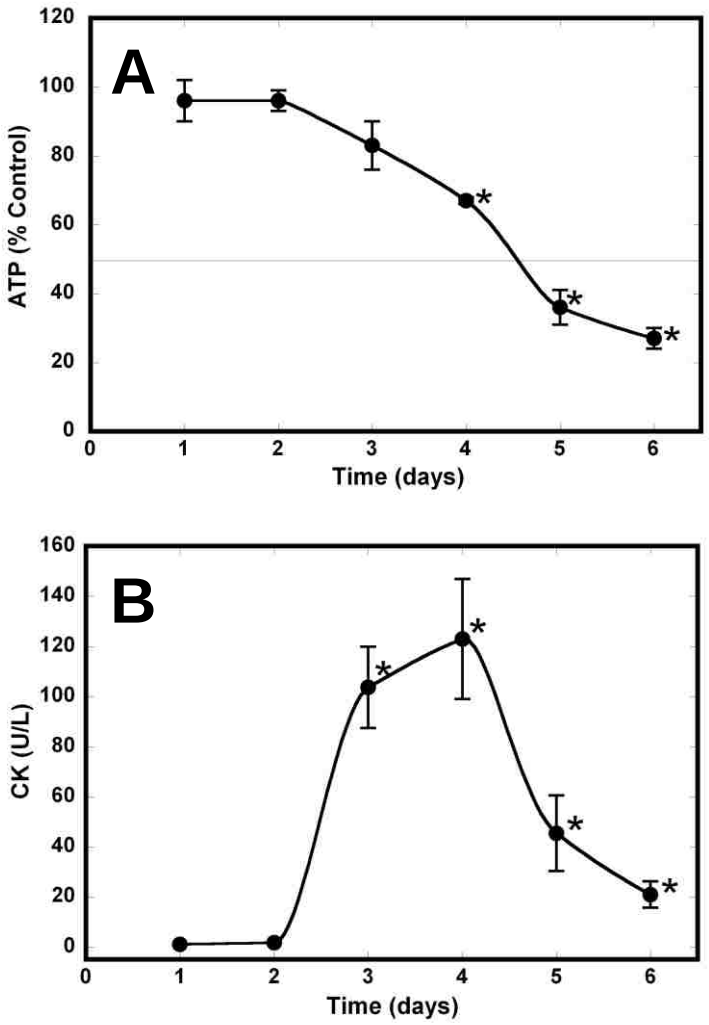

Figure 2.5. Time course of cerivastatin-induced toxicity in female rat myofibers. Myofibers were treated with cerivastatin (300 nM) for up to six consecutive days. On each day, CK (A) and ATP (B) levels were determined and compared to untreated myofibers. Results represent the mean ± SE of four separate experiments.

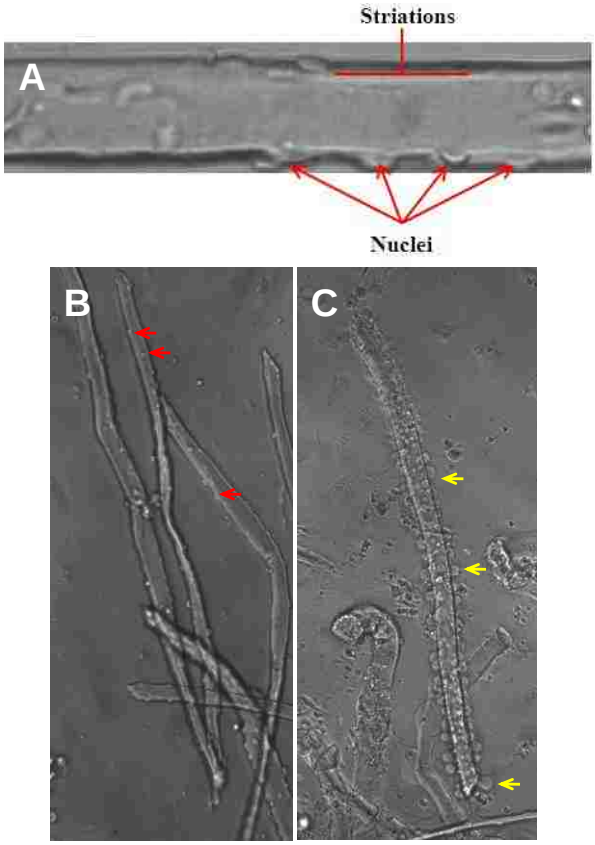

Figure 2.6. Cerivastatin-induced morphological changes in female rat myofibers. Mature differentiated cultured myofibers maintain characteristic striated pattern and peripherally located nuclei (A). Myofibers were treated with vehicle (B) or cerivastatin (C; 1 µM) for 4 days and morphological changes were qualitatively evaluated by light microscopy. Vehicle treated myofibers showed normal morphology with peripherally located nuclei (red arrows) whereas cerivastatin treated myofibers appeared swollen, with the presence of numerous blebs on the plasma membrane which are characteristic of stressed cells releasing cytoplasmic contents (yellow arrows).

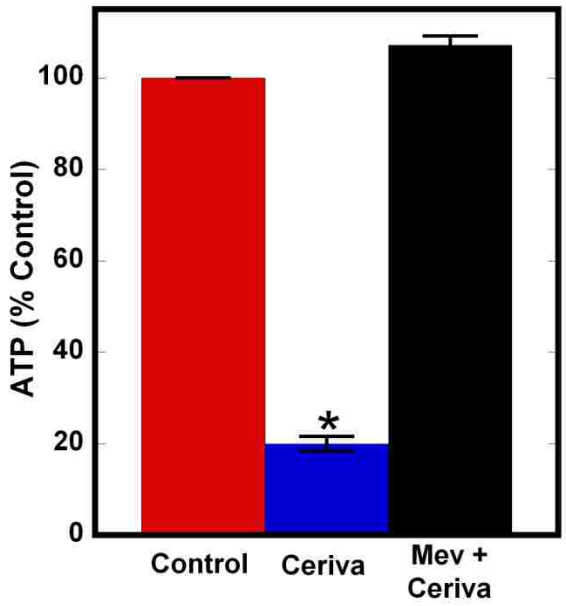

Figure 2.7. Mevalonate supplementation prevents cerivastatin-induced myotoxicity. Female rat myofibers were treated with cerivastatin (1 µM) with or without mevalonate (100 µM) for five days at which time ATP was determined. Results represent the mean ± SE of three separate experiments.

Table 2.1. Muscles collected for histopathology

Muscle	Fiber type, %[a]			Reference
	I [SO]	IIA [FOG]	IIB [FG]	
Soleus (Sol)	84	16	0	Koerker et al., 1990
Diaphragm (Dia)	35	38	27	Kumagai et al., 2001
Quadriceps femoris (Quad)	8	65	27	Koerker et al., 1990
Gastrocnemius (Gastroc)	4	38	58	Ariano et al., 1973
Psoas	1	8	91[b]	Hamalainen and Pette, 1993
Flexor digitorum brevis	6	61	33	Ihlemann et al., 2001

[a]Muscle fiber type - Type I, slow oxidative [SO]; Type IIa, fast oxidative glycolytic [FOG]; Type IIb fast glycolytic [FG]

[b]In the psoas, the FG muscle (91%) consists of IIB (46%) and IIX/D (45%) fibers (Hamalainen and Pette, 1993). Type IIB and IIX/D were used interchangeably in the early literature because of species differences and inconsistent nomenclature. However, humans only express IIX/D even though these are generally referred to as IIB fibers. In contrast, both IIB and IIX/D fibers are expressed in rodents (Scott et al., 2001). Type IIX/D fibers have intermediate characteristics between IIb and IIa (Scott et al., 2001).

Table 2.2. Clinical and histopathologic evaluation of cerivastatin-induced myopathy in female and male rats[a]

	Clinical Pathology				Histopathology[d]				
Treatment (mg/kg)	cTnI (ng/mL)[b]	CK (U/L)	AST (U/L)	ALT (U/L)	Gastroc	Quad	Psoas	Dia	Heart
Females									
Control	<7 ± 1	749 ± 70	114 ± 6	50 ± 2	-	-	-	-	-
0.5	<179 ± 109	1402 ± 319	404 ± 177	97 ± 29	3/9 (1.3)	2/9 (2)	2/9 (1.5)	-	1/9 (2)
1.0	733 ± 234*	3252 ± 1380	1838 ± 772	319 ± 108*	6/9 (2.7)	7/9 (2.7)	7/9 (2.7)	1/9 (2)	7/9 (1.9)
Males									
Control	<6 ± 1	985 ± 61	130 ± 21	49 ± 3	-	-	-	-	-
0.5	<7 ± 1	1082 ± 78	152 ± 12	51 ± 3	-	-	1/9 (1)	-	-
1.0	-	1272 ± 183	151 ± 10	58 ± 2	-	-	3/9 (1)	-	-

[a]Results represent the mean and SE of 6 - 9 rats / sex / group dosed for 14 consecutive days.

[b]< Indicates at least one value in the group is less than the detection limit (5.9 ng/ml). (-) indicates all values in the group were ≤ the detection limit.

[c]This group had two values ≥ 1330 ng/mL, therefore the mean underestimates the actual concentration.

[d]Results represent tissues affected by treatment. No adverse histological effects were observed in the soleus or liver. Number of animals with muscle necrosis and degeneration / number of animals per group. The mean severity score in () is based on an arbitrary severity scale of 1, 2 and 3 (most severe). (-) denotes no significant histopathologic finding. *Significantly different from control ($p < 0.05$).

Table 2.3. Time course of clinical and histopathologic changes associated with cerivastatin induced myopathy in female rats[a]

Days of dosing cerivastatin	Clinical Pathology				Histopathology[c]			
	cTnI (ng/mL)[b]	CK (U/L)	AST (U/L)	ALT (U/L)	Gastroc	Quad	Psoas	Heart
Control	<1.7 ± 0.4	443 ± 42	85 ± 4	47 ± 2	-	-	-	-
1	<1.0 ± 0.1	414 ± 105	88 ± 12	45 ± 4	-	-	-	-
6	<0.8 ± 0.1	344 ± 14	95 ± 3	52 ± 3	-	-	-	-
8	<1.4 ± 0.4	259 ± 32	96 ± 8	55 ± 3	-	4/8 (1.0)	2/8 (1.0)	-
10	<190 ± 133	1282 ± 865	477 ± 251	98 ± 31	5/8 (1.6)	6/8 (1.7)	6/8 (1.7)	5/8 (1.6)
14	1016 ± 306	9747 ± 3239*	2933 ± 651*	363 ± 70*	7/8 (3.0)	8/8 (3.0)	7/8 (3.6)	6/8 (2.3)

[a]Results represent the mean and SE of eight treated rats per day whereas the control group consists of twenty rats representing four animals from days 1, 6, 8, 10 and 14. The histopathology results represent tissues affected by treatment.

[b]< Indicates at least one value in the group is less than the detection limit (0.8 ng/ml).

[c]Results represent tissues affected by treatment. No adverse histological effects were observed in the soleus or liver. Results represent the number of animals with skeletal or cardiac myofiber necrosis and degeneration / number of animals per group. The mean severity score in () is based on an arbitrary score of 1 to 4 (most severe). (-) denotes no significant findings observed.

*Significantly different from control ($p < 0.05$).

Table 2.4. Morphological changes of female rat myofibers treated with cerivastatin.

Days of treatment	Morphological changes	
	Control	**Cerivastatin (1 µM)**
1 - 2	Normal	Normal
3 - 4	Normal	Many of the myofibers were swollen and contained up to 100 blebs.
5 - 6	Normal	The number of myofibers containing blebs increased and many of the myofibers were dark in color, without striations and detached from the laminin covered plate.

Chapter 3

Transcriptional profiles of skeletal muscles with and without cerivastatin treatment in female and male rats

3.1. Introduction

Skeletal muscles are predominately divided into two major fiber types; fast-twitch glycolytic (Type IIB or IIX/D) which are best adapted for rapid activity involving high velocity contractions and slow-twitch oxidative (Type I) which are specialized for continuous activity and possess greater blood supply, myoglobin and mitochondria (Chapter 1.6; Table 1.2; Pett and Staron, 1997; Zierath et al., 2004). Furthermore, fibers known as fast-twitch oxidative (Type IIA) possesses intermediate characteristics when compared to the other two fiber types (Chapter 1.6; Table 1.2; Pett and Staron, 1997; Zierath et al., 2004). Skeletal muscle fiber composition is determined in part by genetic factors, functional and metabolic demands, innervation and differential expression of distinct myofibrillar and metabolism proteins which allow fine tuning of muscle performance (Baldwin and Haddad, 2002; Chemello et al., 2011; Fluck and Hoppeler, 2003; Schiaffino and Reggianai, 1996). Furthermore, sexual dimorphism of skeletal muscle is also well known, with gene expression differences in energy metabolism, which are most pronounced in fast-twitch muscle fibers (Chapter 1.7.2.; Maher et al., 2008; Welle et al., 2008).

Transcriptional profiles of skeletal muscles from mice and humans have been previously determined and are consistent with the known fiber- and sex-specific differences described above (Campbell et al., 2001; Chemello et al., 2011; Kang et al., 2005; Maher et al., 2009; Welle et al., 2008; Yoshioka et al., 2007). However, fiber- and sex-specific gene expression profiles of the rat have not yet been determined. Establishing fiber- and sex-specific gene expression profiles of skeletal muscles in the rat during normal physiology makes it possible to determine differential transcriptional changes associated with pathological conditions mediated by toxicity, and exacerbated by infiltrated immune cells, connective tissue replacement and muscle regeneration (Haslett and Kunkel, 2002; Marotta et al., 2009; Yan et al., 2003). Accordingly, differential transcriptional profiling may provide insight into the molecular events involved with mechanisms of toxicity which can occur in a fiber- and sex-dependent manner (Chapter 1.7). Specifically, it is of particular interest to understand the transcriptional changes associated with statin-induced myotoxicity which predominately occurs in female fast-twitch skeletal muscles (Tables 2.2 and 2.3).

Gene expression analysis has been conducted following statin treatment. However, it has been difficult to develop a unified and compelling transcriptional profile, representing the molecular changes characteristic of statin-induced myopathy, because these studies have either been conducted in undifferentiated cultured muscle cells or in humans with heterogeneous muscle fiber types (Draeger et al., 2010; Hubal et al., 2011; Laaksonen et al., 2006; Morikawa et al., 2005; Urso et al., 2005; Yu et al., 2009). Despite these inconsistencies, transcriptional profiling is considered a powerful and appropriate tool to

investigate the molecular changes associated with statin-induced myotoxicity. However, the approach taken for the current work was significantly different from previous investigations. Specifically, rats were selected because this species is considered a useful model for studying mechanisms of statin-induced myopathy (Chapter 2). Furthermore, homogenous or "pure" skeletal muscles, consisting of >80% fast- or slow-twitch fibers were evaluated (Table 2.1). Using skeletal muscles consisting of a homogenous fiber type enables the determination of a fiber- and sex-specific gene expression profile during normal physiology and the differential effects associated with statin-induced myotoxicity. Therefore, it was hypothesized that gene expression profiles could discriminate fast- and slow-twitch skeletal muscles as well as sex-related differences in fast-twitch skeletal muscles from the rat. Additionally, it was hypothesized that the gene expression profile of these skeletal muscles may be useful in identifying pathways altered with cerivastatin-induced myopathy.

3.2. Methods

Study design. This investigation was conducted on samples obtained from *study 1* described in Chapter 2. Skeletal muscles including a representative fast-twitch fiber (psoas) and slow-twitch fiber (soleus) were harvested from the right side of the rat and stored at -80˚C pending RNA isolation (Table 2.1)

RNA isolation. Frozen muscle tissues were individually pulverized in liquid nitrogen and 50 mg was used for RNA isolation. RNA was isolated using TRIzol RNA extraction (Invitrogen Corporation, Carlsbad, CA) with the RNeasy RNA extraction kit (Qiagen, Valencia, CA) according to the manufacturers' instructions. Complete removal of DNA was achieved by using Qiagen's RNase-Free DNase. RNA concentration (260 nm absorbance) and quality (260 / 280 nm absorbance) were determined with a Nanodrop® ND-1000 spectrophotometer (NanoDrop Technologies, Inc., Wilmington, DE) and the integrity of the 18S and 28S ribosomal RNA bands was assessed by electrophoresis on RNA 6000 Nano labchips with a 2100 Bioanalyzer (Agilent Technologies, Palo Alto, CA).

Expression profiling. RNA labeling, hybridization and staining were carried out according to the Eukaryotic Target Preparation protocol in the Affymetrix® (Santa Clara, CA)Technical Manual for GeneChip® Expression Analysis. Total RNA (5 μg) was used to generate double-stranded cDNA using Superscript reverse transcriptase (Invitrogen Life Technologies) and a T7-oligo (dT) primer (Affymetrix®). The resulting cDNA was purified using the GeneChip Sample Cleanup Module according to the manufacturer's protocol (Affymetrix®). The purified cDNA was amplified using BioArray high yield

RNA transcription labeling kit (Enzo) according to the manufacturer's instructions to produce biotin labeled cRNA (complement RNA) which was then purified using GeneChip Sample Cleanup Module (Affymetrix®) and quantified. Labeled cRNA (20 μg) was fragmented at 94°C for 35 min. Fragmented cRNA (15 μg) was hybridized to the Affymetrix® HT Rat Focus Array containing 24,249 probe sets for 16 hours at 45°C. The hybridized arrays were washed and stained using Streptavidin–Phycoerythrin (Molecular Probes) and amplified with affinity purified biotinylated anti-streptavidin (Vector Laboratories, Inc, Burlingame, CA) using a GeneChip® Fluidics Station 450 (Affymetrix®). The arrays were scanned in Affymetrix® high-resolution GeneChip scanner 3000 at 570 nm using Genechip Operating software (GCOS, Ver.1.2).

Data analysis. All transcriptional data were analyzed with Rosetta Resolver software (Seattle, WA). Initial evaluation of the transcriptional intensity profiles for all skeletal muscles was conducted by principal component analysis (PCA). Skeletal muscle transcriptional profiles for each group were analyzed with an error weighted ANOVA to determine the differential expression of genes based on skeletal muscle fiber type and sex in vehicle treated rats. Furthermore, the differential expression of genes in skeletal muscles from cerivastatin relative to the vehicle treated groups was also determined. For these analyses, 5 female and male fast-twitch muscles and 4 female slow-twitch muscles from vehicle treated rats were used. Additionally, 8 and 6 fast-twitch muscles from female rats receiving 0.5 or 1 mg/kg of cerivastatin, respectively and 5 fast-twitch muscles from male rats receiving 1 mg/kg of cerivastatin were used. For the slow-twitch muscles, 8 female rats receiving 0.5 or 1 mg/kg of cerivastatin were used.

For differential gene expression analysis, probe sets were eliminated if they did not meet a p value of <0.01 and a minimum fold change of ≥ ±1.5. These criteria were selected to increase stringency and reduce false positives. Specifically, probe sets with low intensities tend to have greater variation, therefore a higher fold change was selected to reduce this inherent noise (Stevenson et al., 2003). However, even with these stringent criteria, several thousand transcripts were differentially expressed when comparing skeletal muscle fiber types as well as following cerivastatin (1 mg/kg) treatment in the fast-twitch muscle relative to vehicle treated rats. Therefore, an additional enrichment step was included to further filter the data and focus the analysis.

The HT Rat Focus microarrays contain 24,249 probe sets and approximately 50% of these were expressed in skeletal muscle. Furthermore, probe sets which were expressed at a low level may represent specific binding or result from factors which affect background noise. Accordingly, to reduce the contribution of noise-based error, which could increase the number of differentially expressed transcripts, the most abundant probe sets were determined as this approach has been shown to correlate with the skeletal muscle phenotype (Yoshioka et al., 2007; Table 1.2). For comparison of fiber and sex differences in skeletal muscles, the top 1% most abundantly expressed transcripts were collated and the differential expression of these probe sets was determined with a p value of <0.01 and a minimum fold change of ≥ ±1.5. In a similar manner, the top 2% most abundantly expressed transcripts in fast-twitch muscles from cerivastatin (1 mg/kg) treated female rats was collated and the differential expression of these probe sets was determined relative to vehicle treated female rats with a p value of <0.01 and a minimum fold change

of ≥ ±1.5. A value of 2% was selected for this analysis to include a more representative characterization of the transcriptional changes following cerivastatin treatment.

Additional analysis of the transcriptional data was also conducted to identify common transcripts which were differentially expressed with a p value of <0.01 in both fast- and slow-twitch muscles following cerivastatin (1 mg/kg) treatment and in a dose dependent manner in fast-twitch muscles. Furthermore, common probe sets which were differentially expressed in the fast-twitch muscle from female rats treated with 0.5 mg/kg and male rats treated with 1 mg/kg of cerivastatin were also determined with a p value of <0.01 since these tissues showed minimal to no myopathy. The goal of these additional analyses was to determine whether common differentially expressed transcripts exist in a fiber- or sex-dependent manner in skeletal muscles following cerivastatin treatment which may represent molecular targets or pathways important in the mechanism of cerivastatin-induced myopathy. Additionally, given the pharmacology of statins, a targeted evaluation of transcripts in the mevalonate pathway and cholesterol regulation was also conducted for all analyses.

Established annotations of the differentially expressed transcripts, as well as their accompanying accession numbers were used to categorize genes based on function with an emphasis on skeletal muscle biology and toxicity. These functional categories included energy metabolism (glycolysis, citric acid cycle, oxidative phosphorylation and creatine phosphate synthesis), sarcomere and cytoskeleton, immune, inflammatory response and cell stress, metabolism, proteolysis, extracellular matrix, regulation of

transcription and translation, transporters, calcium homeostasis, miscellaneous and those without ontology. Confirmation of gene ontology was conducted by interrogation of several databases including KEGG, Ingenuity®, Gene Expression Omnibus and the literature.

3.3. Results

PCA analysis of all the transcriptional profiles indicated two points of separation. Specifically, fast-twitch and slow-twitch muscle fibers were separated in principal component 2 regardless of treatment. Additionally, the fast-twitch muscles from both female and male rats were clustered together indicating that the transcriptional profiles were similar. Furthermore, the slow-twitch muscles, regardless of treatment, were generally clustered together indicating the transcriptional profiles were similar. In contrast, fast-twitch muscles from vehicle and cerivastatin treated female rats were separated in principal component 1 indicating the transcriptional profiles were significantly different (Figure 3.1).

In female rats, there were 2,678 differentially expressed transcripts between fast- and slow-twitch muscles. In fast-twitch muscles, the most abundant transcripts, which were differentially expressed relative to slow-twitch muscles were consistent with the established phenotype for this muscle fiber (Tables 1.2, 3.1 and 3.2; Chemello et al., 2011). Specifically, transcripts involved with the glycolytic pathway and glycogen metabolism were more highly expressed. Furthermore, probe sets specific to the fast-twitch muscle sarcomere, including myosin (Mybpc2, Myh1 and Myh4), troponin (Tnni2 and Tnnt3), Actn3, and myozenin 1 had higher constitutive expression relative to the slow-twitch muscle (Chemello et al., 2011). Additionally, parvalbumin which is a calcium binding protein, the sarcoplasmic reticulum calcium ATPase (Atp2a1) and Ldha which are highly expressed in fast-twitch muscles were significantly upregulated relative to slow-twitch muscles (Chemello et al., 2011).

In slow-twitch muscles, the most abundant transcripts, which were differentially expressed relative to fast-twitch muscles were also consistent with the established phenotype for this muscle fiber (Tables 1.2, 3.3 and 3.4; Chemello et al., 2011). Specifically, transcripts involved with the slow-twitch muscle sarcomere, including myosin (Myh7, Myl3 and Mlc2), troponin (Tnnc, Tnni1 and Tnnt1) and myozenin 2 were all significantly upregulated relative to the fast-twitch muscle as previously reported in mice (Chemello et al., 2011). Furthermore, Fabp3, myoglobin and Hadhb, which are predominately expressed in slow-twitch muscles were also significantly higher relative to the fast-twitch muscle. However, myoglobin and Hadhb were only increased by 1.2- and 1.3-fold, respectively. Several additional transcripts specific to the slow-twitch muscle were more highly expressed relative to the fast-twitch muscle, including Ldhb, Atp2a2, fhl1, Cryab, Csrp3 and Ankrd2 (Chemello et al., 2011). Moreover, several heat shock protein transcripts (Hspb7, Cryab, Hspb1), genes involved with redox cycling (Gpx1 and Ca3) and probe sets without ontology were more highly expressed in the slow-twitch muscle. Unexpectedly, transcripts involved with energy metabolism, including oxidative phosphorylation and creatine kinase were ubiquitously abundant in both fiber types which is consistent with the role of skeletal muscle in energy metabolism. Although there was a general correlation between the most abundant transcripts and the muscle fiber phenotype, genes involved with fatty acid oxidation were not highly abundant in the slow-twitch muscle as expected with the current statistical constraints. However, targeted analysis of the 2,678 differentially expressed transcripts revealed many genes involved with fatty acid oxidation, including acyl-CoA dehydrogenases which were more highly expressed in the slow-twitch muscle. Transcripts involved with the mevalonate pathway

and cholesterol regulation were not abundantly or differentially expressed in a fiber-dependent manner.

Differential expression of the most abundant transcripts in female and male fast-twitch muscles revealed no differences. To further investigate sex differences, 137 out of 12,018 detectable probes were differentially expressed in female relative to male fast-twitch muscles, with most transcripts showing less than a ± 2 fold change (Tables 3.5 and 3.6). However, several transcripts, including some without ontology, showed a marked increase of 3 to 51 fold indicating these may be important in contributing to sex differences in the fast-twitch muscle. Specific sex differences were noted for genes involved with energy metabolism, including insulin related transcripts (Igf2, Igfbp6 and Irs1) as well as those involved with Acetyl-CoA formation (Pdk4 and Acas2l), fatty acid oxidation (Ehhadh), oxidative phosphorylation (Ucp3), circadian rhythm (Per2) and transcriptional regulation (Thrb, Atf3, Nr4a1 and Cited2). However, skeletal muscles from females are generally believed to oxidize more fatty acids than males yet this finding was not reflected under the current statistical constraints. Following a more detailed analysis of the data, six additional genes involved with fatty acid oxidation, namely acyl-CoA dehydrogenase, enoyl-CoA hydratase, isovaleryl-CoA dehydrogenase, branched chain keto acid dehydrogenase, methylmalonate-semialdehyde dehydrogenase and methylcrotonyl-CoA carboxylase were all significantly higher in female fast-twitch muscles ($p<0.01$), however the fold increase was between 1.2 and 1.5. Unexpectedly, guanidinoacetate methyltransferase was 1.5-times more highly expressed in the male rat fast-twitch muscle suggesting sex differences in creatine metabolism. A large number of

genes involved with the immune, inflammatory response and cell stress were generally more highly upregulated in females. However, the biological significance of these sex differences is unknown. Most of the differentially expressed transcripts were represented by two categories, including miscellaneous (20%) and without ontology (40%). Transcripts involved with the mevalonate pathway and cholesterol regulation were not differentially expressed in a sex-dependent manner.

In a manner consistent with the lack of myotoxicity observed with cerivastatin (0.5 mg/kg), 26 out of 12,769 probes were transcriptionally altered, with all changes less than 3-fold in the female fast-twitch muscle (Table 2.2). The predominate changes were transcripts involved with glucose and lipid metabolism (Pdk4, Klf15 and G0s2), regulators of muscle mass (Cited2, Lmcd1 and Csrp3), cell stress (Sesn1 and Dnajb1) and the nuclear receptor Nr1d1 suggesting cerivastatin treatment may modulate energy metabolism in the fast-twitch muscle prior to the onset of myopathy (Table 3.7).

Consistent with severe myopathy observed with cerivastatin (1 mg/kg), 7,021 out of 13,947 detectable probes were differentially expressed in the female fast-twitch muscle (Table 2.2). In a retrospective evaluation of transcriptional profiling data, Foster et al. (2007) demonstrated that target organ toxicity was associated with at least 5% of total transcripts changing. Accordingly, the high percentage of transcripts changed in this study was likely reflective of the marked pathology observed in these rats. Therefore, instead of looking at all transcriptional changes, a subset representing the most abundant transcripts following cerivastatin treatment were collated and the differential expression

of these probe sets relative to vehicle treated rats was determined (Tables 3.8 to 3.13). In general, transcripts involved with energy metabolism were downregulated as expected whereas probes involved with the cytoskeleton showed a significant increase which may reflect skeletal muscle remodeling (Table 3.8). In contrast, sarcomeric proteins specific to the fast-twitch muscle were downregulated which is consistent with destruction of the myofibrillar apparatus (Table 3.8). A variety of genes involved with the immune, inflammatory response and cell stress (Spp1, Mt1a, Timp1, Cd68 and Ifitm1), metabolism (Np, Sat, Txn1, Prdx5, Gpx1, Prdx1), proteolysis (Ctsl, Scpep1, Ctsb and Psmb4), and the extracellular matrix (Fn1, Col3a1, Dcn, Colla2, Rpsa) were upregulated along with dysregulation of several transporters and calcium binding proteins consistent with the pathophysiology (Table 3.9, 3.11 and 3.12). Furthermore, a variety of probes involved with regulation of transcription and translation were significantly upregulated, however this change may be independent of myogenesis as the muscle regulator factors did not show a pattern of change reflecting this process (Tables 3.10 and 3.11; Figure 1.6). Unexpectedly, a variety of transcripts in the mevalonate pathway (Hmgcr, Pmvk, Sqle, Lss, Cyp51, Sc4mol, Idil and Fdft1) and those involved with cholesterol regulation (Soat1, Lip1, Abca1, Abcg1, Npc2, Ldlr, Oldlr, Vldlr and Srebf2) were significantly upregulated (Table 3.13). The most profound change in this category was Ch25H which increased 19-fold. Additionally, several other genes involved with bile acid synthesis were also induced including Cyp7b1 and Hsd3b7 whereas Cyp27a1 was downregulated (Table 3.13).

In the fast-twitch muscle from male rats treated with cerivastatin (1 mg/kg) only 54 out of 11,921 detectable probes were differentially expressed and this is consistent with the lack of myopathy (Table 2.2, 3.14). Specifically, several transcripts for nuclear receptors were upregulated, including Nr1d1, Nr1d2 and Nr4a1 whereas the transcription factor Foxo1a was downregulated. Additionally several genes involved with a stress response were transcriptionally induced, including Hspa1a, Hspa1b, Dnajb1 and Cygb.

In the slow-twitch muscles from cerivastatin (0.5 mg/kg) treated female rats 57 out of 13,573 detectable probes were differentially expressed (Table 3.15). Specifically, several transcripts involved with energy metabolism were induced, including Hk2, nuclear receptors Nr4a2 and Nr4a3 and the peroxisome proliferative activated receptor, gamma, coactivator 1 alpha (Ppargc1a or PGC-1α). Alterations in energy metabolism were also supported by transcriptional modulation of Ucp3 and Rrad which results in increased oxidative phosphorylation and modulation of glucose and lipid utilization, respectively (Table 3.15; Bezaire et al., 2007; Casey et al., 2008). More than 50% of the differentially expressed transcripts were without ontology.

In the slow-twitch muscles from cerivastatin (1 mg/kg) treated female rats 29 out of 13,500 detectable probes were differentially expressed (Table 3.16). A perturbation in energy metabolism was suggested by a transcriptional increase in the nuclear receptor Nr1d2 and the kinase Phka1 which increases glycogen degradation for glycolysis. Transcriptional induction of Mt1a was increased 10-fold indicating oxidative stress and Il10 was increased suggesting an anti-inflammatory response (Table 3.16; Chapter 1.6.1).

Additional transcriptional changes were also observed, including upregulation of the transporters Kctd13 and Trpv4 which may indicate a dysregulation of electrolyte (calcium and potassium) homeostasis (Table 3.16).

To further examine the fiber specific response the differential expression of common probes in fast- and slow-twitch muscles from cerivastatin (1 mg/kg) relative to vehicle treated female rats was determined (Table 3.17). Four probes, including the nuclear receptor Nr1d2, the priming enzyme for glycogen synthesis, Gyg1, and two transcripts without ontology (LOC684802 and RGD1307838), showed a differential response relative to the respective vehicle group (Table 3.17). To further examine the dose response, differential expression of common probes in fast-twitch muscles from female rats treated with 0.5 and 1 mg/kg of cerivastatin relative to vehicle treated rats was determined (Table 3.18). Several transcripts involved with energy metabolism (G0s2, Klf15 and Tulp4), regulation of muscle mass (Csrp3 and Lmcd1) as well as the cell stress response (Dnajb1 and Sesn1) were differentially expressed at both dosages (Table 3.18). Furthermore, Nr1d2 was also differentially expressed and was the only transcript to change in a fiber and dose dependent manner. Fast-twitch muscles from female and male rats treated with 0.5 and 1 mg/kg of cerivastatin, respectively showed minimal to no myopathy. Therefore, the differential expression of common probes in these muscles relative to vehicle treated rats was determined (Table 3.19). For this analysis, only three common probes were identified including one involved with the stress response (Dnajb1) as well as the nuclear receptors Nr1d1 and Nr1d2.

3.4. Discussion

Transcriptional profiles of fiber- and sex-specific differences have been previously determined in mice and humans (Campbell et al., 2001; Chemello et al., 2011; Kang et al., 2005; Maher et al., 2009; Welle et al., 2008; Yoshioka et al., 2007; Zierath et al., 2004). Furthermore, differential expression profiles have been useful for investigating specific molecular targets and pathways associated with skeletal muscle injury, atrophy and hypertrophy in several species (Bialek et al., 2011; Chen et al., 2007; De Souza et al., 2006; Komamura et al., 2003; Mahoney et al., 2008; Marotta et al., 2009; Pearen et al., 2009; Sanoudou et al., 2003; Spurlock et al, 2006; Stevenson et al., 2003). Although the rat is commonly used for evaluation of preclinical drug-induced myopathy, fiber- and sex-specific transcriptional profiles have not been established in this species. Therefore, the goal of the current work was to determine the fiber- and sex specific transcriptional profiles of skeletal muscles in naïve rats and use differential gene expression to investigate molecular targets or pathways causally related to statin-induced myopathy (Table 2.2).

In the current work, differential expression of the most abundant transcripts correlated with the skeletal muscle fiber phenotype, including energy metabolism and sarcomeric proteins which has been previously shown in mice (Yoshioka et al., 2007). Furthermore, these results were consistent with the protein expression pattern and biochemistry previously established for these muscle fibers in other species (Campbell et al., 2001; Guyton and Hall, 2006; Kang et al., 2005; Okumura et al., 2005; Zierath et al., 2004). However, some of the transcripts, like hemoglobin and those involved with the extracellular matrix may have originated from other cell types in the muscle, including

fibroblasts in the connective layers, endothelial and smooth cells in the vessel walls, blood cells within the vessels, nerves and Schwann cells around the axons which has been previously described in mice (Chemello et al., 2011). Despite this limitation, transcriptional profiling was able to discriminate between fast- and slow-twitch muscle fibers in the rat.

The most abundant transcripts in female and male fast-twitch muscles were not different, indicating the phenotype of these muscles are similar. However, differential expression of all probe sets indicated subtle changes in several functional categories with a large number of transcripts without ontology. The most profound sex difference was represented by transcripts involved with energy metabolism. Specifically a more oxidative phenotype in female rats was observed which is consistent with literature reports in mice and humans (Haren et al., 2011; Maher et al., 2009; Salehzadeh et al., 2011; Yoshioka et al., 2007).

The fast-twitch muscles from cerivastatin (1 mg/kg) treated female rats showed a severe myopathy which was reflected by the profound transcriptional response in which approximately 50% of the detectable probes were differentially expressed. As noted in the results, differential expression of such a large number of transcripts is associated with pathology (Foster et al., 2007). Therefore, a limitation of the present results is that transcriptional changes were only analyzed after 14 days of dosing cerivastatin (1 mg/kg), a time when there was severe myopathy in the fast-twitch muscles. Since this frank pathology likely obscures subtle, potentially informative transcriptional changes,

while favoring the identification of genes involved with energy metabolism, cell stress and inflammation a comprehensive evaluation of the transcriptional changes was not conducted. Instead, only a survey of the most abundant transcripts was evaluated to determine the major functional categories modulated with myopathy. However, there was an unexpected upregulation for many of the transcripts in the mevalonate pathway and cholesterol regulation. While upregulation of cholesterol biosynthesis transcripts is a common response associated with hepatotoxicity, HMG-CoA reductase inhibition is also known to cause a similar compensatory hepatic effect in the absence of pathology, particularly in the rat (Foster et al., 2007; Fujioka et al., 1995). Therefore, it is unknown whether this skeletal muscle specific response is mediated by pharmacology, toxicity or regeneration. However, Morikawa et al (2005) also showed transcriptional induction of genes in the cholesterol biosynthetic pathway in L6 myotubes and in a human skeletal muscle cell line following statin treatment and suggested this response may be related to the pathogenesis of muscle damage. Furthermore, Draeger et al (2010) observed a similar transcriptional induction of HMG-CoA reductase in human muscles following statin treatment.

In skeletal muscles from cerivastatin treated rats with minimal to no myopathy the transcriptional profiles may be more informative of specific molecular targets which are causally related to the mechanism of statin-induced myopathy. More specifically, while there were a variety of fiber- and sex-specific transcriptional differences which may be important, there was also a common response across muscles characterized by modulation of several nuclear receptors including Nr1d1, Nr1d2, Nr4a1, Nr4a2 and

Nr4a3 as well as transcripts involved with energy metabolism, including the coactivator PGC-1α in the slow-twitch muscle which is necessary and sufficient to increase mitochondrial content, respiratory capacity and fiber switching to a more oxidative phenotype (Wende et al., 2005).

The nuclear receptors Nr1d1 and Nr1d2 regulate a number of physiological functions, including circadian rhythm, carbohydrate and lipid metabolism, skeletal muscle differentiation and inflammation (Burris, 2008). The ligand for Nr1d1 and Nr1d2 is heme which increases affinity of the receptors to promoters thereby modulating repression of genes involved with a variety of physiological functions (Buriss, 2008). Intracellular heme levels are also coupled to PGC-1α expression, therefore a link between nutritional status, heme levels and skeletal muscle function exists (Burris, 2008). Heme is a porphyrin that is an essential prosthetic group for many proteins critical for muscle function including myoglobin and cytochrome oxidase (Buriss, 2008). Heme also increases expression of myoglobin, mitochondrial biogenesis, aerobic capacity and differentiation in skeletal muscle and these effects may be mediated by PGC-1α expression (Burris, 2010). Therefore, a direct link exists between transcriptional induction of Nr1d1 and Nr1d2 and skeletal muscle function. In contrast, the orphan nuclear receptors in the Nr4a subfamily function as ligand-independent transcription factors. These nuclear receptors are early-response genes induced by a variety of stimuli, including growth factors, cell stress and inflammation and are involved with regulating important functions including energy metabolism, proliferation, differentiation, survival and inflammation (Zhao and Bruemmer, 2010). While these transcriptional results do not

demonstrate a mode of action for statin-induced myopathy they do provide potential molecular targets which may be causally related to the mechanism. Furthermore, a common theme of altered energy metabolism and cell stress was observed suggesting differential regulation of these pathways in a fiber- and sex-dependent manner may be important. This conclusion is consistent with recent literature reports indicating that statin-induced myopathy is a metabolic muscle disease in which glucose utilization and mitochondrial function is impaired in fast-twitch muscles (Mallinson et al., 2009; Phillips and Haas, 2008).

An important observation from this work is that female slow-twitch muscles were not resistant to the adverse effects of cerivastatin treatment. While myopathy was not observed, transcriptional induction of Mt1a was noted in the slow-twitch muscle suggesting oxidative stress. However, these changes may have been mediated by severe fast-twitch myopathy, which is associated with oxidative stress in these animals. Accordingly, evidence of oxidative stress in the slow-twitch muscle may be secondary to this effect in the fast-twitch muscle. Recent work by Bouitbir et al (2011) in humans and rats indicated that the generation of reactive oxygen species (ROS) represents the triggering factor which induces mitochondrial dysfunction and reduces mitochondrial biogenesis in fast-twitch muscles and this effect is rescued by antioxidants and overexpression of PGC-1α which induces genes involved with ROS removal. In contrast, significantly less ROS is generated in the heart and transcriptional induction of PGC-1α and β and mitochondrial biogenesis is considered the mediator of cardiac protection from statin treatment (Bouitbir et al., 2011). Given that the slow-twitch phenotype is more

similar to the heart than fast-twitch fibers it may be that similar mechanisms, including PGC-1α expression protects slow-twitch muscle fibers from statin-induced myopathy. Although this is a plausible mechanism, cardiotoxicity was observed with cerivastatin (Table 2.2), whereas the slow-twitch muscles were resistant. Therefore, additional factors are likely important in the mechanism of cerivastatin-induced myopathy in fast-twitch muscles.

In summary, the current work demonstrates that gene expression profiles can discriminate fiber- and sex-specific transcriptional differences in the rat which are consistent with other species. Furthermore, this work provides novel molecular targets in the skeletal muscle which may be important in mediating cerivastatin-induced myopathy. Follow up investigative studies were conducted in subsequent chapters to further explore the role of altered cholesterol homeostasis and energy metabolism as potential mechanisms of cerivastatin-induced myopathy.

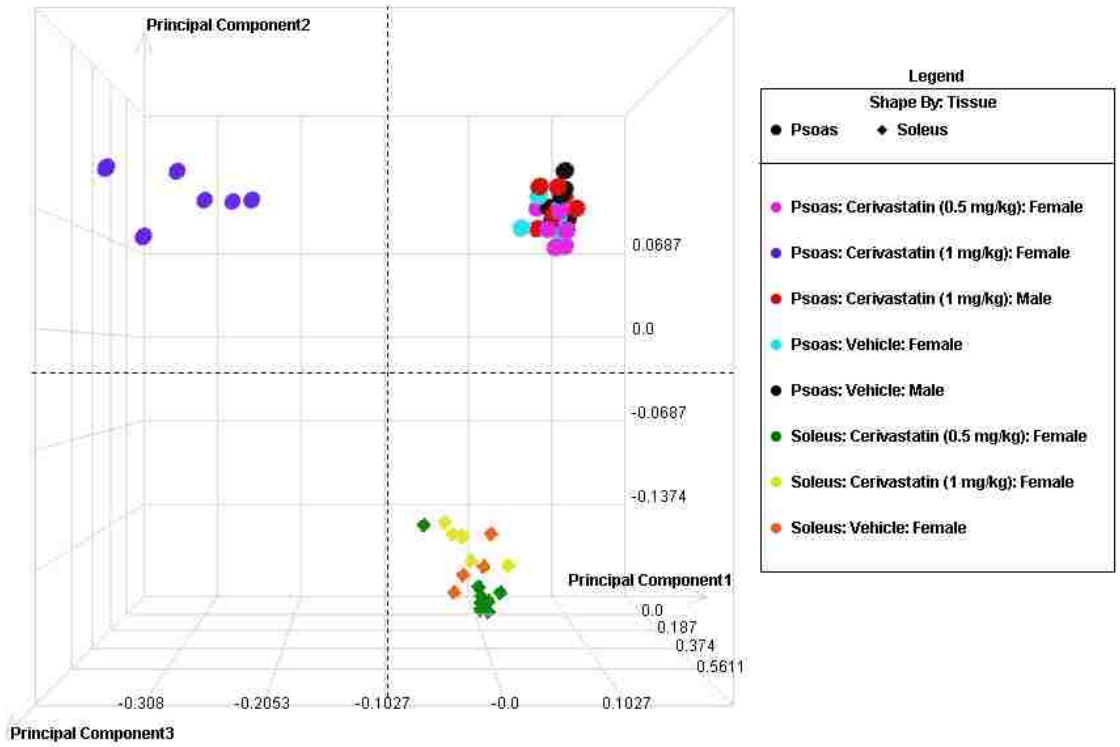

Figure 3.1. PCA analysis of skeletal muscle transcriptional profiles. A PCA analysis of all treatment groups identified two points of separation. Specifically, fast- and slow-twitch muscle fibers from female rats were separated in principal component 2, whereas fast-twitch muscles from vehicle and cerivastatin treated female rats showing evidence of severe myopathy were separated in principal component 1. In contrast, fast-twitch muscles from both female and male rats clustered together, and regardless of treatment all slow-twitch muscles were generally clustered together.

Table 3.1. Differential expression of the most abundantly expressed genes in the female rat fast- relative to slow-twitch skeletal muscles[ab]

Category	Accession #	Differential gene expression[b]	Sequence name	Sequence Description
Glycolysis				
	BI283882	3.6	Gpi	glucose phosphate isomerase
	BI291434	3.5	Pfkm	phosphofructokinase, muscle
	NM_017025	3.2	Ldha	lactate dehydrogenase A
	NM_053297	3.0	Pk	pyruvate kinase isozyme M2 - rat
	NM_031715	2.7	Pfkm	phosphofructokinase, muscle
	NM_017328	2.4	Pgam2	phosphoglycerate mutase 2
	NM_012949	2.0	Eno3	enolase 3, beta
	NM_022922	1.9	Tpi1	triosephosphate isomerase 1
	NM_012495	1.6	Aldoa	aldolase A
	NM_017008	1.5	Gapd	glyceraldehyde-3-phosphate dehydrogenase
Glycogen metabolism				
	AI717476	3.2	Pygm	muscle glycogen phosphorylase
	BI277505	2.9	Pgm1	phosphoglucomutase 1
	AW919180	2.4	Pygm	muscle glycogen phosphorylase
	BI275633	2.3	Pygm	muscle glycogen phosphorylase
Citric acid cycle and oxidative phosphorylation				
	NM_058213	2.2	Atp2a1	ATPase, Ca++ transporting, cardiac muscle, fast twitch 1
	NM_033235	-	Mdh1	malate dehydrogenase 1, NAD (soluble)
	NM_013177	-	Got2	glutamate oxaloacetate transaminase 2 \
	NM_053756	-	Atp5g3	ATP synthase, H+ transporting, mitochondrial F0 complex, subunit c (subunit 9), isoform 3
	AA893531	-	Atp5f1	ATP synthase, H+ transporting, mitochondrial F0 complex, subunit b, isoform 1
	NM_019383	-	Atp5h	ATP synthase, H+ transporting, mitochondrial F0 complex, subunit d
	NM_017311	-	Atp5g1	ATP synthase, H+ transporting, mitochondrial F0 complex, subunit c (subunit 9), isoform 1
	M19044	-	Atp5b	ATP synthase, H+ transporting, mitochondrial F1 complex, beta polypeptide
	BI275939	-	Atp5c1	ATP synthase, H+ transporting, mitochondrial F1 complex, gamma polypeptide 1
	J05266	-	Atp5a1	ATP synthase, H+ transporting, mitochondrial F1 complex, alpha subunit, isoform 1
	AF010323	-	Atp5e	ATP synthase, H+ transporting, mitochondrial F1 complex, epsilon subunit
	BG666921	-	Ndurfb9	NADH dehydrogenase (ubiquinone) 1 beta subcomplex, 9
	BG666002	-	Ndufa4	NADH dehydrogenase (ubiquinone) 1 alpha subcomplex, 4
	AI231358	-	Ndufs7	NADH dehydrogenase (ubiquinone) Fe-S protein 7 (predicted)
	AI555535	-	Ndurfb3	NADH dehydrogenase (ubiquinone) 1 beta subcomplex 3
	NM_012812	-	Cox6a2	cytochrome c oxidase, subunit VIa, polypeptide 2
	NM_019360	-	Cox6c	cytochrome c oxidase, subunit VIc
	NM_012786	-	Cox8h	cytochrome c oxidase subunit VIII-H (heart/muscle)
	X15030	-	Cox5a	cytochrome c oxidase, subunit Va
	AI104240	-	Cycs	cytochrome c, somatic
	NM_017202	-	Cox4i1	cytochrome c oxidase subunit IV isoform 1
	AA866477	-	Cox7b	cytochrome c oxidase subunit VIIb
	NM_022503	-	Cox7a3	cytochrome c oxidase, subunit 7a 3
	NM_053586	-	Cox5b	cytochrome c oxidase subunit Vb
	BI296109	-	Uqcrc2	ubiquinol-cytochrome c reductase core protein II
	BG670074	-	Uqcrb	ubiquinol-cytochrome c reductase binding protein
Creatine phosphate synthesis				
	NM_012530	-	Ckm	creatine kinase, muscle
	AA799557	-	Ckmt2	creatine kinase, mitochondrial 2
Sarcomere and cytoskeleton				
	AW533848	13.4	Mybpc2	myosin binding protein C, fast-type
	BG378588	11.1	Mybpc2	myosin binding protein C, fast-type
	BI277545	9.6	Myh1	type 2X myosin heavy chain
	NM_133424	7.2	Actn3	actinin alpha 3
	BM391169	4.2	Myh4	myosin, heavy polypeptide 4, skeletal muscle
	AI716887	4.2	RGD1561064	similar to myozenin 1
	AF372216	2.4	Tpm1	tropomyosin 1, alpha
	NM_017185	2.3	Tnni2	troponin 1, type 2, skeletal fast
	BF521859	2.2	Tnnt3	troponin T3, skeletal, fast
	NM_019131	2.2	Tpm1	tropomyosin 1, alpha
	NM_012605	1.8	Myl2	myosin, light polypeptide 2
	NM_019212	-	Acta1	actin, alpha 1, skeletal muscle
	NM_020104	-	Myl1	myosin, light polypeptide 1
	BF417385	-	Tpm2	tropomyosin 2, beta
	BI289527	-	Tmod4	tropomodulin 4
	NM_022531	-	Des	desmin
	BF552973	-	Myot	titin immunoglobulin domain protein (myotilin)
	AI104533	-	Ttn	similar to N2B-Titin Isoform

[a]The most abundantly expressed transcripts represent the top 1% (125 probes) of the 12,482 probe sets expressed on the microarray.

[a]The most abundantly expressed transcripts had an arbitrary intensity of 3,017 to 10,822 whereas all other transcripts had an intensity of 12 to 3,016.

[b]Differential gene expression representing the fold change was determined at $p<0.01$ with a fold change $\geq \pm 1.5$. (-) Indicates no transcriptional difference.

Table 3.2. Differential expression of the most abundantly expressed genes in the female rat fast- relative to slow-twitch skeletal muscles[ab]

Category	Accession #	Differential gene expression[b]	Sequence name	Sequence Description
Immune, inflammatory response and cell stress				
	D29960	-	Hspd6	heat shock protein, alpha-crystallin-related, B6
	AA866458	-	Csda	cold shock domain protein A
	NM_024351	-	Hspa8	heat shock protein 8
	NM_012935	-1.9	Cryab	crystallin, alpha B
Metabolism				
	NM_022676	2.1	Pp1r1a	protein phosphatase 1, regulatory (inhibitor) subunit 1A
	J02811	2.1	Ampd1	adenosine monophosphate deaminase 1 (isoform M)
	AB030829	-	Ca3	carbonic anhydrase 3
	AI411388	-	Oaz1	ornithine decarboxylase antizyme 1
	NM_019292	-1.9	Ca3	carbonic anhydrase 3
Regulation of transcription and translation				
	BI281697	-	RPl17a	ribosomal protein L7a
	AI177054	-	Rpl27a	ribosomal protein L27a
	NM_017152	-	Rps17	ribosomal protein S17
	NM_022506	-	Rp131	ribosomal protein L31
	BG666892	-	RP19	ribosomal protein L9
	AI229633	-	RPS29	ribosomal protein S29
	AA848284	-	Rps23	ribosomal protein S23
	BM388159	-	RPl32	ribosomal protein L32
	NM_031103	-	RPl19	ribosomal protein L19
	A1598536	-	RPl26	ribosomal protein L26
	NM_017153	-	Rps3a	ribosomal protein S3a
	BG666872	-	Rps16	ribosomal protein S16
	AA944861	-	Rps2	ribosomal protein S2
	AW914118	-	Rpl35	ribosomal protein L35
	NM_031099	-	Rpl15	ribosomal protein L5
	AA799501	-	Rps4x	ribosomal protein S4, X-linked
	NM_022672	-	Rps14	ribosomal protein S14
	NM_022402	-	Arbp	acidic ribosomal phosphoprotein P0
	NM_012660	-	Eef1a2	Elongation factor 1a2
	BI282111	-	Nsep1	nuclease sensitive element binding protein 1
	NM_133583	-	Ndrg2	N-myc downstream regulated gene 2
	AW434961	-	Hfe2	RGM domain family, member C
	BI279866	-	L18a	similar to 60S ribosomal protein L18a
	BG673187	-1.8	Fhl1	four and a half LIM domains 1
Transporters				
	BG666999	-	Slc25a4	solute carrier family 25 (mitochondrial adenine nucleotide translocator) member 4
	M23984	-	Slc255a3	solute carrier family 25 (mitochondrial carrier; adenine nucleotide translocator), member 3
	NM_031355	-	Vdac3	voltage-dependent anion channel 3
	NM_031353	-	Vdac1	voltage-dependent anion channel 1
	NM_012505	-	ATP1a2	ATPase, Na+/K+ transporting, alpha 2 polypeptide
Miscellaneous				
	A1175539	8.4	Pvalb	parvalbumin
	BI302005	2.3	Mlf1	myeloid leukemia factor 1
	BF284168	1.7	H19	H19 fetal liver mRNA
	NM_021588	-	Mb	myoglobin
	AI179404	-	Hba-a1	hemoglobin alpha 2 chain
	A1179404	-	Hba-a1	hemoglobin alpha 2 chain
	NM_033234	-	Hbb	hemoglobin beta chain complex
	NM_012848	-	Fth1	ferritin, heavy polypeptide 1
	NM_053867	-	Tpt1	tumor protein, translationally-controlled 1
	BI282332	-	MGC105647	similar to Nur77 downstream protein 2
	AA800892	-	RGD1563599	similar to putative SH3BGR protein
	A1012372	-	Sui1-rs1	suppressor of initiator codon mutations, related sequence 1
	D16554	-	Ubb	polyubiquitin
	A1406651	-	Serf2	small EDRK-rich factor 2
	AA944393	-	MGC72942	similar to CG6105-PA
Without ontology				
	BI276959	2.4		
	BG663128	1.8		
	AI230164	-		
	A1170758	-		
	AA849795	-		
	AI180257	-		
	A1104151	-		
	AA799471	-		
	A1008105	-		
	BF395095	-		
	AI228039	-		
	A1104326	-		

[a]The most abundantly expressed transcripts represent the top 1% (125 probes) of the 12,482 probe sets expressed on the microarray.

[a]The most abundantly expressed transcripts had an arbitrary intensity of 3,017 to 10,822 whereas all other transcripts had an intensity of 12 to 3,016.

[b]Differential gene expression representing the fold change was determined at $p<0.01$ with a fold change $\geq \pm 1.5$. (-) Indicates no transcriptional difference.

Table 3.3. Differential expression of the most abundantly expressed genes in the female rat slow- relative to fast-twitch skeletal muscles [ab]

Category	Accession #	Differential gene expression[b]	Sequence name	Sequence description
Glycolysis				
	AA848319	4.9	Ldhb	lactate dehydrogenase B
	NM_017008	-1.5	Gapd	glyceraldehyde-3-phosphate dehydrogenase
	NM_012495	-1.6	aldoa	aldolase A
	NM_022922	-1.9	Tpi1	triosephosphate isomerase 1
	NM_012949	-2.0	Eno3	enolase 3, beta
	NM_017328	-2.4	Pgam2	phosphoglycerate mutase 2
Fatty acid oxidation				
	NM_133618	-	Hadhb	hydroxyacyl-Coenzyme A dehydrogenase/3-ketoacyl-Coenzyme A thiolase/enoyl-Coenzyme A hydratase (trifunctional protein), beta subunit
Citric acid cycle and oxidative phosphorylation				
	NM_017290	4.0	Atp2a2	ATPase, Ca++ transporting, cardiac muscle, slow twitch 2
	AI172491	1.7	LOC361596	similar to NADP+-specific isocitrate dehydrogenase
	NM_033235	-	Mdh1	malate dehydrogenase 1, NAD (soluble)
	AI172320	-	Sdhb	succinate dehydrogenase complex, subunit B, iron sulfur
	NM_024398	-	Aco2	aconitase 2, mitochondrial
	M19044	-	Atp5b	ATP synthase, H+ transporting, mitochondrial F1 complex, beta polypeptide
	NM_053756	-	Atp5g3	ATP synthase, H+ transporting, mitochondrial F0 complex, subunit c (subunit 9), isoform 3
	BI275939	-	Atp5c1	ATP synthase, H+ transporting, mitochondrial F1 complex, gamma polypeptide 1
	J05266	-	Atp5a1	ATP synthase, H+ transporting, mitochondrial F1 complex, alpha subunit, isoform 1
	AF010323	-	Atp5e	ATP synthase, H+ transporting, mitochondrial F1 complex, epsilon subunit
	AA893531	-	Atp5f1	ATP synthase, H+ transporting, mitochondrial F0 complex, subunit b, isoform 1
	NM_019383	-	Atp5h	ATP synthase, H+ transporting, mitochondrial F0 complex, subunit d
	NM_017311	-	Atp5g1	ATP synthase, H+ transporting, mitochondrial F0 complex, subunit c (subunit 9), isoform 1
	BG666921	-	Ndufb9	NADH dehydrogenase (ubiquinone) 1 beta subcomplex, 9
	BG666002	-	Ndufa4	NADH dehydrogenase (ubiquinone) 1 alpha subcomplex, 4
	AI555535	-	Ndurfb3	NADH dehydrogenase (ubiquinone) 1 beta subcomplex 3
	AI231358	-	Ndufs7	NADH dehydrogenase (ubiquinone) Fe-S protein 7
	NM_012786	-	Cox8h	Cytochrome c oxidase subunit VIII-H (heart/muscle)
	NM_019360	-	Cox6c	cytochrome c oxidase, subunit VIc
	NM_017202	-	Cox4i1	cytochrome c oxidase subunit IV isoform 1
	AA866477	-	Cox7b	cytochrome c oxidase subunit VIIb
	X15030	-	Cox5a	cytochrome c oxidase, subunit Va
	NM_022503	-	Cox7a3	cytochrome c oxidase, subunit 7a 3
	NM_053586	-	Cox5b	cytochrome c oxidase subunit Vb
	AI104240	-	Cycs	cytochrome c, somatic
	NM_012812	-	Cox6a2	cytochrome c oxidase, subunit VIa, polypeptide 2
	BI296109	-	Uqcrc2	ubiquinol-cytochrome c reductase core protein II
	BG670074	-	Uqcrb	ubiquinol-cytochrome c reductase binding protein
	NM_058213	-2.2	Atp2a1	ATPase, Ca++ transporting, cardiac muscle, fast twitch 1
Creatine phosphate synthesis				
	NM_012530	-	Ckm	creatine kinase, muscle
	AA799557	-	Ckmt2	creatine kinase, mitochondrial 2
Sarcomere and cytoskeleton				
	AA849895	10.0	Ankrd2	ankyrin repeat domain 2 (stretch responsive muscle)
	BF395647	9.4	Myh7	myosin, heavy polypeptide 7, cardiac muscle, beta
	NM_017184	7.4	Tnni1	troponin I, skeletal, slow 1
	AI104354	7.2	Myoz2	myozenin 2
	NM_017240	6.7	Myh7	myosin, heavy polypeptide 7, cardiac muscle, beta
	AF399874	6.2	Tnnt1	troponin T1, skeletal, slow
	AI710682	5.1	Tncc	troponin C, cardiac/slow skeletal
	NM_057144	4.9	Csrp3	cysteine-rich protein 3
	NM_012606	4.3	Myl3	myosin, light polypeptide 3
	BF419995	3.1	Mlc2	myosin regulatory light chain 2, ventricular/cardiac muscle isoform
	BF284889	2.3	Actn2	actinin alpha 2
	BM386665	1.8	Nrap	nebulin-related anchoring protein
	NM_019212	-	Acta1	actin, alpha 1, skeletal muscle
	BM389619	-	Mybpc1	myosin binding protein C, slow type
	NM_020104	-	Myl1	myosin, light polypeptide 1
	BF417385	-	Tpm2	tropomyosin 2, beta
	BI289527	-	Tmod4	tropomodulin 4
	NM_022531	-	Des	desmin
	AI104533	-	Ttn	similar to N2B-Titin Isoform
	BF552973	-	Myot	titin immunoglobulin domain protein (myotilin)
	BE113393	-	Synpo2	similar to Synaptopodin-2
	BI296011	-	Cfl2	cofilin 2, muscle
	NM_012605	-1.8	Myl2	myosin, light polypeptide 2
	BF521859	-2.2	Tnnt3	troponin T3, skeletal, fast
	NM_019131	-2.2	Tpm1	tropomyosin 1, alpha
	NM_017185	-2.3	Tnni2	troponin 1, type 2

[a]The most abundantly expressed transcripts represent the top 1% (131 probes) of the 13,112 probe sets expressed on the microarray.
[a]The most abundantly expressed transcripts had an arbitrary intensity of 2,927 to 9,916 whereas all other transcripts had an intensity of 12 to 2,922.
[b]Differential gene expression representing the fold change was determined at $p<0.01$ with a fold change $\geq \pm 1.5$. (-) Indicates no transcriptional difference.

Table 3.4. Differential expression of the most abundantly expressed genes in the female rat slow- relative to fast-twitch skeletal muscles [ab]

Category	Accession #	Differential gene expression[b]	Sequence name	Sequence description
Immune, inflammatory response and cell stress				
	BM390305	8.0	Hspb7	heat shock 27kD protein family, member 7 (cardiovascular)
	NM_012935	1.9	Cryab	crystallin, alpha B
	NM_031970	1.8	Hspb1	heat shock 27kDa protein 1
	D29960	-	Hspb6	heat shock protein, alpha-crystallin-related, B6
	NM_024351	-	Hspa8	heat shock protein 8
	AA866458	-	Csda	cold shock domain protein A
Metabolism				
	S41066	2.4	Gpx1	glutathione peroxidase 1
	NM_019292	1.9	Ca3	carbonic anhydrase 3
	AB030829	-	Ca3	carbonic anhydrase 3
Regulation of transcription and translation				
	BI298356	2.3	Fhl1	four and a half LIM domains 1
	BG673187	1.8	Fhl1	four and a half LIM domains 1
	AI177054	-	Rp127a	ribosomal protein L27a
	BI281697	-	Rp17a	ribosomal protein L7a
	NM_017152	-	Rps17	ribosomal protein S17
	AA848284	-	Rps23	ribosomal protein S23
	BI279866	-	MGC72957	similar to 60S ribosomal protein L18a
	BG666892	-	Rpl9	ribosomal protein L9
	NM_031103	-	Rpl19	ribosomal protein L19
	AI229633	-	Rps29	ribosomal protein S29
	NM_022506	-	Rp131	ribosomal protein L31
	NM_017153	-	Rps3a	ribosomal protein S3a
	BG666872	-	Rps16	ribosomal protein S16
	AW914118	-	Rp135	ribosomal protein L35
	NM_022672	-	Rps14	ribosomal protein S14
	BM388159	-	Rp132	ribosomal protein L32
	NM_031706	-	Rps8	ribosomal protein S8
	AI598536	-	Rp126	ribosomal protein L26
	AA799501	-	Rps4x	ribosomal protein S4, X-linked
	NM_031099	-	Rpl5	ribosomal protein L5
	AA944861	-	Rps2	ribosomal protein S2
	BG375811	-	Rps24	ribosomal protein S24
	NM_022402	-	Arbp	acidic ribosomal phosphoprotein P0
	AW914090	-	Rplp1	ribosomal protein, large, P1
Transporters				
	BG666999	-	Slc25a4	solute carrier family 25 (mitochondrial adenine nucleotide translocator) member 4
	M23984	-	Slc25a3	solute carrier family 25 (mitochondrial carrier; adenine nucleotide translocator), member 3
	NM_031353	-	Vdac1	voltage-dependent anion channel 1
Miscellaneous				\
	NM_024162	2.3	Fabp3	fatty acid binding protein 3
	BI285575	2.2	Col1a1	collagen, type 1, alpha 1
	NM_021588	-	Mb	myoglobin
	AI179404	-	Hba-a1	hemoglobin alpha 2 chain
	AI179404	-	Hba-a1	hemoglobin alpha 2 chain
	NM_012848	-	Fth1	ferritin, heavy polypeptide 1
	BI275716	-	Col3a1	collagen, type III, alpha 1
	NM_053867	-	Tpt1	tumor protein, translationally-controlled 1
	AI012372	-	Sui1-rs1	suppressor of initiator codon mutations, related sequence 1
	NM_012512	-	B2m	beta-2 microglobulin
	NM_133583	-	Ndrg2	N-myc downstream regulated gene 2
	BI282111	-	Nsep1	nuclease sensitive element binding protein 1
	AI233054	-	Qpc	low molecular mass ubiquinone-binding protein
	BI282332	-	MGC105647	similar to Nur77 downstream protein 2
	AA891707	-	Usmg5	upregulated during skeletal muscle growth 5
	BF284168	-1.7	H19	H19 fetal liver mRNA
Without ontology				
	AI230220	33.4		
	AI599017	5.5		
	BM384301	2.8		
	AI230164	-		
	AI170758	-		
	AI180257	-		
	AA849795	-		
	AI104151	-		
	AA799471	-		
	AI008105	-		
	AI228039	-		
	AA944393	-		
	BF395095	-		
	BG663128	-1.8		

[a]The most abundantly expressed transcripts represent the top 1% (131 probes) of the 13,112 probe sets expressed on the microarray.
[a]The most abundantly expressed transcripts had an arbitrary intensity of 2,927 to 9,916 whereas all other transcripts had an intensity of 12 to 2,922.
[b]Differential gene expression representing the fold change was determined at $p<0.01$ with a fold change $\geq \pm 1.5$. (-) Indicates no transcriptional difference.

Table 3.5. Differential expression of genes in the fast-twitch muscle from female relative to male rats[a]

Category	Accession #	Differential gene expression[a]	Sequence name	Sequence Description
Energy metabolism				
	NM_031511	2.1	Igf2	insulin-like growth factor 2
	BI303527	2.1	Arrdc3	arrestin domain containing 3
	NM_022290	2.1	Tnmd	tenomodulin
	NM_053551	2.0	Pdk4	pyruvate dehydrogenase kinase, isoenzyme 4
	BI295878	1.8	Kat3	kynurenine aminotransferase III
	NM_134387	1.6	Dcxr	dicarbonyl L-xylulose reductase
	NM_022400	1.6	Bcat2	branched chain aminotransferase 2, mitochondrial
	U92069	1.6	Ucp3	uncoupling protein 3
	AY057895	1.5	Adrb2	adrenergic receptor, beta 2
	NM_133606	1.5	Ehhadh	enoyl-Coenzyme A, hydratase/3-hydroxyacyl Coenzyme A dehydrogenase
	BG673588	1.5	Igfbp6	insulin-like growth factor binding protein 6
	AI176565	1.5	Acas2l	acetyl-Coenzyme A synthetase 2 (AMP forming)-like
	NM_012793	-1.5	Gamt	guanidinoacetate methyltransferase
	NM_012969	-1.6	Irs1	insulin receptor substrate 1
Immune, inflammatory response and cell stress				
	NM_133380	2.1	Il4r	interleukin 4 receptor
	AF307302	1.9	H2-Aa	histocompatibility 2, class II antigen A, alpha
	X89963	2.1	Thbs4	thrombospondin 4
	NM_053843	1.7	Fcgr2a	similar to Fc gamma (IgG) receptor II (low affinity) alpha precursor - rat
	BF387360	1.7	RGD1559482	similar to immunoglobulin superfamily, member 7
	L12458	1.7	Lyz	lysozyme
	NM_013069	1.7	Cd74	CD74 antigen (invariant polypeptide of major histocompatibility class II antigen-associated)
	BG671521	1.6	Hspca	heat shock protein 1, alpha
	NM_031348	1.6	Fcna	ficolin A
	BI285141	1.6	Cd24	CD24 antigen
	BF418957	1.6	C1qa	complement component 1, q subcomponent, alpha polypeptide
	AW915763	1.5	Serping1	serine (or cysteine) peptidase inhibitor, clade G, member 1
	AI411618	1.5	C1qg	complement component 1, q subcomponent, gamma polypeptide
	NM_017079	1.5	CD1d1	CD1d1 antigen
	AA925924	-1.6	Crlf1	cytokine receptor-like factor 1
	AI176519	-1.9	Ler3	immediate early response 3
	AI406687	-1.9	Cklfsf6	chemokine-like factor super family 6
	AI407339	-2.3	Ifi1	interferon inducible protein 1
Metabolism				
	L32601	2.2	Akr1c18	20 alpha-hydroxysteroid dehydrogenase
	NM_031509	1.6	Gsta5	glutathione S-transferase A5
	NM_022547	1.6	Fthfd	formyltetrahydrofolate dehydrogenase
	AI411117	-1.6	Tst	thiosulfate sulfurtransferase
	AF319950	-1.6	Glrx1	glutaredoxin 1 (thioltransferase)
	NM_022278	-1.6	Glrx1	glutaredoxin 1 (thioltransferase)
	AI408948	-1.8	Ca2	carbonic anhydrase 2
Regulation of transcription and translation				
	NM_012912	3.4	Atf3	activating transcription factor 3
	J03933	2.2	Thrb	thyroid hormone receptor beta
	NM_031678	1.8	Per2	period homolog 2
	BM384099	1.8	Ndrg1	N-myc downstream regulated gene 1
	NM_024388	1.7	Nr4a1	nuclear receptor subfamily 4, group A, member 1
	AI013390	-1.6	Cited2	Cbp/p300-interacting transactivator, with Glu/Asp-rich carboxy-terminal domain
	NM_053698	-1.8	Cited2	Cbp/p300-interacting transactivator, with Glu/Asp-rich carboxy-terminal domain, 2
	AI556378	-2.2	Cited 4	Cbp/p300-interacting transactivator, with Glu/Asp-rich carboxy-terminal domain, 4
Extracellular matrix				
	NM_080698	3.3	Fmod	fibromodulin
	AW251280	2.9	Tna	tetranectin (plasminogen binding protein)
	BE116084	2.1	Xlkd1	extra cellular link domain-containing 1
	AA945955	1.9	Ogn	osteoglycin

[a]Differential gene expression representing fold change was determined at $p<0.01$ with a fold change $\geq \pm 1.5$.

Table 3.6. Differential expression of genes in the fast-twitch muscle from female relative to male rats[a]

Category	Accession #	Differential gene expression[a]	Sequence name	Sequence Description
Miscellaneous				
	BG668493	4.6	Stmn2	stathmin-like 2
	NM_053440	3.7	Stmn2	stathmin-like 2
	NM_080892	2.1	Selenbp1	selenium binding protein 2
	BI284420	1.8	STRA6	similar to retinoic acid-responsive protein
	BI279526	1.8	RT1-Db1	RT1 class II, locus Db1
	NM_031832	1.8	Lgals3	lectin, galactose binding, soluble 3
	AA818521	1.7	Thbd	thrombomodulin
	BG667163	1.7	Ddx3x	DEAD/H (Asp-Glu-Ala-Asp/His) box polypeptide 3, X-linked
	NM_053296	1.7	Glrb	glycine receptor, beta subunit
	BG662620	1.7	Eif2s3x	similar to eukaryotic translation initiation factor 2, subunit 3, structural gene X-linked
	AJ131902	1.7	Gas7	growth arrest specific 7
	BM389311	1.6	RGD1564930	similar to novel protein Tensin
	Y00480	1.6	RT1-Da	RT1 class II, locus Da
	BI286025	1.5	Lmod1	leiomodin 1 (smooth muscle)
	BF284017	-1.5	Raph1	Ras association (RalGDS/AF-6) and pleckstrin homology domains 1, transcript variant 2
	AW520792	-1.6	Vasp	vasodilator-stimulated phosphoprotein
	BM389208	-1.6	Gimap4	GTPase, IMAP family member 4
	M58040	-1.6	Tfrc	transferrin receptor
	BI282699	-1.6	Abr	active BCR-related gene
	AW253616	-1.7	Slc8a1	solute carrier family 8 (sodium/calcium exchanger), member 1
	BM387083	-1.7	Sema6a	sema domain, transmembrane domain (TM), and cytoplasmic domain
	BF525047	-1.8	Actc1	actin alpha cardiac 1
	AA800705	-2.0	Actc1	actin alpha cardiac 1
	J05087	-2.2	Atp2b3	ATPase, Ca++ transporting, plasma membrane 3
	AI112577	-2.4	Gng3	guanine nucleotide binding protein (G protein), gamma 3 subunit
	NM_133621	-2.4	Hod	homeobox only domain
Without ontology				
	AI228978	51.2		
	AI103917	33.7		
	BG374488	6.7		
	AA799294	5.7		
	BF418649	3.0		
	BF408611	3.0		
	BM391248	2.4		
	AI103530	2.1		
	BI278231	2.1		
	AI171466	2.0		
	AI598546	2.0		
	AW433665	2.0		
	AA956555	2.0		
	BE111083	1.9		
	BF414266	1.9		
	H32997	1.9		
	AA945579	1.8		
	BI275923	1.8		
	AI043817	1.7		
	AA858930	1.7		
	AI716248	1.7		
	BE107890	1.6		
	BE108345	1.6		
	AA817956	1.6		
	AI411941	1.6		
	BF555488	1.6		
	BI294018	1.6		
	BI282107	1.5		
	AI227627	1.5		
	BF417285	1.5		
	AI406802	-1.5		
	AA859508	-1.5		
	AA891759	-1.6		
	BE113016	-1.6		
	AI043888	-1.6		
	BI280865	-1.7		
	AI711147	-1.7		
	U30831	-1.7		
	H33003	-1.7		
	AA819332	-1.7		
	BF386499	-1.8		
	AI044729	-1.9		
	BI274589	-2.0		
	AA957707	-2.0		
	AI228970	-2.0		
	AI711147	-2.0		
	BF395080	-2.0		
	BF544005	-2.1		
	AA957509	-2.1		
	AW253907	-2.5		
	AI010831	-2.6		

[a]Differential gene expression representing fold change was determined at $p<0.01$ with a fold change $\geq \pm 1.5$.

Table 3.7. Differential expression of genes in the fast-twitch muscle from cerivastatin (0.5 mg/kg) relative to vehicle treated female rats[a]

Category	Accession #	Differential gene expression[a]	Sequence name	Sequence Description
Energy metabolism				
	NM_053551	1.8	Pdk4	pyruvate dehydrogenase kinase, isoenzyme 4
Regulation of transcription and translation				
	M25804	2.2	Nr1d1	nuclear receptor subfamily 1, group D, member 1
	NM_053698	1.9	Cited2	Cbp/p300-interacting transactivator, with Glu/Asp-rich carboxy-terminal domain, 2
	AI013390	1.7	Cited2	Cbp/p300-interacting transactivator, with Glu/Asp-rich carboxy-terminal domain, 2
	AI602501	1.6	Lmcd1	LIM and cysteine-rich domains 1
	NM_057144	1.6	Csrp3	cysteine-rich protein 3
	NM_053536	1.5	Klf15	Kruppel-like factor 15
	BF564195	-1.5	Crem	cAMP responsive element modulator
Immune, inflammatory response and cell stress				
	AI104331	1.6	Sesn1	sestrin 1
	AA945704	-1.7	Dnajb1	DnaJ (Hsp40) homolog, subfamily B, member 1
	BM384926	-2.0	Dnajb1	DnaJ (Hsp40) homolog, subfamily B, member 1
Miscellaneous				
	AW918724	1.5	Enah	enabled homolog (Drosophila)
	BE117201	-1.6	Uxs1	UDP-glucuronate decarboxylase 1
	BI289103	-1.8	Slc44a4	Ng22 protein (Ng22)
	NM_022296	-1.9	Xylt2	xylosyltransferase II
	AI177358	-2.0	Slc25a25	solute carrier family 25 (mitochondrial carrier, phosphate carrier), member 25
	AI406939	-2.6	G0s2	G0/G1 switch gene 2
Without ontology				
	BE100456	1.9	RGD1559442	
	AI231999	1.7	LOC689256	
	AI070270	-1.5	Tob2	
	AI712476	-1.6	1391431	
	BI296430	-1.6	1378055	
	BF414266	-1.7	Sart3	
	AA858930	-1.6	Pde4b	
	AA891759	1.6	RGD1309437	
	BG381715	-1.5	BG381715	

[a]Differential gene expression representing fold change was determined at $p<0.01$ with a fold change $\geq \pm 1.5$.

Table 3.8. Differential expression of the most abundantly expressed genes in the fast-twitch muscle from cerivastatin (1 mg/kg) relative to vehicle treated female rats[ab]

Category	Accession #	Differential gene expression[b]	Sequence name	Sequence Description
Glycolysis				
	NM_012554	2.9	Eno1	Alpha enolase
	NM_017008	-1.8	Gapdh	glyceraldehyde-3-phosphate dehydrogenase
	NM_053297	-2.1	Pkm2	pyruvate kinase
	NM_017025	-2.2	Ldha	lactate dehydrogenase A
	NM_012495	-2.2	Aldoa	aldolase A
	NM_022922	-2.6	Tpi1	triosephosphate isomerase 1
	NM_012949	-4.2	Eno3	enolase 3, beta
Citric acid cycle and oxidative phosphorylation				
	BE111722	13.4	Ndufs2	NADH dehydrogenase (ubiquinone) Fe-S protein 2
	NM_130823	3.1	Atp6v0c	ATPase, H+ transporting, V0 subunit C
	BG673321	2.0	Cox8a	cytochrome c oxidase, subunit VIIIa
	NM_017202	-	Cox4i1	cytochrome c oxidase subunit IV isoform 1
	AI230604	-	Cox6b1	cytochrome c oxidase, subunit VIb polypeptide 1
	BF281400	-1.5	Atp5j2	ATP synthase, H+ transporting, mitochondrial F0 complex, subunit f, isoform 2
	NM_019383	-1.6	Atp5h	ATP synthase, H+ transporting, mitochondrial F0 complex, subunit d
	BG670074	-1.7	Uqcrb	ubiquinol-cytochrome c reductase binding protein
	NM_022503	-1.7	Cox7a2	cytochrome c oxidase, subunit 7a 3
	AA893531	-1.7	Atp5f1	ATP synthase, H+ transporting, mitochondrial F0 complex, subunit b, isoform 1
	M19044	-1.8	Atp5b	ATP synthase, H+ transporting, mitochondrial F1 complex, beta polypeptide
	NM_053586	-1.8	Cox5b	cytochrome c oxidase subunit Vb
	NM_019360	-1.8	Cox6c	cytochrome c oxidase, subunit VIc
	AA866477	-1.8	Cox7b	cytochrome c oxidase subunit VIIb
	AI233054	-1.8	Qpc	low molecular mass ubiquinone-binding protein
	X15030	-1.8	Cox5a	cytochrome c oxidase, subunit Va
	NM_053756	-1.9	Atp5g3	ATP synthase, H+ transporting, mitochondrial F0 complex, subunit c
	BG666002	-1.9	Ndufa4	NADH dehydrogenase (ubiquinone) 1 alpha subcomplex, 4
	BG666921	-1.9	Ndufb9	NADH dehydrogenase (ubiquinone) 1 beta subcomplex, 9
	AF010323	-2.0	Atp5e	ATP synthase, H+ transporting, mitochondrial F1 complex, epsilon subunit
	AI104240	-2.1	Cycs	cytochrome c, somatic
	J05266	-2.1	Atp5a1	ATP synthase, H+ transporting, mitochondrial F1 complex, alpha subunit, isoform 1
	BI275939	-2.2	Atp5c1	ATP synthase, H+ transporting, mitochondrial F1 complex, gamma polypeptide 1
	NM_012812	-2.7	Cox6a2	cytochrome c oxidase, subunit VIa, polypeptide 2
	NM_058213	-3.6	Atp2a1	ATPase, Ca++ transporting, cardiac muscle, fast twitch 1
Creatine phosphate synthesis				
	NM_012530	-2.4	Ckm	creatine kinase, muscle
Sarcomere and cytoskeleton				
	NM_019289	9.7	Arpc1b	actin related protein 2/3 complex, subunit 1B
	BF525047	7.8	Actc1	actin alpha cardiac 1
	BG666614	7.3	Cfl1	cofilin 1
	AA800705	7.0	Actc1	actin alpha cardiac 1
	BI285434	5.0	Tuba6	tubulin, alpha 6
	NM_031140	4.2	Vim	vimentin
	AW920881	3.3	Actr2	ARP2 actin-related protein 2 homolog (yeast)
	NM_031144	3.3	Actb	actin, beta
	NM_031986	3.3	Sdcbp	syndecan binding protein
	AI009775	3.2	Arpc2_predicted	actin related protein 2/3 complex, subunit 2
	NM_031144	3.1	Actb	actin, beta
	BI285502	2.9	LOC684520	myosin, light polypeptide 6, alkali, smooth muscle and non-muscle
	BG666668	2.7	Actg1	similar to cytoplasmic beta-actin, transcript variant 2
	NM_022511	2.7	Pfn1	profilin 1
	BG668902	2.2	Tmsb4x	thymosin, beta 4
	NM_057144	2.4	Csrp3	cysteine-rich protein 3
	NM_053319	1.8	Dynll1	dynein, cytoplasmic, light chain 1
	X05566	-	Mrlcb	similar to Myosin regulatory light chain 2-A, smooth muscle isoform
	NM_053867	-	Tpt1	tumor protein, translationally-controlled 1
	NM_022531	-	Des	desmin
	AF002281	-1.5	Pdlim3	PDZ and LIM domain 3
	NM_019212	-1.6	Acta1	actin, alpha 1, skeletal muscle
	NM_020104	-1.9	Myl1	myosin, light polypeptide 1
	NM_012605	-1.9	Mylpf	myosin, light polypeptide 2
	BF417385	-2.0	Tpm2	tropomyosin 2, beta
	BF521859	-2.2	Tnnt3	troponin T3, skeletal, fast
	NM_019131	-2.6	Tpm1	tropomyosin 1, alpha
	AF372216	-2.6	Tpm1	tropomyosin 1, alpha
	NM_017185	-2.7	Tnni2	troponin 1, type 2
	AI104533	-3.7	Ttn	N2B-Titin Isoform
	NM_133424	-5.4	Actn3	actinin alpha 3

[a]The most abundantly expressed transcripts represent the top 2% (278 probes) of the 13,947 probe sets expressed on the microarray.
[a]The most abundantly expressed transcripts had an arbitrary intensity of 1,411 to 6,526 whereas all other transcripts had an intensity of 14 to 1,410.
[b]Differential gene expression representing the fold change was determined at $p<0.01$ with a fold change $\geq \pm 1.5$. (-) Indicates no transcriptional difference.

Table 3.9. Differential expression of the most abundantly expressed genes in the fast-twitch muscle from cerivastatin (1 mg/kg) relative to vehicle treated female rats[ab]

Category	Accession #	Differential gene expression[b]	Sequence name	Sequence Description
Immune, inflammatory response and cell stress				
	AB001382	100.0	Spp1	secreted phosphoprotein 1
	AF411318	60.1	Mt1a	metallothionein 1
	NM_053819	51.9	Timp1	tissue inhibitor of metalloproteinase 1
	AI177761	31.7	Cd68	CD68 antigen
	BG380285	26.1	Ifitm1	interferon induced transmembrane protein 1
	NM_053843	16.1	Fcgr3	similar to Fc gamma (IgG) receptor II (low affinity) alpha precursor - rat
	L81174	13.3	Ankrd1	ankyrin repeat domain 1
	AF154349	13.2	Lgmn	legumain
	BM389261	12.3	Ifi30	interferon gamma inducible protein 30
	NM_053843	12.1	Fcgr3	Fc receptor, IgG, low affinity III
	NM_031832	11.0	Lgals3	lectin, galactose binding, soluble 3
	L12458	8.2	Lyz	lysozyme
	NM_017125	5.0	Cd63	CD63 antigen
	NM_021989	4.5	Timp2	tissue inhibitor of metalloproteinase 2
	AI178772	3.8	Ptma	prothymosin alpha
	NM_013132	3.6	Anxa5	annexin A5
	NM_022536	3.5	Ppib	peptidylprolyl isomerase B
	NM_012904	3.5	Anxa1	annexin A1
	BG671399	3.0	Ppia	peptidylprolyl isomerase A
	BG057543	2.5	Tra1	tumor rejection antigen gp96
	NM_012512	2.1	B2m	beta-2 microglobulin
	NM_019904	1.8	Lgals1	lectin, galactose binding, soluble 1
	NM_031812	1.6	Cd164	CD164 antigen
	NM_031970	-	Hspb1	heat shock 27kDa protein 1
	BI285700	-	Hspcb	heat shock 90kDa protein 1, beta
	NM_012966	-	Hspe1	heat shock 10 kDa protein 1
	NM_024351	-	Hspa8	heat shock protein 8
	AI237389	-	Hspcb	heat shock 90kDa protein 1, beta
	NM_012935	-	Cryab	crystallin, alpha B
	AA866458	-1.9	Csda	cold shock domain protein A
Metabolism				
	AI102495	10.0	Np	nucleoside phosphorylase
	AA893220	7.5	Sat	spermidine/spermine N1-acetyl transferase
	NM_053800	2.6	Txn1	thioredoxin 1
	NM_053610	2.2	Prdx5	peroxiredoxin 5
	S41066	2.1	Gpx1	glutathione peroxidase 1
	NM_031000	1.8	Akr1a1	aldo-keto reductase family 1, member A1
	NM_057114	1.8	Prdx1	peroxiredoxin 1
	NM_017050	-	Sod1	superoxide dismutase 1
	BI275294	-	Glul	glutamine synthetase 1
	BI296610	-	Glul	glutamine synthetase 1
	NM_013177	-1.8	Got2	glutamate oxaloacetate transaminase 2
	AB030829	-3.0	Ca3	carbonic anhydrase 3
Proteolysis				
	AI176595	7.0	Ctsl	cathepsin L
	BI283159	6.1	Scpep1	serine carboxypeptidase 1
	BM389083	5.5	Ppgb	protective protein for beta-galactosidase
	NM_022597	5.1	Ctsb	cathepsin B
	BG666933	1.9	Cst3	cystatin C
	NM_031687	1.6	Uba52	ubiquitin A-52 residue ribosomal protein fusion product 1
	NM_013013	1.6	Psap	prosaposin
	NM_031629	1.5	Psmb4	proteasome (prosome, macropain) subunit, beta type 4
	AW525776	-	Laptm4a	lysosomal-associated protein transmembrane 4A
	NM_031237	-	Ube2d3	ubiquitin-conjugating enzyme E2D 3
	BG663093	-	Sqstm1	sequestosome 1 (Sqstm1), transcript variant 1
	D16554	-	Ubb	polyubiquitin
	NM_017283	-	Psma6	proteasome (prosome, macropain) subunit, alpha type 6
	D16554	-	Ubb	polyubiquitin
Extracellular matrix				
	AA893484	3.9	Fn1	fibronectin 1
	BI275716	1.8	Col3a1	collagen, type III, alpha 1
	BM390253	1.7	Dcn	decorin
	BM388837	1.6	Col1a2	procollagen, type I, alpha 2
	NM_017138	1.6	Rpsa	laminin receptor 1
	D28875	-	Sparc	secreted acidic cysteine rich glycoprotein
	BI285575	-	Col1a1	collagen, type 1, alpha 1

[a]The most abundantly expressed transcripts represent the top 2% (278 probes) of the 13,947 probe sets expressed on the microarray.
[a]The most abundantly expressed transcripts had an arbitrary intensity of 1,411 to 6,526 whereas all other transcripts had an intensity of 14 to 1,410.
[b]Differential gene expression representing the fold change was determined at $p<0.01$ with a fold change $\geq \pm 1.5$. (-) Indicates no transcriptional difference.

Table 3.10. Differential expression of the most abundantly expressed genes in the fast-twitch muscle from cerivastatin (1 mg/kg) relative to vehicle treated female rats[ab]

Category	Accession #	Differential gene expression[b]	Sequence name	Sequence Description
Regulation of transcription and translation				
	AA892367	4.6	Rpl3	ribosomal protein L3
	BI284436	4.2	Eif4a1	eukaryotic translation initiation factor 4A1
	NM_134353	3.8	Pabpc1	poly(A) binding protein, cytoplasmic 1
	AI177503	3.2	H3f3b	H3 histone, family 3B
	BI279561	2.7	Naca	nascent-polypeptide-associated complex alpha polypeptide
	NM_017172	2.4	Zfp36l1	zinc finger protein 36, C3H type-like 1
	NM_0+B205335	2.3	Eef1a1	eukaryotic translation elongation factor 1 alpha 1
	AW251450	2.2	Mustn1	musculoskeletal, embryonic nuclear protein 1
	NM_031709	2.0	Rps12	ribosomal protein S12
	BG665124	2.0	Rps3	ribosomal protein S3
	X61043	2.0	Eef1a1	eukaryotic translation elongation factor 1 alpha 1
	NM_031109	1.9	Rps10	ribosomal protein S10
	NM_013043	1.9	Tsc22d1	TSC22 domain family, member 1
	NM_031101	1.8	Rpl13	ribosomal protein L13
	AI175551	1.8	Eef1b2	eukaryotic translation elongation factor 1 beta 2
	NM_022179	1.8	Hk3	ribosomal protein L13A
	AA799768	1.8	Rps9	ribosomal protein S9
	NM_031102	1.8	Rpl18	ribosomal protein L18
	BG668512	1.7	Rps19	ribosomal protein S19
	AI170643	1.7	LOC499782	similar to 60S ribosomal protein L12
	NM_017151	1.7	Rps15	ribosomal protein S15
	BF281388	1.7	Rps18	ribosomal protein S18
	NM_031065	1.6	Rpl10a	ribosomal protein L10A
	BF410811	1.6	Rps21	ribosomal protein S21
	AW142090	1.6	Rpl36a	ribosomal protein L36a
	AW914097	1.6	Rps20	ribosomal protein S20
	AI237597	1.6	Hspca	heat shock protein 1, alpha
	NM_031706	1.6	Rps8	ribosomal protein S8
	AA944073	1.6	Rpl41	ribosomal protein L41
	AA874811	1.6	Rpl14	ribosomal protein L14
	BM390456	1.5	H3f3b	H3 histone, family 3A, transcript variant 1
	AA800007	1.5	Rpl15	ribosomal protein L15
	NM_017150	1.5	Rpl29	ribosomal protein L29
	BG671311	1.5	Rpl17	ribosomal protein L17
	AI013910	1.5	Rpl34	ribosomal protein L34
	NM_053597	1.5	Rps27	ribosomal protein S27
	NM_013224	1.5	Rps26	ribosomal protein S26
	AI407731	1.5	Rps28	ribosomal protein S28
	BE107613	1.5	Rps13	ribosomal protein S13
	H35210	1.5	LOC681221	similar to 60S ribosomal protein L38
	NM_053971	1.5	Rpl6	ribosomal protein L6

[a]The most abundantly expressed transcripts represent the top 2% (278 probes) of the 13,947 probe sets expressed on the microarray.
[a]The most abundantly expressed transcripts had an arbitrary intensity of 1,411 to 6,526 whereas all other transcripts had an intensity of 14 to 1,410.
[b]Differential gene expression representing the fold change was determined at $p<0.01$ with a fold change $\geq \pm 1.5$. (-) Indicates no transcriptional difference.

Table 3.11. Differential expression of the most abundantly expressed genes in the fast-twitch muscle from cerivastatin (1 mg/kg) relative to vehicle treated female rats[ab]

Category	Accession #	Differential gene expression[b]	Sequence name	Sequence Description
Regulation of transcription and translation				
	NM_031570	1.5	Rps7	similar to ribosomal protein S7
	NM_017160	-	Rps6	ribosomal protein S6
	AA848284	-	Rps23	ribosomal protein S23
	NM_022697	-	Rpl28	ribosomal protein L28
	BI284252	-	Rpl11	ribosomal protein L11
	NM_031113	-	Rps27a	ribosomal protein S27a
	BG375811	-	Rps24	ribosomal protein S24
	NM_021264	-	Rpl35a	ribosomal protein L35a
	NM_031100	-	Rpl10	ribosomal protein L10
	BI283681	-	Eif5a	eukaryotic translation initiation factor 5A
	AI177054	-	Rpl27a	ribosomal protein L27a
	BI282255	-	Rps5	ribosomal protein S5
	NM_031103	-	Rpl19	ribosomal protein L19
	NM_031110	-	Rps11	ribosomal protein S11
	AI409193	-	Rpl8	ribosomal protein L8
	BM388159	-	Rpl32	ribosomal protein L32
	AW914118	-	Rpl35	ribosomal protein L35
	NM_022672	-	Rps14	ribosomal protein S14
	AI228150	-	Rpl22	ribosomal protein L22
	NM_022402	-	Arbp	acidic ribosomal phosphoprotein P0
	NM_022514	-	Rpl27	ribosomal protein L27
	NM_022510	-	Rpl4	ribosomal protein L4
	AA925327	-	Rpl23	ribosomal protein L23
	BI279866	-	MGC72957	similar to 60S ribosomal protein L18a
	NM_017245	-	Eef2	eukaryotic translation elongation factor 2
	U92700	-	Rps2	ribosomal protein S2
	BG667162	-	Eif4g2	eukaryotic translation initiation factor 4, gamma 2
	AI172199	-	Rpl23a	similar to 60S ribosomal protein L23a
	NM_022506	-	Rpl31	ribosomal protein L31
	NM_022699	-	Rpl30	ribosomal protein L30
	AA944861	-	Rps2	ribosomal protein S2
	NM_017153	-	Rps3a	ribosomal protein S3a
	NM_031099	-	Rpl5	ribosomal protein L5
	NM_017152	-	Rps17	ribosomal protein S17
	BF281221	-	Rpl7	ribosomal protein L7
	AI598536	-	Rpl26	ribosomal protein L26
	AA799501	-	Rps4x	ribosomal protein S4, X-linked
	BG666872	-	Rps16	ribosomal protein S16
	NM_031106	-	Rpl37	ribosomal protein L37
	BG666892	-	Rpl9	ribosomal protein L9
	BI297634	-	Rpl24	ribosomal protein L24
	AW914090	-	Rplp1	ribosomal protein, large, P1
	NM_017283	-	Psma6	proteasome (prosome, macropain) subunit, alpha type 6
	BF281215	-	Rpl37a	ribosomal protein L37a
	BI281697	-	Rpl7a	ribosomal protein L7a
	BM391203	-	Eef1g	eukaryotic translation elongation factor 1 gamma
	AI229633	-	Rps29	ribosomal protein S29
	AF388527	-	Serbp1	PAI-1 mRNA-binding protein
	NM_022674	-	H2afz	H2A histone family, member Z
	AI012372	-	Sui1-rs1_predicted	suppressor of initiator codon mutations, related sequence 1
	BI282111	-	Nsep1	nuclease sensitive element binding protein 1
	AF242550	-	Cnbp1	cellular nucleic acid binding protein 1
	AA799736	-	Chchd2	coiled-coil-helix-coiled-coil-helix domain containing 2
	BG673187	-	Fhl1	four and a half LIM domains 1
	BI298356	-	Fhl1	four and a half LIM domains 1
	AA891707	-1.7	Usmg5	upregulated during skeletal muscle growth 5
Transporters				
	AI012445	4.0	Slc25a5	solute carrier family 25 (mitochondrial carrier; adenine nucleotide translocator), member 5
	AF161588	1.8	Gabarap	gamma-aminobutyric acid receptor associated protein
	M23984	-1.9	Slc25a3	solute carrier family 25 (mitochondrial carrier; adenine nucleotide translocator), member 3
	BG666999	-2.6	Slc25a4	solute carrier family 25 (mitochondrial adenine nucleotide translocator) member 4
Calcium homeostasis				
	NM_012618	16.6	S100a4	S100 calcium-binding protein A4
	BG378926	5.6	S100a11	S100 calcium binding protein A11
	AF140232	4.7	S100a6	S100 calcium binding protein A6
	NM_031114	4.1	S100a10	S100 calcium binding protein A10
	X13933	1.5	Calm1	calmodulin 1
	BI279113	-	Calm1	calmodulin 1

[a]The most abundantly expressed transcripts represent the top 2% (278 probes) of the 13,947 probe sets expressed on the microarray.
[a]The most abundantly expressed transcripts had an arbitrary intensity of 1,411 to 6,526 whereas all other transcripts had an intensity of 14 to 1,410.
[b]Differential gene expression representing the fold change was determined at $p<0.01$ with a fold change $\geq \pm 1.5$. (-) Indicates no transcriptional difference.

Table 3.12. Differential expression of the most abundantly expressed genes in the fast-twitch muscle from cerivastatin (1 mg/kg) relative to vehicle treated female rats[ab]

Category	Accession #	Differential gene expression[b]	Sequence name	Sequence Description
Miscellaneous				
	NM_133298	45.1	Gpnmb	glycoprotein (transmembrane) nmb
	U13253	14.5	Fabp5	fatty acid binding protein 5, epidermal
	J02582	9.4	Apoe	apolipoprotein E
	NM_017113	8.5	Grn	granulin
	AA945178	8.4	Srprb	Transferrin
	L01122	6.1	Ftl1	ferritin light chain 2
	NM_019905	5.7	Anxa2	annexin A2
	BM385031	5.3	Plp2	proteolipid protein 2
	BF550246	5.0	Crip1	cysteine-rich protein 1
	NM_012862	4.0	Mgp	matrix Gla protein
	BI287960	4.0	Npc2	Niemann Pick type C2 (Npc2)
	BM386513	2.5	Cltc	clathrin, heavy polypeptide
	BG671677	2.1	App	amyloid beta (A4) precursor protein
	AA799627	2.0	Sepp1	selenoprotein P, plasma, 1
	BE329198	1.6	Arf1	ADP-ribosylation factor 1
	NM_130734	1.5	Gnb2l1	Bos taurus guanine nucleotide binding protein (G protein), beta polypeptide 2-like 1
	BI278308	-	Itm2b	integral membrane protein 2B
	AA925473	-	Cdc42	cell division cycle 42 homolog (S. cerevisiae)
	AI177362	-	Fau	Finkel-Biskis-Reilly murine sarcoma virus ubiquitously expressed
	BF282337	-	Itm2b	integral membrane protein 2B
	NM_130743	-	Ifi27l	putative ISG12(a) protein
	NM_012848	-	Fth1	ferritin, heavy polypeptide 1
	AI411388	-	Oaz1	ornithine decarboxylase antizyme 1
	U30789	-	Txnip	upregulated by 1,25-dihydroxyvitamin D-3
	AI406651	-	Serf2	small EDRK-rich factor 2
	BI277035	-	Gnas	GNAS complex locus
	AI179404	-	Hba-a1	hemoglobin alpha 2 chain
	AI179404	-	Hba-a1	hemoglobin alpha 2 chain
	NM_033234	-	Hbb	hemoglobin beta chain complex
	AA944393	-1.7	MGC72942	similar to CG6105-PA
	BF284168	-1.8	H19	H19 fetal liver mRNA (H19) on chromosome 7
Without ontology				
	BM383531	37.6		
	BI294018	12.1		
	NM_017154	4.8		
	AA799542	1.7		
	BI282748	1.5		
	AI180257	-		
	AI170758	-		
	AI104151	-		
	AA849795	-		
	AI577319	-		
	AI230164	-		
	AI008105	-		
	NM_017314	-		
	BG663128	-2.4		

[a]The most abundantly expressed transcripts represent the top 2% (278 probes) of the 13,947 probe sets expressed on the microarray.
[a]The most abundantly expressed transcripts had an arbitrary intensity of 1,411 to 6,526 whereas all other transcripts had an intensity of 14 to 1,410.
[b]Differential gene expression representing the fold change was determined at $p<0.01$ with a fold change $\geq \pm 1.5$. (-) Indicates no transcriptional difference.

Table 3.13. Differential expression of genes in the fast-twitch muscle related to the mevalonate pathway and cholesterol regulation from cerivastatin (1 mg/kg) relative to vehicle treated female rats[a]

Category	Accession #	Differential gene expression[a]	Sequence name	Sequence Description
Mevalonate pathway and cholesterol regulation				
	AI169398	19.2	Ch25h	cholesterol 25-hydroxylase
	NM_031118	18.8	Soat1	Acyl-CoA: cholesterol acyltransferase 1
	NM_031118	11.9	Soat1	Acyl-CoA: cholesterol acyltransferase 1
	NM_017136	10.3	Sqle	squalene epoxidase
	NM_080886	6.6	Sc4mol	sterol-C4-methyl oxidase-like
	NM_053539	5.6	Idi1	isopentenyl-diphosphate delta isomerase
	NM_012941	4.8	Cyp51	cytochrome P450, subfamily 51
	NM_013134	4.5	Hmgcr	3-hydroxy-3-methylglutaryl-Coenzyme A reductase
	D45252	4.5	Lss	lanosterol synthase
	NM_012732	4.3	Lip1	lipase A, lysosomal acid
	AW918387	4.0	Abca1	ATP-binding cassette, sub-family A, member 1
	NM_053502	4.0	Abcg1	ATP-binding cassette, sub-family G, member 1
	BI287960	4.0	Npc2	Niemann Pick type C2
	NM_133306	3.7	Oldlr1	oxidized low density lipoprotein receptor 1
	BM390399	2.9	Hmgcr	3-hydroxy-3-methylglutaryl-Coenzyme A reductase
	BG664123	2.9	Cyp51	cytochrome P450, subfamily 51
	BF283070	2.3	Cyp7b1	cytochrome P450, family 7, subfamily b, polypeptide 1
	BI294974	1.8	Ldlr	Low density lipoprotein receptor
	BG378288	1.5	Pmvk	phosphomevalonate kinase
	AI170663[b]	1.3	Srebf2	Sterol regulatory element binding factor 2
	AW530769	-1.9	Fdft1	farnesyl diphosphate farnesyl transferase 1
	M73231	-3.1	Cyp27a1	cytochrome P450, family 27, subfamily a, polypeptide 1
	AA849857	-3.3	Vldlr	very low density lipoprotein receptor
	NM_013155	-3.8	Vldlr	very low density lipoprotein receptor
	AF286470	-7.3	Srebf1	sterol regulatory element binding factor 1
	BF398848	-7.5	Srebf1	sterol regulatory element binding factor 1

[a]Differential gene expression in the female fast-twitch muscle from cerivastatin (1 mg/kg) relative to vehicle treated rats ($p<0.01$ with a fold change $\geq \pm 1.5$).
[b]Srebf2 was only induced by 1.3 fold but was included given its relevance to cholesterol regulation ($p<0.01$).

Table 3.14. Differential expression of genes in the fast-twitch muscle from cerivastatin (1 mg/kg) relative to vehicle treated male rats[a]

Category	Accession #	Differential gene expression[a]	Sequence name	Sequence Description
Regulation of transcription and translation				
	M25804	2.0	Nr1d1	nuclear receptor subfamily 1, group D, member 1
	BF288243	1.8	Klf2	Kruppel-like factor 2
	BM385790	1.8	Klf2	Kruppel-like factor 2
	AI230048	1.8	Dbp	D site albumin promoter binding protein
	NM_024385	1.6	Hhex	hematopoietically expressed homeobox
	U15660	1.6	Nr1d2	nuclear receptor subfamily 1, group D, member 2
	NM_024388	1.6	Nr4a1	nuclear receptor subfamily 4, group A, member 1
	AF000942	1.6	Id3	Inhibitor of DNA binding 3, dominant negative helix-loop-helix protein
	M86708	1.5	Id1	Inhibitor of DNA binding 1, helix-loop-helix protein
	BI291626	-1.5	Ell2	elongation factor RNA polymerase II 2
	BG671389	-1.5	Cpeb4	cytoplasmic polyadenylation element binding protein 4
	AI010275	-1.5	Cpeb2	cytoplasmic polyadenylation element binding protein 2
	BF406350	-1.9	Foxo1a	forkhead box protein O1A
	AB012600	-2.0	Arntl	aryl hydrocarbon receptor nuclear translocator-like
Immune, inflammatory response and cell stress				
	NM_031971	2.7	Hspa1a	heat shock 70kD protein 1B
	BI278231	2.7	Hspa1b	heat shock 70kDa protein 1B
	BM384926	2.2	Dnajb1	DnaJ (Hsp40) homolog, subfamily B, member 1
	AA945704	2.1	Dnajb1	DnaJ (Hsp40) homolog, subfamily B, member 1
	NM_130744	1.6	Cygb	cytoglobin
	BI285141	1.5	Cd24	CD24 antigen
	NM_053843	-1.5	Fcgr3	Fc receptor, IgG, low affinity III
	AI406687	-1.5	Cmtm6	chemokine-like factor super family 6
	NM_053843	-1.5	Fcgr3	Fc receptor, IgG, low affinity III
	AW534837	-1.6	Fkbp5	FK506 binding protein 5
	NM_053727	-1.7	Nfil3	nuclear factor, interleukin 3 regulated
Metabolism				
	L32601	1.9	Akr1c18	20 alpha-hydroxysteroid dehydrogenase
	BG374483	1.7	Per3	period homolog 3 (Drosophila)
	BE110108	1.6	Dusp1	dual specificity phosphatase 1
	U02553	1.6	Dusp1	dual specificity phosphatase 1
	NM_019292	-1.5	Ca3	carbonic anhydrase 3
Miscellaneous				
	AW143798	1.8	Ccnd1	cyclin D1
	AI028877	1.5	Smoc2	SPARC related modular calcium binding 2
	AI104533	-1.5	Ttn	similar to N2B-Titin Isoform
	AW530219	-1.5	Ryr1	ryanodine receptor 1, skeletal muscle
	AI235468	-1.6	Dst	dystonin
	BI299621	-1.6	Igf2r	Insulin-like growth factor receptor 2
	AA818910	-1.7	Arrdc3	arrestin domain containing 3
	BF408410	-2.2	Phf13	PHD finger protein 13
Without ontology				
	AI235245	2.0		
	AW529368	1.9		
	BG380221	1.8		
	AI407827	1.6		
	AA957707	1.6		
	BE096504	1.5		
	BF284190	1.5		
	AI548649	-1.5		
	BI289300	-1.5		
	BI288556	-1.5		
	AA850695	-1.6		
	BF284310	-1.6		
	BG381541	-1.6		
	BE096356	-1.6		
	BI291447	-1.7		
	AI639159	-1.7		
	AA818846	-1.8		

[a]Differential gene expression representing fold change was determined at $p<0.01$ with a fold change $\geq \pm 1.5$.

Table 3.15. Differential expression of genes in the slow-twitch muscle from cerivastatin (0.5 mg/kg) relative to vehicle treated female rats[a]

Category	Accession #	Differential gene expression[a]	Sequence name	Sequence Description
Energy metabolism				
	NM_053338	2.9	Rrad	Ras-related associated with diabetes
	NM_031347	2.4	Ppargc1a	peroxisome proliferative activated receptor, gamma, coactivator 1 alpha
	NM_012735	2.0	Hk2	hexokinase 2
	U92069	-2.3	Ucp3	uncoupling protein 3
Regulation of transcription and translation				
	AI548994	2.3	Sox9	SRY-box containing gene 9
	AI013512	2.0	Zfp297b	zinc finger protein 297B
	AI072788	2.0	1385978	SRY-box containing gene 9
	AI008458	1.6	Sox9	elongation factor RNA polymerase II
	BF284716	-1.5	Ankrd15	ankyrin repeat domain 15
	BE109033	-1.9	Eif2c1	eukaryotic translation initiation factor 2C, 1
	AI102530	-2.1	Nab2	Ngfi-A binding protein 2
	NM_017352	-3.1	Nr4a3	nuclear receptor subfamily 4, group A, member 3
	L08595	-4.1	Nr4a2	nuclear receptor subfamily 4, group A, member 2
Immune, inflammatory response and cell stress				
	NM_053352	1.5	Cmkor1	chemokine orphan receptor 1
	BF285187	-2.2	Ier5	immediate early response 5
Metabolism				
	AB062758	1.6	Dhrs4	dehydrogenase/reductase (SDR family) member 4
Extracellular matrix				
	BM388837	-1.8	Col1a2	procollagen, type I, alpha 2
	Z78279	-2.2	Col1a1	collagen, type 1, alpha 1
Miscellaneous				
	AW531877	2.5	Efna1	ephrin A1
	NM_053599	2.3	Efna1	ephrin A1
	BM392291	2.0	Rab30	RAB30, member RAS oncogene family
	AA799330	1.7	Pelo	pelota homolog
	AI102065	1.5	Hebp1	heme binding protein 1
	NM_031135	-1.7	Klf10	TGFB inducible early growth response
	AI175728	-1.8	Pepd	growth arrest specific 1
	BG666712	-1.8	Gpm6b	glycoprotein m6b
	NM_021835	-1.9	Jun	v-jun sarcoma virus 17 oncogene homolog
	AI406939	-3.1	G0s2	G0/G1 switch gene 2
Without ontology				
	AW535970	4.6		
	BF398967	2.9		
	BG376846	2.6		
	AI410107	2.5		
	BF402138	2.5		
	BF404786	2.4		
	BF410417	2.1		
	AI638990	2.0		
	BF408105	2.0		
	AI029813	2.0		
	BF283075	1.9		
	BF387399	1.9		
	BI285697	1.8		
	BM390772	1.8		
	BI294137	1.7		
	BF559640	1.7		
	BE114414	1.6		
	BF282700	1.6		
	AI104846	1.5		
	AW531902	-1.5		
	BM391419	-1.5		
	BI291229	-1.5		
	AF109674	-1.6		
	BF414338	-1.7		
	BI289462	-1.7		
	BE116111	-1.7		
	AI548601	-2.1		
	BF418649	-2.7		
	BF405036	-3.2		
	AI170665	-4.1		

[a]Differential gene expression representing fold change was determined at $p<0.01$ with a fold change $\geq \pm 1.5$.

Table 3.16. Differential expression of genes in the slow-twitch muscle from cerivastatin (1 mg/kg) relative to vehicle treated female rats[a]

Category	Accession #	Differential gene expression[a]	Sequence name	Sequence Description
Energy metabolism				
	BF418932	-1.7	Phka1	phosphorylase kinase alpha 1
Regulation of transcription and translation				
	U15660	1.8	Nr1d2	nuclear receptor subfamily 1, group D, member 2
	AI230048	1.6	Dbp	D site albumin promoter binding protein
	AW921151	1.5	Nola2	nucleolar protein family A, member 2
	BE102391	-1.8	Crebl2	cAMP responsive element binding protein-like 2
Immune, inflammatory response and cell stress				
	AF411318	9.5	Mt1a	metallothionein 1
	L02926	1.8	Il10	interleukin 10
Metabolism				
	L32601	-2.0	Akr1c18	20 alpha-hydroxysteroid dehydrogenase
Transporters				
	AI045333	2.1	Kctd13	potassium channel tetramerisation domain containing 13
	NM_023970	1.8	Trpv4	transient receptor potential cation channel, subfamily V, member 4
Calcium homeostasis				
	AI175539	-6.8	Pvalb	parvalbumin
Miscellaneous				
	BF282632	1.9	Tspan4	transmembrane 4 superfamily member 7
	BF283227	-1.5	Garnl1	GTPase activating RANGAP domain-like 1, transcript variant 2
	BM388946	-1.5	Wsb1	WD repeat and SOCS box-containing 1
	AI070638	-1.5	LOC679252	myeloid/lymphoid or mixed-lineage leukemia 3, transcript variant 3
	BF554226	-1.5	Trio	triple functional domain (PTPRF interacting), transcript variant 5
	AW530903	-1.6	Arid5b	AT rich interactive domain 5B
	BG666712	-2.0	Gpm6b	glycoprotein m6b
Without ontology				
	BM383531	8.3		
	BF391448	2.5		
	AI501145	1.8		
	AA818474	1.5		
	AI103917	-1.5		
	BI300794	-1.5		
	BI273855	-1.6		
	AI412155	-1.7		
	BI289460	-1.7		
	BF391129	-1.9		
	BI274506	-2.5		

[a]Differential gene expression representing fold change was determined at $p<0.01$ with a fold change $\geq \pm 1.5$.

Table 3.17. Differential expression of common genes in muscles from cerivastatin (1 mg/kg) relative to vehicle treated female rats [a]

	Differential gene expression[a]	
Sequence description	**Fast-twitch muscle**	**Slow-twitch muscle**
metallothionein 1a (Mt1a)	60.1	9.5
LOC682651	37.6	8.3
transmembrane 4 superfamily member 7 (tspan4)	6.7	1.9
interleukin 10 (Il10)	3.1	1.8
glucosamine (N-acetyl)-6-sulfatase (Gns)	2.3	1.3
TAF9 RNA polymerase II, TATA box binding protein (TBP)-associated factor (Taf9)	2.8	1.3
transient receptor potential cation channel, subfamily V, member 4 (Trpv4)	2.2	1.8
nucleolar protein family A, member 2 (Nola2)	1.8	1.5
LOC684802	1.8	-1.6
RGD1307838	1.4	-1.1
parvalbumin (Pvalb)	-11.7	-6.8
phosphorylase kinase alpha 1 (Phka1)	-10.1	-1.7
LOC683555	-5.3	-1.2
glycoprotein m6b (Gpm6b)	-3.8	-2.0
malic enzyme 1 (Me1)	-3.2	-1.4
20 alpha-hydroxysteroid dehydrogenase (Akr1c18)	-2.9	-2.0
cryptochrome 1 (Cry1)	-2.8	-1.7
Sos2	-2.5	-1.3
golgi autoantigen, golgin subfamily a, 4 (Golga4)	-2.3	-1.2
cAMP responsive element binding protein-like 2 (Crebl2)	-2.0	-1.8
Nuclear receptor subfamily 1, group D, member 2 (Nr1d2)	-2.1	1.4
radixin (Rdx)	-2.0	-1.2
myeloid/lymphoid or mixed-lineage leukemia 3, transcript variant 5 (Mll3)	-1.8	-1.3
H19 fetal liver mRNA (H19)	-1.8	-1.2
GTPase activating RANGAP domain-like 1, transcript variant 2 (Garnl1)	-1.8	-1.5
glycogenin 1 (Gyg1)	-1.7	1.1
1373634	-1.3	-1.2

[a]Differential gene expression in female muscles from cerivastatin (1 mg/kg) relative to vehicle treated rats ($p<0.01$).

Table 3.18. Dose response of differentially expressed common genes in the fast-twitch muscle from cerivastatin relative to vehicle treated female rats[a]

	Differential gene expression[a]	
Sequence description	**0.5 mg/kg**	**1 mg/kg**
RGD15594	1.9	3.0
Cysteine-rich protein 3 (Csrp3)	1.6	2.4
Amyloid beta precursor protein (Appbp1)	-1.2	2.1
Sart3	-1.7	1.6
DNAjb1 (Hsp40), subfamily B, member 1 (Dnajb1)	-2.0	1.4
Solute carrier family 25, member 25 (Slc25a25)	-2.0	-8.8
G0/G1 switch gene 2 (GOs2)	-2.6	-7.6
ADP ribosylation factor-like 6 interacting protein 2	-1.1	-4.1
Kruppel-like factor 15 (Klf15)	1.5	-4.0
1378055	-1.6	-3.8
Sestrin 1 (Sesn1)	1.6	-3.4
Transducer of ERBB2 (Tob2)	-1.5	-3.2
RGD13094	1.6	-3.0
unc-51 like kinase 2 (Ulk2)	-1.2	-2.8
1391431	-1.6	-2.7
Transmembrane protein 23 (Tmem23)	1.3	-2.4
RGD73502	1.3	-2.4
RGD13076	-1.2	-2.3
Nuclear receptor subfamily 1, member 2 (Nr1d2)	1.3	-2.1
LOC68925	1.7	-2.0
Nuclear transcription factor Y gamma (Nfyc)	1.2	-1.8
Zinc finger protein 541 (Znf541)	1.2	-1.8
1372308	-1.3	-1.8
LIM and cysteine rich domains 1 (Lmcd1)	1.6	-1.8
tubby-like protein 4 (Tulp4)	-1.4	-1.4

[a]Differential expression of common genes in female muscles from cerivastatin (0.5 and 1 mg/kg) relative to vehicle treated rats ($p<0.01$).

Table 3.19. Differentially expressed common genes in the fast-twitch muscle from cerivastatin treated female (0.5 mg/kg) and male (1 mg/kg) relative to vehicle treated rats[a]

	Differential gene expression[a]	
Sequence description	**Female (0.5 mg/kg)**	**Male (1 mg/kg)**
DnaJ (Hsp40), subfamily B, member 1 (Dnajb1)	-2.0	2.2
Nuclear receptor subfamily 1, member 2 (Nr1d2)	1.3	1.6
Nuclear receptor subfamily 1, member 1 (Nr1d1)	2.2	2.0

[a]Differential expression of common genes in the fast-twitch muscle from cerivastatin treated female (0.5 mg/kg) and male (1 mg/kg) relative to vehicle treated rats ($p<0.01$).

Chapter 4

Metabolomic profiles of skeletal muscles with and without cerivastatin treatment in female and male rats

4.1. Introduction

Gene expression analysis of skeletal muscles from cerivastatin treated rats indicated that alterations in energy metabolism and cholesterol homeostasis may be involved with the mechanism of cerivastatin-induced myopathy (Chapter 3). However, there remains a significant gap in knowledge regarding how alterations in skeletal muscle energy metabolism and cholesterol homeostasis may be causally related to statin-induced myopathy. Accordingly, it was hypothesized that understanding the metabolic changes in skeletal muscle following cerivastatin treatment may provide further insight into the specific biochemical targets and pathways involved with the development of myopathy.

Metabolomics is a systems biology approach for studying metabolic profiles representing the total metabolite pool in tissue extracts or biofluids (Nicholson et al., 2002). This approach combines analytical technologies like ^{1}H nuclear magnetic resonance spectrometry (NMR) with statistics to provide a quantitative, comprehensive and ubiased assessment of the metabolic response to physiological or pathophysiological changes (Gatzidou et al., 2007; Nicholson et al., 2002). Although NMR metabolomics provides an assessment of the total metabolic pool, the sensitivity of this technique is limited to compounds in the concentration range >0.1 µM. Despite this limitation, NMR

metabolomics has been successfully applied to investigate metabolite profiles associated with a variety of myopathies and physiological stress in vivo as well as in myotubes, and these studies have revealed significant changes in biochemical pathways, including early alterations in mitochondrial energetics (Griffin et al., 2001, 2009; Lin et al., 2011; Sharma et al., 2003a, 2003b; Slade et al., 2006; Straadt et al., 2010a, 2010b; Sprott et al., 2000; Xu et al., 2011; Wu et al., 2011). Separately, metabolomic profiling of urine has been useful for identifying metabolite changes originating from skeletal muscle and representing biomarkers of disease progression (Chung et al., 2003, 2005). Importantly, these studies suggest NMR metabolomic profiling of skeletal muscles may also be useful for evaluating metabolic changes associated with statin-induced myopathy.

Fast-twitch muscles from female rats are most sensitive to statin-induced myopathy (Figure 2.1 and Table 2.2). Therefore, a major goal of this work was to use NMR metabolomic profiling to determine whether fiber- and sex-specific metabolite differences are present in naïve rats. An additional goal of this work was to use NMR metabolomic profiling to determine metabolite changes in skeletal muscles, representing potential biochemical targets and pathways, involved with cerivastatin-induced myopathy. For this work, metabolomic profiling was conducted on both aqueous and lipophilic extracts of skeletal muscles from representative fast-twitch (psoas) and slow-twitch (soleus) fibers from female and male rats (Table 2.1). Separately, metabolomic profiling of urine was also conducted in Chapter 7 to identify skeletal muscle specific metabolites which may represent potential biomarkers of cerivastatin-induced myopathy.

4.2 Methods

***Study design*.** This investigation was conducted on fast-twitch (psoas) and slow-twitch (soleus) skeletal muscles obtained from *study 1*, described in Chapter 2.2.

Folch extraction of skeletal muscle. Frozen muscle tissues were individually pulverized in liquid nitrogen and a portion (100 mg psoas and 50 mg soleus) was extracted according to the method of Folch (1957). The psoas represents a large muscle, therefore to maximize the NMR signal 100 mg of tissue was used. In contrast, the soleus weighs approximately 100 mg so only 50 mg was used, with the remaining tissue used for RNA isolation. Metabolite extraction was performed by homogenizing the tissue in a bead mill (Retsch MM 300, Haan Germany) for 4 minutes (30 Hz) with 10 volumes of ice-cold methanol. Following centrifugation (8000g, 4˚C) for 15 minutes, the supernatant (0.6 ml for psoas; 0.3 ml for soleus) was transferred to water/chloroform (0.4 ml / 1 ml for psoas; 0.2 ml / 0.6 ml for soleus) and vortexed for 10 seconds and then shaken in a bead mill (30 Hz) for 10 minutes at room temperature. Samples were centrifuged (6000g, 4˚C) for 25 minutes and the methanol / aqueous (hydrophilic phase) and chloroform (lipophilic phase) were separated, dried under nitrogen at room temperature and analyzed by ^{1}H NMR. Samples were stored at -80˚C until analysis.

^{1}H NMR metabolomic profiling. Aqueous extracts were reconstituted in 0.6 ml of deuterated water (D_2O) with trimethylsilyl propionate (TSP) as an internal standard. Samples were measured in a 5 mm NMR tube using Iconnmr (NMR software) in a Bruker 600 MHz spectrometer with a 5 mm TCI MicroCryoProbe at 300K with standard

1D proton parameters as follows: 256 scans, 8 dummy scans, 16 ppm spectral width, 2 seconds of relaxation delay, noesy1dpr pulse sequence program with water suppression and 32K of free induction decay. Chloroform samples were dissolved in 0.6 ml of deuterated chloroform ($CDCl_{3)}$ with 0.05% tetramethylsilane (TMS) as an internal standard, and measured with the conditions described for the aqueous extracts, however a zg30 pulse sequence program was used without water suppression. All samples in each group were measured using a constant receiver gain to allow for quantitation.

LC-MS analysis. The lipophilic skeletal muscle extracts were also analyzed for a panel of sterols by LC-MS based on a proprietary method at Lipomics Technologies (West Sacramento, California).

Data analysis. NMR spectra were visually inspected to determine qualitative differences. Metabolites showing a marked change, with well resolved signals were identified using standard spectra from The Human Metabolome Database and the Bruker proprietary database. The intensity of each metabolite resonance was assessed by integration of the signal and normalization to the internal standard (TSP or TMS) signal. For each metabolite, the relative mean ± SE fold change was determined for each treatment group. Sterol results from Lipomics Technologies were reported as either nmol or µmol / g of tissue. Group means were compared with a Student's t-test or ANOVA using StatView (SAS Institute, Cary, NC) at $p<0.05$ prior to determining the relative fold change.

4.3. Results

To determine sex differences in metabolites from naïve rats, NMR metabolomic profiles of aqueous extracts of the psoas from female and male rats were compared. In general, the metabolomic profiles showing the aliphatic (Figure 4.1; 0.5–4.5 ppm) and aromatic (Figure 4.2; 5.7-9.5 ppm) regions of the psoas were similar between female and male rats. However, creatine was 16% ($p = 0.01$) higher in male rats, with no difference in phosphocreatine. The chemical shift (3.1-3.5 ppm) for the two taurine triplets was highly variable because of pH differences across samples. The non-muscle metabolite, 1,2-propanediol was also detected in both muscles and attributed to the use of sodium pentobarbital, as this anesthesia contains 1,2-propanediol as the vehicle for delivery of the barbiturate.

The metabolomic profiles of the lipophilic extracts of the psoas were similar between female and male rats (Figure 4.3). In general, the resonances in the lipophilic extracts were typically broad, which was expected. However, this broadening reduced resolution and limited metabolite identification. Despite this limitation, cholesterol was identified based on sharp resonances at 0.68 and 1.01 ppm, representing the C18 and C19 methyl groups, respectively (Figures 4.3 and 6.1). Furthermore, phosphatidylcholine was identified based on the resonance at 3.30 ppm, representing the $(CH_3)_3$-N group, and several resonances consistent with CH_2 groups in phospholipids were identified. There were no sex differences in the concentration of cholesterol or phosphatidylcholine. Additionally, methanol was also present in these samples (3.50 ppm) resulting from the extraction.

To determine fiber differences in metabolites from naïve female rats, NMR metabolomic profiles of aqueous extracts of the psoas were compared to the soleus. The metabolomic profiles indicated that the fiber types have a similar distribution and concentration of metabolites (Figure 4.4 and 4.5). However, lactate was higher in the psoas whereas taurine, fumarate and an unknown metabolite at 1.25 ppm were higher in the soleus.

The metabolomic profiles of the lipophilic extracts of the psoas and soleus appeared qualitatively different in female rats and this was likely related to better resolution for many of the metabolites in the soleus as a result of less tissue used in the Folch extraction (Figure 4.6). Despite better resolution, further characterization of specific phospholipids in muscles was not pursued. However, higher levels of cholesterol were noted in the soleus.

The fiber- and sex-specific histopathology of the skeletal muscles from cerivastatin treated rats was previously described in Chapter 2.3 (Figure 2.1 and Table 2.2). To determine metabolomic changes associated with cerivastatin treatment aqueous extracts from the psoas and soleus were evaluated by NMR. Metabolomic profiles of the aqueous extracts of the psoas from female rats indicated several metabolite changes associated with cerivastatin (1 mg/kg) treatment (Figure 4.7 and 4.8; Table 4.1). Metabolites representing a perturbation in energy metabolism (lactate, phosphocreatine, creatine and NAD^+) and histidine-containing moieties (anserine and carnosine) were reduced by up to 3-fold with cerivastatin (1 mg/kg) treatment (Table 4.1). In contrast, resonances of two unknown metabolites (1.27 and 1.77 ppm) and glutamine were significantly increased

with cerivastatin (1 mg/kg) treatment (Table 4.1). Changes in nucleotides (AMP, ADP, ATP) were also observed with cerivastatin treatment. However, since ATP is labile and tissues were not freeze clamped, these metabolites were not quantitated. In contrast to the high dose, a reduction in NAD^+ was the only change observed at the low dose of cerivastatin (0.5 mg/kg) in the aqueous extracts of the psoas from female rats (Table 4.1; spectra not shown).

Since cerivastatin modulates cholesterol synthesis, lipophilic extracts of skeletal muscles were evaluated to determine the effects on sterols. Representative NMR spectra of the lipophilic extracts of the psoas from female rats indicated a dose dependent increase in cholesterol, phosphatidylcholine and an unknown metabolite at 3.15 ppm (Figure 4.9; Table 4.2). Further evaluation of the spectra indicated that the increase in cholesterol was specific to the free and not the esterified form. Specificity of this change in free cholesterol was determined based on an increase in the resonance at 3.55 ppm, representing the proton on the carbon for the CHOH group which is absent in esterified cholesterol (Figure 4.9; Table 4.2).

The metabolomic profile of the aqueous extracts of the psoas from cerivastatin (1 mg/kg) treated male rats was similar to control, with one exception phosphocreatine showed a significant increase (Figure 4.10 and 4.11; Table 4.1). Similarly, the lipophilic extracts of the psoas from cerivastatin (1 mg/kg) treated male rats were similar to control, with only phosphatidylcholine showing an increase (Table 4.2; spectra not shown).

The metabolomic profile of the aqueous extracts of the soleus from cerivastatin (1 mg/kg) treated female rats was similar to control (Figures 4.12, 4.13 and Table 4.1). However anserine and phosphocreatine were reduced by almost 2-fold, whereas a significant increase in the nucleotide region was observed. In the lipophilic soleus extracts from cerivastatin (1 mg/kg) treated female rats there were no changes observed in cholesterol, phosphatidylcholine or phospholipids (Table 4.2; spectra not shown). Additionally, no changes were observed in either the aqueous or lipophilic soleus extracts from rats receiving 0.5 mg/kg cerivastatin (Table 4.2; spectra not shown).

To further investigate the effects of cerivastatin treatment, a panel of sterols was measured in lipophilic extracts of the psoas from cerivastatin treated female rats (Table 4.3). The LC-MS results corroborated the NMR findings demonstrating an increase in total cholesterol. Furthermore, the LC-MS results indicated a marked increase in the cholesterol precursors, desmosterol and 7-dehydrocholesterol and the downstream product 7α-hydroxycholesterol in the psoas from cerivastatin (1 mg/kg) treated rats. In contrast, cholesterol precursors including lanosterol and lathosterol as well as the phytosterols β-sitosterol, campesterol, and stigmasterol were unchanged or reduced in skeletal muscles from cerivastatin treated rats compared to control.

4.4. Discussion

The major goal of this work was to use metabolomic profiling to determine whether sex- and fiber-specific metabolite differences were present in skeletal muscles from naïve rats, and to determine metabolic changes associated with cerivastatin-induced myopathy. Accordingly, it was hypothesized that determining the metabolic changes in skeletal muscle following cerivastatin treatment may provide further insight into the specific biochemical targets and pathways involved with the development of myopathy. Although NMR metabolomics has the potential to provide an unbiased and comprehensive assessment of the total metabolite pool in skeletal muscle, the current investigation was limited to resonances which could be identified against standard spectra, and metabolites with concentrations above the limit of detection (>0.1 μM). Therefore, compounds like isoprenoids and mevalonate which may be important in the mechanism of toxicity were not measured as their concentrations were below the limit of detection.

The current work demonstrates that metabolomic profiles of both aqueous and lipophilic extracts of fast-twitch skeletal muscles from naïve female and male rats were similar, with only creatine showing higher levels in the male. Although the biological implication of this difference is unknown, it is consistent with a higher gene expression of the enzyme that catalyzes creatine formation (guanidinoacetate methyltransferase) in the male rat psoas (Table 3.5). In general, the lack of sex-specific metabolite changes is consistent with the transcriptional data, indicating that there is no difference in the most abundant genes which define the muscle fiber phenotype (Chapter 3.3, Tables 3.5 and 3.6).

Metabolomic profiling of fast- and slow-twitch skeletal muscles from naïve female rats was also generally similar with only a few changes noted. In particular, lactate was higher in the psoas whereas taurine, fumarate and cholesterol were higher in the soleus, and these changes have been previously reported by other methods (Froberg, 1967; Nikolaidis et al., 2006; Pierno et al., 2011; Stefanyk et al., 2010; Yoshioka et al., 2002). The higher level of lactate and fumarate is consistent with anaerobic glycolysis in the fast-twitch muscle and oxidative energy metabolism in the slow-twitch muscles, respectively. In contrast, taurine is present in most tissues at millimolar levels, and in slow-twitch muscles it has been proposed to have several roles including attenuation of the atrophy process by reducing expression of the atrophy genes (Pierno et al., 2011). It is important to note that while only a few metabolites changed in a fiber-dependent manner, the gene expression data indicated that several thousand transcripts were differentially expressed (Chapter 3.3). Together, these results demonstrate that transcriptional profiling is more sensitive at detecting both sex- and fiber-specific changes which are consistent with the muscle fiber phenotype, whereas metabolomic profiling is more useful for monitoring changes in metabolites which are highly concentrated in the skeletal muscle.

Since cerivastatin inhibits cholesterol synthesis, metabolomic profiling was also conducted on lipophilic extracts from cerivastatin treated female rats. Metabolomic evaluation of lipophilic extracts is not a common practice because of poor resolution mediated by a reduction in the chemical shifts, leaving few distinct resonances for metabolite identification (Srivastava et al., 2010). Despite this limitation, the NMR data revealed dose-dependent increases in free cholesterol and phosphatidylcholine in the

psoas from female rats. This observation was unexpected given the pharmacology of statins and the hypothesis that statin-induced myopathy is mediated by a decrease in skeletal muscle cholesterol (London et al., 1991). However, the current results are consistent with transcriptional induction of genes in the mevalonate pathway and cholesterol regulation, including HMG-CoA reductase and the Ldl receptor (Table 3.13). A similar increase in cholesterol has also been observed clinically in the quadriceps of patients on simvastatin, in the absence of an increase in CK, suggesting this change may precede myopathy (Paiva et al., 2005; Phillips et al., 2010). The accumulation and abnormal localization of free cholesterol adversely effects cellular functions and can lead to cell death (Ridgway et al., 1999). Furthermore, an abnormal accumulation of free cholesterol, representing 2 to 3-fold increase is associated with the pathogenesis of other myopathies, like inclusion body myositis, muscular dystrophy, chloroquine-induced myopathy, statin-induced myopathy in mice and muscle atrophy (Jaworska-Wilczynska et al., 2002; Kuhn and Logan, 1990; Kumar and Sharma, 2009; Nilsson et al., 1981; Owens and Hughes, 1970; Williams and Smith, 1989; Yokoyama et al., 2007). However, an inflammatory response in non-muscle tissues increases cholesterol as well as desmosterol and 7-dehydrocholesterol which were both noted in the current investigation (Fon Tacer et al., 2010). Therefore, additional experiments are needed to determine whether these changes represent pathology or are causally related to statin-induced myopathy.

Metabolomic profiling of aqueous skeletal muscle extracts from cerivastatin treated female rats revealed several metabolites which were mostly decreased. In the female

psoas, metabolites involved with energy metabolism (lactate, NAD^+, creatine, and phosphocreatine) were significantly decreased, and NAD^+ was the only metabolite which was reduced in a dose-dependent manner. Similar metabolite changes have been reported in skeletal muscle and myotubes during conditions of physiological stress and myopathy (Brault et al., 2003; Gupta et al., 2000; Sharma et al., 2003a, 2003b; Straadt et al., 2010a, 2010b). Accordingly, the current findings are consistent with alterations in energy homeostasis related to myopathy, and this conclusion is consistent with the gene expression data indicating a reduction in transcripts involved with energy metabolism (Table 3.8). In contrast, glutamine was significantly increased, and a similar response has been observed with other catabolic conditions in skeletal muscle (Huang et al., 2007; Salehian et al., 2006). Additionally, there was a significant reduction in histidine-containing dipeptides, including both carnosine and anserine. These dipeptides are highly concentrated in skeletal muscle (1 – 50 mM) and play a role in pH-buffering and antioxidant activity (Aldini et al., 2004; Chan et al., 1994; Penafiel et al., 2004). The decrease in these metabolites is consistent with skeletal muscle degeneration.

There were several unexpected findings in the aqueous extracts, including a decrease in anserine and phosphocreatine in the soleus from cerivastatin treated female rats, in the absence of histological evidence of toxicity (Table 2.2). Although the biological basis for these changes is unknown, they may be indicative of oxidative stress which would be consistent with transcriptional induction of Mt1a noted in the soleus (Table 3.16). Furthermore, a decrease in phosphocreatine may suggest a perturbation in energy homeostasis, and this conclusion is corroborated by transcriptional changes in several

genes involved with alterations in energy metabolism (Tables 3.15 and 3.16). Together, these results suggest that cerivastatin also affects the slow-twitch muscle, albeit in the absence of myopathy. However, it is also possible that changes observed in the slow-twitch muscle are secondary to the observation that some of the rats were moribund.

An additional unexpected finding in this study was that phosphocreatine increased in the psoas from male rats treated with cerivastatin. Given that constitutive levels of creatine were higher in the psoas from naïve male rats, these data may indicate that sex-specific differences in creatine metabolism are mechanistically important. Clinical evidence indicates phosphocreatine recovery time is prolonged in skeletal muscles of statin treated patients while exercising, thereby indicating an impairment in mitochondrial oxidative phosphorylation (Wu et al., 2011). Furthermore, in a separate clinical study, creatine supplementation prevented statin-induced myopathy (Shewmon and Craig, 2010). Together, these results may suggest that statins impair energy metabolism in the skeletal muscle. However, additional experiments are needed to determine whether these changes represent pathology or are causally related to statin-induced myopathy.

In summary, metabolomic profiling of skeletal muscles from cerivastatin treated rats revealed alterations in cholesterol homeostasis and energy metabolism, and these findings were consistent with transcriptional changes noted in skeletal muscles (Chapter 3). To determine whether these changes are associated with pathology or causally related to cerivastatin-induced myopathy, additional experiments were conducted in Chapters 5 and 6. Furthermore, in Chapter 7 metabolomic profiling was conducted on urine collected

from cerivastatin treated rats to determine whether specific skeletal muscle metabolites can be identified which would be useful as biomarkers of myopathy.

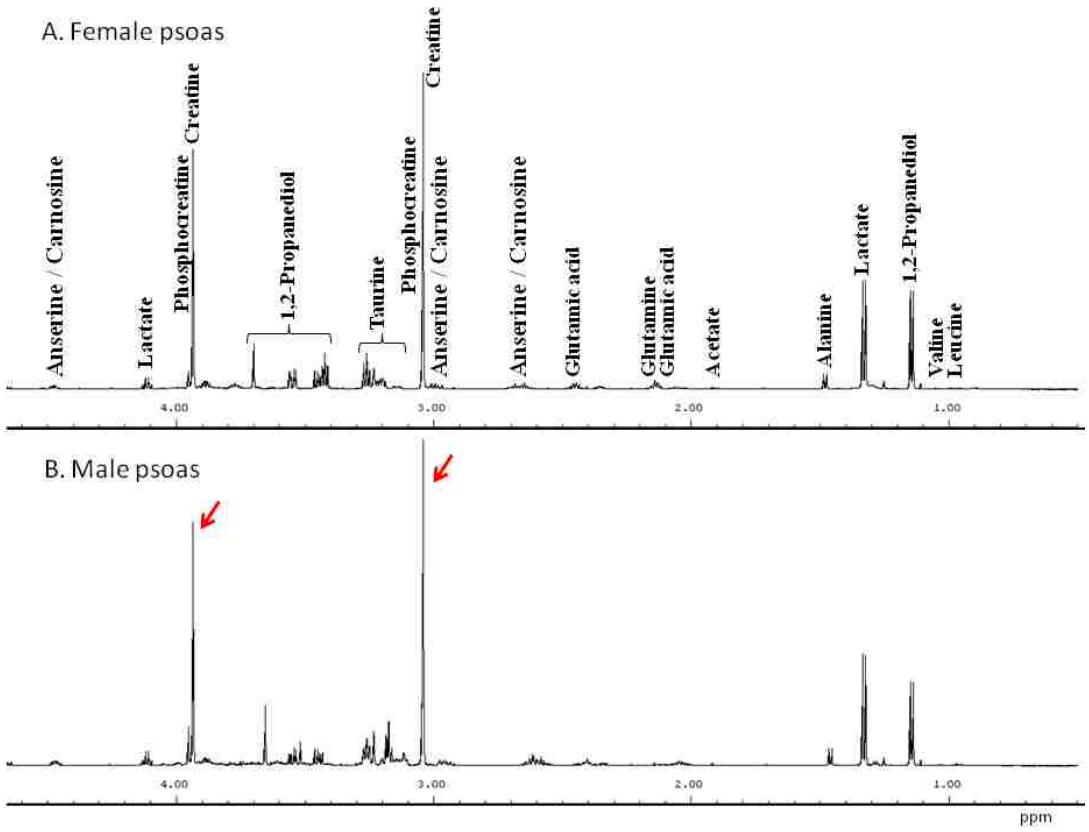

Figure 4.1. ^{1}H NMR spectra of aqueous extracts of the psoas from female and male rats (aliphatic region: 0.5-4.5 ppm). Representative spectra of the psoas from A) female and B) male rats showing similar metabolomic profiles. However, creatine (↓) was increased in the male relative to the female rats.

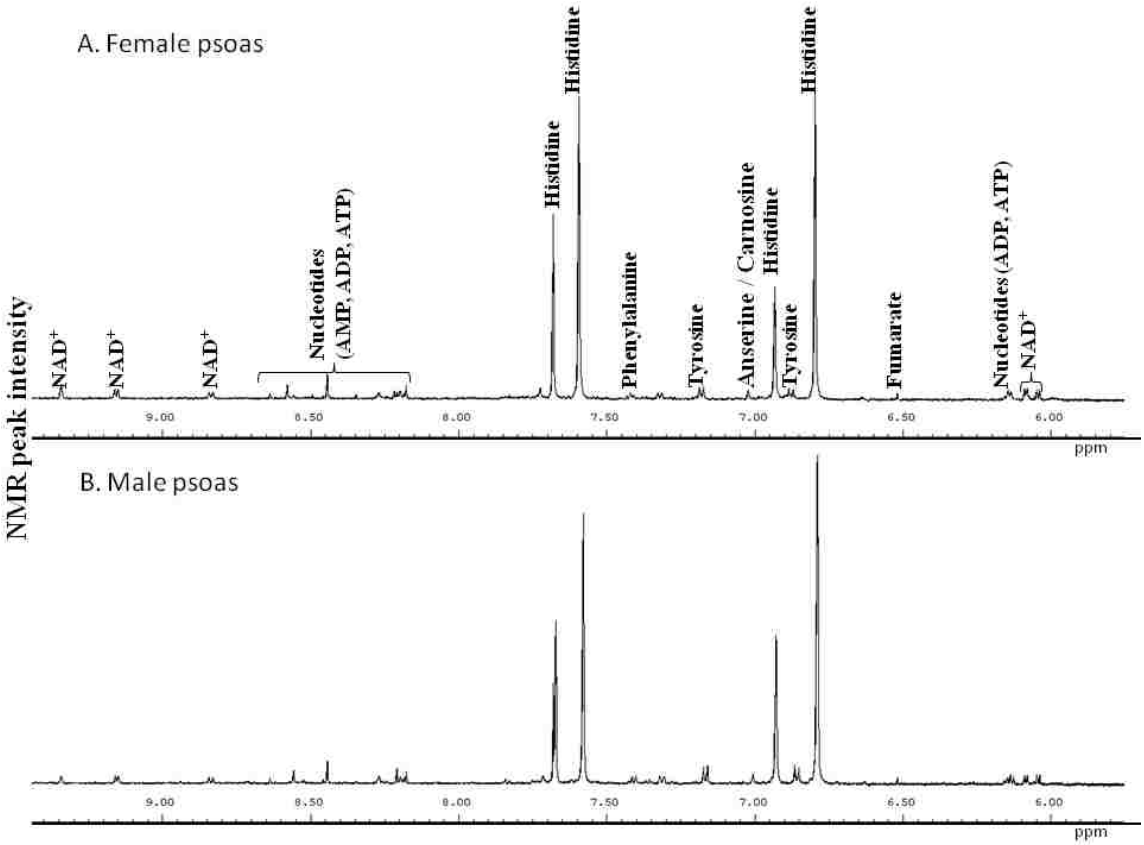

Figure 4.2. ^{1}H NMR spectra of aqueous extracts of the psoas from female and male rats (aromatic region: 5.7-9.5 ppm). Typical spectra of the psoas from A) female and B) male rats showing similar metabolomic profiles.

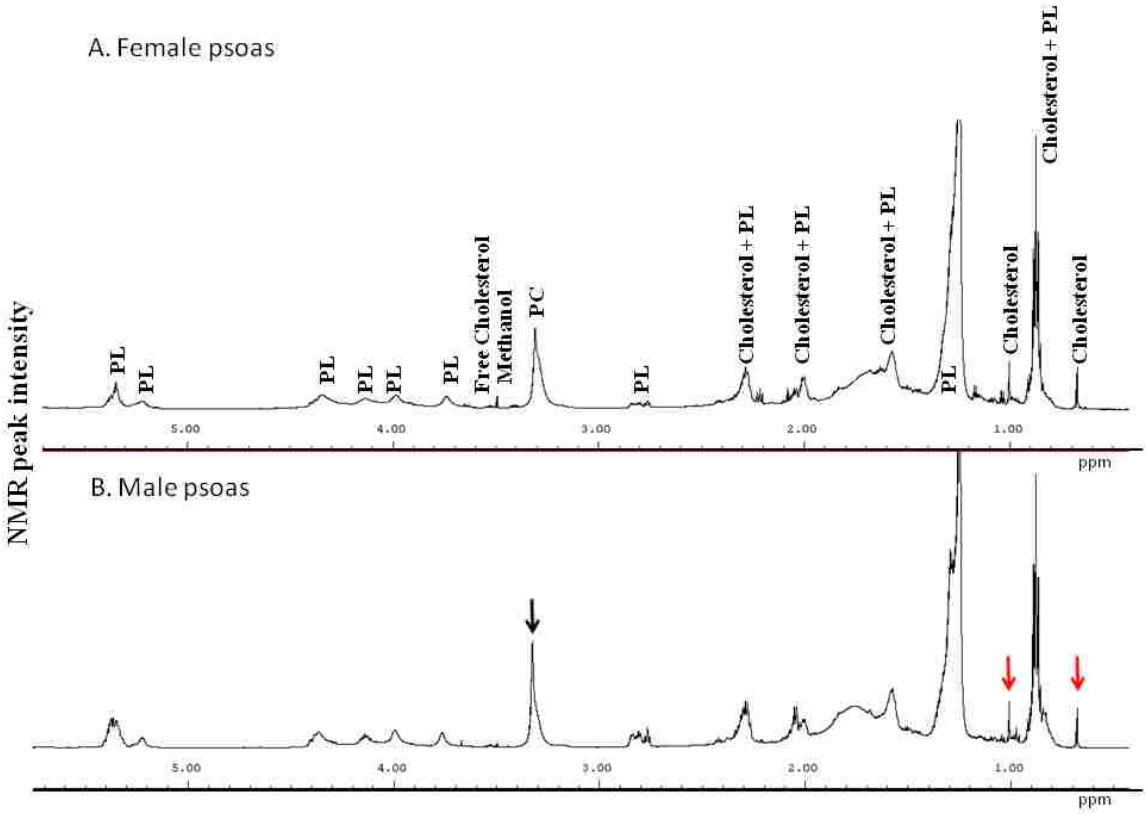

Figure 4.3. ^{1}H NMR spectra of lipophilic extracts of the psoas from female and male rats. Representative spectra of the psoas from A) female and B) male rats showing similar metabolomic profiles including sharp resonances for cholesterol (↓) and phosphatidylcholine (↓) and broad resonances for the CH_2 groups from phospholipids (PL). In general, resonances in the lipophilic extracts were broad which reduced resolution and limited metabolite identification.

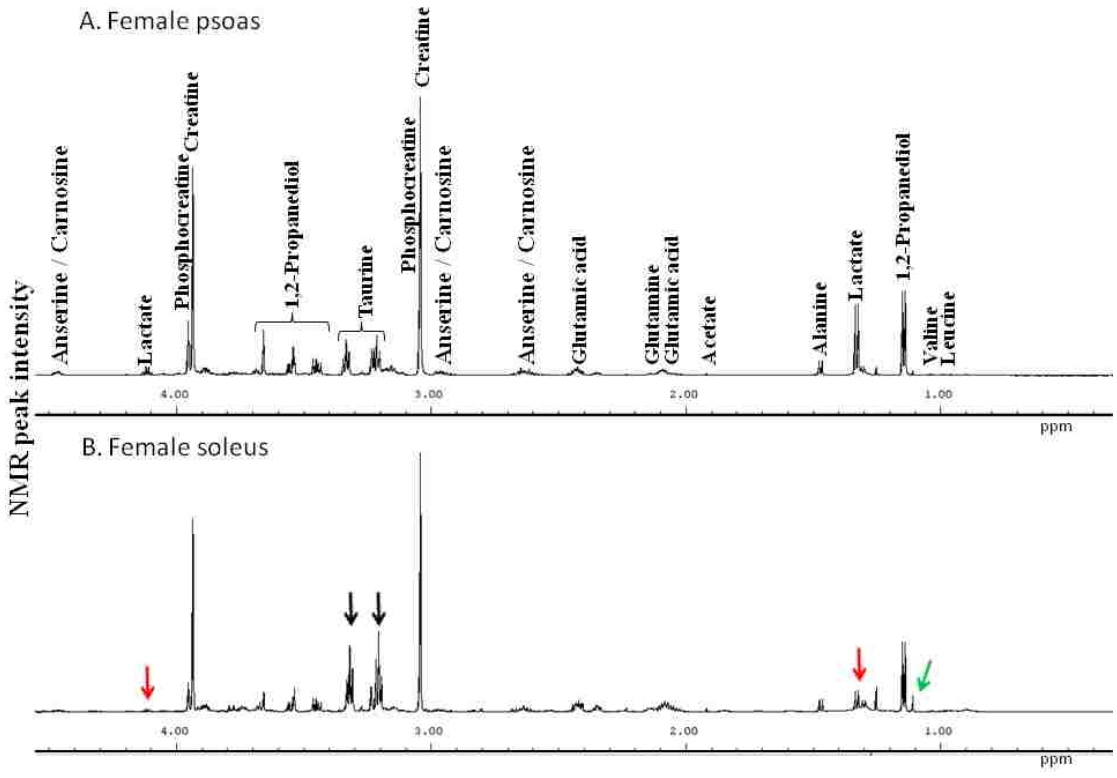

Figure 4.4. ^{1}H NMR spectra of aqueous extracts of the psoas and soleus from female rats (aliphatic region: 0.5-4.5 ppm). Representative spectra of the A) psoas and B) soleus from female rats. Fiber differences in several metabolites was observed including higher levels of lactate (↓) in the psoas, whereas higher levels of taurine (↓) and an unknown metabolite at 1.25 ppm (↓) were noted in the soleus.

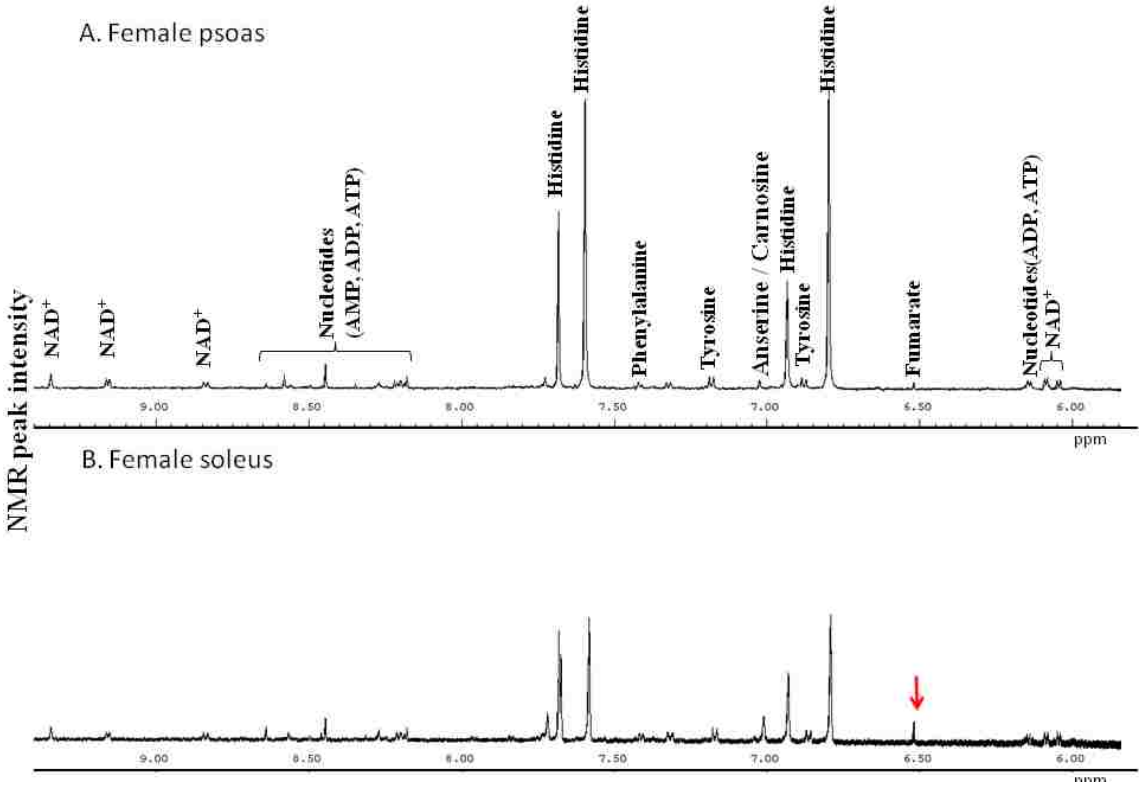

Figure 4.5. ^{1}H NMR spectra of aqueous extracts of the psoas and soleus from female rats (aromatic region: 5.7-9.5 ppm). Representative spectra of the A) psoas and B) soleus from female rats illustrating a similar distribution of metabolites in both muscle fiber types with one noted exception, higher levels of fumarate (↓) were noted in the soleus.

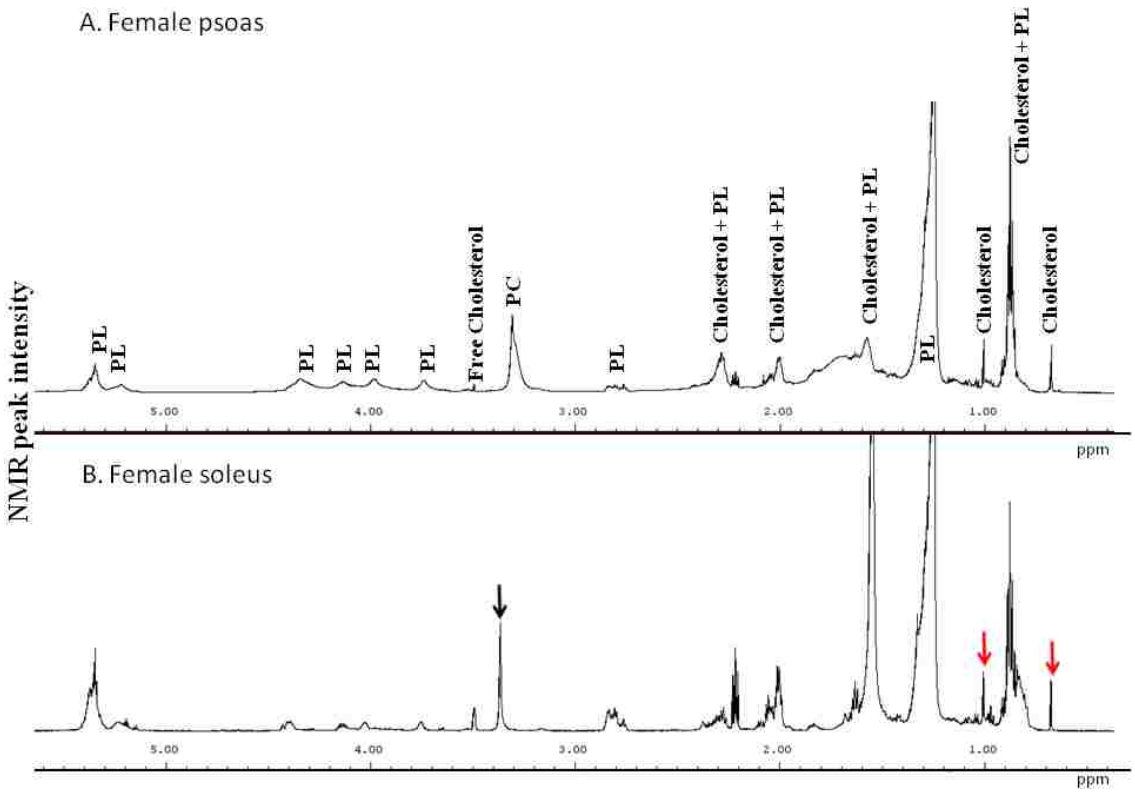

Figure 4.6. ^{1}H NMR spectra of lipophilic extracts of the psoas and soleus from female rats. Typical spectra of the A) psoas and B) soleus from female rats showing sharp resonances for cholesterol (↓) and phosphatidylcholine (↓) and broad resonances for the CH_2 groups from phospholipids (PL). Several PL resonances showed better resolution in the soleus which was likely the result of less tissue comapred to the psoas. Cholesterol levels were higher in the soleus relative to the psoas.

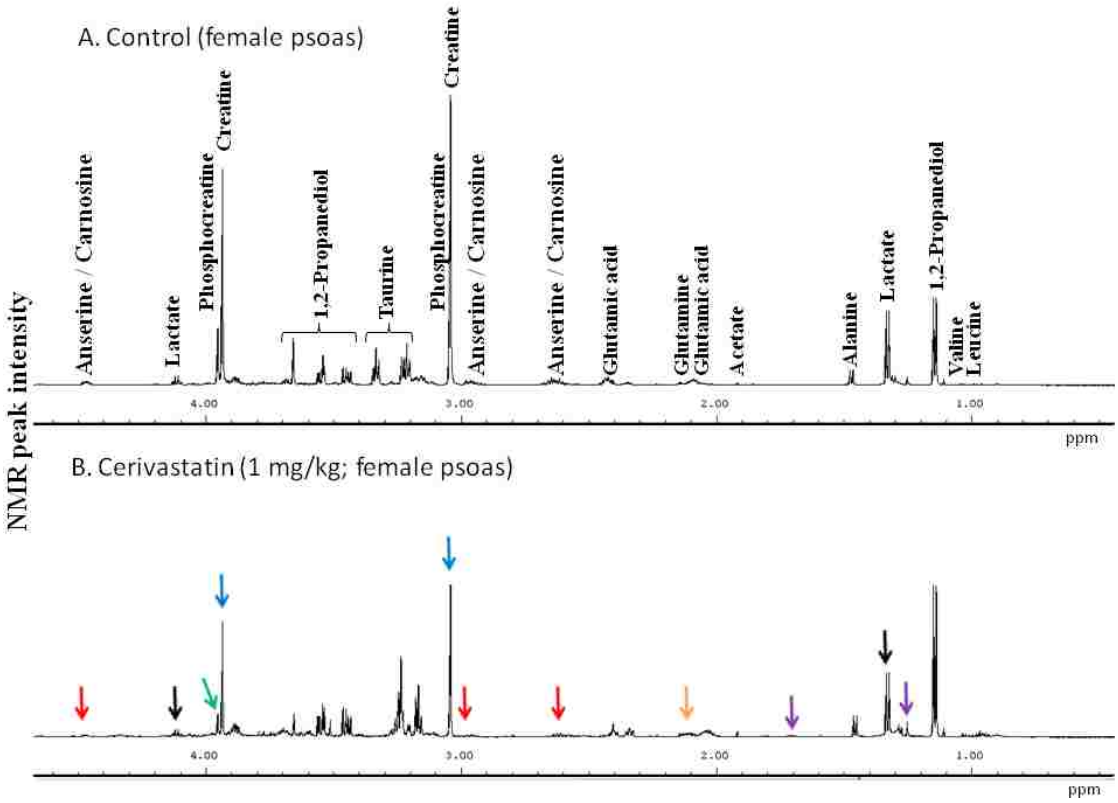

Figure 4.7. ^{1}H NMR spectra of aqueous extracts of the psoas from cerivastatin treated female rats (aliphatic region: 0.5-4.5 ppm). Representative spectra of the psoas from A) control and B) cerivastatin (1 mg/kg) treated female rats showing the major metabolic changes including a decrease in anserine (↓), carnosine (↓), lactate (↓), phosphocreatine (↓), creatine (↓) and two unknown metabolites at 1.27 and 1.77 ppm (↓). In contrast, glutamine increased (↓) in the psoas following cerivastatin treatment.

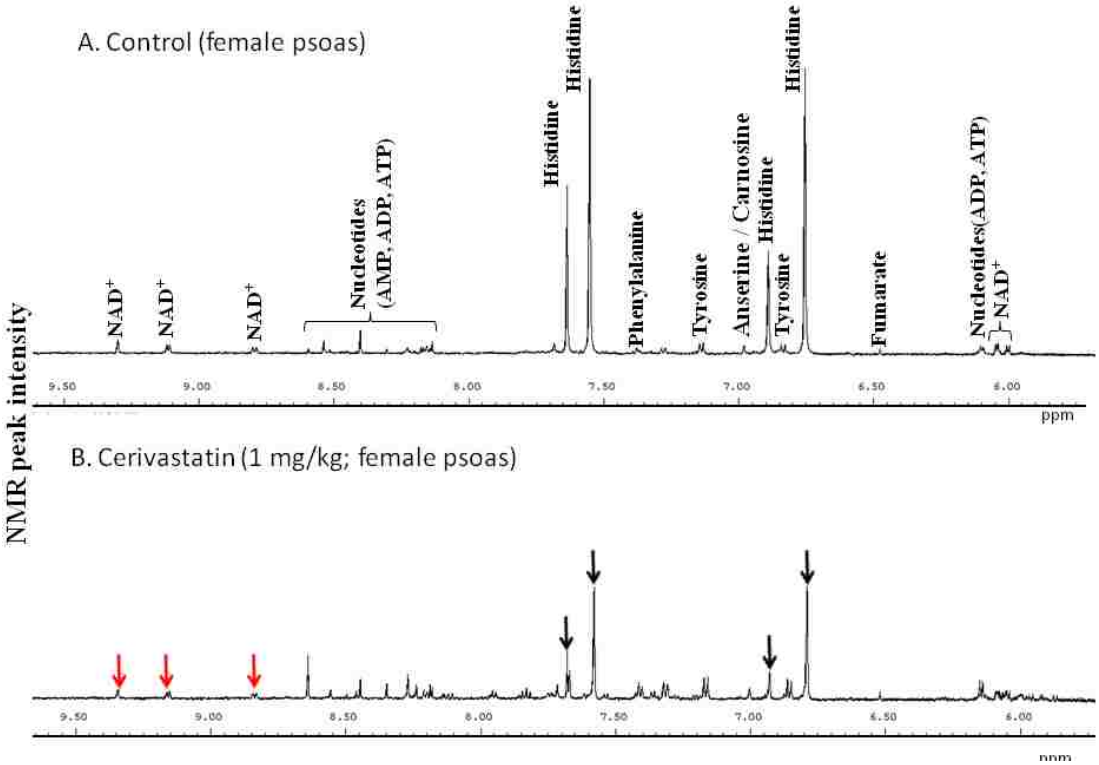

Figure 4.8. ^{1}H NMR spectra of aqueous extracts of the psoas from cerivastatin treated female rats (aromatic region: 5.7-9.5 ppm). Typical spectra of the psoas from A) control and B) cerivastatin (1 mg/kg) treated female rats illustrating the major metabolic changes including a reduction in NAD^+ (↓) and histidine-containing moities (↓).

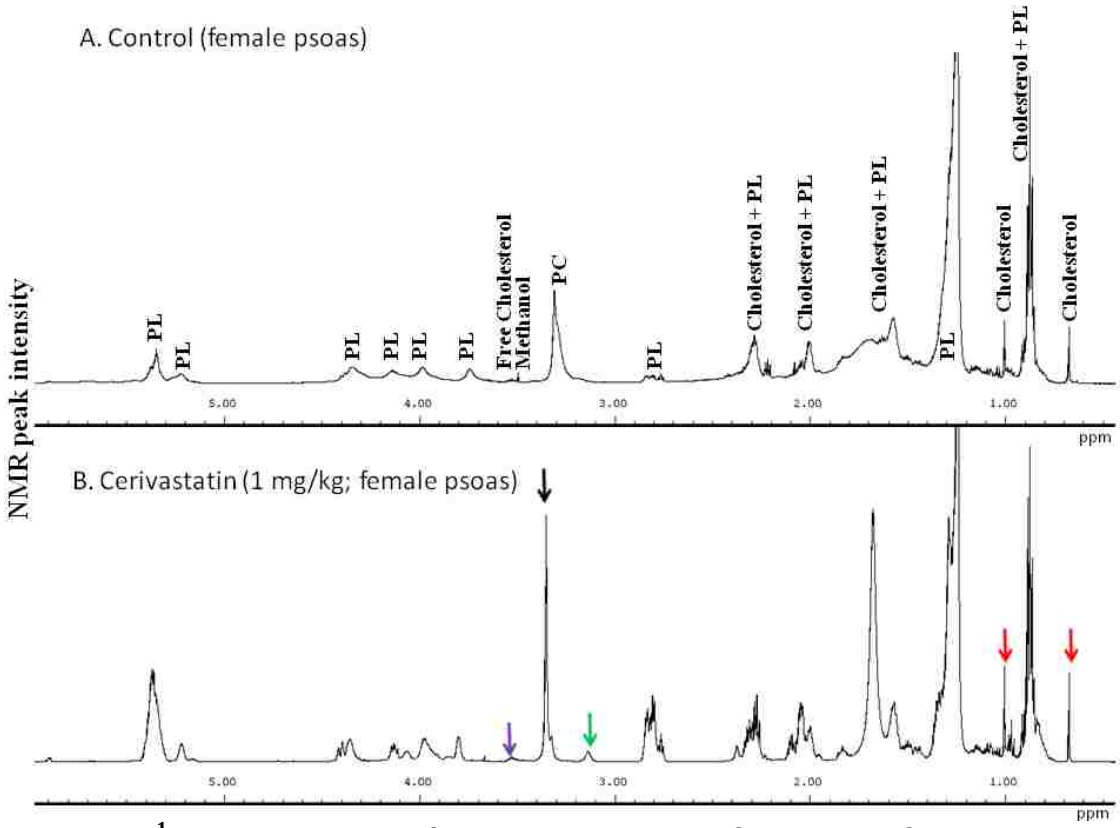

Figure 4.9. ^{1}H NMR spectra of lipophilic extracts of the psoas from cerivastatin treated female rats. Representative spectra of the psoas from A) control and B) cerivastatin (1 mg/kg) treated female rats showing the major metabolic changes including an increase in cholesterol (↓), phosphatidylcholine (PC) (↓), phospholipids (PL) and an unknown metabolite at 3.15 ppm (↓). The increase in cholesterol was confirmed as the free and not the esterified form based on the resonance at 3.55 ppm (↓) representing the proton on the carbon for the CHOH group which is absent in esterified cholesterol.

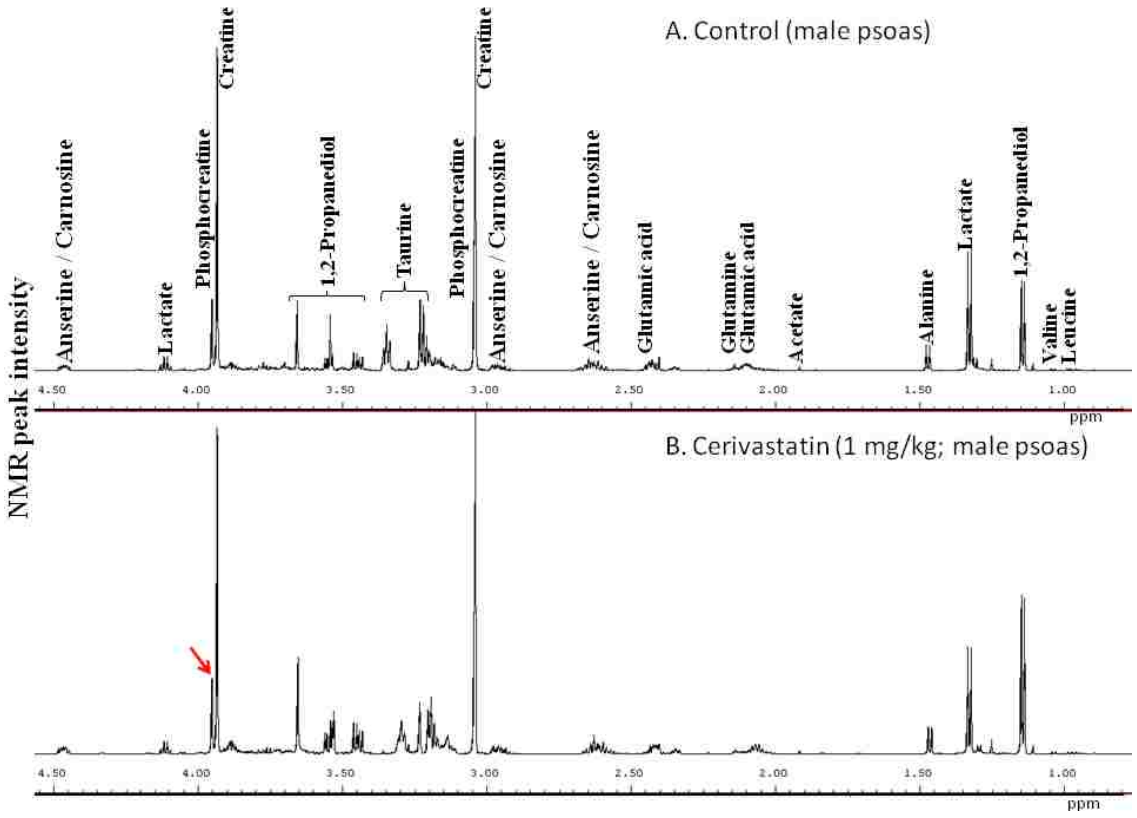

Figure 4.10. ^{1}H NMR spectra of aqueous extracts of the psoas from cerivastatin treated male rats (aliphatic region: 0.5-4.5 ppm). Representative spectra of the psoas from A) control and B) cerivastatin (1 mg/kg) treated male rats were generally similar but phosphocreatine (↓) was significantly higher following cerivastatin treatment.

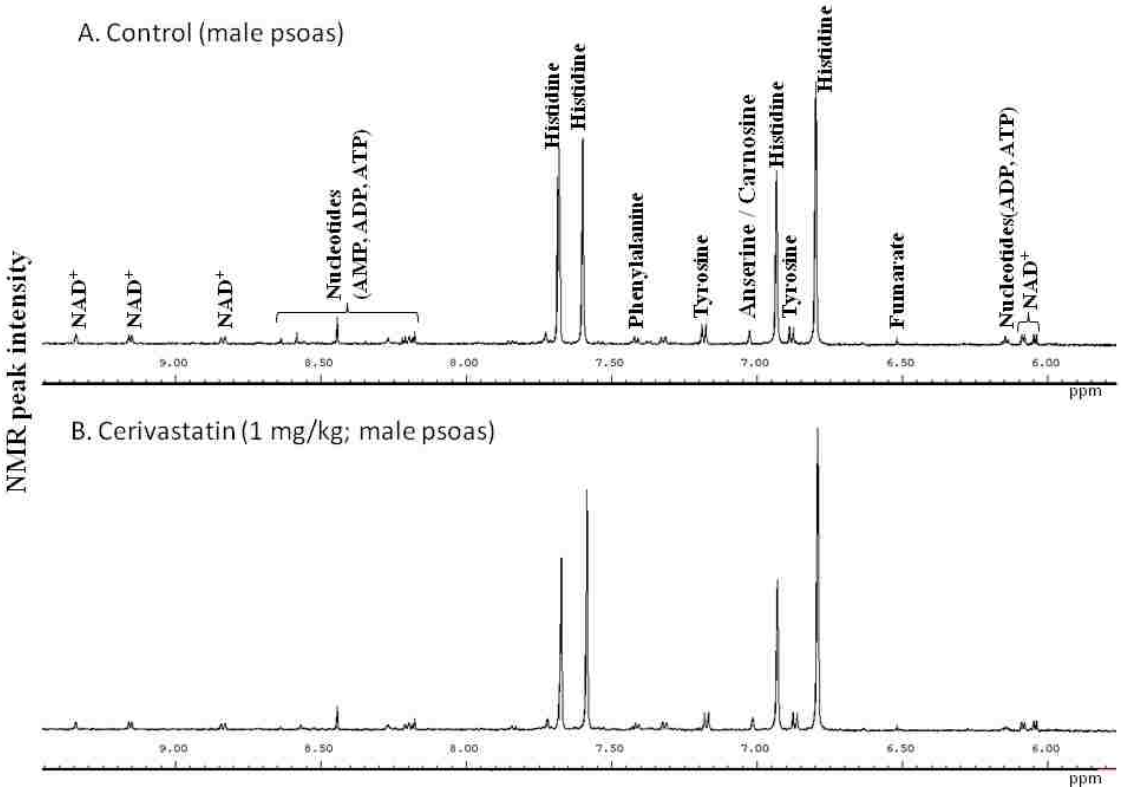

Figure 4.11. ^{1}H NMR spectra of aqueous extracts of the psoas from cerivastatin treated male rats (aromatic region: 5.7-9.5 ppm). Representative spectra of the psoas from A) control and B) cerivastatin (1 mg/kg) treated male rats illustrating similar metabolomic profiles.

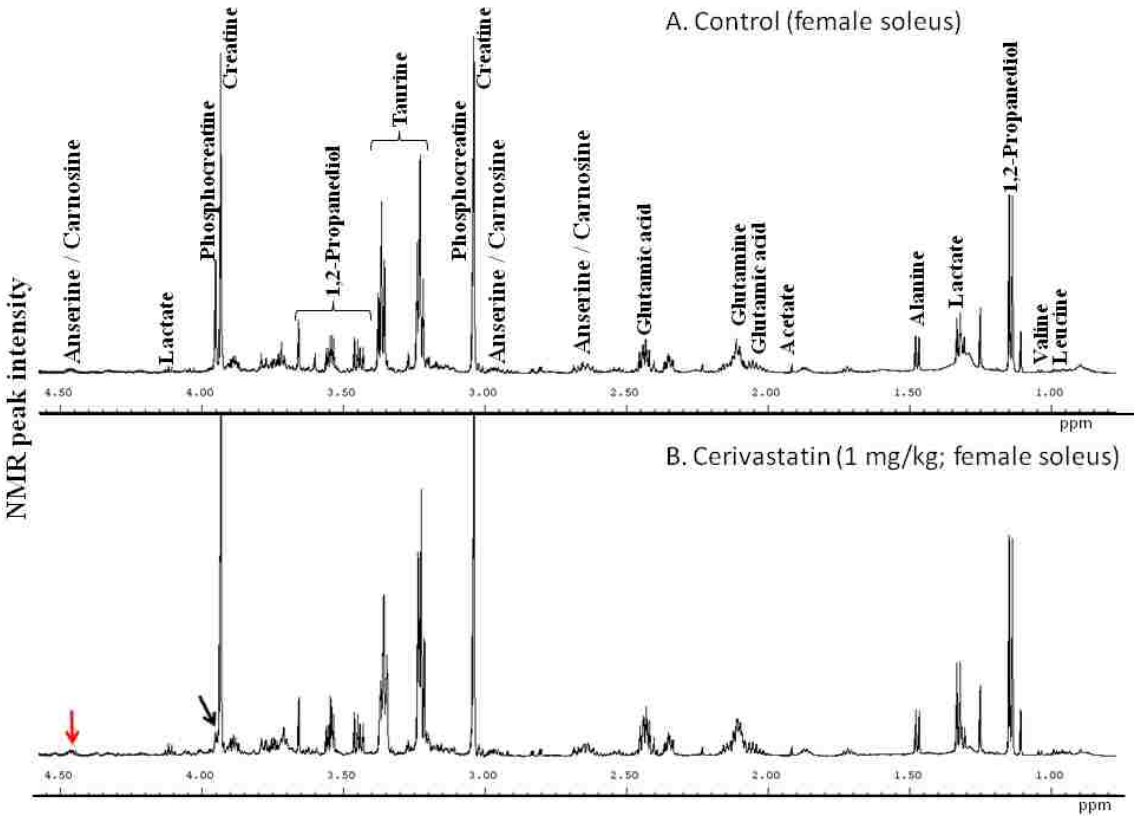

Figure 4.12. ^{1}H NMR spectra of aqueous extracts of the soleus from cerivastatin treated female rats (aliphatic region: 0.5-4.5 ppm). Representative spectra of the soleus from A) control and B) cerivastatin (1 mg/kg) treated female rats illustrating a decrease in anserine (↓) and phosphocreatine (↓). Anserine was quantitated based on a unique resonance at 3.79 ppm and a pH chemical shift at 4.6 ppm.

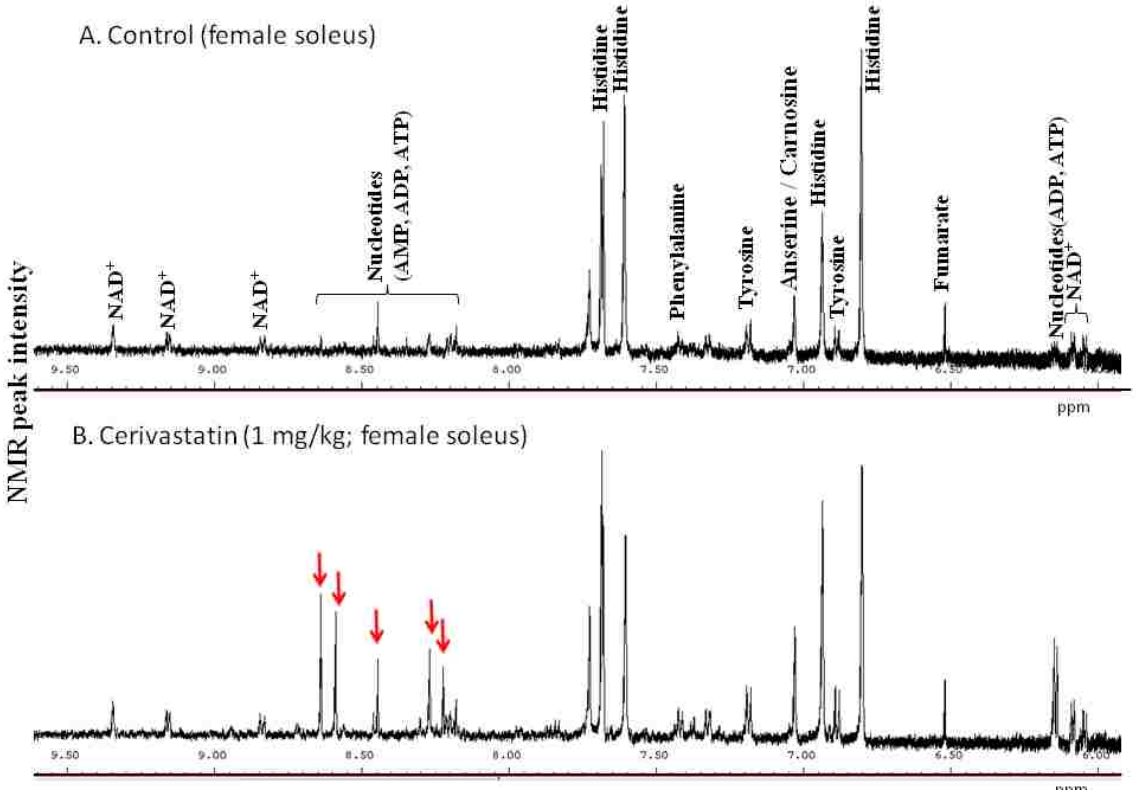

Figure 4.13. ^{1}H NMR spectra of aqueous extracts of the soleus from cerivastatin treated female rats (aromatic region: 5.7-9.5 ppm). Representative spectra of the soleus from A) control and B) cerivastatin (1 mg/kg) treated female rats shows an increase in several of the nucleotides (↓).

Table 4.1. Relative metabolite changes in aqueous skeletal muscle extracts following cerivastatin treatment[a]

Metabolite	Chemical shift (ppm) and assignment	Female Psoas		Male Psoas	Female Soleus	
		0.5 mg/kg	1 mg/kg	1 mg/kg	0.5 mg/kg	1 mg/kg
Metabolites involved with energy metabolism						
Glucose	4.64 (H')	-	-	-	-	-
Lactate	1.33 (CH_3), 4.11 (CH)	-	**-1.7 ± 0.1***	-	-	-
NAD^+	6.04 (H1'), 8.84, 9.15, 9.34 (nicotinamide and base)	**-1.4 ± 0.1***	**-2.5 ± 0.1***	-	-	-
Creatine	3.02 (CH_3), 3.93 (CH_2)	-	**-3.3 ± 0.1***	-	-	
Phosphocreatine	3.04 (CH_3), 3.95 (CH_2)	-	**-2.5 ± 0.1***	**1.3 ± 0.1***		**-1.7 ± 0.1***
Fumarate	6.53 (CH=CH)	-	-	-	-	-
Amino acids						
Alanine	1.47 (β-CH_3), 3.75 (α-CH)	-	-	-	-	-
Glutamic acid	2.04 (β-CH_2), 2.31 (γ-CH_2), 3.65 (α-CH_2)	-	-	-	-	-
Glutamine	2.08 (β-CH_2), 2.34 (γ-CH_2), 3.66 (α-CH_2)	-	**1.5 ± 0.1***	-	-	-
Leucine	0.94, 0.95 (δ-CH3), 1.69 (γ-CH2), 1.72 (β-CH), 3.64 (α-CH)	-	-	-	-	-
Phenylalanine	7.32 (2,6 H), 7.36 (4 H), 7.42 (3,5 H)	-	-	-	-	-
Tyrosine	6.88 (3,5 H), 7.16 (2,6 H)	-	-	-	-	-
Valine	1.00 (γ-CH_2), 2.20 (β-CH)	-	-	-	-	-
Other compounds						
Acetate	1.92 (CH_3)	-	-	-	-	-
Carnosine	Histidine: 2.95, 3.12 (β-CH), 4.46 (α-CH), 6.94 (4H), 7.68 (2H); β-alanine: 2.61 (β-CH3), 3.12 (α-CH)	-	**-2.5 ± 0.1***	-	-	-
Anserine[b]		-	**-2.5 ± 0.1***	-	-	**-1.7 ± 0.1***
Taurine	3.25 (CH_2NH), 3.41 (CH_2SO_3)	-	-	-	-	-

[a]Results represent the mean fold change ± SE for each metabolite in aqueous skeletal muscle extracts from cerivastatin treated compared to control rats measured by NMR.

[b]The 1H NMR spectra for anserine and carnosine are similar with one noted exception, anserine has a resonance at 3.79 ppm representing the NCH_3 group. Additionally, the two spectra show a chemical and pH shift at 4.6 ppm which enabled quantitation.

(-) = no change relative to control.

*Statistically significant at $p<0.05$.

Table 4.2. Relative metabolite changes in lipophilic skeletal muscle extracts following cerivastatin treatment[a]

Metabolite	Chemical shift and assignment	Female Psoas		Male Psoas	Female Soleus	
		0.5 mg/kg	1 mg/kg	1 mg/kg	0.5 mg/kg	1 mg/kg
Cholesterol[b]	0.68, 0.90, 1.01(CH_3), 1.64, 1.96, 2.26 (CH_2), 3.55 (CHOH)	**1.4 ± 0.1***	**1.8 ± 0.2***	-	-	-
Phosphatidylcholine (PC)	3.30 $(CH_3)_3$-N	**5.0 ± 0.6***	**5.5 ± 0.6***	**1.8 ± 0.1***	-	-
Phospholipids[c] (PL)	0.90 (CH_3), 3.74 (CH_2-N), 1.3, 1.7, 2.1, 2.35, 2.8, 3.7, 3.98, 4.14, 4.29 (CH_2), 5.4 (CH=CH)					

[a]Results represent the mean fold change ± SE of lipophilic skeletal muscle extracts from cerivastatin treated compared to control rats measured by NMR.

[b]There were two distinct resonances at 0.68 and 1.01 ppm which originate from C18 and C19 methyl groups of cholesterol (free + esterified forms), respectively. Specificity of the change in free cholesterol was determined based on an increase in the resonance at 3.55 ppm representing the proton on the carbon for the CHOH group which is absent in esterified cholesterol.

[c]Phospholipids as a class were identified but specific changes were not determined.

(-) = no change relative to control.

*Statistically significant at $p<0.05$.

Table 4.3. Concentration of sterols in the psoas[a]			
Sterol	**Control**	**Cerivastatin (0.5 mg/kg)**	**Cerivastatin (1 mg/kg)**
	nmol/g tissue[b]		
Total cholesterol[b]	1.6 ± 0.7	1.9 ± 0.1	2.8 ± 0.5*
7-Dehydrocholesterol	2.2 ± 0.3	2.8 ± 0.3	4.4 ± 0.9*
Desmosterol	1.4 ± 0.1	1.5 ± 0.2	5.4 ± 1.7*
7α-Hydroxycholesterol	1.1 ± 0.1	1.2 ± 0.1	2.9 ± 1.0*
Lanosterol	0.6 ± 0.1	0.7 ± 0.1	1.0 ± 0.2
Lathasterol	8.6 ± 1.9	9.5 ± 2.3	10.3 ± 1.8
β-Sitosterol	82.2 ± 8.1	52.7 ± 4.6*	58.7 ± 15.0
Campesterol	18.0 ± 1.4	12.1 ± 0.9*	13.7 ± 3.8
Stigmasterol	1.2 ± 0.1	1.0 ± 0.1	1.2 ± 0.5

[a]Results represent the mean ± SE of sterols in extracts of the female psoas from cerivastatin treated and control rats measured by LC-MS.

[b]Cholesterol, representing free and esterified is presented as μmol/g tissue.

*Statistically significant at $p<0.05$.

Chapter 5

Cerivastatin-induced myopathy is associated with alterations in cholesterol homeostasis and upregulation of the 25-hydroxycholesterol pathway

5.1. Introduction

Transcriptomic and metabolomic profiling of fast-twitch muscles in the rat indicated cerivastatin-induced myopathy is associated with alterations in cholesterol homeostasis (Tables 3.13 and 4.2). Specifically, these changes were characterized by a 2-fold increase in cholesterol and transcriptional upregulation of HMG-CoA reductase and the LDL receptor. Furthermore, transcriptional induction was also noted for genes involved with removing excess cholesterol through esterification (acyl-CoA: cholesterol acyltransferase), efflux (ABCG1 and ABCA1) and synthesis to 25-hydroxycholesterol (cholesterol 25-hydroxylase) (Table 3.13).

Given that the pharmacology of cerivastatin is inhibition of HMG-CoA reductase (IC_{50}=1 nM), and the plasma Cmax associated with myopathy is 221 nM (Reinoso et al., 2002; Steinke et al., 1996), an increase in skeletal muscle cholesterol was unexpected. However, the increase in cholesterol may in fact be mediated by the pharmacology, as statins cause a compensatory upregulation of cholesterol biosynthesis in the rat liver (Fujioka et al., 1995). Likewise, cerivastatin may also cause a pharmacological upregulation of cholesterol biosynthesis in the muscle and this could lead to pathological

consequences as accumulation and abnormal localization of cholesterol adversely affects cellular functions and promotes necrosis (Ikonen, 2006, 2008; Ridgway et al., 1999; Warner et al., 1995). Furthermore, accumulation of cholesterol in fast-twitch muscles has been associated with the pathogenesis of myopathies like inclusion body myositis, muscular dystrophy, chloroquine-induced myopathy, and muscle atrophy indicating this fiber type may be sensitive to changes in cholesterol homeostasis (Jaworska-Wilczynska et al., 2002; Kuhn and Logan, 1990; Kumar and Sharma, 2009; Nilsson et al., 1981; Williams and Smith, 1989). Accordingly, it was hypothesized that alterations in cholesterol homeostasis are causally related to the mechanism of statin-induced myopathy in rats.

The goal of this work was to determine whether alterations in cholesterol homeostasis occur prior to, or as a consequence of the myopathy. To determine the relationship between alterations in cholesterol homeostasis and toxicity a time course of cerivastatin-induced myopathy was conducted and alterations in cholesterol homeostasis were monitored in the sensitive fast-twitch muscle, the unaffected slow-twitch muscle and in the liver.

5.2. Methods

Chemicals. Cerivastatin (Na salt) was purchased from Sequoia Research Products (Pangbourne, United Kingdom). Methylcellulose A15C premium was purchased from the Dow Chemical Company (West Point, PA). Nondeuterated sterols including 7-Dehydrocholesterol 7α-hydroxycholesterol, 7α, 25-dihydrocholesterol, 7α,25-dihydro-4-cholesten-3-one were purchased from Avanti Polar Lipids (Alabaster, Alabama) and 24(S)-hydroxycholesterol was purchased from Enzo Life Sciences (Plymouth Meeting, PA) (Figure 6.1). Deuterated (D) sterols with the number of hydrogens replaced with deuterium (D3-7), including cholesterol (D7), desmosterol (D6), 7β-hydroxycholesterol (D7), 25-hydroxycholesterol (D3 and D6), 27-hydroxycholesterol (D6) were purchased from Avanti Polar Lipids (Figure 6.1).

Study design. This investigation was conducted on samples obtained from *study 1 and 2* described in Chapter 2. Skeletal muscle muscles representing slow-twitch (soleus) and fast-twitch (quadriceps femoris and psoas) twitch fiber composition (Table 2.1) and the left lateral lobe of the liver were fixed in 10% neutral buffered formalin for histopathological assessment whereas the same skeletal muscles on the right side of the animal, including the right lateral lobe of the liver were flash frozen and used for sterol analysis and RNA isolation.

Histopathology. Tissues were processed for histopathologic evaluation as described in Chapter 2.2.

Evaluation of sterols in skeletal muscle and liver. A pilot study was initially conducted on the quadriceps from control and cerivastatin treated rats treated for 14 days (*study 1*; 1 mg/kg) to determine the relative changes in sterols and hydroxycholesterols. Based on these results, a panel of sterols and hydroxycholesterols were selected and quantitated in the psoas across the time course, and soleus and liver after 14 days of treatment (*study 2).* Frozen muscle tissues (quadriceps, psoas and soleus) and the right lateral lobe of the liver were individually pulverized in liquid nitrogen and a portion (100 mg psoas and liver, and 50 mg of soleus) was extracted according to the method of Folch (1957). Metabolite extraction was performed by homogenizing the tissue in a bead mill (Retsch MM 300, Haan Germany) for 4 minutes (30 Hz) with 10 volumes of ice-cold methanol. To each sample, 5 µl (60 ng/µl) of deuterated 25-hydroxycholesterol (D6) (internal standard) was added. Following centrifugation (8000g, 4˚C) for 15 minutes, the supernatant (0.6 ml for psoas and liver; 0.3 ml for soleus) was transferred to water/chloroform (0.4 ml / 1 ml for psoas and liver; 0.2 ml / 0.6 ml for soleus) and vortexed for 10 seconds and then shaken in a bead mill (30 Hz) for 10 minutes at room temperature. Samples were centrifuged (6000g, 4˚C) for 25 minutes and the chloroform (lipophilic phase) was collected and dried under nitrogen at room temperature and reconstituted in 200 µl of methanol, vortexed and centrifuged for 10 minutes at 12,000g. The supernatant was transferred to a new tube and sterols were measured by LC/MS.

Sterol standard curves. For the pilot study, standards representing a panel of relevant sterols and hydroxycholesterols were prepared, including cholesterol (D7), 7-dehydrocholesterol, desmosterol (D6), 7α-hydroxycholesterol, 7β-hydroxycholesterol

(D7), 24(S)-hydroxycholesterol, 25-hydroxycholesterol (D3), 7α, 25-dihydrocholesterol, 7α,25-dihydro-4-cholesten-3-one, and 27-hydroxycholesterol (D6) (Figure 5.1). For quantitation of sterols in the psoas, soleus and liver standard curves were prepared for cholesterol (D7; 1-500 µg/ml), 7-dehydrocholesterol (5-5000 ng/ml), desmosterol (D6; 5-50,000 ng/ml), 7β-hydroxycholesterol (D7; 5-5000 ng/ml), 25-hydroxycholesterol (D3; 5-5000 ng/ml). Each sterol standard was prepared in 200 µl of methanol containing 300 ng of the internal standard 25-hydroxycholesterol (D6) with a final concentration of 1.5 µg/ml.

***LC/MS*:** Sterols were separated by a Thermo-Fisher Accela reversed-phase UPLC with a Waters Acquity UPLC BEH C18 analytical column (2.1×100 mm, 1.7 µm) at 65˚C. A gradient mobile phase was used consisting of (Mobile Phase A) 0.1% formic acid in water and (Mobile Phase B) methanol with 0.1% formic acid with a flow rate of 0.6 ml/min and an injection volume of 5 µl. Initial mobile phase conditions were 60% A and 40% B for 0.2 minutes, followed by a linear gradient to 25% A and 75% B over 0.3 minutes and a linear gradient to 100% B over 8.5 minutes. Initial mobile phase conditions for system equilibration were established after 9 minutes for a total sample analysis time of 10 minutes. Between each sample analysis the needle was washed in 0.1% formic acid in acetonitrile and then with 0.1% formic acid in 80:20 (methanol:water). A Thermo-Fisher Oribtrap Exactive MS with APCI positive mode was used for sterol detection. Identification of each sterol was based on an external standard curve, elution time and accurate m/z. Although sensitivity for each sterol was not determined the concentration

of all the sterols but 25-hydroxycholesterol was within the range of the standard curve. The LOQ for 25-hydroxycholesterol was 0.01 µg/g of wet tissue weight.

RNA isolation. Frozen tissues from *study 2* were pulverized and 50 mg of muscle (psoas and soleus) and liver was used for RNA isolation. RNA was isolated with TRIzol (Invitrogen Corporation, Carlsbad, CA) and an RNeasy spin column (Qiagen, Valencia, CA) according to the manufacturers' instructions. Removal of DNA was achieved by using Qiagen's RNase-Free DNase. The quantity (260 nm absorbance) and quality (260 / 280 nm absorbance ratio) of total RNA was determined on a ND-1000 spectrophotometer (NanoDrop Technologies, Inc., Wilmington, DE).

Quantitative RT-PCR. RNA (2 µg) was reverse transcribed to cDNA using a High Capacity cDNA reverse transcription kit (Applied Biosystems, Foster City, CA). Quantitative RT-PCR was performed on the ABI Prism 7900HT Sequence Detection System (Applied Biosystems) using 2X Power SYBR® Green PCR master mix (Applied Biosystems). Primer Express (v2.0, Applied Biosystems) was used to design primers which were synthesized by Invitrogen (Table 5.1) (Invitrogen Corporation, Carlsbad, CA). The 18S rRNA primers from Applied Biosystems were used as an endogenous control. Primer specificity was confirmed by BLAST searches and melting curve analysis demonstrated that primers only generated a single amplicon. The amplification conditions used were 2 min at 50°C, 10 min at 95°C, followed by 40 cycles at 95°C for 15 s and 60°C for 30 s. To create dissociation curves, additional steps were added to the end of the

amplification reaction: 95°C for 15 s, 60°C for 15 s and then gradually increasing to 95°C for 20 min.

Isolation of rat fast-twitch myofibers. Isolation of rat fast-twitch myofibers is described in Chapter 2.2. To each well, 30 µl of vehicle (maintenance medium) or cerivastatin (final concentration was 300 nM) was added to the myofibers. This concentration was selected because a toxic dose of cerivastatin in female rats is associated with a Cmax of 221 nM (Reinoso et al., 2002; Steinke et al., 1996). Therefore, for the current work a slightly higher concentration was selected for testing. Furthermore, 3-4 days of cerivastatin (300 nM) treatment is associated with morphological changes characteristic of a stressed and dying cell and reduced viability (Figure 2.5). On days, 1, 2, 3, and 4 the medium from one plate was gently removed with a pipette and the myofibers were washed twice with pre-warmed PBS (100 µl).

Myofiber sterol extraction. Ice-cold methanol (200 µl) was added to 24 control and 24 treated wells. The bottom of the wells was scrapped with a pipette tip to remove the myofibers. The methanol was also pipetted up and down several times to remove myofibers. The methanol was removed and pooled together giving two samples (control and treated) for each of the four days. Following collection, these samples were frozen at -80˚C. To each sample (approximately 5 ml of methanol) one volume of chloroform and 0.4 volumes of water was added. The samples were vortexed and centrifuged at 12,000g for 25 minutes. The bottom layer was transferred to a new glass vial and dried. For LC/MS analysis, samples were reconstituted in 200 µl of methanol, vortexed and centrifuged for 10 minutes at 12,000g. The supernatant was transferred to a new tube and

cholesterol, 7-dehydrocholesterol, desmosterol and 25-hydroxycholesterol were measured by LC/MS as described above for tissues.

Myofiber RNA isolation. Lysis buffer (50 µl) (Qiagen RLT buffer) was added to 24 control and 24 treated wells. The bottom of the wells were scrapped with a pipette tip to remove myofibers. The buffer was also pipetted up and down several times to remove the cells. The buffer was removed from 24 control and 24 treated wells and pooled together giving two samples (control and treated) for each of the four days. The lysis buffer was pipetted up and down with a 20 gauge needle on a syringe to lyse the cells. Following collection, these samples were frozen at -80˚C. RNA was isolated with an RNeasy spin column according to the manufacturers' instructions. The quantity and quality of RNA as well as the RT-PCR conditions were was conducted as described above.

Cholesterol 25-hydroxylase immunohistochemistry. The quadriceps from control and cerivastatin (*study 1*; 1 mg/kg; 14 days) treated rats were sectioned at 4 µm, mounted on slides, deparaffinized, rehydrated and treated with cell conditioning 1 antigen retrieval buffer at 100˚C for 30 minutes (Ventana, Medical Inc., Tucson, AZ). Sections were incubated separately with CH25H mouse monoclonal antibody (Abcam, Cambridge, MA) at 1:50 or CD68 (ED1) mouse monoclonal antibody (AbD Serotec, Oxford, UK) at 1:500 for one hour at room temperature. Following incubation, tissues were incubated with anti-mouse IgG biotin and streptavidin-HRP and developed in DAB substrate. Positive expression (brown signal) was confirmed by observation of distinct granular deposits by light microscopy. For double staining, DABMAP and REDMAP detection

kits were used (Ventana Medical Inc.). CH25H signals were developed with DAB chromagen (brown signal) and CD68 signals were developed with fast red substrate (red/purple signal). Colocalization of CH25H with CD68 shows a double positive orange signal.

Data analysis. Sterol identification and relative changes following cerivastatin treatment were assessed based on a single standard in the pilot study (*study 1*) and in myofibers. Quantitation of sterols in muscle and liver were determined in *study 2* with standard curves (correlation coefficient>0.99). For quantitative RT-PCR, relative changes in gene expression were determined by the ΔΔCt method. The Ct values for each gene were normalized to 18S Ct values and the fold change in treated muscles was determined relative to control. Group means for all analyses were compared with a Student's t-test or ANOVA using StatView (SAS Institute, Cary, NC) at $p<0.05$. However, statistics for the RT-PCR results were conducted on the values following normalization to 18S.

5.3. Results

Cerivastatin caused fast-twitch specific myofiber degeneration in the quadriceps and psoas in female rats after 14 days of dosing whereas the slow-twitch fibers of the soleus were unaffected as previously described (*Study 1*; Figure 2.2; Table 2.2). In the cerivastatin time course, skeletal muscle toxicity was initially observed in the fast-twitch muscles (quadriceps and psoas) after 8 days of dosing and increased in severity after 10 and 14 days of dosing as previously described (*Study 2*; Figure 2.3; Table 2.3). In contrast, no myopathy was observed in the soleus at any time. Furthermore, no evidence of hepatotoxicity was observed in either of these studies. (Tables 2.2 and 2.3).

Cerivastatin-induced myopathy was associated with alterations in cholesterol homeostasis in the quadriceps, including an increase in cholesterol, 7-dehydrocholesterol, desmosterol and 7α/β-hydroxycholesterol as previously observed in the psoas (*Study 1*; Table 4.3; Table 5.2). Furthermore, 25-hydroxycholesterol was increased 31-fold relative to control and the downstream sterol in the 25-hydroxylation pathway, 7α,25-dihydro-4-cholesten-3-one was also increased 14-fold (*Study 1*; Table 5.2; Figure 5.2). In contrast, 24- and 27-hydroxycholesterol were non-detectable in the quadriceps showing myopathy (*Study 1*; Table 5.2). Accordingly, these results demonstrate that upregulation of the 25-hydroxylation pathway is a specific response associated with cerivastatin-induced myopathy (Figure 5.2).

To determine whether alterations in cholesterol homeostasis are causally related to toxicity the concentration of sterols was determined in a time course of cerivastatin-

induced myopathy (*Study 2*). In the psoas, cholesterol, 7-dehydrocholesterol, desmosterol and 25-hydroxycholesterol were all increased but only in the presence of myopathy (≥ day 11), indicating these changes are not causally related to toxicity (Table 5.3). In contrast, these sterols were unchanged in the soleus, consistent with the absence of myopathy. In the liver, sterol increases were noted on day 15, indicating increased hepatic cholesterol synthesis and uptake (Table 5.3).

To further investigate alterations in cholesterol homeostasis, transcriptional changes in a subset of genes induced with cerivastatin-induced myopathy, and involved with cholesterol regulation, were evaluated in tissues from the time course (*Study 2*; Table 3.13). In the psoas, transcriptional induction of these genes was associated with the manifestation of myopathy whereas similar changes were not observed in the soleus (Figure 5.3). The expression of these genes in the time course after 14 days of dosing cerivastatin (1 mg/kg) were similar to the microarray results for skeletal muscles observed in the cerivastatin (1 mg/kg) dose response *study 1* (Table 3.13). In the liver, HMG-CoA reductase showed an immediate and sustained transcriptional induction across the time course, suggesting this response is likely mediated by cerivastatin pharmacology (Figure 5.3). In contrast, cholesterol 25-hydroxylase, Acyl-CoA: cholesterol acyltransferase and ABCG1 were only minimally increased or unchanged (Figure 5.3).

To determine whether alterations in cholesterol homeostasis are muscle specific, fast-twitch myofibers were isolated and treated with cerivastatin (300 nM) for up to 4 days. After 3-4 days, light microscopy revealed that the myofibers developed blebs on the plasma membrane consistent with a stressed / dying cell (Table 2.4; Figures 2.5 and 2.6). However, unlike the in vivo psoas response, cholesterol, 7-dehydrocholesterol, and desmosterol were not increased relative to control and 25-hydroxycholesterol was below the limit of detection following cerivastatin treatment (Figure 6.4). The transcriptional profile was also different in the myofibers compared to the psoas but similar to the liver, with HMG-CoA reductase showing a sustained transcriptional induction across the 4-day time course whereas cholesterol 25-hydroxylase, ABCG1 and Acyl-CoA: cholesterol acyltransferase showed no change or a reduction relative to control (Figure 5.5). Together, the sterol and transcriptional profile in the treated myofibers did not recapitulate changes observed in the psoas, suggesting alterations in cholesterol homeostasis are mediated in part by in vivo factors.

Transcriptional induction of cholesterol 25-hydroxylase has not been reported in models of myopathy. Therefore, to determine whether the increase in cholesterol 25-hydroxylase is specific to the muscle, immunohistochemical staining of the quadriceps following cerivastatin treatment was conducted (*Study 1*). In the quadriceps from control rats, there was no expression of cholesterol 25-hydroxylase or CD68 (constitutive marker of macrophages) (Figure 5.6A). However, cholesterol 25-hydroxylase (Figure 5.6B) and CD68 (Figure 5.6C) were both readily detectable in muscle cells and macrophages, respectively with cerivastatin-induced myopathy. Furthermore, no double staining of

these proteins was observed indicating that the cholesterol 25-hydroxylase response is specific to the muscle cell (Figure 5.6D).

5.4. Discussion

All nucleated cells can synthesize cholesterol from acetyl-CoA through the mevalonate pathway. However during normal physiological conditions the rate of cholesterol biosynthesis in rat skeletal muscle is less than 1% of the liver and significantly less than other major organs (Spady and Dietschy, 1983). Furthermore, skeletal muscle shows the lowest uptake of LDL-C compared to other major organs (Stange and Dietschy, 1984; Turley et al., 1981). The reduced need for cholesterol synthesis in skeletal muscle is likely related to the fact that under normal physiological conditions differentiated skeletal muscle is comprised of predominately post-mitotic cells and there is a minimal need for membrane synthesis. However, increases in skeletal muscle cholesterol synthesis and uptake are associated with processes involving membrane synthesis like myogenesis, hypertrophy and injury repair (Martini et al., 2009; Riechman et al., 2009; Trapani et al., 2010; Vinagre et al., 2007). This tight regulation of cholesterol homeostasis is important because abnormal accumulation of cholesterol adversely affects cellular functions, promotes necrosis and has been associated with the pathophysiology of various myopathies (Cui et al., 2002; Ikonen, 2006, 2008; Jaworska-Wilczynska et al., 2002; Kuhn and Logan, 1990; Kumar and Sharma, 2009; Nilsson et al., 1981; Ridgway et al., 1999; Warner et al., 1995; Williams and Smith, 1989).

In humans, statins inhibit hepatic HMG-CoA reductase resulting in transcriptional induction of the LDL receptor, increased hepatic uptake and reduction in serum cholesterol. In rats, there is a compensatory response in which HMG-CoA reductase is transcriptionally induced resulting in increased liver and serum cholesterol levels (Fujioka et al., 1995). However, serum cholesterol was unchanged with cerivastatin

treatment in the current study (results not shown). Instead, cerivastatin was shown to increase cholesterol levels in fast-twitch muscles in association with myopathy, suggesting this tissue may respond similar to the liver (Chapters 3 and 4). Since abnormal accumulation of cholesterol is potentially toxic it was hypothesized that alterations in skeletal muscle cholesterol homeostasis are causally related to the development of cerivastatin-induced myopathy. (Ikonen, 2006, 2008; Ridgway et al., 1999; Warner et al., 1995). Therefore, the goal of this work was to determine the temporal relationship between alterations in skeletal muscle cholesterol homeostasis and the development of cerivastatin-induced myopathy.

In the cerivastatin time course the sterol and transcriptional profile of the fast-twitch muscle demonstrated that altered cholesterol homeostasis is a manifestation of the myopathy and unrelated to the mechanism of toxicity. Importantly, this profile was different from the soleus in which there was no evidence of toxicity or changes in cholesterol homeostasis. Furthermore, the profile was also different from the liver which showed an immediate and sustained compensatory transcriptional induction in HMG-CoA reductase consistent with the pharmacology.

Although the mechanism of increased cholesterol and transcriptional induction of HMG-CoA reductase was not directly probed in this work, this response may be mediated by the need to repair damaged skeletal muscle and remove excess cholesterol (Figure 6.7). Similarly, transcriptional induction of HMG-CoA reductase was also observed in vitro although cholesterol concentrations were unchanged indicating that the in vitro model did

not recapitulate changes observed in vivo. The disparity between the in vivo and in vitro results may be related to undefined in vivo factors or the fact that the myofiber medium did not contain serum or cholesterol. Accordingly, the myofibers may not have been able to synthesize or acquire cholesterol from the medium. Importantly, cerivastatin caused toxicity in vitro in the absence of alterations in cholesterol homeostasis. Therefore, this work further demonstrates that an increase in cholesterol is a response to myofiber damage and unrelated to the mechanism of toxicity.

One limitation of this study was that the location of the increased cholesterol in the muscle was not directly determined. Specifically, the increase in cholesterol could be occurring intracellularly or extracellularly in the muscle as a consequence of necrosis. However, transcriptional induction of genes involved with cholesterol esterification (acyl-CoA: cholesterol acyltransferase), efflux (ABCG1 and ABCA1) and conversion (cholesterol 25-hydroxylase) to 25-hydroxycholesterol represent a profile consistent with a response involving removal of excess intracellular cholesterol (Bjorkhem et al., 2009). Furthermore, since cholesterol 25-hydroxylase protein was specifically expressed in muscle cells it is reasonable to conclude that alterations in cholesterol homeostasis occurred within the skeletal muscle and not in macrophages or extracellularly.

Activation of the 25-hydroxylation pathway has not been previously reported with skeletal muscle necrosis. Therefore, it is unknown whether this response is specific to statin myopathy or commonly associated with other muscle pathologies. However, various biological roles for 25-hydroxycholesterol have been previously identified.

Specifically, this oxysterol is more hydrophilic than cholesterol and is able to passively diffuse across the membrane and is reverse transported to the liver where it is converted to bile acids (Bjorkhem et al., 2009). Moreover, 25-hydroxycholesterol is a ligand for LXR which activates the efflux transporters and further increases removal of cholesterol (Bjorkhem et al., 2009). At the same time, 25-hydroxycholesterol suppresses cholesterol synthesis when levels are in excess (Figure 1.3). Additionally, a pro-inflammatory role has also been described in which cholesterol 25-hydroxylase is transcriptionally induced through Toll-like receptor signaling and 25-hydroxycholesterol stimulates IL-8 production and recruits inflammatory cells (Bauman et al., 2009; Vejux et al., 2008). Similar hydroxylation pathways have also been identified, which are induced in a tissue specific manner, and regulate cholesterol homeostasis including, 27-hydroxycholesterol in macrophages, 24S-hydroxycholesterol in the brain and 7α-hydroxycholesterol in the liver (Bjorkhem, 2009; Vejux et al., 2008). Accordingly, the current results suggest that 25-hydroxylation of cholesterol is an important pathway in skeletal muscle which regulates cholesterol homeostasis with statin-induced myopathy (Figure 5.7).

In summary, the current work demonstrates that cerivastatin increases skeletal muscle cholesterol levels but these alterations are not causally related to the mechanism of cerivastatin-induced toxicity. Instead, the increase in cholesterol is likely associated with the tissue repair process triggered by muscle injury (Figure 6.7). Furthermore, in the face of ongoing toxicity, the muscle is unable to repair itself, resulting in cholesterol accumulation and triggering pathways, including esterification, efflux and conversion to 25-hydroxycholesterol which facilitate removal of excess cholesterol (Figure 5.7).

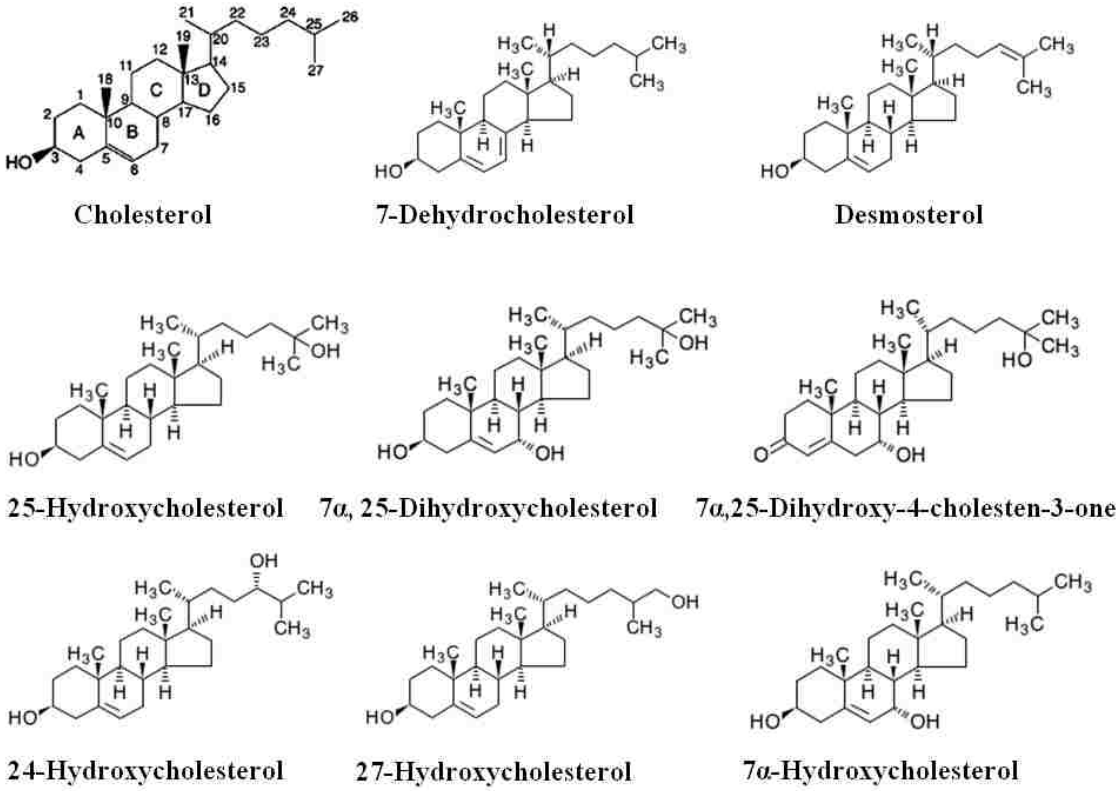

Figure 5.1. Chemical structures of sterols measured in tissues. For several sterols, hydrogens on carbons 25, 26 and 27 were replaced with deuterium.

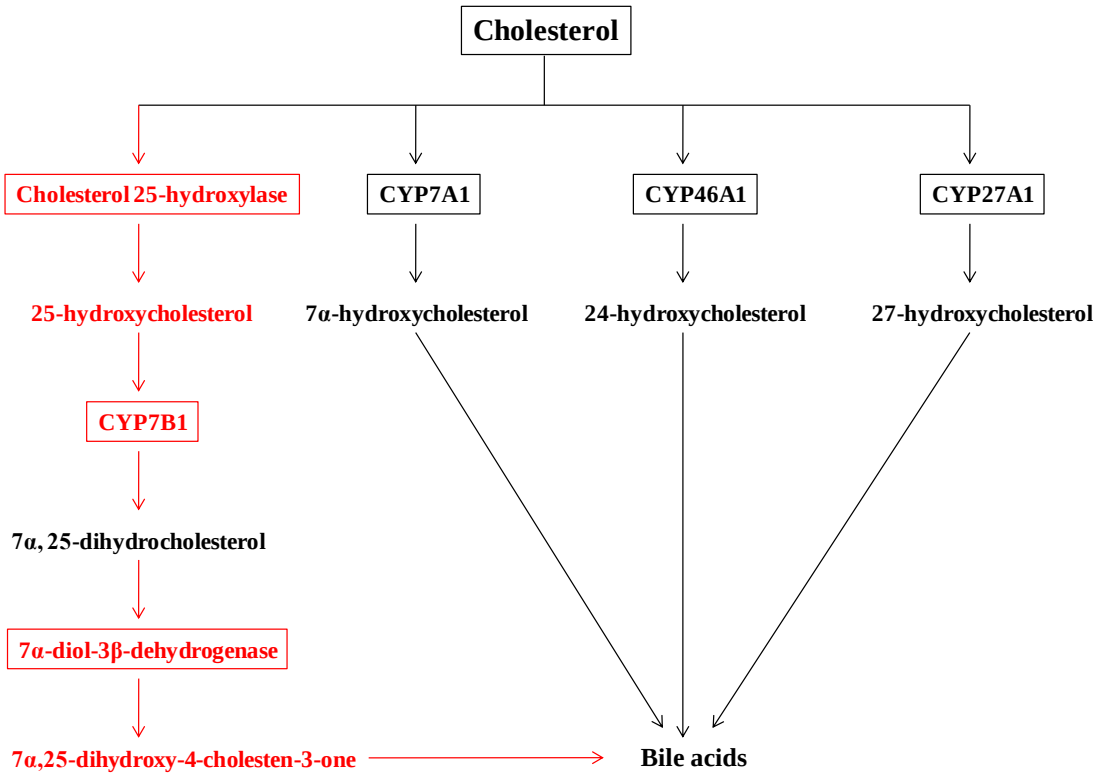

Figure 5.2. Cerivastatin-induced myopathy upregulates the cholesterol 25-hydroxylase pathway. Cholesterol 25-hydroxylase was transcriptionally induced with cerivastatin-induced myopathy and this was accompanied by an increase in 25-hydroxycholesterol and 7α, 25-dihydroxy-4-cholesten-3-one. Although not evaluated in the current work, both CYP7B1 and 7α-diol-3β-dehydrogenase were also transcriptionally induced with cerivastatin (1 mg/kg) myopathy after 14 days of dosing (Table 3.13). In contrast, levels of 7α-, 24- and 27-hydroxycholesterol were minimally increased or unchanged and this is consistent with the previous observation indicating that CYP7A1 and CYP46A1 are not transcriptionally induced and CYP27A1 is downregulated with cerivastatin (Table 3.13). Accordingly, these results demonstrate that cerivastatin-induced myopathy is associated with a specific upregulation of the cholesterol 25-hydroxylase pathway.

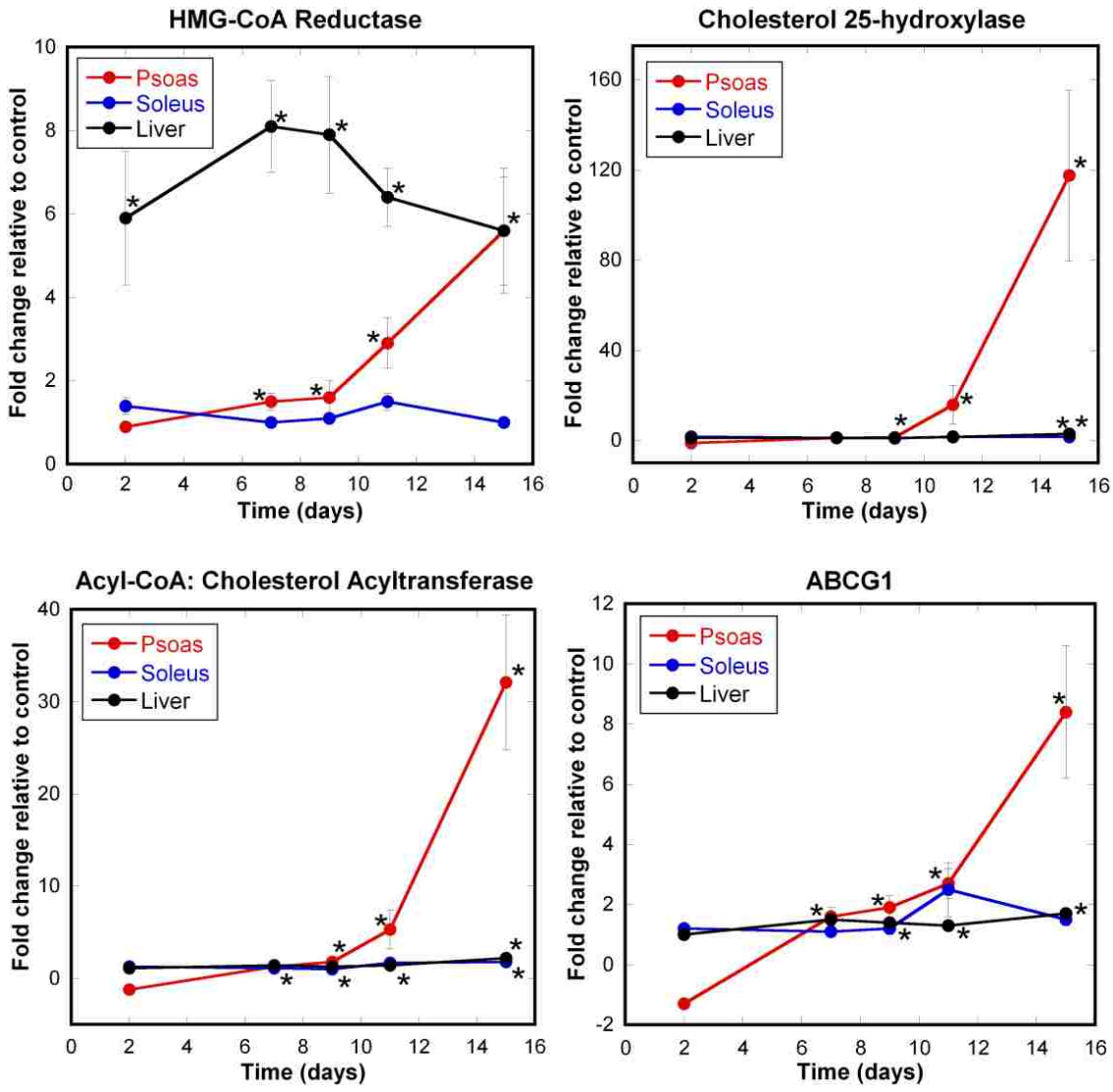

Figure 5.3. Genes involved with cholesterol homoeostasis are transcriptionally induced with cerivastatin-induced myopathy. A subset of genes involved with cholesterol regulation, and induced with myopathy after dosing cerivastatin (1 mg/kg) for 14 days (Table 3.13), were evaluated in a time course to determine whether these changes are causally related to toxicity. In the psoas, these genes were transcriptionally induced as a manifestation of myopathy (≥ 8 days of cerivastatin) whereas in the soleus these genes were unchanged. In the liver, HMG-CoA reductase was transcriptionally induced as expected in response to the pharmacological activity of cerivastatin.

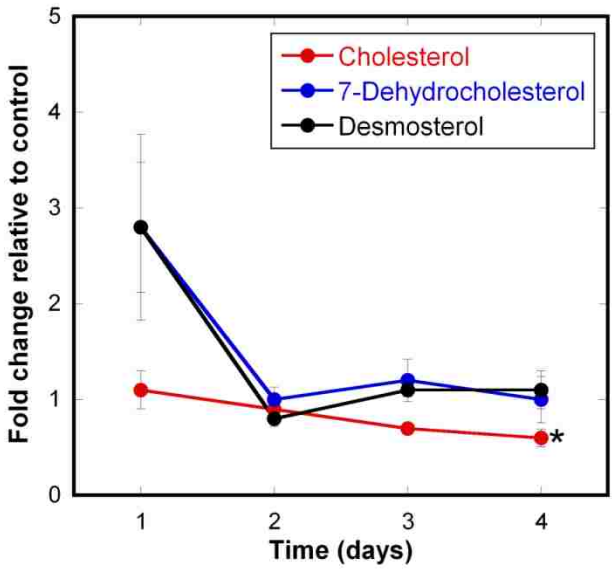

Figure 5.4. Sterol changes in cerivastatin treated isolated myofibers. Myofibers cultured in medium without serum were treated with cerivastatin (300 nM) for up to four days and sterol levels were measured by LC/MS. The concentration of these sterols was either unchanged or decreased with cerivastatin treatment. These results do not recapitulate the in vivo findings suggesting other in vivo factors contribute to an increase in these sterols.

Results represent the mean fold change relative to control ± SE of three separate experiments.

25-Hydroxycholesterol was non-detectable.

Statistically significant at $p<0.05$.

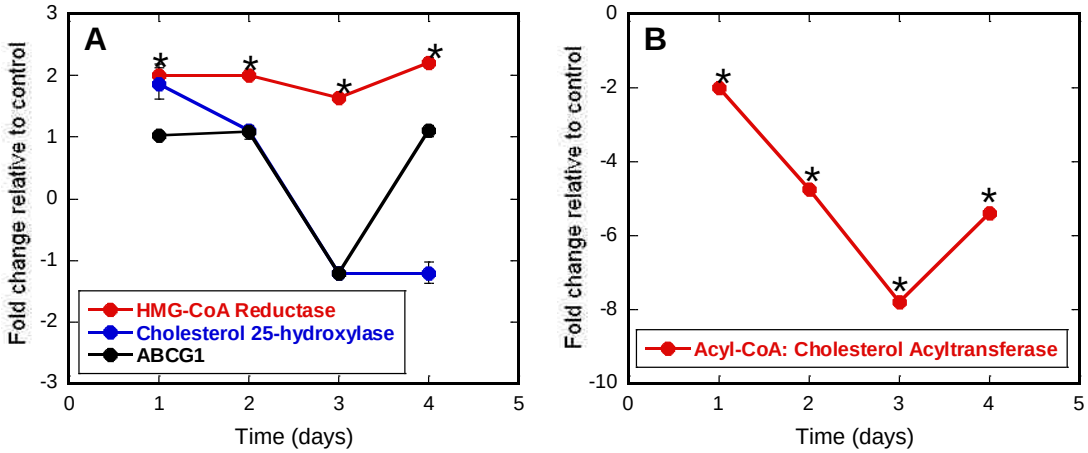

Figure 5.5. Myofiber transcriptional changes in genes involved with cholesterol homeostasis following cerivastatin treatment. Myofibers cultured in medium without serum were treated with cerivastatin (300 nM) for up to four days and a subset of genes involved with cholesterol homeostasis were evaluated by RT-PCR. HMG-CoA reductase showed a sustained transcriptional induction indicating cholesterol deficiency (A). In contrast, the other genes were either reduced or unchanged across the time course (A and B). This transcriptional profile is different than the psoas following cerivastatin treatment suggesting in vivo factors mediate alterations in cholesterol homeostasis.

Results represent the mean fold change relative to control ± SE of three separate experiments.

*Statistically significant at $p<0.05$.

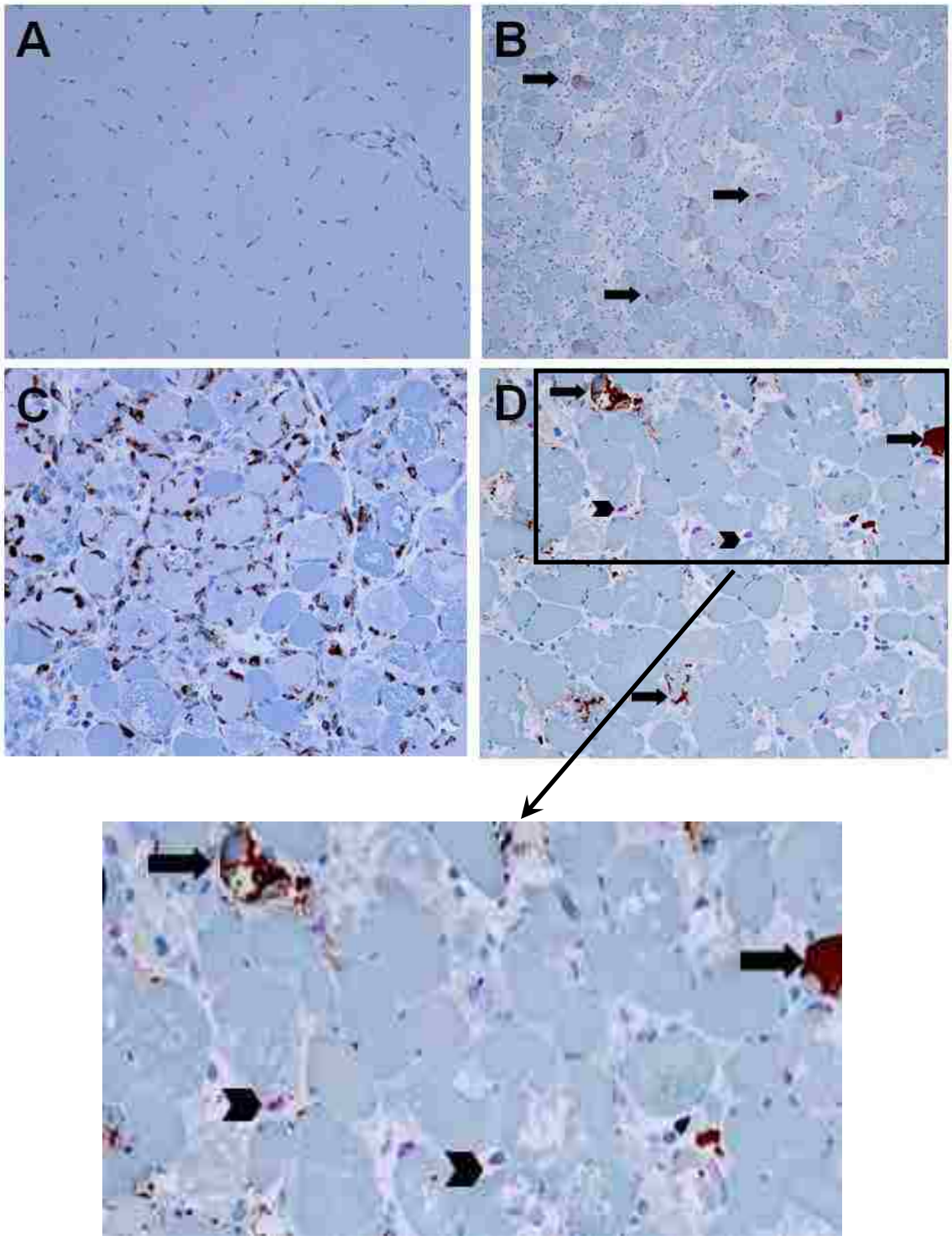
A
B
C
D

Figure 5.6. Cholesterol 25-hydroxylase expression in rat skeletal muscle from cerivastatin treated rats. CH25H and CD68 (macrophage marker) expression were not detected in the quadriceps from control rats (A), whereas a brown signal (■) for CH25H in skeletal muscle (B), and CD68 in macrophages (C) was observed in the quadriceps from cerivastatin (1 mg/kg; 15 days) treated rats. Double staining with CH25H (■; showing a brown signal) and CD68 (■; showing a red/purple signal) in the quadriceps from cerivastatin (1 mg/kg; 15 days) treated rats demonstrates expression in skeletal muscle and macrophages, respectively with no colocalization of these positive signals (D; magnified to illustrate expression). Similar results were observed in muscles from other rats (n = 3 control and 3 treated).

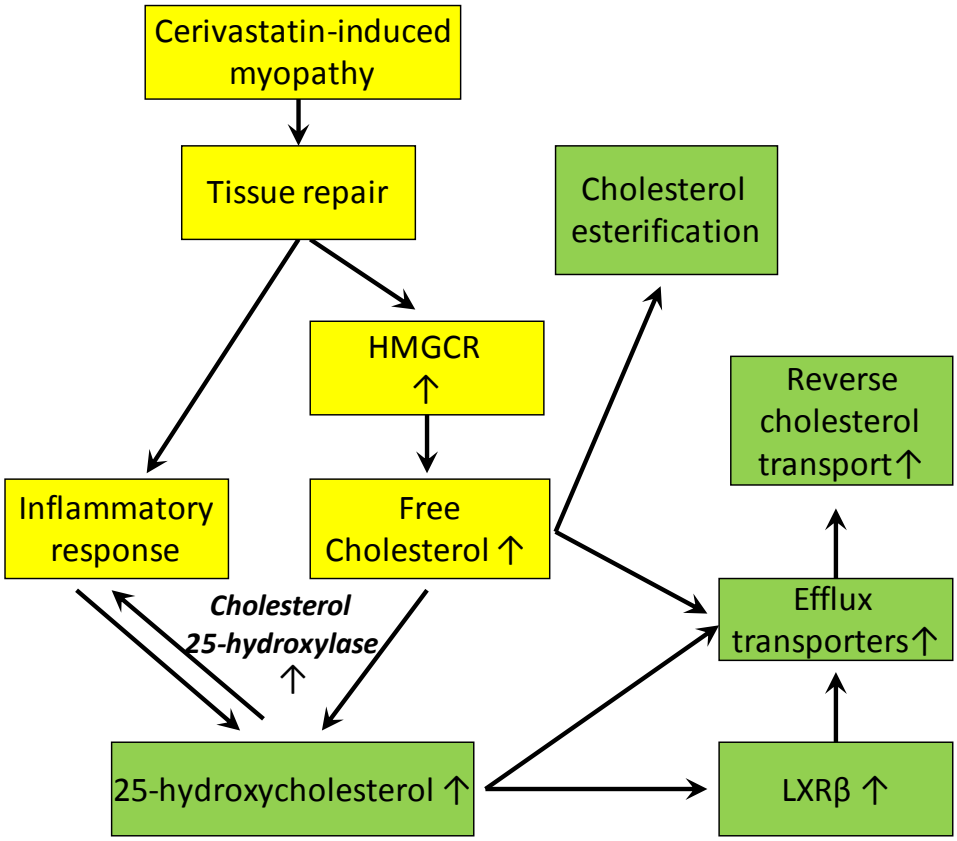

Figure 5.7. Proposed mechanism of cerivastatin-induced alterations in cholesterol homeostasis. Cerivastatin-induced myopathy triggers a tissue repair response characterized by inflammation, transcriptional induction of HMG-CoA reductase and the LDL receptor as well as an increase in free cholesterol (yellow boxes). However, in the face of ongoing toxicity, excess cholesterol accumulates in the muscle causing an increase in esterification, efflux and conversion to 25-hydroxycholesterol (green boxes).

Table 5.1. Quantitative RT-PCR primers

Gene	Description	Forward Primer	Reverse Primer
18srRNA	18s Ribosomal RNA	CGGCTACCACATCCAAGGAA	GCTGGAATTACCGCGGCT
HMGCR	3-hydroxy-3-methylglutaryl-Coenzyme	CGACATCATCATCCTCACGATAA	AGCTGACGCAGGTTCTGGAA
CH25H	Cholesterol 25-hydroxylase	CCAGAAGAAGAAACAGACTTGAGTTATTT	CGGGCTGCAGAAACACATTA
SOAT1	Acyl-CoA: Cholesterol acyltransferase	AGGTGTGCTGATGCTGTTCCT	AACATTTCAGCAAAGGCATTGA
ABCG1	ATP binding cassette subfamily G member 1 (Efflux transporter)	TACCTTGGGATTGGGAACGA	AGGGCGGCGAACATGAG

Table 5.2. Sterol changes in skeletal muscle with cerivastatin-induced myopathy[a]

Sterol	Fold change relative to control	Chemical formula	Molecular weight	m/z	Retention time (min)
Cholesterol	1.5 ± 0.1*	$C_{27}H_{46}O$	386.6	369 ($M+H^+-H_2O$)	5.1
7-Dehydrocholesterol	2.5 ± 0.5*	$C_{27}H_{44}O$	384.6	367 ($M+H^+-H_2O$	4.9
Desmosterol	12.9 ± 2.7*	$C_{27}H_{44}O$	384.6	367 ($M+H^+-H_2O$	4.7
7α,β-hydroxycholesterol[b]	3.1 ± 0.5*	$C_{27}H_{46}O_2$	402.7	367 ($M+H^+-H_2O$	3.5
24S-Hydroxycholesterol	-	$C_{27}H_{46}O_2$	402.7	367 ($M+H^+-2H_2O$)	2.5
27-Hydroxycholesterol	-	$C_{27}H_{46}O_2$	402.7	367 ($M+H^+-2H_2O$)	2.6
Cholesterol 25-hydroxylase pathway					
25-Hydroxycholesterol	30.6 ± 5.9*	$C_{27}H_{46}O_2$	402.7	367 ($M+H^+-2H_2O$)	2.4
7α, 25-Dihydrocholesterol	-	$C_{27}H_{46}O_3$	418.7	401 ($M+H^+-H_2O$)	2.0
7α,25-Dihydroxy-4-cholesten-3-one	14.1 ± 4.1*	$C_{27}H_{44}O_3$	416.6	417 ($M+H^+$)	1.9

[a]Results represent the mean fold change relative to control ± SE in the quadriceps from cerivastatin (study 1; 1 mg/kg; day 15) treated rats (n = 6 control and 9 treated rats / group).

[b]7α- and 7β-hydroxycholesterol were not resolved under these conditions.

(-) indicates no change.

*Statistically significant at $p<0.05$.

Table 5.3. Time course of sterol changes in the psoas, soleus and liver with cerivastatin-induced myopathy[a]

Day	Cholesterol (mg/g)	7-Dehydrocholesterol (µg/g)	Desmosterol (µg/g)	25-Hydroxycholesterol (µg/g)	7α/β-Hydroxycholesterol (µg/g)
Psoas					
Control	1.29 ± 0.02	1.79 ± 0.16	0.69 ± 0.06	<LOQ	0.71 ± 0.14
2	1.36 ± 0.03	2.12 ± 0.16	0.76 ± 0.10	<LOQ	0.60 ± 0.12
7	1.30 ± 0.05	1.92 ± 0.34	0.78 ± 0.24	<LOQ	0.88 ± 0.27
9	1.31 ± 0.04	2.23 ± 0.21	0.58 ± 0.07	<LOQ	0.44 ± 0.11
11	1.42 ± 0.04*	2.76 ± 0.31*	0.90 ± 0.22	0.07 ± 0.06	0.54 ± 0.12
15	1.89 ± 0.17*	4.01 ± 0.87*	6.31 ± 2.13*	0.49 ± 0.13	0.26 ± 0.06
Soleus					
Control	1.40 ± 0.01	0.74 ± 0.17	0.23 ± 0.04	<LOQ	2.15 ± 0.89
15	1.31 ± 0.01	0.49 ± 0.07	0.21 ± 0.05	<LOQ	3.49 ± 0.28
Liver					
Control	2.43 ± 0.13	1.24 ± 0.18	0.75 ± 0.17	0.06 ± 0.01	0.32 ± 0.06
15	3.08 ± 0.07*	1.92 ± 0.12*	1.34 ± 0.18*	0.20 ± 0.02*	7.75 ± 3.03

[a]Results represent the mean concentration ± SE of sterols per wet tissue weight from control (n=4) and cerivastatin (1 mg/kg; n=8) treated rats.

LOQ for 25-hydroxycholesterol was 0.01 µg/g of wet tissue weight.

*Statistically significant at $p<0.05$.

Chapter 6

Cerivastatin-induced myopathy is associated with alterations in energy metabolism

6.1. Introduction

Skeletal muscle energy metabolism relies on oxidative phosphorylation, and a critical step in this process is glucose oxidation followed by conversion of pyruvate to acetyl-CoA, in a reaction catalyzed by the pyruvate dehydrogenase complex (PDC) (Pilegaard and Neufer, 2004). This irreversible process plays a major role in energy metabolism, particularly in fast-twitch skeletal muscles, as it represents the only entry point for glucose derived from uptake or glycogen degradation into the mitochondria for oxidation and ATP synthesis. However, under certain conditions like fasting, diabetes and exercise, glucose availability becomes limited and the skeletal muscle is required to adapt via metabolic switch to fatty acids or amino acids for energy metabolism (Pilegaard and Neufer, 2004). The metabolic switch to alternative fuel substrates occurs with transcriptional induction of pyruvate dehydrogenase kinase 4 (PDK4) followed by phosphorylation of serine residues in PDC which inactivates the enzyme thereby limiting glucose oxidation.

In Chapter 3, PDK4 was transcriptionally induced by 2-fold in fast-twitch muscles prior to the onset of cerivastatin-induced myopathy and this change has been shown to significantly reduce PDC activity (Table 3.7; Sidaway et al., 2010). Furthermore, PDK4

was transcriptionally induced by more than 10-fold in fast-twitch muscles from rats treated with simvastatin and this effect was accompanied by impaired glucose oxidation (Mallinson et al., 2009). Similar effects of PDK4 induction have also been demonstrated in skeletal muscles from mice treated with various statins (Motojima, 2002; Motojima and Seto, 2003). Together, these studies suggest statin therapy may impair normal glucose metabolism in fast-twitch muscles.

Biochemical abnormalities reflecting deficiencies in fatty acid metabolism and impaired muscle energetics are also commonly observed in patients sensitive to statin-induced myopathy (Hubal et al., 2011; Phillips and Haas, 2008; Phillips et al., 2009). In the absence of normal glucose and fatty acid oxidation, fast-twitch muscles rely on amino acids from myofibrillar protein degradation for energy. Recent evidence in several species, including humans, has demonstrated that transcriptional induction of the muscle specific ubiquitin ligases atrogin-1 and MuRF-1 are causally related to statin-induced myopathy (Hanai et al., 2007; Mallinson et al., 2009). Transcriptional induction of these muscle specific ubiquitin ligases are considered hallmark changes associated with myofibrillar protein degradation, and abnormal activation of this process during impaired energy metabolism can lead to myopathy (Hanai et al., 2007; Mallinson et al., 2009; Motojima, 2002; Motojima and Seto, 2003). However, transcriptional profiling in Chapter 3 indicated that these genes were not transcriptionally induced. However, RT-PCR results demonstrated that these genes were transcriptionally induced in the cerivastatin time course study described in Chapter 2.2 (*study 2*), but expression was

significantly lower after 14 days of dosing relative to 8 and 10 days, which may reflect severe myopathy (Table 8.2).

In Chapter 3, PGC-1α was transcriptionally induced in the slow-twitch muscles following cerivastatin treatment, and this may represent an adaptive response in this fiber type as overexpression of this gene mediates the oxidative phenotype, prevents myofibrillar protein degradation and statin-induced myopathy (Table 3.15; Brault et al., 2010; Hanai et al., 2007; Lin et al., 2002). Specifically, physiological stress and altered energy metabolism cause transcriptional induction of PGC-1α which induces the estrogen receptor α (ERRα) and together they bind the PDK4 promoter and induce gene expression which increases mitochondrial biogenesis and represses the muscle specific ubiquitin ligases (Figure 6.1; Brault et al., 2010; Hanai et al., 2007; Zhang et al., 2006; Wende et al., 2005). Accordingly, these results suggest a specific transcriptional program related to impaired energy metabolism may occur in a fiber dependent manner following statin treatment.

Together, these studies suggest fiber specific differences in energy metabolism may be important in the mechanism of statin-induced myopathy. Therefore, it was hypothesized that cerivastatin-induced myopathy is mediated by alterations in energy metabolism which occur in a fiber dependent manner. The major goal of this work was to determine whether PDK4 inhibition in fast-twitch skeletal muscles is causally related to cerivastatin-induced myopathy. An additional goal of this work was to determine the

temporal relationship between transcriptional induction of PDK4, PGC-1α and the muscle specific ubiqutin ligases with the development of cerivastatin-induced myopathy.

6.2. Methods

***Study design*.** This investigation was conducted on skeletal muscles obtained from *study 2* described in Chapter 2. *Study 2:* For this study, muscles representing slow-twitch (soleus) and fast-twitch (psoas) fiber composition (Table 2.1) were collected from the left side and fixed in 10% neutral buffered formalin for histopathological assessment whereas the same tissues on the right side were flash frozen and used for RNA isolation.

Histopathology. Tissues were processed for histopathologic assessment as described in Chapter 2.2 (*study 2).*

Gene expression analysis. Constitutive PGC-1α expression in fast- and slow-twitch muscles from naïve rats was determined based on microarray data as described in Chapter 3.

Determination of transcriptional changes in cerivastatin treated rat fast-twitch FDB myofibers Female rat fast-twitch FDB myofibers were isolated and cultured as previously described in Chapter 2.2. To each well, 30 μl of vehicle (maintenance medium) or cerivastatin (final concentration was 300 nM) was added to the myofibers. This concentration was selected because a toxic dose of cerivastatin in female rats is associated with a Cmax of 221 nM (Reinoso et al., 2002; Steinke et al., 1996). Therefore, for the current work a slightly higher concentration was selected for testing. Furthermore, 3-4 days of cerivastatin (300 nM) treatment is associated with morphological changes characteristic of a stressed / dying cell and reduced viability (Figure 2.4). On days 1, 2, 3,

and 4 the media was gently removed with a pipette and the myofibers were washed twice with pre-warmed PBS (100 μl). This incubation time was selected because 4 days of cerivastatin treatment was required to cause a significant reduction in viability as measured by ATP (Figure 2.4). This experiment was conducted in triplicate with 24 wells per treatment on three separate days.

Determination of cerivastatin treated rat fast-twitch FDB myofiber viability with dichloroacetate. Female rat fast-twitch FDB myofibers were isolated and cultured as previously described in Chapter 2.2. To each well, 30 μl of vehicle (maintenance medium), cerivastatin (final concentration was 300 nM), dichloroacetate (DCA; an inhibitor of PDK4; final concentration was 5 mM) or cerivastatin (300 nM) and dichloroacetate (5 mM) were added to the myofibers. This concentration of dichloroacetate was selected because the Ki for PDK4 is 0.5 mM (Bowker-Kinley et al., 1998; Philp et al., 2010). On a daily basis, the media was removed and replenished with the treatments described above. After 4 days of treatment, viability (ATP) was determined. Myofibers were treated for 4 days because previous experiments indicated this treatment time caused a marked reduction in viability (Figure 2.4). This experiment was conducted in triplicate with 24 wells per treatment on three separate days.

Myofiber RNA isolation. Total RNA isolation was conducted as described in Chapter 5.2.

RNA isolation from skeletal muscles. Total RNA was isolated from flash-frozen skeletal muscle as described in Chapter 5.2.

RT-PCR. RT-PCR experiments were conducted as described in Chapter 5.2. The forward and reverse primer sequences are given in Table 6.1.

Data analysis. The mean mRNA fold change ± SE of PDK4, PGC-1α, atrogin-1 and MuRF1 was determined in fast- and slow-twitch muscles following cerivastatin treatment and in myofiber cultures representing three separate experiments. For the dichloroacetate experiment, the mean viability ± SE representing three separate experiments was determined. Group means were determined and compared with a Student's t-test or ANOVA using StatView (SAS Institute, Cary, NC) at $p<0.05$. However, statistics for the RT-PCR results were conducted on the values following normalization to 18S.

6.3. Results

Cerivastatin (1 mg/kg) caused a time dependent, fast-twitch specific myofiber degeneration in female rats whereas no evidence of myopathy was observed in the slow-twitch muscle (Figure 2.2; Table 2.3). These changes were first noted in 25% of the animals after 8 days of cerivastatin treatment and the incidence of myopathy increased to 75% and 100% of the animals after 10 and 14 days, respectively (Table 2.3). The severity of cerivastatin-induced myotoxicity also increased with time from a minimal injury after 8 days (Figure 2.2, panel B) to a severe myopathy after 14 days of cerivastatin treatment (Figure 2.2, panel D).

In fast-twitch muscles, transcriptional induction of PDK4 was first observed prior to evidence of myopathy after 6 days of cerivastatin (1 mg/kg) treatment and continued to show a sustained increase throughout the time course (Table 6.2). Similarly, PGC-1α was transcriptionally induced after 6 and 8 days but was unchanged after 10 days and reduced after 14 days of cerivastatin treatment (Table 6.2). In contrast, transcriptional induction of atrogin-1 and MuRF1 was only observed from days 8 to 10 when myopathy was present (Table 6.2). However, transcriptional induction of 2-fold or greater was observed in all rats on days 8 and 10. These results are consistent with an early metabolic switch in the fast-twitch muscle followed by impaired energy metabolism and evidence of myofibrillar degradation.

In the slow-twitch muscle, transcriptional induction of PDK4, atrogin-1 and MuRF1 were only observed after 14 days of cerivastatin treatment whereas PGC-1α was unchanged

across the time course (Table 6.3). To further probe skeletal muscle differences in PGC-1α constitutive expression this gene was interrogated in the gene expression profiles (Chapter 3). The differential expression of PGC-1α was 4.4-times higher ($p<0.0001$) in the slow- compared to the fast-twitch muscle of naïve female rats. These results demonstrate that cerivastatin treatment results in a different metabolic response in the slow- compared to the fast-twitch muscle which may be related to transcriptional induction of PDK4 and the higher constitutive expression of PGC-1α resulting in an oxidative phenotype.

To further examine the temporal relationship between these transcriptional changes, alterations in energy metabolism, and toxicity an in vitro culture of isolated FDB fast-twitch myofibers was used. Following cerivastatin (300 nM) treatment, PDK4 was transcriptionally induced on all days indicating an early and sustained response consistent with a metabolic switch in energy metabolism (Table 6.4). In contrast, PGC-1α, atrogin-1 and MuRF1 were only transcriptionally induced after 4 days, when viability was reduced (Table 6.4). For all transcripts evaluated, expression was unchanged across the time course in control myofibers. These data are generally consistent with the in vivo results indicating an early metabolic switch in the fast-twitch muscle followed by impaired energy metabolism and evidence of myofibrillar degradation.

To test the hypothesis that impaired energy metabolism, mediated by PDK4 induction in the fast-twitch muscle was causally related to cerivastatin-induced myopathy FDB

myofibers were treated with dichloroacetate (PDK4 inhibitor) (Figure 6.2). However, dichloroacetate treatment did not prevent cerivastatin-induced toxicity (Figure 6.2).

6.4. Discussion

Skeletal muscle is capable of rapidly adapting to different fuel substrates for energy metabolism in response to a variety of physiological conditions. To adapt to these ever changing energy demands muscle substrate utilization pathways are tightly controlled. Determining the gene expression changes and metabolic consequences associated with cerivastatin treatment is important in understanding the molecular pathogenesis of the myopathy in which substrate utilization for energy metabolism is impaired (Mallinson et al., 2009; Phillips and Haas, 2008).

The current results demonstrate that cerivastatin triggers an early and sustained transcriptional induction of PDK4 in fast-twitch muscles which is consistent with a metabolic switch in energy metabolism to a more oxidative phenotype. However, inhibition of this metabolic switch by dichloroacetate was insufficient to protect the fast-twitch muscle from cerivastatin-induced toxicity. Therefore, these results suggest that transcriptional induction of PDK4 may be necessary but insufficient to mediate cerivastatin-induced myopathy. Consistent with this observation, previous investigators have also demonstrated that statins transcriptionally induce PDK4 and reduce mitochondrial oxidative capacity resulting in impaired energy metabolism in fast-twitch muscles (Hubal et al., 2011; Mallinson et al., 2009; Motojima, 2002; Motojima and Seto, 2003; Phillips and Haas, 2008; Phillips et al., 2009; Sidaway et al., 2010). Consistent with this hypothesis, transcriptional induction of PGC-1α expression was observed supporting a metabolic demand for a more oxidative phenotype. However, this metabolic adaptation was insufficient in protecting the muscle, as transcriptional markers of protein

degradation, indicative of impaired energy metabolism, were induced in association with myopathy.

In contrast to the current work, it was recently demonstrated that DCA administered with simvastatin prevents myopathy in rats, thereby supporting a role for PDK4 in mediating toxicity (Sidaway et al., 2010). In that study, the authors demonstrated simvastatin (40 mg/kg) caused a 2-fold transcriptional induction of PDK4 which was associated with a significant reduction in PDC activity, a 2-fold transcriptional induction of atrogin-1 and myopathy. All of these changes were prevented when simvastatin was administered with DCA (50 mg/kg/day). The fact that DCA did not protect against cerivastatin-induced myopathy in the current experiment may be related to the in vitro conditions. As noted in Chapter 5 the in vitro response did not recapitulate alterations in cholesterol homeostasis observed in vivo.

There were several limitations of this work which make it difficult to completely interpret the results. Specifically, glycolytic and oxidative flux were not measured. Therefore, it is unknown whether there was a direct correlate between transcriptional changes and functional consequences in energy metabolism. This would have been particularly valuable for the dichloroacetate experiment by confirming that PDK4 was inhibited.

Although slow-twitch muscles are generally considered insensitive to cerivastatin-induced myopathy the current results suggest this fiber type simply shows a delayed response, as PDK4 and markers of protein degradation were transcriptionally induced

after 14 days of treatment (Obayashi et al., 2011; Westwood et al., 2005). However, unlike the fast-twitch muscle, PGC-1α was not transcriptionally induced in the slow-twitch muscle following cerivastatin treatment. Instead, constitutive levels of PGC-1α were 4-times higher in the slow-twitch muscle which may offer protection against myofibrillar degradation in this fiber type (Brault et al., 2010). Furthermore, 14 days of cerivastatin (1 mg/kg) treatment led to a significant increase in metallothionein 1, indicating oxidative stress in addition to transcriptional evidence of altered energy metabolism along with a reduction in phosphocreatine (Tables 3.16 and 4.1). Together, these results suggest that additional cellular stress factors, which occur in a fiber dependent manner, may be important in mediating impaired energy metabolism associated with cerivastatin-induced myopathy. Alternatively, the effects in the slow-twitch muscle may be related to physiological stress as these changes only occurred in animals with severe fast-twitch myopathy.

Recent work by Bouitbir et al (2011), indicated significantly greater ROS formation in fast-twitch muscles along with reduced oxidative capacity, and collapse of PGC-1α expression compared to the heart following statin treatment. These authors also demonstrated attenuation of ROS formation with antioxidants and overexpression of PGC-1α which prevented statin-induced myopathy (Bouitbir et al., 2011). Accordingly, since the slow-twitch muscle phenotype is more similar to the heart in regard to energy metabolism than fast-twitch muscles, a similar mechanism involving less ROS formation and higher PGC-1α expression may delay oxidative stress, impaired energy metabolism and toxicity in this fiber type. In contrast to this hypothesis, cerivastatin also caused

cardiac toxicity suggesting these results may not fully explain the mechanism of fiber-specific toxicity. However, the role of ROS in this mechanism was not pursued in the current work and it is unknown whether this is a cause or an effect.

In summary, the current work demonstrates fundamental transcriptional differences in female rat fast- and slow-twitch muscles in response to cerivastatin treatment. In the fast-twitch muscle, transcriptional changes were consistent with impaired energy metabolism as a mediator of myotoxicity whereas in the slow-twitch muscle alterations in energy metabolism were only observed after 14 days of cerivastatin treatment which did not result in myopathy. Furthermore, these results demonstrate that PDK4 inhibition in the fast-twitch muscle was insufficient to prevent cerivastatin-induced myotoxicity, thereby implicating additional factors in mediating toxicity. Alternatively, the lack of protection by DCA may be related to the in vitro culture conditions as rats treated with a toxic dose of simvastatin and DCA prevents myopathy (Sidaway et al., 2010). The current in vitro results, in addition to those presented in Chapter 6, indicate that this model does not always recapitulate the in vivo findings.

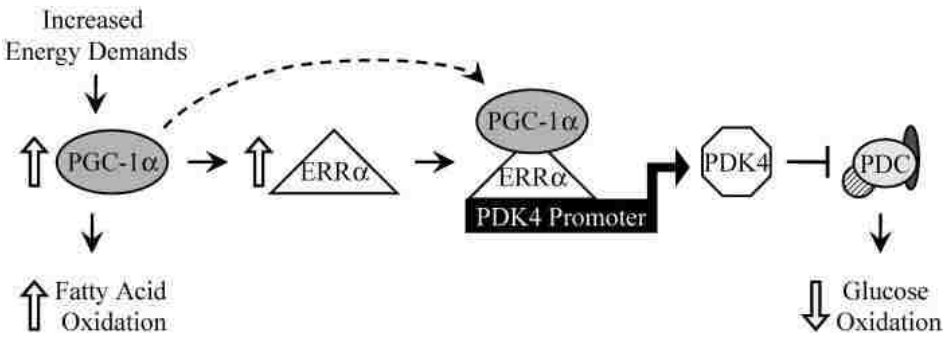

Figure 6.1. Proposed mechanism for the regulation of glucose metabolism involving PGC-1α / ERRα and PDK4 (Wende et al., 2005). Physiological stress increases energy demands causing induction of skeletal muscle PGC-1α, which in turn induces ERRα and together bind to the PDK4 promoter to activate gene expression. PDK4 activation results in a negative regulation of PDC and reduced glucose oxidation coincident with increased mitochondrial biogenesis and fatty acid oxidation mediated by PGC-1α in the slow-twitch muscle.

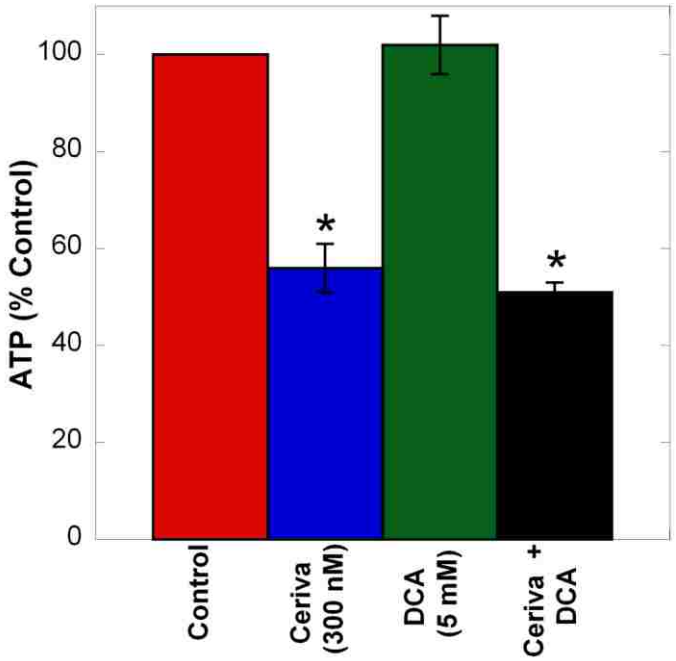

Figure 6.2. Dichloroacetate inhibition of PDK4 does not prevent cerivastatin-induced toxicity in isolated FDB fast-twitch myofibers. FDB myofibers were isolated from female rats and treated with cerivastatin (ceriva; 300 nM), dichloroacetate (DCA; 5 mM) or cerivastatin and dichloroacetate for 5 days and viability (ATP) was determined. Results represent the mean ± SE of three separate experiments.

Table 6.1. Quantitative RT-PCR Primers

Gene	Description	Forward Primer	Reverse Primer
18srRNA	18s Ribosomal RNA	CGGCTACCACATCCAAGGAA	GCTGGAATTACCGCGGCT
PDK4	Pyruvate dehydrogenase kinase 4	CTCCCTGAACGCTTAGTGAACA	TGGGCTCTTTTCGTGGAACT
PGC1α	Peroxisome proliferator-activated receptor-gamma coactivator	CACAACGCGGACAGAACTGA	CCGCAGATTTACGGTGCATT
Atrogin-1	Muscle specific ubiquitin E3 ligase, Muscle atrophy f-box (MAFBX), Atrogin-1	ATCCGCAAGCGATTGATCTT	ATCGCACAAGCTTAAAGTACATCTTC
MuRF-1	Muscle specific ubiquitin E3 ligase, Muscle RING finger-1 (MuRF-1)	AGGCAGCCACCCGATGT	CACCTCGCACGTGAGACAGT

Table 6.2. Time course of cerivastatin-induced histopathological and transcriptional changes in the fast-twitch muscle[a]

Day	Histopathology[b]	PDK4	PGC1α	Atrogin-1	MuRF1
1	-	NC	NC	NC	NC
6	-	1.9 ± 0.1*	1.9 ± 0.5*	NC	NC
8	2/8 (1.0)	2.6 ± 0.5*	1.5 ± 0.2*	5.0 ± 1.1*	1.8 ± 0.1*
10	6/8 (1.7)	4.1 ± 0.9*	NC	6.2 ± 1.3*	2.1 ± 0.8*
14	7/8 (3.6)	1.8 ± 0.4*	-2.5 ± 0.2*	2.5 ± 0.6*	2.4 ± 0.6*

[a]Results represent the mean mRNA expression ± SE normalized to 18s and relative to control following cerivastatin (1 mg/kg) treatment. Results for all control rats (n = 20) were pooled together.

NC = no change relative to control.

[b]Results represent the number of animals with skeletal myofiber necrosis and degeneration / number of animals per group. The mean severity score in () is based on an arbitrary score of 1 to 4 (most severe). (-) Denotes no significant findings observed.

*Significantly different from control ($p<0.05$).

Table 6.3. Time course of cerivastatin-induced histopathological and transcriptional changes in the slow-twitch muscle[a]

Day	Histopathology[b]	PDK4	PGC1α	Atrogin-1	MuRF1
1	-	NC	NC	NC	NC
6	-	NC	NC	NC	NC
8	-	NC	NC	NC	NC
10	-	NC	NC	NC	NC
14	-	2.6 ± 0.5*	NC	1.5 ± 0.3*	2.9 ±0.9*

[a]Results represent the mean mRNA expression ± SE normalized to 18s and relative to control following cerivastatin (1 mg/kg) treatment. Results for all control rats (n = 20) were pooled together.

NC = no change relative to control.

[b]No adverse histological effects were observed in the soleus. (-) Denotes no significant findings observed.

*Significantly different from control ($p<0.05$).

Table 6.4. Time course of cerivastatin-induced transcriptional changes in the fast-twitch FDB muscles in culture[a]

Day	ATP (% control)	PDK4	PGC1α	Atrogin-1	MuRF1
1	96 ± 4	2.3 ± 0.4*	NC	NC	NC
2	96 ± 4	1.7 ± 0.1*	NC	NC	NC
3	94 ± 3	1.6 ± 0.1*	NC	NC	NC
4	69 ± 2*	5.6 ± 1.1*	3.1 ± 0.7*	2.1 ± 0.5*	3.6 ± 0.9*

[a]Results represent the mean mRNA expression ± SE normalized to 18s and relative to control following cerivastatin (300 nM) treatment for three separate experiments.

NC = no change relative to control.

*Significantly different from control ($p<0.05$).

Chapter 7

Identification of 1- and 3-methylhistidine as biomarkers of skeletal muscle toxicity by nuclear magnetic resonance-based metabolic profiling **(Anal. Biochem. 2011 Mar 1;410(1):84-91)**

This work was conducted in collaboration with Dr. Nelly Aranibar. Specifically, I was responsible for designing and conducting all in vivo portions of this work, whereas Dr. Nelly Aranibar conducted all NMR analysis, including identification of 1- and 3-MH.

7.1. Introduction

Drug-induced skeletal muscle injury is commonly associated with the use of a variety of medications including statins, fibrates and glucocorticoids (Singh et al., 2005). The potential severity of this adverse effect is illustrated by withdrawal of cerivastatin from the market after more than 100 rhabdomyolysis-related deaths were associated with this drug (Thompson et al., 2003). Early evaluation of myotoxic potential is important in drug development, and preclinically has relied mainly on serological biomarkers, such as creatine kinase (CK) and aspartate aminotransferase (AST). Unfortunately, the diagnostic utility of these analytes is limited by their lack of sensitivity and specificity, particularly in rats (Bohlmeyer et al., 1994; Sorichter et al., 1999). As a result, histopathologic assessments are most often used to confirm drug-induced myotoxicity. Consequently, the need for specific biomarkers of myopathy from peripheral biological fluids has been recognized, and several new potential serum biomarkers of drug-induced myotoxicity, including skeletal muscle troponin I (sTnI), myosin light chain 3 (Myl3) and fatty acid binding protein 3 (fabp3), have recently been reported (Berna et al., 2007; Pritt et al., 2008; Tonomura et al., 2009; Vassallo et al., 2009).

Transcriptional profiling of skeletal muscles has been used to develop insight into the etiology of idiopathic or disease-related myopathies in humans and rats and has helped to identify gene expression profiles that suggest possible new biomarkers of myotoxicity (Casey et al., 2008; De Souza et al., 2006; Jagoe et al., 2002; Laaksonen et al., 2006; Morikawa et al., 2005; Yu et al., 2009). However, transcriptional profiling is not an ideal platform for routine monitoring of drug-induced myotoxicity in the preclinical setting.

In direct contrast to global transcriptional profiling, metabolomic evaluation of biological fluids affords the opportunity to assess systemic metabolic changes that may be directly related to myotoxicity. Metabolomics has been widely used in the last decade to define tissue metabolic profiles, investigate mechanisms of toxicity and to identify biomarkers of pharmacologic or adverse effect, with nuclear magnetic resonance (NMR) and mass spectrometry representing the commonly used analytical platforms (Xu et al., 2011). However, there is presently very little information available on the global metabolic effects observed with drug-induced myopathy in laboratory animals. In Chapter 4, metabolomic profiling of fast-twitch muscles identified several metabolites which decreased in association with cerivastatin-induced myopathy. Therefore, it was hypothesized that metabolomic profiling of urine from that study would show an increase in skeletal muscle specific metabolites which may represent biomarkers of myopathy.

In the present research, the urinary NMR metabolomic profile of cerivastatin-induced myopathy in rats was evaluated. Changes in relevant endogenous metabolites including creatine were noted. However, a predominant but unknown moiety was also detected that

directly correlated with the sex-, dose-, and time-dependent development of myopathy. The work described herein summarizes the analytical effort to identify these unknown analytical signals as 1- and 3-methylhistidine and to characterize their relevance to muscle biology and function with respect to their potential utility as biomarkers of muscle toxicity.

7.2. Methods

Chemicals. Cerivastatin (Na salt) was purchased from Sequoia Research Products (Pangbourne, United Kingdom). Isoproterenol hydrochloride, anserine, 1-methylhistidine (1-MH), 3-methylhistidine (3-MH), and corn oil were purchased from the Sigma-Aldrich Company (St Louis, MO). Methylcellulose A15C premium was purchased from the Dow Chemical Company (West Point, PA); HPLC grade methanol from Mallinckrodt Baker (Phillipsburg NJ, USA); ammonium acetate and formic acid from Aldrich (Milwaukee, WI). TSP (trimethylsilyl-2,2,3,3-tetradeuteropropionic acid) was purchased from ISOTEC (Miamisburg, Ohio).

Animals. Male (250-300 g) and female (175-225 g) Sprague-Dawley rats (8-9 weeks old; Charles River Laboratories, Portage, MI) were individually housed in temperature and humidity controlled rooms with a 12-h light/dark cycle. Animals were allowed free access to water and a standard lab diet (Harlan Teklad 2018C, Madison, WI) and were acclimated for one week prior to dosing. The conduct of all animal studies was approved by the Bristol-Myers Squibb Animal Care and Use Committee.

Treatment and sample collection. The metabolomic investigation was conducted on urine samples obtained from a previously published study in which male and female rats were dosed orally with cerivastatin (0.5 and 1 mg/kg; 5 mL/kg) or methylcellulose vehicle (n = 6 - 9 animals / group / sex) for 14 days (Vassallo et al., 2009). Cerivastatin dosages were selected based on the literature indicating that 0.5 mg/kg was associated

with a minimal and variable myopathy whereas 1 mg/kg caused a mild to severe myotoxicity (Westwood et al., 2005).

In a second study, female rats (n = 4 – 8 animals / group) were dosed orally with a myotoxic dose of cerivastatin (1 mg/kg) for 14 days. Only female rats were used for this study because the initial results indicated this sex was more sensitive to cerivastatin-induced myotoxicity than male rats. Isoproterenol (0.5 mg/kg; 1 mL/kg) was administered (sc) as a single dose to male rats (n = 5 – 6 animals per group) as previously described (Vassallo et al., 2009). This dosing paradigm was selected because it was associated with mild to severe cardiac myopathy with no skeletal muscle toxicity. Only male rats were used for this study because previous research indicated that isoproterenol caused skeletal muscle hypertrophy in this sex (Agrawal et al., 2003)

Urine was collected over 24 hours from cerivastatin-treated rats housed in metabolism cages immediately after dosing on days 7 and 14 or after dosing isoproterenol. Serum from cerivastatin-treated rats was collected as previously described after 14 doses of cerivastatin (Vassallo et al., 2009). Urine and serum samples were stored at -80°C pending analysis.

NMR metabolomics. Rat urine samples were thawed on ice and 400 μL aliquots were mixed with 200 μL buffer: 0.2 M sodium phosphate, pH 7.2, containing 20% D_2O for field-lock and 1 mM TSP (trimethylsilyl-2,2,3,3-tetradeuteropropionic acid) as an internal standard. Each sample was placed into a 5 mm NMR tube and data were acquired

on a 600 Avance III Bruker NMR spectrometer (Bruker Analytic GmbH, Germany) equipped with a 5 mm TCI cryoprobe operating at 600.53 MHz for ^{1}H. Samples were measured in batches of 20 at a probe temperature of 27°C using standard 1D proton parameters as follows: 256 transients following 8 dummy transients, 16 ppm spectral width, and a 90 pulse of 7.7 us. The water suppression was accomplished using the standard Bruker sequence 'noesy1dpr', with irradiation during the 0.05 s mixing time and 2 s relaxation delay. The size of the time domain data (free induction decay) was 32k points. The NMR spectra were Fourier transformed and phase and baseline corrected in a consistent manner. For principal component analysis (PCA) and region integration for metabolite quantification, AMIX software version 3.8 (Bruker Analytik) was used. For input, reduced NMR spectra were prepared by integrating 0.01 ppm wide regions from 10 to -0.5 ppm, scaled to total intensity, excluding the water residual signal regions (4.7 to 5 ppm) with a total of 525 regions considered for the analysis. Pareto scaling was used to calculate the three first principal components and loadings. For NMR-based metabolite quantitation, regions containing well isolated peaks were integrated across all relevant spectra, normalized to TSP and analyzed statistically (ANOVA, t-test and regression calculations) with Partek Pro (v. 6.0 Partek Inc. Missouri, USA).

Evaluation of unknown urinary metabolites. To aid in the identification of unknown metabolites, preparative HPLC followed by NMR analyses was used to isolate individual urine fractions for more detailed analytical evaluation. Briefly, the preparative HPLC system (Varian Prostar, Palo Alto, CA, USA) was equipped with two solvent delivery modules, a UV-Vis detector, an autosampler, and fraction collector. Urinary metabolites

were separated on a Luna NH2 (Phenomenex, Torrance, CA, USA) column (100 mm × 21.2 mm I.D, 5 μm) and eluted with a gradient of A: 20 mM NH_4Ac and B: 100% methanol. Chromatographic preparative separation was made at a flow rate of 22 mL/min at ambient temperature. The elution solvent gradient started with 5% A/ 95% B, changing to 90% B/10% A in 15 minutes and held at this composition for 5 minutes. The column was then washed with 100% methanol with 0.02% formic acid for 2 minutes, followed by 2 minutes washing with HPLC-grade water containing 0.02% formic acid. Urine from two female rats showing the greatest intensities of the unknown NMR signals were pooled and concentrated for HPLC analysis. After sample injection, fractions were collected at 0.5 minute fractions over the course of the gradient, and two additional fractions were collected during the wash period.

After collection, all the chromatographic fractions were dried under nitrogen. To facilitate removal of any residual mobile phase, samples were rinsed and dried again overnight under nitrogen. After the last drying procedure, 250 μL of 0.2 N phosphate buffer in D_2O: H_2O (20:80) with 1mM TSP and 500 μL DI water were added to each sample. Reconstituted samples were mixed thoroughly and subjected to centrifugation at 8000 rpm for 10 min to remove any particulates. Aliquots (600 μL) were used for NMR spectroscopy in 5 mm tubes with the same pulse sequence and parameters as described above. Selected fractions containing the peaks of interest were analyzed by 2D proton-carbon NMR, including one-bond and multiple-bond experiments. The one bond (HMQC) experiments were recorded using a pulse sequence for proton-carbon correlation via heteronuclear zero and double quantum coherence with decoupling during

acquisition, using gradient pulses for selection (called ‘hmqcgpqf’ in the Bruker pulse library) with 64 dummy transients, 112 transients, 400 T1 increments and 1k points in F2. The sweep width was 12 ppm for proton and 220 ppm for carbon. The 90 degree pulse for proton was 7.7 us and for carbon was 15.4 us. A 1.5 sec relaxation delay was used between scans. Decoupling was performed utilizing a GARP sequence, and a sine shape was used for the gradient selection. The evolution time was optimized for a one bond C-H scalar coupling of 145 Hz. Multiple bond proton-carbon (HMBC) experiments were acquired with a pulse sequence for proton-carbon multiple bond correlation via heteronuclear zero and double quantum coherence, optimized on long range couplings with low-pass J-filter to suppress one-bond correlations, no decoupling during acquisition, using gradient pulses for selection (identified as ‘hmbcgplpndqf’ in the Bruker pulse library), with 64 dummy transients, 128 transients, 400 increments in T1 and 4k points in F2. The sweep width was 12 ppm for proton and 240 ppm for carbon. Pulses and delays used as for HMQC, except that the evolution time was optimized for a multiple C-H bond coupling of 10 Hz.

Constitutive tissue concentrations of 1- and 3-methylhistidine in rats The distribution and concentration of 1- and 3-MH were determined in select muscles and all other major organs from male and female Sprague Dawley rats (n=3). Tissues analyzed included skeletal muscles representing fast-twitch muscles (quadriceps, psoas, and gastrocnemius), slow-twitch muscles (soleus) and mixed muscle fibers (diaphragm), along with heart, stomach, duodenum, jejunum, ileum, colon, spleen and lung, kidney, liver, testes, ovaries, brain and serum (Ariano et al., 1973; Hamalainen and Pette, 1993; Koerker et al.,

1990; Kumagai et al., 2001). Rats were anesthetized with isoflurane and exsanguinated, after which all tissues were flash-frozen and stored at -80°C pending analysis. The concentration of 1- and 3-MH was determined in each tissue by GC-MS. Briefly, the internal standards (20 nmol) 1-[methyl-$^2H_3$]methylhistidine (d_3-1MH) (MSD Isotopes, Montreal, Canada) and 3-methyl-[methyl-$^2H_3$]-histidine (d_3-3MH) (MassTrace, Woburn, MA), and 4 mL of 6 N HCl were added to approximately 50 mg of tissue. The tissue was homogenized with a Tissue Tearor™ (BioSpec Products, Inc.) and then hydrolyzed to free the methylhistidines from the acetylated form, by heating at 100° C for 20h. The resultant methylhistidine isomers in tissue hydrolysates were absorbed on a cation exchange column (Dowex-50W in the hydrogen form Sigma Chemical, St. Louis, MO), after which the column was washed with 0.01 *N* HCl (4x1mL) and deionized water (2x1ml). The methylhistidine isomers were eluted with 25% NH_4OH and dried at 65°C under nitrogen. The samples were derivatized with acetonitrile and N-methyl-N-(t-butyldimethylsilyl)-trifluoroacetamide (MTBSTFA, Regis Technologies, Inc., Morton Grove, IL) and analyzed by GC-MS (Rathmacher et al. 1992). Both 1- and 3-MH were quantified based on the isotope ratios of the unknowns compared to the internal standard curves.

Urine and serum 1- and 3-MH were analyzed by a similar method. Urine and serum samples (75 µL) and 20 nmol of the internal standards were hydrolyzed in 100 µL 6 N HCl with heat (110 °C) for 15 h. Urine hydrolysates were subjected to cation exchange, derivatized and analyzed by GC-MS as described above.

Statistics. Urine from vehicle-treated male (n=15) and female (n=17) rats, representing samples collected across the cerivastatin and isoproterenol studies described herein, were used for determining the population mean concentration of 1- and 3-MH. The mean urine concentrations of 1- and 3-MH in treated rats were compared to respective experimental controls with a Student's t-test ($p < 0.05$).

7.3. Results

Metabolomics. PCA scores plot of the reduced NMR spectra indicated that urine from female rats treated with cerivastatin (1 mg/kg) separated from control, low dose (0.5 mg/kg) females and high dose (1 mg/kg) males after 14 (but not 7) days of dosing (results not shown). When the loadings were investigated, resonances contributing to the separation included the citrate and 2-oxoglutarate regions along with resonances 3.05 and 3.95 ppm, which correspond to creatine. In addition, two unknown singlets at 3.83 (U1) and 2.01 ppm (U2) showed high discriminating power between the treatment and control groups (Figure 7.1A). The mean values and distributions of selected metabolites, including the two unknown peaks are shown in Figure 7.1B. The most notable changes were increased excretion of creatine, U1 and U2 in rats with myopathy.

To identify the origin of the unknown resonances, 4 mL of urine from two female animals which showed the greatest intensities of the unknown NMR signals were pooled, concentrated 2-fold and chromatographically separated into fractions by preparative HPLC. Proton NMR revealed that the singlets of interest (2.01 and 3.83 ppm) appeared in four fractions (20 through 23). The ^{1}H NMR spectra from two of these critical fractions, shown in Figure 7.2, showed significant enrichment of two similar molecules which carry the 2.01 ppm resonance. Key features in both spectra include an AMX-type spin system with multiplets at 4.49 or 4.45 ppm, 3.25 or 3.17 and 3.06 or 3.01 ppm, singlets at 3.83 or 3.81 and 2.01 or 1.99 ppm for fractions 20 and 23, respectively. The singlets at low field are consistent with N-methyl groups whereas the singlets at high field are consistent with acetyl groups. Finally, there were two pairs of singlets in the aromatic region (7.19 or

7.13 ppm and 8.47 or 8.28 ppm) consistent with an imidazole moiety in fractions 20 and 23, respectively. Based on the relative signal intensities between fractions 20 and 23, there was at least an order of magnitude more material in fraction 20. These fractions were pure enough to conduct rigorous multi-dimensional NMR assessment without further purification. The single and multiple bond proton-carbon correlations allowed confident assignment of the unknown resonances to N-acetylated 1- and N-acetylated 3-methylhistidine for fractions 20 and 23, respectively. The HMBC spectrum for the N-acetyl-1-methylhistidine is shown in Figure 7.3, along with key correlations indicated.

The nomenclature of the positional isomers of methylhistidine in the literature has been inconsistent. To clarify the names associated with each of these molecules, the structures for the two isomers are shown in Figure 7.4. 1-Methylhistidine is also known as N^{π}-methylhistidine, N-δ-methylhistidine, or pros-methylhistidine, and 3-methylhistidine has been identified as N^{τ}–methylhistidine or N-γ–methylhistidine. The IUPAC names for these compounds are as follows: 1-MH is 2-amino-3-(1-methyl-1H-imidazol-5-yl) propanoic acid and 3-MH is 2-amino-3-(1-methyl-1H-imidazol-4-yl) propanoic acid. 1-MH is a known component of anserine, a cytosolic dipeptide found in muscle of many species including the rat (Abe, 2000; Aldini et al., 2004, Crusch, 1970; Christman 1976; Tamaki et al., 1980) whereas 3-MH is a known post-translational modification of one histidine residue in actin of skeletal and smooth muscle and one residue in fast-twitch myosin of skeletal muscle (Johnson et al. 1967; Young and Munro, 1978).

In light of the relevance of the methylhistidines to skeletal muscle, the distribution and concentration of 1- and 3-MH in 18 tissues from female and male rats was determined. (Figure 7.5; Table 7.1). In the five skeletal muscles evaluated, the concentration of 1-MH was higher than 3-MH, and there were no sex differences observed for either methylhistidine isomer (Table 7.1). Across evaluated muscles, 1-MH was highest in the quadriceps with a concentration of approximately 7 μmol/g (or about 7 mM), whereas the concentration of 3-MH was about 1 mM across the 5 muscles evaluated (Figure 7.5A; Table 7.1). In the heart, both isomers were lower than in skeletal muscles with 3-MH somewhat higher than 1-MH. (Figure 7.5B; Table 7.1). In smooth muscle-containing tissues (stomach, duodenum, jejunum, ileum, colon, spleen and lung) 3-MH was more abundant than 1-MH, and both isomers were lower than skeletal muscle (Figure 7.5B; Table 7.1). Other organs (liver, ovaries, testes and brain) had low levels of methylhistidine isomers compared to skeletal muscles, with higher levels of 1-MH compared to 3-MH. No sex differences were observed for either methylhistidine isomer (Figure 7.5B; Table 7.1). Together, these data suggest that 1- and 3-MH are highly abundant in skeletal muscle relative to other tissues. The high concentration of 1-MH in skeletal muscles suggests that its excretion in urine may be diagnostic for skeletal muscle damage. In contrast, excretion of 3-MH might reflect damage to skeletal, cardiac or smooth muscle, or a combination of these.

In vehicle-treated rats, GC-MS determined urine 1-MH was 451 ± 29 and 583 ± 39 nmol/mg creatinine, in males and females, respectively, while 3-MH was 253 ± 13 and

257 ± 12 nmol/mg creatinine, respectively (Tables 7.2 and 7.3). There did not appear to be any vehicle-related effects on 1- or 3-MH levels in urine.

The absolute change in urinary concentrations of 1- and 3-MH following cerivastatin treatment was determined (Table 7.4). At 0.5 mg/kg, a dose that caused only minimal myotoxicity (Vassallo et al. 2009), 1-MH excretion was variable and not significantly increased in female rats and 3-MH was unchanged. In contrast, 1- and 3-MH increased by 6- and 2-fold, respectively in female rats dosed at 1 mg/kg and showing a mild to severe myotoxicity (Table 2.1). In cerivastatin-treated male rats, urinary excretion of 1- and 3-MH was unchanged consistent with the absence of histologic evidence of myopathy (Table 2.1).

In serum, 1-MH was readily detected with concentrations of 6 and 16 μM in female and male, rats respectively. Additionally, 3-MH was detected in serum with concentrations of 2 and 3 μM in female and male rats, respectively. For both methylhistidine isomers, the serum concentration was higher in male rats. Following a myotoxic dose of cerivastatin (1 mg/kg), serum levels of 1- and 3-MH increased significantly by 12- and 3-fold, respectively (Table 7.4). Similar to the urine data, serum levels of 1- and 3-MH were unchanged in cerivastatin-treated male rats.

Urinary excretion of 1- and 3-MH was also evaluated in male rats dosed with isoproterenol (0.5 mg/kg), a dosing regimen known to cause frank cardiac necrosis (Ng et al. 2002). No increase in urinary levels of 1- and 3-MH was observed in isoproterenol-

treated rats, suggesting specificity of these metabolites for skeletal muscle toxicity. Surprisingly however, isoproterenol decreased the excretion of 1- and 3-MH by 2-fold compared to vehicle-treated rats (Table 7.5).

7.4. Discussion

The evaluation of skeletal muscle toxicity has long relied on serum markers such as AST and CK. Although CK is a useful diagnostic tool for assessing muscle toxicity in humans, its utility in preclinical species has been limited by its marked variability, and other preclinical markers like AST suffer from a lack of muscle specificity (Bohlmeyer et al., 1994). With these limitations, there has been considerable effort invested over the past several years to identify more specific and sensitive biomarkers of skeletal muscle toxicity particularly in preclinical species. These efforts have focused primarily on proteins that are highly expressed in or unique to skeletal muscles such as sTnI, Myl3, fabp3 and myoglobin (Berna et al., 2007; Pritt et al., 2008; Tonomura et al., 2009; Vassallo et al., 2009). In contrast, minimal effort has been invested in pursuing endogenous small molecules or metabolites as potential markers of myotoxicity. Urinary excretion of creatine has been associated with a variety of myopathies and this metabolite was also observed to increase with cerivastatin-induced myotoxicity (Bohlmeyer et al., 1994; Chung et al., 2003, 2005; Draper et al., 1994). However, creatine excretion is also known to increase with testicular damage and hepatotoxicity indicating that it may not be a specific biomarker of skeletal muscle damage despite the fact that it is highly abundant in this tissue (Clayton et al., 2004; Draper and Timbrell, 1996).

In the present work, the urinary excretion of two metabolites, 1- and 3-MH were identified in female rats following the development of cerivastatin-induced myotoxicity. Moreover, this observation was extended to serum, indicating that either biological

matrix may be useful for monitoring changes in these biomarkers in association with drug-induced myotoxicity.

Although this is the first report showing increased excretion of 1- and 3-MH in response to a muscle toxicant such as cerivastatin, these metabolites have been used for studying muscle protein turnover for more than 30 years Young et al. 1973, Elia et al. 1981). 1-MH is a component of anserine (β-alanyl-1-MH), which is found in the cytoplasm of skeletal muscles in millimolar concentrations (Abe, 2000; Aldini et al., 2004; Christman, 1976; Penafiel et al. 2004). Anserine can be synthesized either from β-alanine and 1-MH (Tamaki, 1980) or from the N-methylation of carnosine (β-alanyl-histidine) (McManus, 1967). Either biosynthetic pathway occurs primarily in skeletal muscle but not in other organs including the liver (Bauer and Schulz, 1994). The present data show that in rats, 1-MH is highly abundant in skeletal muscles, regardless of sex or fiber type, with substantially lower concentrations detected in cardiac muscle or in organs that have abundant smooth muscle (i.e. gastrointestinal tract). Constitutive levels of 1-MH ranged from 1 – 7 μmol/g tissue in the skeletal muscles evaluated, results that are consistent with reported variability in anserine levels (Aldini et al., 2004; Christman, 1976; Penafiel et al., 2004).

Anserine is stored in muscle cells and is hydrolyzed into its amino acid components, 1-MH and β-alanine, under the action of carnosinase. β-alanine can be reused to synthesize anserine or other metabolites including dipeptides or molecules such as pantothenate (and subsequently Coenzyme A) and quinolinate. As such, β-alanine would not be expected to

be a useful marker of skeletal muscle toxicity and in fact did not increase with cerivastatin-induced myotoxicity (results not shown). In contrast, the current data indicate that 1-MH excretion and serum levels increase with cerivastatin-induced skeletal muscle necrosis and thus may represent a potentially useful marker of toxicity.

3-MH is a post-translational modification of myofibrillar actin and fast-twitch myosin in all species. Conditions that cause skeletal muscle atrophy result in degradation of these proteins and increased urinary excretion (Haverberg et al., 1975; Young and Munro, 1978; Lowell et al., 1986, Segaud et al., 2007). In the present work, constitutive concentrations of 3-MH were lower than 1-MH in skeletal muscles, whereas 3-MH was typically higher than 1-MH in cardiac and smooth muscle. 1-MH increased to a much greater extent than 3-MH following cerivastatin treatment, a result that is consistent with the relative levels of these metabolites in skeletal muscles.

The marked increase in excretion and serum levels of 1- and 3-MH in response to cerivastatin, coupled with their recognized relevance to skeletal muscle biology, suggests that these metabolites may be useful biomarkers of skeletal muscle toxicity. An important attribute of a useful biomarker for skeletal muscle toxicity is its ability to distinguish between cardiac and skeletal myofiber damage. Accordingly, excretion of 1- and 3-MH was evaluated in an acute model of cardiac necrosis with isoproterenol. If skeletal muscle specific, excretion of 1- and 3-MH should remain unchanged by isoproterenol treatment. Unexpectedly, a significant decrease in excretion of both 1- and 3-MH was observed in this model, despite evidence of marked cardiac necrosis. However, β-adrenergic agonists

are known to have a direct anabolic effect on skeletal muscle, and the action of building muscle will reduce urinary excretion of these metabolites. In support of this concept, there is evidence that clenbuterol (β_2-adrenergic agonist) decreases 3-MH excretion in rats (Waterfield et al., 1995). These results suggest that serum or urine levels of 1- and 3-MH may be useful markers for skeletal muscle necrosis and anabolic effects, thereby providing information on the totality of skeletal muscle protein turnover in rats.

This is the first report showing an increase in urinary excretion and serum levels of 1- and 3-MH in association with drug-induced skeletal muscle injury. As such, additional work will be required to extend analysis of these metabolites in response to other skeletal muscle toxicants, additional models of cardiac toxicity, particularly models devoid of skeletal muscle hypertrophy, and other general models of hepatic or renal toxicity. Furthermore, there is a need to consider the utility of these biomarkers across species. In this regard, anserine, which contains 1-MH, is most likely not present in human skeletal muscles (Abe, 2000; Christman, 1976), however basal urinary excretion of 1-MH in humans has been observed even in the absence of dietary meat intake (Sjolin et al., 1987). 1-MH has the most potential utility in preclinical species such as rodents, dogs and non-human primates (Abe, 2000, Christman, 1976, Harris et al., 1990; Penafiel et al.,, 2004). In contrast, 3-MH is highly conserved, and although its basal levels can be altered by diet, age or disease, it should translate across species such as rodents, dogs and non-human primates (Asatoor and Armstrong, 1967; Johnson et al., 1967), under pre-clinical experimental conditions, in which diet and other conditions are highly controlled. In humans, its utility as a biomarker of drug-induced muscle toxicity would be restricted to

controlled diet and exercise, as well as in the absence of any other physiological or pathological conditions which would affect skeletal muscle.

The present study has focused on the identification of 1- and 3-MH in rat urine and their potential significance in preclinical evaluation of myopathy, however the work also highlights the impact of urinary metabolomic profiling in toxicology. Although not as sensitive as liquid or gas chromatographic methods, the MH isomers were originally detected as unique, unknown moieties from NMR-based profiling. Several other endogenous metabolites, including intermediates in the Krebs cycle and creatine were also observed to change with cerivastatin-induced skeletal muscle injury. However, untargeted NMR profiling provided a rapid and reproducible method wherein global metabolite changes were noted, and in light of the extent of changes noted, the method enabled the targeted identification of these metabolites. Many research efforts have focused on applying NMR metabolomic profiling to assessing mechanisms of toxicity or developing signatures of metabolites that are associated with specific organ toxicity or adaptive responses (Griffin, 2003). In addition to these approaches, the present work provides a novel example in which metabolomic profiling can be directly applied to biomarker discovery.

In summary, the present work illustrates the ability of untargeted metabolomics analysis to identify relevant biomarkers and describes the utility of 1- and 3-MH as putative biomarkers of drug-induced skeletal muscle necrosis and hypertrophy in the rat. Quantitative measurements of both methylated species are straightforward and can be

evaluated in a single sample by GC-MS. Evaluation of these metabolites in urine provides for non-invasive and repeated collection such that the onset, progress, and potential recovery of skeletal muscle toxicity can be followed. Further investigation into the use and limitations of these metabolites as markers of muscle necrosis, hypertrophy and atrophy is warranted. However, given that 3-MH translates across species additional experiments will be conducted in Chapter 8 to further determine the utility of this biomarker for assessing preclinical drug-induced myopathy.

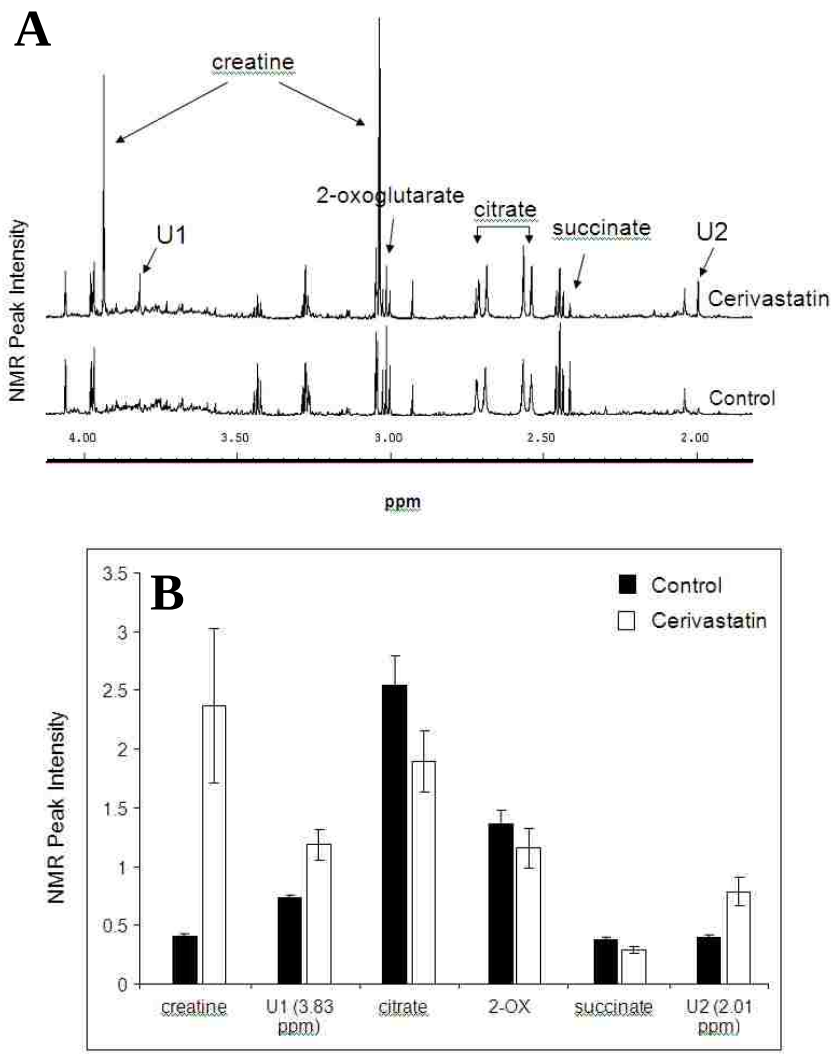

Figure 7.1. Metabolic profiles of urine ^{1}H NMR spectra. A. Representative spectra of urine from control (bottom trace) and cerivastatin (1 mg/kg/day; top trace) treated female rats, showing some of the major metabolic changes: creatine (3.05, 3.93 ppm), citrate (2.55, 2.71 ppm), 2-oxoglutarate (2.45, 2.47 ppm), succinate (2.41 ppm), U1 = unknown peak at 3.82 ppm, U2 = unknown peak at 2.01 ppm. B: Mean peak areas with standard errors for selected metabolites in urine from control and cerivastatin (1 mg/kg) treated female rats. The y-axis is relative NMR peak intensity normalized to creatinine.

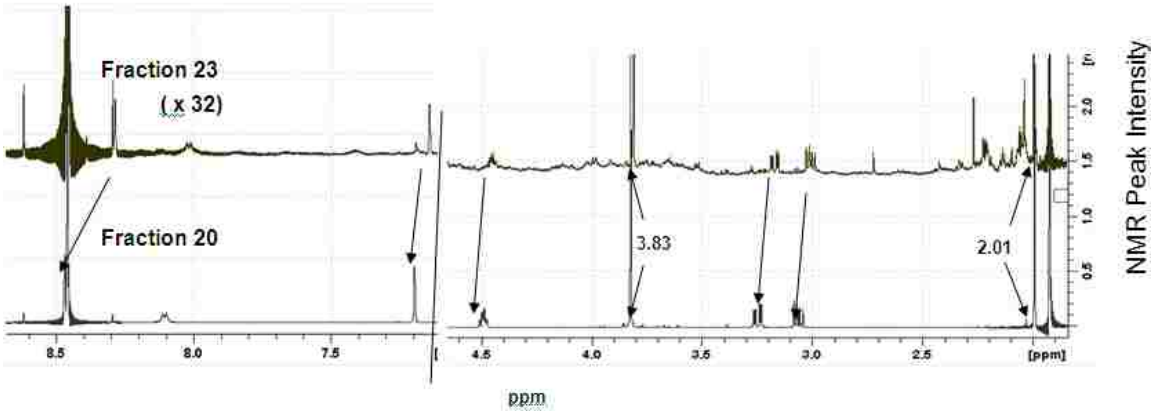

Figure 7.2. ^{1}H NMR spectra of unknown metabolites. 600 MHz ^{1}H NMR spectra of HPLC fractions 20 (bottom trace) and 23 (top trace, with vertical scale increased 32-fold relative to bottom trace) showing two well resolved sets of signals of different but structurally similar molecules, including the diagnostic singlets at 3.83 or 3.81 and 2.01 or 1.99 ppm for fractions 20 and 23, respectively.

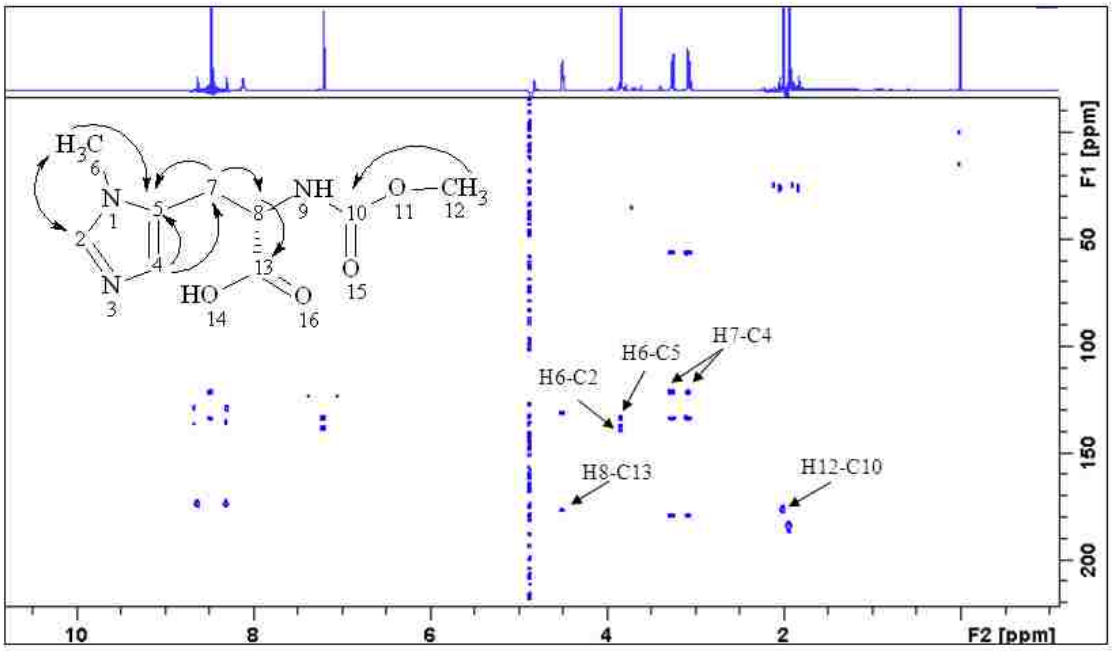

Figure 7.3. 2D NMR spectrum of N-acetyl-1-methylhistidine. Proton-carbon cross correlations observed in the HMBC 2D NMR spectrum of fraction 20. Inset: key correlations that identified the compound as N-acetylated 1-methylhistidine. Selected cross peaks crucial to the structural assignment are indicated.

1-Methylhistidine

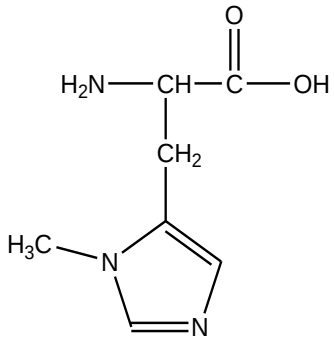

3-Methylhistidine

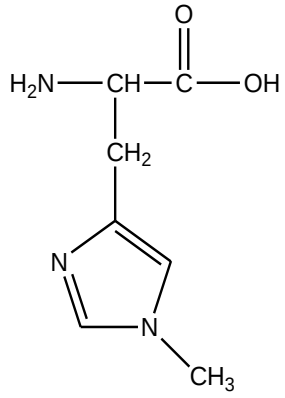

Figure 7.4. **Structures of 1- and 3-methylhistidine.** The structures of 1- and 3-methylhistidine were identified as the unknown metabolites from cerivastatin-treated rats.

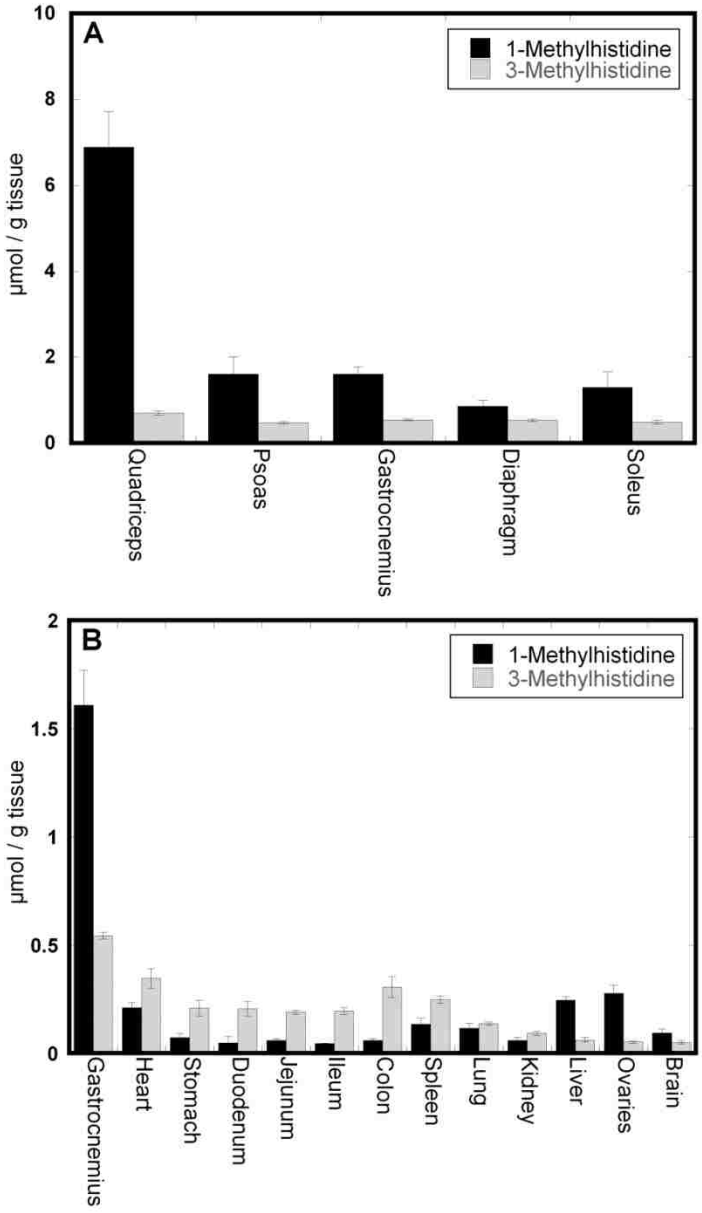

Figure 7.5. Tissue distribution and concentration of 1- and 3-methylhistidine in female rats. The concentration of the methylhistidine isomers was determined by GC-MS in A) five skeletal muscles, representing predominately fast- (quadriceps, psoas, gastrocnemius), slow- (soleus) and mixed- (diaphragm) twitch fibers. In panel B, the gastrocnemius muscle is presented for direct comparison to other tissues.

Table 7.1. Tissue distribution and concentration of 1- and 3-methylhistidine in male and female rats.

	1-Methylhistidine (µmol / g tissue)	SE	3-Methylhistidine (µmol / g tissue)	SE
Quadriceps Male	5.416	1.198	0.611	0.034
Quadriceps Female	6.892	0.822	0.701	0.046
Psoas Male	1.626	0.228	0.415	0.027
Psoas Female	1.611	0.399	0.474	0.026
Gastrocnemius Male	1.503	0.238	0.526	0.019
Gastrocnemius Female	1.609	0.161	0.544	0.017
Diaphram Male	0.787	0.212	0.488	0.037
Diaphram female	0.860	0.139	0.537	0.030
Soleus Male	1.344	0.124	0.539	0.031
Soleus Female	1.296	0.362	0.493	0.041
Heart Male	0.182	0.005	0.281	0.016
Heart female	0.211	0.023	0.345	0.045
Stomach Male	0.026	0.007	0.200	0.048
Stomach Female	0.072	0.019	0.209	0.036
Duodenum male	0.031	0.004	0.184	0.003
Duodenum female	0.048	0.030	0.207	0.033
Jejunum male	0.054	0.005	0.184	0.004
Jejunum female	0.060	0.007	0.190	0.010
Ileum male	0.067	0.014	0.232	0.012
Ileum female	0.044	0.002	0.195	0.016
Colon male	0.078	0.015	0.293	0.017
Colon female	0.059	0.009	0.306	0.049
Spleen Male	0.131	0.022	0.215	0.008
Spleen Female	0.134	0.028	0.248	0.016
Lung Male	0.128	0.014	0.154	0.005
Lung Female	0.116	0.023	0.137	0.007
Kidney Male	0.062	0.025	0.105	0.008
Kidney Female	0.060	0.014	0.092	0.009
Liver Male	0.196	0.040	0.067	0.005
Liver Female	0.245	0.016	0.062	0.010
Testes	0.230	0.024	0.050	0.002
Ovaries	0.276	0.037	0.052	0.005
Brain Male	0.100	0.024	0.038	0.006
Brain Female	0.094	0.018	0.050	0.007

Table 7.2. 1- and 3-Methylhistidine urine concentrations in vehicle-treated male rats[a]

Animal #	Vehicle	1-MH (nmol/mg creatinine)	3-MH (nmol/mg creatinine)
1	0.5% Methylcellulose[b]	438	268
2	(Cerivastatin vehicle)	582	228
3		412	232
4		510	275
5		430	222
6		340	154
7	Saline[c]	502	349
8	(Isoproterenol vehicle)	337	257
9		384	279
10		445	333
11		418	301
12	Saline[c]	340	235
13		672	242
14		652	248
15		305	173
Mean concentration ± SE		**451 ± 29**	**253 ± 13**

[a]The concentration of 1- and 3-MH in male rat urine collected for 24 hrs was determined across 3 studies.

[b]Rats were given 14 doses of 0.5 methylcellulose.

[c]Rats were given a single dose of saline.

Table 7.3. 1- and 3-methylhistidine urine concentrations in vehicle-treated female rats[a]

Animal #	Vehicle	1-MH (nmol/mg creatinine)	3-MH (nmol/mg creatinine)
1	0.5% Methylcellulose[b]	504	321
2	(Cerivastatin vehicle)	459	278
3		456	262
4		306	136
5		535	257
6		701	284
7	Saline[c]	742	283
8	(Isoproterenol vehicle)	672	286
9		492	251
10		430	162
11		714	323
12	Saline[c]	804	306
13		808	272
14		658	253
15		752	261
16		545	238
17		334	202
Mean concentration ± SE		**583 ± 39**	**257 ± 12**

[a]The concentration of 1- and 3-MH in female rat urine collected for 24 hrs was determined across 3 studies.

[b]Rats were given 14 doses of 0.5% methylcellulose.

[c]Rats were given a single dose of saline.

Table 7.4. 1- and 3-Methylhistidine in urine and serum from cerivastatin treated female and male rats[a]

	1-Methylhistidine		3-Methylhistidine	
Treatment (mg/kg)	**Urine (nmol/mg creatinine)**	**Serum (μM)**	**Urine (nmol/mg creatinine)**	**Serum (μM)**
Females				
Control	494 ± 52	6.0 ± 0.9	256 ± 26	1.9 ± 0.2
0.5	829 ± 199	*nd*	278 ± 23	*nd*
1.0	3142 ± 966*	69.7 ± 22.8*	512 ± 98*	5.5 ± 0.9*
Males				
Control	452 ± 34	15.8 ± 2.1**	230 ± 18	3.0 ± 0.2**
0.5	446 ± 18	*nd*	230 ± 8.5	*nd*
1.0	381 ± 45	14.0 ± 0.8	252 ± 36	2.8 ± 0.1

[a]Results represent the mean and SE of 4 - 9 rats dosed daily with cerivastatin or vehicle for 14 consecutive days.

(nd) not determined.

*Significantly different from control ($p < 0.05$).

**Significantly different from female control ($p < 0.05$).

Table 7.5. 1- and 3-Methylhistidine in urine from isoproterenol treated male rats[a]

Treatment (mg/kg)	1-MH (nmol/mg creatinine)	3-MH (nmol/mg creatinine)
Control	417 ± 28	304 ± 17
0.5	170 ± 28*	153 ± 21*

[a]Results represent the mean and SE of 5 - 6 rats given a single dose of isoproterenol.

*Significantly different from control ($p < 0.05$).

Chapter 8

Utility of 3-methylhistidine as a preclinical biomarker of drug-induced myopathy

8.1. Introduction

Preclinical skeletal muscle injury is routinely evaluated by histopathology because commonly used serological proteins, including CK and AST lack sensitivity and specificity (Bohlmer et al., 2004; Loeb, 1999). Although histopathology is a definitive indicator of myopathy, it is invasive, labor intensive, and it is not feasible to assess all muscles from a rat. Thus, there is a significant need for more reliable preclinical biomarkers of skeletal muscle toxicity. This need is further underscored by the increased incidence of skeletal muscle injury in the preclinical evaluation of new therapeutic targets and the fact that drug-induced skeletal muscle toxicity is a serious clinical liability highlighted by cerivastatin, which was withdrawn from the market after it was associated with more than 100 rhabdomyolysis-related deaths (Thompson et al., 2003).

NMR metabolomic profiling of urine from cerivastatin treated rats indicated that 3-methylhistidine (3-MH), an endogenous metabolite originating from skeletal muscle, increased with the severity of myopathy in the rat (Chapter 7; Aranibar et al., 2011). Methylation of histidine at the 3-position represents a post-translational modification of actin and myosin heavy chain which is most abundant in skeletal muscle (Aranibar et al., 2011; Johnson et al., 1967, 1970; Tomas et al., 1979; Young et al., 1972; Young and

Munro, 1978). When skeletal myofibrillar proteins are degraded under various catabolic conditions, 3-MH is not reutilized for protein synthesis but rather is excreted in a manner that is directly related to the rate of degradation (Young and Munro, 1978). Over the last 30 years, urinary 3-MH normalized to creatinine (3-MH/creatinine), and representing the fractional excretion relative to muscle mass, has been used for the preclinical and clinical evaluation of myofibrillar protein degradation in various catabolic (atrophy) and anabolic (hypertrophy) skeletal muscle conditions (Agrawal et al., 2003; Asatoor and Armstrong, 1967; Johnson et al., 1967, 1970; Kuhl et al., 1998; Li and Wasner, 1981; Long et al., 1975; Young et al., 1972; Young and Munro, 1978). Accordingly, the observation that 3-MH levels in urine and serum increase with cerivastatin-induced myopathy may further extend the utility of this metabolite as a potential biomarker of drug-induced skeletal muscle toxicity.

There are several mechanisms which contribute to intracellular protein degradation, however the ubiquitin-proteasome pathway (UPP) is responsible for 80-90% of myofibrillar protein degradation which occurs in response to various catabolic conditions like fasting, sarcopenia, cachexia, denervation, and drugs like glucocorticoids, chloroquine and statins (Chapter 1.7.3., Buettner and Lecker, 2008; Goll et al., 2008; Kimura et al., 2009; Lecker et al., 2004; Mallinson et al., 2009; Mitch and Goldberg, 1996; Murton et al., 2008; Solomon and Goldberg, 1996). In these conditions, there is a common and coordinated transcriptional and biochemical adaptation which mediates rapid catabolism of myofibrillar proteins through the UPP (Cohen et al., 2009; Fielitz et al., 2007; Lecker et al., 2004). Within the UPP, there are two skeletal muscle specific

ubiquitin ligases, atrogin-1 and MuRF-1 which are transcriptionally induced and considered hallmark changes associated with increased myofibrillar protein degradation (Chapter 1.7.3.; Bodine et al., 2001; Buettner and Lecker, 2008; Cohen et al., 2009; Foletta et al., 2011; Kimura et al., 2009; Lecker et al., 2004; Mitch and Goldberg, 1996). In chapter 6 it was shown that both atrogin-1 and MuRF-1 are transcriptionally induced in fast-twitch muscles with cerivastatin-induced myopathy. Furthermore, in Chapter 7 it was demonstrated that urine and serum 3-MH were also increased with cerivastatin-induced myopathy. Therefore, since transcriptional induction of the muscle specific ubiquitin ligases, and increased excretion of 3-MH are both indicators of myofibrillar protein degradation, it was hypothesized that upregulation of atrogin-1 and MuRF-1 precedes an increase in urine and serum levels of 3-MH associated with skeletal muscle atrophy and necrosis.

The goal of this work was to further investigate the potential utility of 3-MH as a preclinical urine and serum biomarker of drug-induced myopathy. An additional goal of this work was to determine the temporal relationship between transcriptional induction of the muscle specific ubiquitin ligases with changes in urine and serum levels of 3-MH. For this work, several different models known to induce skeletal muscle catabolism were employed, including necrosis and, atrophy, thereby providing a range of experimental conditions to assess changes in 3-MH compared to more traditional endpoints including CK, AST and histopathology. Specifically, a time course of cerivastatin-induced myotoxicity was conducted in non-fasted rats to further investigate the utility of 3-MH in this model. Additionally, since rats are typically fasted during routine preclinical studies,

and this experimental manipulation is associated with myofibrillar protein degradation, a fasting time course study was conducted to determine the effect on 3-MH. Moreover, a dosing paradigm, using the muscle toxicant BMS-600149 (p38 kinase inhibitor) was performed to determine whether 3-MH could detect a minimal drug-induced myotoxicity in fasted rats (Vassallo et al., 2009).

8.2. Methods

Chemicals. Cerivastatin was prepared as previously described in Chapter 2.2. BMS-600149 ((S)-2-(sec-butylamino)-N-(5-(cyclopropylcarbamoyl)-2-methylphenyl)thiazole-5-carboxamide) was synthesized at Bristol-Myers Squibb (Princeton, NJ). Polyethylene glycol 400 was purchased from EMD Chemicals Inc. (Gibbstown, NJ).

Animals. Female and male rats were used for this study as previously described in Chapter 2.2.

Study design. Rats were randomized by weight and treated as outlined in Table 8.1. The cerivastatin time course was conducted as previously described in Chapter 2 (*study 2).* Evaluation of fasting in rats was conducted for up to 16 hours because this time is routinely used during the conduct of preclinical safety studies and has been previously demonstrated to increase 3-MH (Robertson et al., 2011). The BMS-600149 dosing paradigm was selected based on the literature indicating 100 mg/kg dosed for 3 days causes minimal skeletal muscle damage (Vassallo et al., 2009).

After the last dose, rats treated with cerivastatin and BMS-600149 were placed in metabolism cages (Nalgene, Rochester, NY) and urine was collected at 4°C over a 24 hour period. Fasted rats were placed in metabolism cages upon removal of food at 2, 4, 8, 12 and 16 hours prior to necropsy. Animals treated with cerivastatin and BMS-600149 were anesthetized with isoflurane prior to exsanguination (vena cava) approximately 24 hours after the last dose. Fasted rats were anesthetized with isoflurane prior to

exsanguination (vena cava) between 6 and 8 am. Blood was collected for serum separation and tissues were harvested as described below.

Skeletal muscle collection. For all studies, skeletal muscles, including representative fast-twitch (quadriceps femoris and gastrocnemius) and slow-twitch (soleus) fiber type composition were harvested from the right side of the animal along with the right coronal section of the heart and the right lobe of the liver and stored at -80˚C pending RNA isolation (Table 2.1).

Histopathology. For all studies, skeletal muscles including representative fast-twitch (quadriceps femoris and gastrocnemius) and slow-twitch (soleus) fiber type composition were harvested from the left side of the animal along with the left coronal section of the heart and left lateral lobe of the liver were collected for histopathologic evaluation as described in Chapter 2.2 (Table 2.1; Armstrong and Phelps, 1984; Hamalainen and Pette, 1993; Koerker et al., 1990).

Clinical chemistry analysis. Serum and urine samples were stored at -80°C immediately after collection and analyzed for CK, AST and ALT on a Seimens Advia 1800 chemistry autoanalyzer (Seimens Healthcare Diagnostics, Tarrytown, NY). Creatinine (Roche Hitachi 917 instrument) was determined for each urine sample.

Serum and urine methylhistidine. Quantitation of serum and urine 3-MH was determined by GC-MS as previously described in Chapter 7.2 (Aranibar et al., 2010; Rathmacher et al., 1992).

RNA isolation and RT-PCR. RNA was isolated from frozen skeletal muscles and quantitative RT-PCR was conducted as previously described in Chapter 5.2 with primers listed in Table 6.1.

Data analysis. The mean ± SE concentration of 3-MH, CK, AST and ALT were determined for each treatment group. For quantitative RT-PCR, relative changes in gene expression were determined by the ΔΔCt method. The Ct values for each gene were normalized to 18S Ct values and the fold change in treated muscles was determined relative to control. Group means for all analyses were compared with a Student's t-test or ANOVA using StatView (SAS Institute, Cary, NC) at $p<0.05$. However, statistics for the RT-PCR results were conducted on the values following normalization to 18S.

8.3. Results

To investigate the utility of 3-MH as a biomarker of drug-induced myotoxicity a time course with cerivastatin was conducted. Cerivastatin caused a time dependent, fast-twitch specific myofiber necrosis and degeneration whereas the slow-twitch muscle (soleus) was unaffected as previously described (Figure 2.2; Table 8.2). In the quadriceps, a minimal myopathy was first observed in 50% of the animals after 8 days of cerivastatin treatment (Figure 2.2; Table 8.2). At this time, serum 3-MH increased in conjunction with the muscle specific ubiquitin ligases in all rats, whereas all other markers were unchanged (Table 8.2). After 10 days of cerivastatin treatment, 75% of the animals had evidence of a mild myopathy in the quadriceps and urine and serum 3-MH increased in conjunction with transcriptional induction of the muscle specific ubiquitin ligases in all rats (Figure 2.2; Table 8.2). An increase in the other serum biomarkers, including CK, AST and ALT was noted, however these changes were highly variable and not significant (Table 8.2). Following 14 days of cerivastatin treatment, 100% of the animals had evidence of myopathy in the quadriceps, generally characterized as moderate to severe, and all biomarkers were significantly increased along with the muscle specific ubiquitin ligases (Figure 2.2; Table 8.2). Although the muscle specific ubiquitin ligases were significantly increased relative to control, the magnitude of increase was significantly less compared to muscles from rats after 10 days of cerivastatin treatment which may reflect dissolution of the myofibers after 14 doses (Figure 2.2; Table 8.2). Together, these results suggest a temporal relationship between transcriptional induction of the muscle specific ubiquitin ligases and increases in serum 3-MH with cerivastatin-induced myopathy. Specifically, there was a correlation between an increase in the muscle specific ubiquitin ligases and 3-

MH for individual animals. Furthermore, these results demonstrate that serum 3-MH was more sensitive than urine 3-MH, CK and AST for detecting cerivastatin-induced myopathy.

Overnight (16 hours) fasting is commonly employed in routine rodent toxicological studies. However, the temporal effects on myofibrillar protein degradation associated with this experimental manipulation are unknown. Following 16 hours of fasting, there was no evidence of myopathy or atrophy by histopathology or clinical chemistry (Figure 8.1; Table 8.3). However, serum 3-MH increased after 8 hours of fasting and continued to stay elevated at 16 hours whereas urine 3-MH was only elevated at the later time point (Table 8.3). Consistent with fasting-induced myofibrillar protein degradation, the muscle specific ubiquitin ligases were also transcriptionally induced in a time-dependent manner, with atrogin-1 preceding an increase in MuRF-1 (Table 8.3). Collectively, these results demonstrate that 16 hours of fasting causes a time-dependent transcriptional induction in the muscle specific ubiquitin ligases and increases in serum and urine 3-MH. Furthermore, these results demonstrate that serum was more sensitive than urine 3-MH for detecting fasting-induced myofibrillar protein degradation.

Since both cerivastatin-induced myopathy as well as fasting-induced myofibrillar protein degradation resulted in a similar increase in 3-MH, a study was conducted to determine whether 3-MH was useful for detecting drug-induced myopathy in fasted rats (Tables 8.2 and 8.3). For this study, BMS-600149 was used as a model compound because it has previously been shown to cause a consistent but minimal myotoxicity. Following 3 days

of dosing, BMS-600149 caused a minimal myopathy, with 100% incidence in the quadriceps characterized by necrosis, atrophy and cellular infiltration which was corroborated by a slight increase in AST but not CK (Figure 8.1; Table 8.4). As expected, an underlying myofibrillar protein degradation was likely present in control fasted rats as 3-MH levels were similar to those observed in the 16 hour fasting time course study (Tables 8.3 and 8.4). However, serum but not urine 3-MH, was further increased in BMS-600149 treated rats relative to control, suggesting a minimal drug-induced myopathy was detected in the presence of fasting-induced myofibrillar protein degradation. Furthermore, these results are consistent with a slight, but significant transcriptional induction of atrogin-1 and MuRF-1 which may represent an effect above fasting alone (Tables 8.3 and 8.4).

8.4. Discussion

Skeletal muscle mass is determined by the balance between myofibrillar protein synthesis and degradation and these processes are highly regulated to meet the functional needs of this tissue as well as whole body energy metabolism (Murton et al., 2008). Despite this tight regulation, skeletal muscle rapidly adapts to catabolic and anabolic conditions by modulating the rates of myofibrillar protein synthesis and degradation (Figure 8.2). Although both of these processes are important, the focus of this work was on the evaluation of myofibrillar protein degradation. Specifically, this work was designed to further investigate the potential utility of 3-MH as a preclinical biomarker of myofibrillar protein degradation resulting from drug-induced myopathy, and to determine the temporal relationship between transcriptional induction of the muscle specific ubiquitin ligases with changes in urine and serum levels of 3-MH.

For this work, several different models known to induce skeletal muscle catabolism were employed, including necrosis and atrophy, thereby providing a range of experimental conditions to assess changes in 3-MH compared to more traditional endpoints including CK, AST and histopathology. Specifically, a time course of cerivastatin-induced myotoxicity was conducted in non-fasted rats to further investigate the utility of 3-MH in this model. Additionally, since rats are typically fasted during routine preclinical studies, and this experimental manipulation is associated with myofibrillar protein degradation, a fasting time course was conducted to determine the effect on 3-MH. Moreover, a dosing paradigm, using the muscle toxicant BMS-600149 was performed to determine whether

3-MH could detect a minimal drug-induced myotoxicity in fasted rats (Vassallo et al., 2009).

Historically, urine 3-MH has been useful for monitoring skeletal muscle atrophy and the current work further confirms the utility of this biomarker for catabolic conditions (Figure 8.2). Additionally, the current work provides perspective on the utility of urine 3-MH for evaluating drug-induced myopathy (Figure 8.2). Based on the current results, urine 3-MH showed similar utility as CK and AST for monitoring cerivastatin-induced myopathy in non-fasted rats. However, an important experimental variable needs to be considered when using this biomarker in the urine. Specifically, overnight fasting, which is typically employed in routine safety studies, increases myofibrillar protein degradation and urine 3-MH in the absence of myopathy. Accordingly, this urine biomarker may be most useful for monitoring drug-induced myopathy in non-fasted rats.

In contrast to the urine, serum levels of 3-MH were more sensitive than the standard biomarkers of myopathy, and increases were generally correlated with evidence of myofibrillar protein catabolism, including histopathology and transcriptional induction of the muscle specific ubiquitin ligases (Figure 8.2). However, similar to the urine, fasting also increased serum 3-MH. Therefore, this biomarker may be most useful for monitoring drug-induced myopathy in non-fasted rats.

It was hypothesized that transcriptional induction of the muscle specific ubiquitin ligases would precede an increase in 3-MH. In general, there was a correlation between

transcriptional induction of the muscle specific ubiquitin ligases and increases in 3-MH which is consistent with the notion that atrogin-1 and MuRF-1 are considered strong predictors of increased myofibrillar protein catabolism (Foletta et al., 2011). Despite this correlation, the temporal relationship and the magnitude of transcriptional induction for atrogin-1 and MuRF-1 were not always in absolute concordance with an increase in serum 3-MH, and this was particularly the case in the fasting time course. However, this pattern has also been observed by other investigators and may reflect the fact that atrogin-1 and MuRF-1 are differentially regulated with separate targets in protein synthesis and degradation, respectively (Figure 8.2; Foletta et al., 2011; Mikura et al., 2009; Nakashima and Yakabe, 2007; Pruznak et al., 2008; Sachek et al., 2004; Vary et al., 2008). Furthermore, several other factors, including proteasome activity and enzymes like calpains, tripeptidyl-peptidase II and exopeptidases contribute to the rate of myofibrillar protein degradation (Figure 1.15; Taillandier et al., 2004). Despite the complex regulation involved with myofibrillar protein degradation, transcriptional induction of the muscle specific ubiquitin ligases was temporally correlated with an increase in serum 3-MH.

The totality of these results confirms the utility of urine 3-MH as a useful preclinical biomarker for monitoring catabolic conditions in skeletal muscle, including cerivastatin-induced myopathy in non-fasted rats. This work also provides additional perspective on the utility of serum 3-MH as a potential biomarker of drug-induced myopathy. Specifically, serum 3-MH was more sensitive than CK, AST and urine 3-MH for assessing drug-induced myopathy. Furthermore, the ability of 3-MH to monitor skeletal muscle atrophy provides an advantage over the standard biomarkers which are limited to

detecting necrosis (Table 1.5). Accordingly, this biomarker may be particularly useful for compounds which cause skeletal muscle atrophy in the absence of myopathy. Moreover, the sensitivity of serum 3-MH to changes in myofibrillar protein degradation which may indicate that this biomarker has potential utility in providing early evidence that an adverse skeletal muscle may develop. However, additional studies are needed to further investigate this hypothesis.

One limitation of 3-MH is the dynamic range in both matrices. Therefore, both urine and serum 3-MH may be most useful as a qualitative, and not a quantitative biomarker of myofibrillar protein degradation in non-fasted rat studies. Although the current investigation was conducted in rats, 3-MH is highly conserved and these findings may translate across species including dogs, nonhuman primates and humans under conditions in which factors like diet, exercise, physiological or pathological changes which could affect skeletal muscle protein metabolism are controlled (Asatoor and Armstrong, 1967; Johnson et al., 1967).

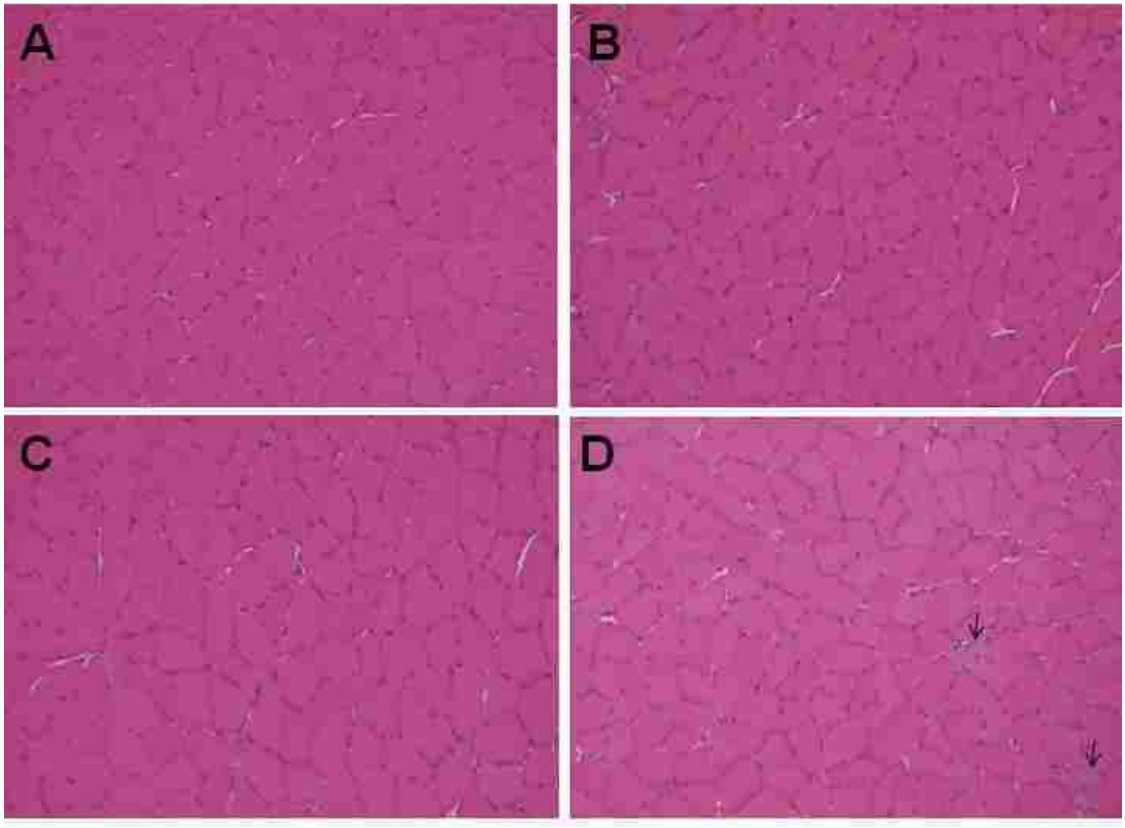

Figure 8.1. Histopathology of quadriceps femoris muscle from fasted and BMS-600149 treated rats.

Skeletal muscles from control (A) and 16 hour fasted (B) rats demonstrates no evidence of myopathy or atrophy. Skeletal muscles from control (C) and BMS-600149-treated (D) rats illustrates myopathy (arrow) characterized by hyalinization, atrophy and cellular infiltration.

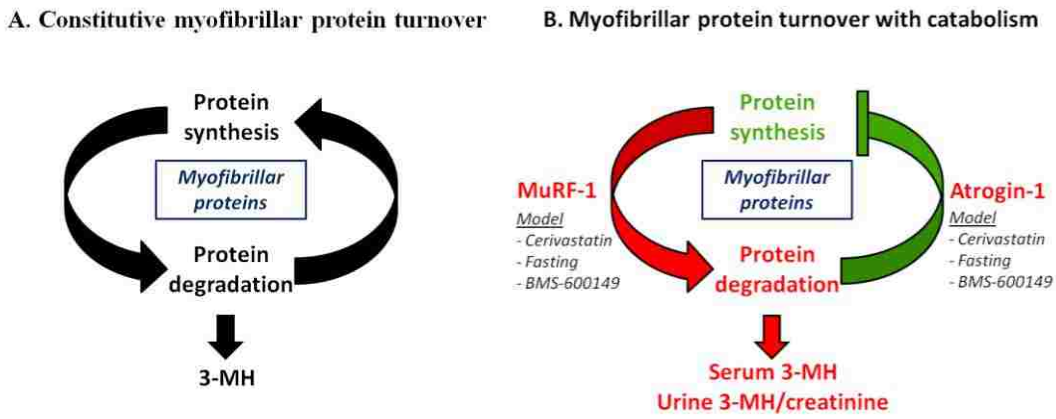

Figure 8.2. Regulation of myofibrillar protein turnover. A) Myofibrillar protein turnover is a constitutively active process involving de novo synthesis and degradation. Under normal physiological conditions, the rate of myofibrillar protein synthesis and degradation are tightly regulated to prevent changes in muscle mass. **B)** During catabolic conditions, transcriptional induction of atrogin-1 and MuRF-1 inhibits protein synthesis and increases protein degradation, respectively resulting in an increase in serum 3-MH and urine 3-MH/creatinine.

Note: Black indicates constitutive protein turnover under normal physiological conditions whereas red and green indicates an increase or decrease, respectively in atrogin-1 or MuRF-1 transcription, protein synthesis, protein degradation and 3-MH.

Table 8.1. Study design										
Treatment and effect[a]	Muscle target	Sex	Fasting	Dosage (mg/kg)	Volume of administration (ml/kg)	Vehicle[b]	Route of administration[c]	Number of doses[d]	Necropsy day[e]	References
Cerivastatin-induced myopathy	Fast-twitch	Female	No	1	5	MC	Oral	1,6,8,10,14	2,7,9,11,15	Westwood et al., 2005
Fasting-induced muscle atrophy[f]	Fast-twitch	Male	Yes							Jagoe et al., 2002; Wassner et al., 1977
BMS-680149-induced myopathy	Fast-, Slow-twitch	Male	Yes	100	5	PEG	Oral	3	4	Vassallo et al., 2009

[a]Dosing paradigms and related effects were based on previously published literature.

[b]MC, 0.5% methylcellulose; PEG, polyethylene glycol 400.

[c]Oral, oral gavage.

[d]Dosing was conducted once daily before noon.[e]Necropsy was conducted before noon and 24 hours after the last dose for all treated animals.

[f]Rats were fasted for 2, 4, 8, 12 and 16 hours with necropsy between 6-8 am.

Table 8.2. Evaluation of clinical, histopathological and transcriptional changes associated with cerivastatin-induced myopathy[a]										
Days of dosing cerivastatin	Urine[b]	Serum				Histopathology[c]			Relative mRNA expression in muscle[d]	
	3-MH (nmol / mg creatinine)	3-MH (μM)	CK (U/L)	AST (U/L)	ALT (U/L)	Quad	Gastroc	Heart	Atrogin-1	MuRF-1
Control	295 ± 10	1.9 ± 0.1	443 ± 42	85 ± 4	47 ± 2	-	-	-	1	1
1	307 ± 12	1.9 ± 0.1	414 ± 105	88 ± 12	45 ± 4	-	-	-	-1.2 ± 0.1	-1.3 ± 0.2
6	295 ± 12	2.0 ± 0.1	344 ± 14	95 ± 3	52 ± 3	-	-	-	1.2 ± 0.2	1.3 ± 0.2
8	321 ± 17	2.5 ± 0.2*	259 ± 32	96 ± 8	53 ± 3	4/8 (1.0)	-	-	5.5 ± 1.1*	3.2 ± 0.7*
10	441 ± 58*	3.5 ± 0.6*	1282 ± 865	477 ± 251	98 ± 31	6/8 (1.7)	5/8 (1.6)	5/8 (1.6)	7.9 ± 1.5*	7.3 ± 1.8*
14	794 ± 166*	5.5 ± 1.0*	9747 ± 3239*^	2933 ± 651*^	363 ± 70*^	8/8 (3.0)	7/8 (3.0)	6/8 (2.3)	2.8 ± 0.7*^	2.4 ± 0.0.7*^

[a]Results represent the mean and SE of eight treated and four control rats per day. Results for all control rats (n = 20) were pooled together. Rats in this study were not fasted prior to necropsy.

[b]3-MH levels were measured in a 24 hour urine collection and total excretion was normalized to creatinine.

[c]Results represent the number of animals with skeletal or cardiac myofiber necrosis and degeneration / number of animals per group. The mean severity score in () is based on an arbitrary score of 1 to 4 (most severe). (-) Denotes no significant findings observed. No adverse histological effects were observed in the soleus or liver.

[d]Values represent the mean mRNA expression ± SE normalized to 18s and relative to control in the quadriceps femoris. (-) No values were entered because the transcriptional data are presented as fold change over control.

*Significantly different from control ($p<0.05$). ^Significantly different from day 10 ($p<0.05$).

Table 8.3. Evaluation of clinical, histopathological and transcriptional changes associated with fasting[a]				
Hours of fasting[b]	Urine[c]	Serum	Relative mRNA expression in muscle[d]	
	3-MH (nmol / mg creatinine)	3-MH (μM)	Atrogin-1	MuRF-1
Control	343 ± 14	2.3 ± 0.2	1	1
2	307 ± 15	2.2 ± 0.1	1.2 ± 0.3	-1.2 ± 0.1
4	337 ± 5	2.8 ± 0.3	2.3 ± 0.4*	1.2 ± 0.1
8	345 ± 8	3.9 ± 0.2*	2.9 ± 0.4*	1.3 ± 0.1
12	348 ± 17	3.8 ± 0.4*	5.6 ± 0.5*	1.6 ± 0.1*
16	437 ± 32*	4.6 ± 0.7*	7.7 ± 1.5*	1.8 ± 0.2*

[a]Results represent the mean and SE of five rats per group.

[b]Control rats were given food ad libitum for 16 hours whereas all other rats were fasted for the time indicated prior to necropsy. All rats were necropsied between 6-8 am.

[c]3-MH levels were measured in urine collected for the respective fasting time and total excretion was normalized to a 24 hour collection and creatinine. CK, AST and ALT were unchanged and no adverse histological effects were observed in the muscles or liver.

[d]Values represent the mean mRNA expression ± SE normalized to 18s and relative to control in the quadriceps femoris. (-) No values were entered because the transcriptional data are presented as fold change over control.

*Significantly different from control ($p < 0.05$).

Table 8.4. Evaluation of clinical, histopathological and transcriptional changes associated with BMS-600149-induced myopathy[a]

Treatment (mg/kg)	Urine[b]	Serum				Histopathology[c]			Relative mRNA expression in muscle[d]	
	3-MH (nmol / mg creatinine)	3-MH (µM)	CK (U/L)	AST U/L)	ALT (U/L)	Quad	Gastroc	Sol	Atrogin-1	MuRF-1
Control	391 ± 23	4.5 ± 0.4	308 ± 7	82 ± 3	42 ± 2	-	-	1/6 (1.0)	1	1
100	374 ± 19	5.4 ± 0.1*	288 ± 37	139 ± 12*	53 ± 5	6/6 (1.0)	3/6 (1.0)	5/6 (1.2)	1.6 ± 0.2*	1.5 ± 0.2*

[a]Results represent the mean and SE of six rats per group. Rats in this study were fasted for 16 hours prior to necropsy.

[b]3-MH levels were measured in urine collected for 16 hours and total excretion was normalized to a 24 hour collection and creatinine.

[c]Results represent the number of animals with skeletal myofiber necrosis and degeneration / number of animals per group. The mean severity score in () is based on an arbitrary score of 1 to 4 (most severe). (-) Denotes no significant findings observed. No adverse histological effects were observed in the heart or liver.

[d]Values represent the mean mRNA expression ± SE relative to control and normalized to 18s in the quadriceps. (-) No values were entered because the transcriptional data are presented as fold change over control.

*Significantly different from control ($p < 0.05$).

Chapter 9

Summary, conclusions and future research

Despite extensive research efforts indicating statin-induced myotoxicity is an on-target effect mediated by HMG-CoA reductase inhibition, the underlying pathophysiology remains unknown. The purpose of this dissertation was to use transcriptomic and metabolomic profiling to identify potential mechanisms and biomarkers of statin-induced myopathy. To determine transcriptional and metabolite changes, global gene expression analysis and metabolomic profiling, respectively were conducted on skeletal muscles from naïve and cerivastatin treated rats. Integration of these results led to the development of specific hypotheses regarding potential mechanisms of toxicity which were further investigated in a time course of cerivastatin-induced myopathy, as well as in primary cultures of isolated fast-twitch rat myofibers. An additional objective of this work was to identify biomarkers of myopathy by conducting metabolomic profiling on urine collected from cerivastatin treated rats. These results led to the identification of new biomarkers of myopathy which were further investigated to determine their utility for detecting preclinical drug-induced myopathy. A brief summary of this work is described below.

<u>Hypothesis 1:</u> Cerivastatin-induced myopathy in rats occurs in a fiber- and sex-dependent manner which is recapitulated in isolated rat fast-twitch differentiated myofibers (Chapter 2).

The goal of this work was to determine the dose response and time course of cerivastatin-induced myopathy in rats and isolated primary fast-twitch FDB myofibers. Cerivastatin-induced myopathy occurred in a dose-, time-, fiber- and sex-dependent manner with female fast-twitch muscles showing the greatest sensitivity whereas slow-twitch muscles were resistant to myotoxicity. Furthermore, dose- and time-dependent cerivastatin-induced myotoxicity was recapitulated in isolated primary fast-twitch myofibers and was prevented with mevalonate supplementation, confirming toxicity is an on-target effect. In contrast, sex-specific differences in cerivastatin-induced myopathy were not observed in vitro, suggesting in vivo factors may be important in mediating the pathophysiology.

<u>Hypothesis 2:</u> Transcriptional profiles of skeletal muscles from rats are useful for identifying molecular targets causally related to the mechanism of cerivastatin-induced myotoxicity (Chapter 3).

The goal of this work was to determine the fiber- and sex specific transcriptional profiles of skeletal muscles from naïve and cerivastatin treated rats, and to identify potential molecular targets or pathways causally related to myopathy. Transcriptional profiling of skeletal muscles from naïve rats demonstrated genes involved with energy metabolism and the sarcomere were differentially expressed in a fiber- and sex-dependent manner consistent with the phenotype of these muscles. Furthermore, the gene expression

changes were most significant between muscle fiber types whereas fast-twitch muscles from female and male rats were similar.

In fast-twitch muscles from cerivastatin (1 mg/kg) treated female rats approximately 50% of the probes were differentially expressed. Transcriptional changes of this magnitude are typically associated with pathology. Therefore, it was not possible to identify specific pathways causally related to the mechanism of statin-induced myopathy. However, an unexpected increase in a number of transcripts in the mevalonate pathway and cholesterol regulation was observed. Although this is a common response associated with hepatotoxicity, the pharmacology of hepatic HMG-CoA reductase inhibition with statin treatment in rats causes similar transcriptional effects in the absence of liver damage. Therefore, this skeletal muscle specific response may be mediated by pharmacology and causally related to the mechanism of statin-induced myopathy.

In skeletal muscles from cerivastatin treated rats, with minimal to no myopathy, the transcriptional changes were typically subtle, and potentially more informative of molecular changes or pathways involved with myopathy. Specifically, a variety of fiber- and sex-specific transcriptional changes were observed which may be important. However, there was also a common gene expression response across skeletal muscles characterized by modulation of a stress response, nuclear receptors, including Nr1d1, Nr1d2, Nr4a1, Nr4a2 and Nr4a3 as well as transcripts involved with energy metabolism, including PDK4 which is considered a metabolic energy switch. Together, these results

suggest cellular stress and altered energy metabolism may be causally related to the mechanism of statin-induced myopathy.

<u>Hypothesis 3:</u> Metabolomic profiles of skeletal muscles from rats are useful for identifying metabolite changes causally related to the mechanism of cerivastatin-induced myotoxicity (Chapter 4).

The goal of this work was to determine the fiber- and sex specific metabolomic profiles of skeletal muscles from naïve and cerivastatin treated rats, and to identify potential metabolites or pathways causally related to myopathy. Metabolomic profiling of skeletal muscles from naïve rats were similar with only a few changes noted. In aqueous and lipophilic extracts of skeletal muscles, lactate was higher in fast-twitch muscles, whereas taurine, fumarate and cholesterol were higher in slow-twitch muscles from female rats. Metabolomic profiles of aqueous and lipophilic extracts of fast-twitch muscles from female and male rats were similar, with creatine showing higher levels in male rats. Although metabolomic profiling did not reveal as many fiber- and sex-specific changes as transcriptomic profiling, these results were limited to highly concentrated metabolites with resolved resonances, in which the identification of the chemical structure could be confirmed with standard spectra. Furthermore, similar metabolomic profiles may also indicate that mRNA and protein expression are more important in defining the skeletal muscle phenotype.

In cerivastatin (1 mg/kg) treated female rats, metabolic profiles of lipophilic extracts of fast-twitch muscles indicated cholesterol and phosphatidylcholine were increased in a

manner that was consistent the transcriptional changes. Furthermore, these changes occurred in dose-dependent manner whereas similar effects were not observed in skeletal muscles without myopathy. To further determine the effects on the cholesterol pathway, a panel of sterols was measured which indicated that the cholesterol biosynthesis precursors, desmosterol and 7-dehydrocholesterol were also increased in the fast-twitch muscles from female rats treated with cerivastatin. While the origin and implication of these changes was unknown, abnormal accumulation of cholesterol is toxic. Therefore, additional experiments were conducted in Chapter 5 to determine whether alterations in cholesterol homeostasis were causally related to the mechanism of cerivastatin-induced myopathy or whether these changes represent an effect associated with toxicity.

In cerivastatin (1 mg/kg) treated female rats, metabolic profiles of aqueous extracts of fast-twitch muscles indicated a decrease in a variety of metabolites, including lactate, NAD^+, creatine, phosphocreatine, carnosine and anserine which were likely associated with myopathy. Skeletal muscles from cerivastatin treated rats with minimal to no myopathy were also evaluated and the metabolomic changes were typically subtle, and potentially more informative of metabolites and pathways involved with myopathy. Specifically, in the aqueous extracts of skeletal muscles from cerivastatin treated rats, fiber- and sex-specific changes in NAD^+, phosphocreatine and anserine were noted and consistent with the transcriptional changes indicating cellular stress and alterations in energy metabolism may be causally related to the mechanism of cerivastatin-induced myopathy. Additional experiments were conducted in Chapter 6 to further investigate the

role of altered energy metabolism as a potential mechanism of cerivastatin-induced myopathy.

<u>Hypothesis 4:</u> Cerivastatin-induced myopathy is causally related to alterations in cholesterol homeostasis (Chapter 5).

The goal of this work was to determine whether alterations in cholesterol homeostasis are causally related to the mechanism of cerivastatin-induced myopathy. To determine the temporal relationship between alterations in cholesterol homeostasis and the development of myopathy a cerivastatin (1 mg/kg) time course study was conducted in female rats. Alterations in cholesterol homeostasis were monitored in the sensitive fast-twitch muscle, the unaffected slow-twitch muscle and in the liver by measuring transcriptional and sterol changes.

In the cerivastatin time course, transcriptional and sterol changes in the fast-twitch muscle demonstrated that altered cholesterol homeostasis was a manifestation of the myopathy and unrelated to the mechanism of toxicity. Importantly, these changes were different from the soleus in which there was no evidence of toxicity or changes in cholesterol homeostasis. Furthermore, the time course profile was also different from the liver, which showed an immediate and sustained compensatory transcriptional induction of HMG-CoA reductase consistent with the pharmacology of cerivastatin. Although the mechanism of altered cholesterol homeostasis was not directly probed in this work skeletal muscle regeneration requires activation of HMG-CoA reductase. However, in the face of ongoing toxicity, skeletal muscle is unable to regenerate, and this causes

cholesterol accumulation and activation of several pathways including, cholesterol esterification (acyl-CoA: cholesterol acyltransferase), efflux (ABCG1 and ABCA1) and conversion (cholesterol 25-hydroxylase) to 25-hydroxycholesterol. An important observation of this work was that the in vitro model did not recapitulate the in vivo changes in cholesterol suggesting in vivo factors are important in mediating this process.

Activation of the 25-hydroxylation pathway has not been previously reported with skeletal muscle necrosis. Therefore, it is unknown whether this response is specific to statin myopathy or commonly associated with other muscle pathologies. However, various biological roles for 25-hydroxycholesterol have been previously identified. Specifically, this oxysterol is more hydrophilic than cholesterol and is able to passively diffuse across the membrane and is reverse transported to the liver where it is converted to bile acids. Moreover, 25-hydroxycholesterol is a ligand for LXR which activates the efflux transporters and further increases removal of cholesterol. Accordingly, the current results demonstrate that cholesterol 25-hydroxylation may be an important pathway in skeletal muscle which regulates cholesterol homeostasis with statin-induced myopathy.

<u>Hypothesis 5:</u> Cerivastatin-induced myopathy is causally associated with alterations in energy metabolism (Chapter 6).

Skeletal muscle energy metabolism relies on oxidative phosphorylation, and a critical step in this process is glucose oxidation followed by conversion of pyruvate to acetyl-CoA, in a reaction catalyzed by PDC. This irreversible process plays a major role in energy metabolism, particularly in fast-twitch skeletal muscles, as it represents the only

entry point for glucose into the mitochondria for oxidation and ATP synthesis. PDK4 is transcriptionally upregulated in fast-twitch muscles prior to the onset of statin-induced myopathy and chronic induction can impair energy metabolism and lead to extensive myofibrillar protein degradation and myotoxicity. Therefore, a major goal of this work was to determine whether PDK4 inhibition in fast-twitch skeletal muscles is causally related to cerivastatin-induced myopathy. An additional goal of this work was to determine the temporal relationship in fast- and slow-twitch muscle fibers between transcriptional induction of PDK4, PGC-1α which increases mitochondrial content and oxidative capacity, and markers of myofibrillar protein degradation, including atrogin-1 and MuRF1 indicating impaired energy metabolism.

Results from this work demonstrated that cerivastatin triggers an early and sustained transcriptional induction of PDK4 in fast-twitch muscles which is consistent with a metabolic switch in energy metabolism to a more oxidative phenotype. However, inhibition of this metabolic switch by dichloroacetate was insufficient in protecting the fast-twitch muscle from cerivastatin-induced toxicity. Therefore, these results suggest that transcriptional induction of PDK4 may be necessary but insufficient to mediate cerivastatin-induced myopathy. Consistent with this observation, previous investigators have also demonstrated that statins reduce mitochondrial oxidative capacity resulting in impaired energy metabolism in fast-twitch muscles. Further evidence to support a deficiency in oxidative capacity is based on the observation that NAD^+ is significantly decreased in the female rat fast-twitch muscles following cerivastatin (0.5 mg/kg) treatment which is associated with reduced oxidation capacity of substrates in glycolysis,

fatty acid oxidation and the citric acid cycle. Together, these results implicate a deficiency in both glycolytic and oxidative energy metabolism in mediating cerivastatin-induced myopathy. Consistent with this hypothesis, transcriptional induction of PGC-1α expression was observed supporting a metabolic demand for a more oxidative phenotype. However, this metabolic adaptation was insufficient in protecting the muscle, as transcriptional markers of protein degradation, indicative of impaired energy metabolism, were transcriptionally induced in association with toxicity. In contrast to the current results, a recent in vivo study demonstrated that DCA treatment prevents simvastatin-induced myopathy in rats. While the disparity in these results is unknown, it may be related to the in vitro model which also did not recapitulate alterations in cholesterol homeostasis observed in Chapter 5.

Previous transcriptional and metabolomic results (Chapters 3 and 4) demonstrated that cerivastatin causes altered energy metabolism and a cell stress response in the slow-twitch muscle. Similarly, in the current work, slow-twitch fibers showed a transcriptional response represented by upregulation of PDK4, atrogin-1 and MuRF1, indicating impaired energy metabolism, however this was a delayed response and only observed after 14 days of cerivastatin treatment. Unlike the fast-twitch muscle, PGC-1α was not transcriptionally induced in the slow-twitch muscle following cerivastatin treatment, however constitutive levels were 4-times higher in this fiber type. Together, these results implicate additional fiber specific factors in mediating impaired energy metabolism and toxicity.

<u>Hypothesis 6:</u> Metabolomic profiling of urine is useful for identifying biomarkers of cerivastatin-induced myopathy (Chapter 7).

In Chapter 4, metabolomic profiling of skeletal muscles from cerivastatin treated rats indicated several metabolites which were decreased with myopathy. The goal of this work was to use metabolic profiling of urine to identify metabolites originating from skeletal muscle, which may represent potential biomarkers of cerivastatin-induced myopathy. The urinary excretion of two metabolites, 1- and 3-MH were identified and correlated with cerivastatin-induced myotoxicity. Further analysis indicated that these metabolites also increase in the serum with myopathy. Although this is the first report showing increased excretion of 1- and 3-MH in response to a muscle toxicant such as cerivastatin, these metabolites have been used for studying muscle protein turnover for more than 30 years. 1-MH is a component of anserine (β-alanyl-1-MH), which is found in the cytoplasm of skeletal muscles in millimolar concentrations, regardless of sex or muscle fiber type, with substantially lower concentrations detected in cardiac muscle or in organs that have abundant smooth muscle (i.e. gastrointestinal tract). In contrast, 3-MH is a post-translational modification of myofibrillar actin and fast-twitch myosin. Conditions that cause skeletal muscle atrophy result in degradation of these proteins and increased urinary excretion. In this work, constitutive concentrations of 3-MH were lower than 1-MH in skeletal muscles, whereas 3-MH was typically higher than 1-MH in cardiac and smooth muscle. 1-MH increased to a much greater extent than 3-MH following cerivastatin treatment, a result that is consistent with the relative levels of these metabolites in skeletal muscles.

A marked increase in excretion and serum levels of 1- and 3-MH in response to cerivastatin, coupled with their recognized relevance to skeletal muscle biology, suggests these metabolites may be useful biomarkers of skeletal muscle toxicity. However, anserine, which contains 1-MH, is most likely not present in human skeletal muscles and thus has the most potential utility in preclinical species such as rodents, dogs and non-human primates. In contrast, 3-MH is highly conserved, and although its basal levels can be altered by diet, age or disease, it should translate across species such as rodents, dogs, non-human primates and humans under highly controlled experimental conditions. Given the need for more reliable biomarkers, additional investigative studies were conducted in Chapter 8 to determine the preclinical utility of 3-MH for the preclinical assessment of drug-induced myopathy.

Hypothesis 7: 3-Methylhistidine is a preclinical biomarker of drug-induced myopathy (Chapter 8).

The goal of this work was to further investigate the potential utility of 3-MH as a preclinical biomarker of drug-induced myopathy, and to determine the temporal relationship between transcriptional induction of the muscle specific ubiquitin ligases with changes in urine and serum levels of 3-MH. For this work, several different models known to induce skeletal muscle myofibrillar catabolism were employed, including a time course of cerivastatin-induced myopathy, fasting-induced atrophy, and BMS-600149-induced myopathy, thereby providing a range of experimental conditions to assess changes in 3-MH compared to more traditional endpoints including CK, AST and histopathology.

This work confirmed the utility of urine 3-MH as a preclinical biomarker for monitoring skeletal muscle atrophy, an advantage not currently offered with the standard biomarkers of myopathy, including CK and AST. Furthermore, serum 3-MH was more sensitive than CK, AST and urine 3-MH for assessing drug-induced myopathy. However, overnight fasting, which is typically employed in routine preclinical safety studies increases myofibrillar protein degradation and 3-MH in the absence of myopathy. Accordingly, this biomarker would be most useful for monitoring drug-induced myopathy in non-fasted rats. Moreover, this biomarker may be particularly useful for providing early evidence that an adverse skeletal muscle effect may develop as transcriptional induction of the muscle specific ubiquitin ligases and an increase in myofibrillar degradation can occur prior to the onset of myopathy. However, additional studies are needed to further investigate this hypothesis. One limitation of 3-MH is the dynamic range in both matrices. Therefore, both urine and serum 3-MH may be most useful as a qualitative, and not a quantitative biomarker of myofibrillar protein degradation in non-fasted rat studies.

Conclusions

This dissertation demonstrates the utility of transcriptomic and metabolomic profiling for identifying potential mechanisms and biomarkers of cerivastatin-induced myopathy. Specifically, integration of transcriptomic and metabolomic technologies was synergistic, enabling characterization of both molecular and biochemical changes in skeletal muscles, representing common pathways which were perturbed in conjunction with the development of myopathy. Importantly, the use of these platforms led to the development of specific hypotheses regarding modes of toxicity which were further investigated. Together, these technologies and follow up investigative studies enabled a more thorough understanding of the molecular and biochemical changes associated with statin-induced myopathy. Furthermore, the utility of urinary metabolomic profiling was highlighted by the identification of novel biomarkers of drug-induced myopathy.

Future research

Future research should be directed towards determining the mechanism by which statins alter energy metabolism in skeletal muscle, and whether these changes are causally related to the mode of toxicity. Based on the current research, as well as the literature, several potential targets have been identified which play a significant role in skeletal muscle energy metabolism and are modulated with statin treatment. Specifically, PDK4, PGC-1α, the muscle specific ubiquitin ligases and several nuclear receptors identified in chapter 3 represent potential targets which may play a role in altering energy metabolism in skeletal muscle with statin therapy. Therefore, future research should be conducted to determine the relationship between mevalonate depletion, alterations in energy metabolism and the development of statin-induced myopathy.

References

1. Abe, H. (2000). Role of histidine-related compounds as intracellular proton buffering constituents in vertebrate muscle. Biochemistry (Mosc). 65(7), 757-765.

2. Adachi, J., Asano, M., Ueno, Y., Niemela, O., Ohlendieck, K., Peters, T.J., and Preedy, V.R. (2003). Alcoholic muscle disease and biomembrane perturbations. J. Nutr. Biochem. 14(11), 616-625.

3. Agrawal, S., Thakur, P., and Katoch, S.S. (2003). Beta adrenoreceptor agonists, clenbuterol, and isoproterenol retard denervation atrophy in rat gastrocnemius muscle: use of 3-methylhistidine as a marker of myofibrillar degeneration. Jpn. J. Physiol. 53(3), 229-237.

4. Ahmed, W., Khan, N., Glueck, C.J. Pandey, S., Wang, P., Goldenberg, N., Uppal, M., and Khanal, S. (2009). Low serum 25 (OH) vitamin D levels (<32 ng/mL) are associated with reversible myositis-myalgia in statin-treated patients. Transl. Res. 153(1), 11-16.

5. Aizawa, K., Iemitsu, M., Maeda, S., Jesmin, S., Otsuki, T., Mowa, C.N., Miyauchi, T., and Mesaki, N. (2007). Expression of steroidogenic enzymes and synthesis of sex steroid hormones from DHEA in skeletal muscle from rats. Am. J. Physiol. Endocrinol. Metab. 292(2), E577-E584.

6. Aizawa, K., Iemitsu, M., Maeda, S., Otsuki, T., Sato, K., Ushida, T., Mesaki, N., and Akimoto, T. (2010). Acute exercise activates local bioactive androgen metabolism in skeletal muscle. Steroids. 75(3), 219-223.

7. Aldini, G., Orioli, M., Carini, M., and Maffei Facino, R. (2004). Profiling histidine-containing dipeptides in rat tissues by liquid chromatography/electrospray ionization tandem mass spectrometry. J. Mass Spectrom. 39(12), 1417-1428.

8. Alegret, M., and Silvestre, J.S. (2006). Pleiotropic effects of statins and related pharmacological experimental approaches. Methods Find. Exp. Clin. Pharmacol. 28(9), 627-656.

9. Allen, D.D., Caviedes, R., Cardenas, A.M., Shimahara, T., Segura-Aguilar, J., and Caviedes, P.A. (2005). Cell lines as in vitro models for drug screening and toxicity studies. Drug Dev. Ind. Pharm. 31(8), 757-768.

10. Allen, D.L., Roland, R.R., and Edgerton, V.R. (1999). Myonuclear domains in muscle adaptation and disease. Muscle Nerve. 22(10), 1350-1360.

11. Anderson, K.M., Castelli, W.P., and Levy, D. (1987). Cholesterol and mortality: 30 years of follow-up from the Framingham study. JAMA. 257(16), 2176-2180.

12. Antons K,A., Williams C.D., Baker S.K., and Phillips P.S. (2006). Clinical perspective of statin-induced rhabdomyolysis. Am. J. Med. 119(5), 400-9.

13. Appell, H.J., Forsberg, S., and Hollman, W. (1988). Satellite cell activation in human skeletal-muscle after training evidence for muscle-fiber neoformation. Int. J. Sports Med. 9(4), 297-302.

14. Apple, F.S., Rogers, M.A., Sherman, W.M., Costill, D.L., Hagerman, F.C., and Ivy, J.L. (1984). Profile of creatine kinase isoenzymes in skeletal muscles of marathon runners. Clin. Chem. 30(3), 413-416.

15. Armstrong, R.B., and Phelps, R.O. (1984). Muscle fiber type composition of the rat hindlimb. Am. J. Anat. 171(3), 259-272.

16. Aranibar N, Vassallo JD, Rathmacher J, Stryker S, Zhang Y, Dai J, Janovitz EB, Robertson D, Reily M, Lowe-Krentz L, and Lehman-McKeeman L. (2011). Identification of 1- and 3-methylhistidine as biomarkers of skeletal muscle toxicity by nuclear magnetic resonance-based metabolic profiling. Anal. Biochem. 410(1), 84-91.

17. Araki, M., and Motojima, K. (2008). Hyrophobic statins induce autophagy in cultured human rhabdomyosarcoma cells. Biochem. Biophys. Res. Commun. 367(2), 462-467.

18. Ariano, M.A., Armstrong, R.B., and Edgerton, V.R. (1973). Hindlimb muscle fiber populations of five mammals. J. Histochem. Cytochem. 21(1), 51-55.

19. Arif, S.H. (2009). A Ca(2+)-binding protein with numerous roles and uses: parvalbumin in molecular biology and physiology. Bioessays 31(4), 410-421.

20. Armitage, J. (2007). The safety of statins in clinical practice. Lancet. 370(9601), 1781-1790.

21. Asatoor, A.M., and Armstrong, M.D. (1967). 3-methylhistidine, a component of actin. Biochem Biophys. Res. Commun. 26(2), 168-74.

22. Ashizawa, T., and Sarkar, P.S. (2011). Myotonic dystrophy types 1 and 2. Handb. Clin. Neurol. 101, 193-237.

23. Bakker-Arkema, R.G., Davidson, M.H., Goldstein, R.J., Davignon, J., Isaacsohn, J.L., Weiss, S.R., Keilson, L.M., Brown, W.V., Miller, V.T., Shurzinske, L.J., and Black, D.M. (1996). Efficacy and safety of new HMG-CoA reductase inhibitor, atorvastatin, in patients with hypertriglyceridemia. JAMA. 275(2), 128-133.

24. Baldwin, K.M., and Haddad, F. (2002). Skeletal muscle plasticity: cellular and molecular responses to altered physical activity paradigms. Am. J. Phys. Med. Rehabil. 81(11 Suppl), S40-51.

25. Barros, R.P.A., and Gustafsson, J.A. (2011). Estrogen receptor and the metbolic network. Cell Metab. 14(3), 289-299.

26. Bartels, E.M., Dreyer, L., Jacobsen, S., Jespersen, A., Bliddal, H., and Dannaeskiold-Samsoe, B. (2009). Fibromyalgia, diagnsosis, and prevalence. Are gender differences explainable? Ugeskr Laeger. 171(49), 3588-3592.

27. Bauer, K., and Schulz, M. (1994). Biosynthesis of carnosine and related peptides by skeletal muscle cells in primary culture. Eur. J. Biochem. 219(1-2), 43-47.

28. Bauman, D.R., Bitmansour, A.D., McDonald, J.G., Thompson, B.M., Liang, G., and Russell D,W. (2009). 25-Hydroxycholesterol secreted by macrophages in response to Toll-like receptor activation suppresses immunoglobulin A production. Proc. Natl. Acad. Sci. USA. 106(39), 16764-16769.

29. Bekoff, A., and Betz, W.J. (1977). Physiological properties of dissociated muscle fibres obtained from innervated and denervated adult rat muscle. J. Physiol. 271(1), 25-40.

30. Bellosta, S., Ferri, N., Bernini, F., Paoletti, R., and Corsini, A. (2000). Non-lipid-related effects of statins. Ann. Med. 32(3), 164-176.

31. Berchtold, M.W., Celio, M.R., and Heizmann, C.W. (1984). Parvalbumin in non-muscle tissues of the rat. Quantitation and immunohistochemical localization. J. Biol. Chem. 259(8), 5189-5196.

32. Bergman M., Salman H., Djaldetti M., Alexandrova S., Punsky I., Bessler H. (2003). Ultrastructure of mouse striated muscle fibers following pravastatin administration. J. Muscle Res. Cell Motil. 24(7),417-420.

33. Berna, M.J., Zhen, Y., Watson, D.E., Hale, J.E., and Ackerman, B.L. (2007). Strategic use of immunoprecipitation and LC/MS/MS for trace-level protein quantitation: myosin light chain 1, a biomarker of cardiac necrosis. Anal. Chem. 79(11), 4199-4205.

34. Bezaire, V., Seifert, E.L., and Harper, M.E. (2007). Uncoupling protein-3: clues in an ongoing mitochondrial mystery. FASEB J. 21(2), 312-324.

35. Bhardwaj, S.S., and Chalasani, N. (2007). Lipid lowering agents that cause drug-induced hepatotoxicity. Clin. Liver Dis. 11(3), 597-613.

36. Bhasin, S., Calof, O.M., Storer, T.W., Lee, M.L., Mazer, N.A., Jasuja, R., Montori, V.M., Gao, W., and Dalton, J.T. (2006). Drug insight: testosterone and selective androgen receptor modulators as anabolic therapies for chronic illness and aging. Nat. Clin. Pract. Endocrinol. Metab. 2(3), 146-159.

37. Bialek, P., Morris, C., Parkington, J., St. Andre, M., Owens, J., Yaworsky, P., Seeherman, H., and Jelinsky, S.A. (2011). Distinct protein degradation profiles are induced by diferent disuse models of skeletal muscle atrophy. Physiol. Genomics. 43(19), 1075-1086.

38. Billis, A.G., Kastanakis, S., Giamarellou, H., and Daikos, G.K.. (1971). Acute renal failure after a meal of quail. Lancet. 2(7726), 702.

39. Bischoff, H., Angerbauer, R., Boberg, M., Petzinna, D., Schmidt, D., Steinke, W., and Thomas, G. (1998). Preclinical review of cerivastatin sodium- a step forward in HMG-CoA reductase inhibition. Atherosclerosis. 139(suppl. 1), S7-S13.

40. Bjorkhem, I. (2009). Are side-chain oxidized oxysterols regulators also in vivo? J. Lipid Res. 50(Suppl), S213-S218.

41. Blankenberg Skottheim, I., Gedde-Dahl, A., Hejazifar, S., Hoel, K., and Asberg, A. (2008). Statin induced myotoxicity: the lactone forms are more potent than the acid forms in human skeletal muscle cells in vitro. Eur. J. Pharm. Sci. 33(4-5), 317-325.

42. Bodine, S.C., Latres, E., Baumhueter, S., Lai, V.K., Nunez, L., Clarke, B.A. Poueymirou, W.T., Panaro, F.J., Na, E., Dharmarajan, K., Pan, Z-Q., Valenzuela, D.M., DeChiara, T.M., Stitt, T.N., Yancopoulos, G.D. and Glass, D.J. (2001). Identification of ubiquitin ligases required for skeletal muscle atrophy. Science. 294(5547), 1704-1708.

43. Bohlmeyer, T.J., Wu, A.H.B., and Perryman, M.B. (1994). Evaluation of laboratory tests as a guide to diagnosis and therapy of myositis. Rheum. Dis. Clin. North Am. 20(4). 845-856.

44. Boonyarom, O., and Inui, K. (2006). Atrophy and hypertrophy of skeletal muscles: structural and functional aspects. Acta. Physiol. 188(2), 77-89.

45. Bouitbir, J., Charles, A., Echaniz-Laguna, A., Kindo, M., Daussin, F., Auwerx, J., Piquard, F., Geny, B., and Zoll, J. (2011). Opposite effects of statins on mitochondria of cardiac and skeletal muscles: a ‘mitohormesis’ mechanism involving reactive oxygen species and PGC-1. Eur. Heart J. Published ahead of print.

46. Bowker-Kinley, M.M., Davis, W.I., Wu, P., Harris, R.A., and Popov, K.M. (1998). Evidence for existence of tissue-specific regulation of the mammalian pyruvate dehydrogenase complex. Biochem. J. 329(Pt 1), 191-196.

47. Brancaccio, P., Lippi, G., and Maffulli, N. (2010). Biochemical markers of muscular damage. Clin. Chem. Lab Med. 48(6), 757-767.

48. Brault, J.J., Jespersen, J.G., and Goldberg, A.L. (2010). Peroxisome proliferator-activated receptor γ coactivator 1α or 1β overexpression inhibits muscle protein degradation, induction of ubiquitin ligases, and disuse atrophy. J. Biol. Chem. 285 (25), 19460-19470.

49. Brault, J.J., and Terjung, R.L. (2003). Creatine uptake and creatine transporter expression among rat skeletal muscle fiber types. Am. J. Physiol. Cell Physiol. 284(6), C1481-C1489.

50. Brown, A.S., Bakker-Arkema, R.G., Yellen, L., Henley, R.W., Guthrie, R., Campbell, C.F., Koren, M., Woo, W., McLain, R., and Black, D.M. (1998). Treating patients with documented atherosclerosis to National Cholesterol Education Program-recommended low-density-lipoprotein cholesterol goals with atorvastatin, fluvastatin, lovastatin and simvastatin. J. Am. Coll. Cardiol. 32(3), 665-672.

51. Brown, M.S., and Goldstein, J.L. (1986). A receptor-mediated pathway for cholesterol homeostasis. Science. 232(4746), 34-37.

52. Brown, M.S., and Goldstein, J.L. (1997). The SREBP pathway: Regulation of cholesterol metabolism by proteolysis of a membrane-bound transcription factor. Cell. 89(3), 331-340.

53. Brown, M.S., and Goldstein, J.L. (1999). A proteolytic pathway that controls the cholesterol content of membranes, cells, and blood. Proc. Natl. Acad. Sci. USA. 96(20), 11041-11048.

54. Brown, M.S., and Goldstein, J.L. (2004). Lowering plasma cholesterol by raising LDL receptors. Atheroscler. Suppl. 5(3), 57-59.

55. Bruno, C., and DiMauro, S. (2008). Lipid storage myopathies. Curr. Opin. Neurol. 21(5), 601-606.

56. Bruusgaard, J.C., Liestol, K., Ekmark, M., Kollstad, K., and Gundersen, K. (2003). Number and spatial distribution of nuclei in the muscle fibres of normal mice studied in vivo. J. Physiol. 551(Pt 2), 467-478.

57. Buettner, C., and Lecker, S.H. (2008). Molecular basis for statin-induced muscle toxicity: implications and possibilities. Pharmacogenomics. 9(8), 1133-1142.

58. Buhaescu, I., and Izzedine, H. (2007). Mevalonate pathway: A review of clinical therapeutical implications. Clin. Biochem. 40(9-10), 575-584.

59. Burris, T.P. (2008). Nuclear hormone receptors for heme: rev-erbalpha and rev-erbbeta are ligand-regulated components of the mammalian clock. Mol. Endocrinol. 22(7), 1509-1520.

60. Bursch, W., Karwan, A., Mayer, M., Dornetshuber, J., Frohwein, U., Schulte-Hermann, R., Fazi, B., DiSano, F., Piredda, L., Piacentini, M., Petrovski, G., Fesus, L., and Gerner, C. (2008). Cell death autophagy: Cytokines, drugs and nutritional factors. Toxicology. 254(3), 147-157.

61. Bywaters, E.G.L., and Beall, D. (1941). Crush injuries with impairment of renal function. Br. Med. J. 1, 427-432.

62. Calderon, J.C., Bolanos, P., Torres, S.H., Rodriguez-Arroyo, G., and Caputo, C. (2009). Different fibre populations distinguished by their calcium transient characteristics in enzymatically dissociated murine flexor digitorum brevis and soleus muscles. J. Muscle Res. Cell. Motil. 30(3-4), 125-137.

63. Campbell, W.G., Gordon, S.E., Carlson, C.J., Pattison, J.S., Hamilton, M.T., and Booth, F.W. (2001). Differential global gene expression in red and white skeletal muscle. Am. J. Physiol. Cell Physiol. 280(4), C763-C768.

64. Cao, P., Hanai, J., Tanksale, P., Imamura, S., Sukhatme, V.P., and Lecker, S.H. (2009). Statin-induced muscle damage and atrogin-1 induction result of a geranylgeranylation defect. FASEB J. 23(9), 2844-2854.

65. Casey, W.M., Brodie, T., Yoon, L., Ni, H., Jordan, H.L., and Cariello, N.F. (2008). Correlation analysis of gene expression and clinical chemistry to identify biomarkers of skeletal myopathy in mice treated with PPAR agonist GW610742X, Biomarkers 13(4), 364-76.

66. Castelli, W.P., Garrison, R.J., Wilson, P.W., Abbott, R.D., Kalousdian, S., and Kannel, W.B. (1986). Incidence of coronary heart disease and lipoprotein cholesterol levels. The Framingham Study. JAMA. 256, 2835-2838.

67. Ceglia, L. (2008). Vitamin D and skeletal muscle tissue and function. Mol. Aspects Med. 29(6), 407-414

68. Chatzizisis, Y.S., Koskinas, K.C., Misirli, G., Vaklavas, C., Hatzitolios, A., and Giannoglou, G.D. (2010). Risk factors and drug interactions predisposing to statin-induced myopathy. Implications for risk assessment, prevention and treatment. Drug. Saf. 33(3), 171-187.

69. Celio, M.R., and Heizmann, C.W. (1982). Calcium-binding protein parvalbumin is associated with fast contracting muscle fibres. Nature. 297, 504-506.

70. Chan, K.K., Oza. A.M., and Siu, L. (2003). The statins as anticancer agents. Clin. Cancer Res. 9(1), 10-9.

71. Chan, K.M., and Decker, E.A. (1994). Endogenous skeletal muscle antioxidants. Crit. Rev. Food Sci. Nutr. 34(4), 403-426.

72. Chemello, F., Bean, C., Cancellara, P., Laveder, P., Reggiana, C., and Lanfranchi, G. (2011). Microgenomic analysis in skeletal muscle: expression signatures of individual fast and slow myofibers. PloS ONE. 6(2), e16807, 1-14.

73. Chen, Y., Gregory, C.M., Scarborough, M.T., Shi, R., Walter, G.A., and Vandenborne, K. (2007). Transcriptional pathways associated with skeletal muscle disuse atrophy in humans. Physiol. Genomics, 31(3), 510-520.

74. Chen, Y., Zajac, D., and MacLean, H.E. (2005). Androgen regulation of satellite cell function. J. Endocrinol. 186(1), 21-31.

75. Christman, A.A. (1976). Factors affecting anserine and carnosine levels in skeletal muscles of various animals. Int. J. Biochem. 7, 519-527.

76. Chucrallah, A., De Girolami, U., Freeman, R., and Federman, M. (1992). Lovastatin / gemfibrozil myopathy: a clinical, histochemical, and ultrastructural study. Eur. Neurol. 32(5), 293-296.

77. Chung, Y.L., Rider, L.G., Bell, J.D., Summers, R.M., Zemel, L.S., Rennebohm, R.M., Passo, M.H., Hicks, J., Miller, F.W., and Scott, D.L. (2005). Muscle metabolites, detected in urine by proton spectroscopy, correlate with disease damage in juvenile idiopathic inflammatory myopathies. Arthritis. Rheum. 53(4), 565-570.

78. Chung, Y.L., Wassif, W.S., Bell, J.D., Hurley, M., and Scott, D.L. (2003). Urinary levels of creatine and other metabolites in the assessment of polymyositis and dermatomyositis. Rheumatology (Oxford). 42(2), 298-403.

79. Clarke, C.F., Fogelman, A.M., and Edwards, P.A. (1984). Diurnal rhythm of rat liver mRNAs encoding 3-hydorxy-3-methylglutaryl coenzyme a reductase. J. Biol. Chem.. 259(16), 10439-10447.

80. Clayton, T.A., Lindon, J.C., Everett, J.R., Charuel, C., Hanton, G., Le Net, J-L., Provost, J-P., and Nicholson, J.K. (2004). Hepatotoxin-induced hypercreatinaemia and hypercreatinuria: their relationship to one another, to liver damage and to weakened nutritional status. Arch. Toxicol. 78(2), 86-96.

81. Cohen, S., Brault, J.J., Gygi, S.P., Glass, D.J., Valenzuela, D.M., Gartner, C., Latres, E., and Goldberg, A.L. (2009). 81. During muscle atrophy, thick, but not thin, filament components are degraded by MuRF1-dependent ubiquitylation. J. Cell Biol. 185(6), 1083-1095.

82. Collings, F.B., and Vaidya, V.S. (2008). Novel technologies for the discovery and quantitation of biomarkers of toxicity. Toxicology. 245(3), 167-174.

83. Coresh, J., and Kwiterovich, P.O. (1996). Small, dense low-density lipoprotein particles and coronary heart disease risk: A clear association with uncertain implications. JAMA. 276(11), 914-915.

84. Costill, D.L., Daniels, J., Evans, W., and Fink W., Krahenbuhl, G. (1976). Skeletal muscle enzymes and fiber composition in male and female track atheletes. J. Appl. Physiol. 40(2), 149-154.

85. Costelli, P., Reffo, P., Penna, F., Autelli, R., Bonelli, G., and Baccino, F.M. (2005). Ca2+-dependent proteolysis in muscle wasting. Int. J. Biochem. Cell Biol. 37(10), 2134-2146.

86. Crush, K.G. Carnosine and related substances in animal tissues. (1970). Comp. Biochem. Physiol. 34(1), 3-30.

87. Cui, Z., and Houweling, M. (2002). Phosphatidylcholine and cell death. Biochim. Biophys. Acta. 1585(2), 87-96.

88. Cziraky MJ, Willey VJ, and McKenney J.M. (2006). Statin safety: an assessment using an administrative claims database. Am. J. Cardiol. 97(Suppl. 8A),61C–68C.

89. Dare, T.O., Davies, H.A., Turton, J.A., Lomas, L., Williams, T.C., and York, M.J. (2002). Application of surface-enhanced laser desorption/ionization technology to the detection and identification of urinary parvalbumin-α: A biomarker of compound-induced skeletal muscle toxicity in the rat. Electrophoresis. 23(18), 3241-3251.

90. DeBose-Boyd, R.A. (2008). Feedback regulation of cholesterol synthesis: sterol-accelerated ubiquitination and degradation of HMG-CoA reductase. Cell Res. 18(6), 609-621.

91. Dent, T.H. (2010). Predicting the risk of coronary heart disease I. The use of conventional risk markers. Atherosclerosis. 213(2), 345-351.

92. De Pinieux, G., Chariot, P., Ammi-Saïd, M., Louarn, F., Lejonc, J.L., Astier, A., Jacotot, B., and Gherardi, R. (1996). Lipid-lowering drugs and mitochondrial function: effects of HMG-CoA reductase inhibitors on serum ubiquinone and blood lactate/pyruvate ratio. Br. J. Clin. Pharmacol. 42(3), 333-337.

93. De Souza, A. T., Cornwell, P.D., Dai, X., Caguyong, M.J., and Ulrich, R.G. (2006). Agonsits of the peroxisome proliferator-activated receptor alpha induce a fiber-type-selective transcriptional response in rat skeletal muscle. Toxicol. Sci. 92(2), 578-586.

94. Dirks, A.J., and Jones, K.M. (2006). Statin-induced apoptosis and skeletal myopathy. Am. J. Physiol. Cell Physiol. 291(6), C1208-C1212.

95. Dirks-Naylor, A.J., and Griffiths, C.L. (2009). Glucocorticoid-induced apoptosis and cellular mechanisms of myopathy. J. Steroid Biochem. Mol. Biol. 117(1-3), 1-7.

96. Doroshow, J.H., Tallent, C., and Schecter, J.E. (1985). Ultrastructural features of adriamycin-induced skeletal and cardiac muscle toxicity. Am. J. Pathol. 118(2), 288-297.

97. Draeger, A., Monastyrskaya, K., Mohaupt, M.H., Savolainen, H., Allemann, C., and Babiychuk, E.B. (2006). Statin therapy induces ultrastructural damage in skeletal muscle in patients without myalgia. J. Pathol. 210(1), 95-102.

98. Draeger, A., Sanchez-Freire, Monastyrekaya, K., Hoppeler, H., Mueller, Breil, F., Mohaupt, M.G., and Babiychuk, E.B. (2010). Statin therapy and the expression of genes that regulate calcium homeostasis and membrane repair in skeletal muscle. Am. J. Pathol. 177(1), 1-9.

99. Draper, R.P., and Timbrell, J.A. (1996). Urinary creatine as a potential marker of testicular damage: effect of vasectomy. Reprod. Toxicol. 10(1), 79-85.

100. Draper, R.P., Waterfield, C.J., York, M.J., and Timbrell, J.A. (1994). Studies on the muscle toxicant 2,3,5,6-tetramethyl *p*-phenylenediamine: effects on various biomarkers including urinary creatine and taurine. Arch. Toxicol. 69(2), 111-117.

101. Duell, P.B., and Connor, W.E. (2008). Vitamin D deficiency is associated with myalgias in hyperlipidemic subjects taking statins. Circulation. 118, S_470.

102. Dupont-Versteegden, E.E. (2006). Apoptosis in skeletal muscle and its relevance to atrophy. World J. Gastroenterol. 12(46), 7463-7466.

103. Elia, M., Carter, A., Bacon, S., Winearls, C.G., and Smith, R. (1981). Clinical usefulness of urinary 3-methylhistidine in indicating muscle protein breakdown. Br. Med. J. (Clin. Res. Ed). 282(6261), 351-254.

104. Endo, A., and Kuroda, M., (1976). Citrinin, an inhibitor of cholesterol synthesis. J. Antibiot (Tokyo). 29(8), 841-843.

105. Endo, A., Kuroda, M., and Tsujita, Y. (1976). ML-236A, ML-236B, and ML-236C, new inhibitors of cholesterogenesis produced by Penicillium citrinium. J. Antibiot. (Tokyo). 29(12), 1346-1348.

106. Endo, A., Tsujita, Y., Kuroda, M., and Tanzawa, K. (1977). Inhibition of cholesterol synthesis in vitro and in vivo by ML-236A and ML-236B, competitive inhibitors of 3-hydroxy-3-methylglutaryl-coenzyme A reductase. Eur. J. Biochem. 77(1), 31-36.

107. Fernandez, G., Spatz, E.S., Jablecki, C., and Phillips, P.S. (2011). Cleve. Clin. J. Med. 78(6), 393-403.

108. Fielding, P.E., and Fielding, C.J. (1996). Intracellular transport of low density lipoprotein derived free cholesterol begins at clathrin-coated pits and terminates at cell surface caveolae. Biochemistry. 35(47), 14932-14938.

109. Fielitz, J., Kim, M.S., Shelton, J.M., Latif, S., Spencer, J.A., Glass, D.J., Richardson, J.A., Bassel-Duby, R., and Olson, E.N. (2007). Myosin accumulation and striated muscle myopathy result from the loss of muscle RING finger 1 and 3. J. Clin. Invest. 117(9), 2486-2495.

110. Fisher, N.M., Meksawan, K., Limprasertkul, A., Isackson, P.J., Pendergast, D.R., and Vladutiu, G.D. (2007). Statin therapy depresses total body fat oxidation in the absence of genetic limitations to fat oxidation. J. Inherit. Metab. Dis. 30, 388-399.

111. Flint, O.P., Masters, B.A., Gregg, R.E., and Durham, S.K. (1997a). HMG-CoA reductase inhibitor-induced myotoxicity: pravastatin and lovastatin inhibit the geranylgeranylation of low-molecular-weight proteins in neonatal rat muscle cell culture. Toxicol. Appl. Pharmacol. 145(1), 99-110.

112. Flint, O.P., Masters, B.A., Gregg, R.E., and Durham, S.K. (1997b). Inhibition of cholesterol synthesis by squalene synthase inhibitors does not induced myotoxicity in vitro. Toxicol. Appl. Pharmacol. 145(1), 91-98.

113. Fluck, M., and Hoppeler, H. (2003). Molecular basis of skeletal muscle plasticity--from gene to form and function. Rev. Physiol. Biochem. Pharmacol. 146, 159-216.

114. Folch, J., Lees, M., and Stanley, G.H.S. (1957). A simple method for the isolation and purification of total lipids from animal tissues. J. Biol. Chem. 226, 497-509.

115. Foletta, V.C., White, L.J., Larsen, A.E., Leger, B., and Russell, A.P. (2011). The role and regulation of MAFbx/atrogin-1 and MuRF1 in skeletal muscle atrophy. Pflugers Arch. 461(3), 325-335.

116. Folkers, K., Langsjoen, P., Willis, R., Richardson, P., Xia, L.J., Ye, C.Q., and Tamagawa, H. (1990). Lovastatin decreases coenzyme Q levels in humans. Proc. Natl. Acad. Sci. USA. 87(22), 8931-8941.

117. Fon Tacer, K., Pompon, D., and Rozman, D. (2010). Adaptation of cholesterol synthesis to fasting and TNF-α: Profiling cholesterol intermediates in the liver, brain and testis. J. Steroid Biochem. Mol. Biol. 121(3-5), 619-625.

118. Foryst-Ludwig, A., and Kintscher, U. (2010). Metabolic impact of estrogen signalling through ERalpha and ERbeta. J. Steroid Biochem. Mol. Biol. 122(1-3), 74-81.

119. Foster, W. R., Chen, S-J., He, A., Truong, A., Bhaskaran, V., Nelson, D.M., Dambach, D.M., Lehman-McKeeman, L.D., and Car, B.D. (2007). A retrospective analysis of toxicogenomics in the safety assessment of drug candidates. Toxicol. Pathol. 35(5), 621-635.

120. Friesen, J.A., and Rodwell, V.W. (2004). The 3-hydroxy-3-methylglutaryl coenzyme-A (HMG-CoA) reductases. Genome Biol. 5, 248-252.

121. Froberg, S.O. (1967). Determination of muscle lipids. Biochim. Biophys. Acta. 144, 83-93.

122. Fujioka, T., Nara, F., Tsujita, Y., Fukushige, J., Fukami, M., and Kurado, M. (1995). The mechanism of lack of hypocholesterolemic effects of pravastatin sodium, a 3-hydroxy-3-methylglutaryl coenzyme A reductase inhibitor in rats. Biochim. Biophys. Acta. 1254(1), 7-12.

123. Garcia, M.J., Reinoso, R.F., Sanchez Navarro, A., and Prous, J.R. (2003). Clinical pharmacokinetics of statins. Methods Find. Exp. Clin. Pharmacol. 25(6), 457-481.

124. Gatzidou, E.T., Zira, A.N., and Theocharis, S.E. (2007). Toxicogenomics: a pivotal piece in the puzzle of toxicological research. J. Appl. Toxicol. 27, 302-309.

125. Gaussin, V., Skarlas, P., Ching, Y.P., Hardie, D.G., and Hue, L., (1997). Distinct type-2A protein phosphatases activate HMG-CoA reductase and acetyl-CoA carboxylase in liver. FEBS Lett. 4131, 115-118.

126. Ginsberg, H.N., Le, N.A., Short, M.P., Ramakrishnan, R., and Desnick, R.J. (1987). Suppression of apolipoprotein B production during treatment of cholesteryl ester storage disease with lovastatin. Implications for regulation of apolipoprotein B synthesis. J. Clin. Invest. 80(6), 1692-1697.

127. Glueck, C.J., Budhani, S.B., Masineni, S.S., Abuchaibe, C., Khan, N., Wang, P., and Goldenberg, N. (2011). Vitamin D deficinecy, myositis-myalgia, and reversible statin intolerance. Curr. Med. Res. Opin. 27(9), 1683-1690..

128. Goldstein, J.L., and Brown, M.S. (1990). Regulation of the mevalonate pathway. Nature. 343(6257), 425-430.

129. Goldstein, J.L., DeBose-Boyd, R.A., and Brown, M.S. (2006). Protein sensors for membrante sterols. Cell. 124(1), 35-46.

130. Goll, D.E., Neti, G., Mares, S.W., and Thompson, V.F. (2008). Myofibrillar protein turnover: the proteasome and the calpains. J. Anim. Sci. 86(14 Suppl), E19-E35.

131. Goodsaid, F.M., Frueh, F.W., and Mattes, W. (2008). Strategic paths for biomarker qualification. Toxicology 245(3), 219-223.

132. Griffin, J.L., (2003). Metabonomics: NMR spectroscopy and pattern recognition analysis of body fluids and tissues for characterization of xenobiotic toxicity and disease diagnosis, Curr. Opin. Chem. Biol. 7(5), 648–54.

133. Griffin, J.L., and Des Rosiers, C. (2009). Applications of metabolomics and proteomics to the mdx mouse model of Duchene muscular dystrophy: lessons from downstream of the transcriptome. Genome Med. 1(3), 32.1-32.11.

134. Griffin, J.L., Williams, H.J., Sang, E., and Nicholson, J.K. (2001). Abnormal lipid profile of dystrophic cardiac tissue as demonstrated by one- and two-dimensional magic-angle spinning 1H NMR spectroscopy. Magn. Reson. Med. 46(2), 249-255.

135. Grimby, G. (1995). Muscle performance and structure in the elderly as studied cross-sectionally and longitudinally. J. Gerontol. 50A, 17-22.

136. Grosshans, B.L., Ortiz, D., and Novick, P. (2006). Rabs and their effectors: Achieving specificity in membrane traffic. PNAS. 103(32). 11821-11827.

137. Grundy, S.M. (1988). Consensus statement: Role of therapy with “statins” in patients with hypertriglyceridemia. Am. J. Cardiol. 81(4A), 1B-6B.

138. Guis, S. Figarella-Branger, D., Mattei, J.P., Nicoli, F., Le Fur, Y., Kozak-Ribbens, G., Pellissier, J.F., Cozzone, P.J., Amabile, N., and Bendahan, D. (2006). In vivo and in vitro characterization of skeletal muscle metabolism in patients with statin-induced adverse effects. Arthritis Rheum. 55(4), 551-557.

139. Gundersen, K., and Bruusgaard, J.C. (2008). Nuclear domains during muscle atrophy: nuclei lost or paradigm lost? J. Physiol. 586, 2675-2681.

140. Gupta, R.C., and Goad, J.T. (2000). Role of high-energy phosphates and their metabolites in protection of carbofuran-induced biochemical changes in diaphragm by memantine. Arch. Toxicol. 74(1), 13-20.

141. Gupta, A., and Thompson, P.D. (2011). The relationship of vitamin D deficiency and statin myopathy. Athersclerosis. 215(1), 23-29.

142. Guyton, A.C., and Hall, J.E. (2006). Texbook of medical physiology. Elsevier Saunders, 11th edition.

143. Gupta, R.P., Hollis, B.W., Patel, S.B., Patrick, K.S., and Bell, N.H. (2004). CYP3A4 is a human microsomal vitamin D 25-hydroxylase. J. Bone. Miner. Res. 19(4), 680-688.

144. Hall, S.A., Page, S.T., Travison, T.G., Montgomery, R.B., Link, C.L., and McKinlay, J.B. (2007). Do statins affect androgen levels in men? Results from the Boston area community health survey. Cancer Epidemiol. Biomarkers Prev. 16(8), 1587-1594.

145. Hamalainen, N., and Pette, D. (1993). The histochemical profiles of fast fiber types IIB, IID, and IIA in skeletal muscle of mouse, rat and rabbit. J. Histochem. Cytochem. 41(5), 733-743.

146. Hanai, J-I., Cao, P., Tanksale, P., Imamura, S., Koshimizu, E., Zhao, J., Kishi, S., Yamashita, M., Phillips, P.S., Sukhatme, V.P., and Lecker, S.H. (2007). The muscle-specific ubiquitin ligase atrogin-1/MAFbx mediates statin-induced muscle toxicity. J. Clin. Invest. 117(12), 3940-3951.

147. Hardie, D.G. (1992). Regulation of fatty acid and cholesterol metabolism by the AMP-activated protein kinase. Biochim. Biophys. Acta. 1123, 231-238.

148. Haren, M.T., Siddiqui, A.M., Armbrecht, H.J., Kevorkian, R.T., Kim, M.J., Haas, M.J., Mazza, A., Kumar, V.B., Green, M., Banks, W.A., and Morley, J.E. (2011). Testosterone modulates gene expression pathways regulating nutrient accumulation, glucose metabolism and protein turnover in mouse skeletal muscle. Int. J. Androl. 34(1), 55-68.

149. Hargreaves, I.P., Duncan, A.J., Heales, S.J., and Land, J.M. (2005). The effect of HMG-CoA reductase inhibitors on coenzyme Q10: possible biochemical/clinical implications. Drug Saf. 28(8), 659-676.

150. Harris, R.C., Marlin, D.J., Dunnett, M., Snow, D.H., and Hultman, E. (1990). Muscle buffering capacity and dipeptide content in the thoroughbred horse, greyhound dog and man. Comp. Biochem. Physiol. A. Comp. Physiol. 97, 249-51.

151. Hart, D.A., Archambault, J.M., Kydd, A., Reno, C., Frank, C.B., and Herzog, W. (1998). Gender and neurogenic variables in tendon biology and repetitive motion disorders. Clin. Orthop. Relat. Res. 351, 44-56.

152. Haslett, J.N., and Kunkel, L.M. (2002). Microarray analysis of normal and dystrophic skeletal muscle. Int. J. Dev. Neurosci. 20(3-5), 359-65.

153. Haverberg, L.N., Deckelbaum, L., Bilmazes, C., Munro, H.N., and Young, V. R. (1975). Myofibrillar protein turnover and urinary N-tau-methylhistidine output. Response to dietary supply of protein and energy. Biochem. J. 152(3), 503-10.

154. Hegarty, B.D., Furler, S.M., Ye, J., Cooney, G.Y., and Kraegen, E.W. (2003). The role of intramuscular lipid in insulin resistance. Acta. Physiol. Scand. 178(4), 373-383.

155. Horton, J.D., Goldstein, J.L., and Brown, M.S. (2002). SREBPs: Activators of the complete program of cholesterol and fatty acid synthesis in the liver. J. Clin. Invest. 109(9). 1125-1131.

156. Horton, J.D., and Shimomura, I. (1999). Sterol regulatory element-binding proteins: Activators of cholesterol and fatty acid biosynthesis. Curr. Opin. Lipidol. 10(2), 143-150.

157. Huang, Y.F., Wang, Y., and Watford, M. (2007). Glutamine directly downregulates glutamine synthesis protein levels in mouse C2C12 skeletal muscle myotubes. J. Nutr. 137(6), 1357-1362.

158. Hubal, M.J., Reich, K.A., De Biase, A., Bilbie, C., Clarkson, P.M., Hoffman, E.P., and Thompson, P.D. (2011). Transcriptional deficits in oxidative phosphorylation with statin myopathy. Muscle Nerve. 44(3), 393-401.

159. Hudson, C.S., Foster, R.E., and Kahng, M.W. (1985). Neuromuscular toxicity of pyridostigmine bromide in the diaphragm, extensor digitorum longus and soleus muscles of the rat. Fundam. Appl. Toxicol. 5(6 Pt 2), S260-S269.

160. Ihlemann, J., Ploug, T., and Galbo, H. (2001). Effect of force development on contraction induced glucose transport in fast twitch rat muscle. Acta. Physiol. Scand. 171(4), 439-444.

161. Ikonen, E. (2006). Mechanisms for cellular cholesterol transport defects and human disease. Physiol. Rev. 86(4), 1237-1261.

162. Ikonen, E. (2008). Cellular cholesterol trafficking and compartmentalization. Nat. Rev. Mol. Cell Biol. 9(2), 125-137.

163. Irwin, W., Fontaine, E., Agnolucci, L., Penzo, D., Betto, R., Bortolotto, S., Reggiani, C., Salviati, G., and Bernardi, P. (2002). Bupivacaine myotoxicity is mediated by mitochondria. J. Biol. Chem. 277(14), 12221-12227.

164. Istvan, E.S., and Deisenhofer, J. (2000). The structure of the catalytic portion of human HMG-CoA reductase. Biochim. Biophys. Acta. 1529(1-3), 9-18.

165. Istvan, E.S., Palnitkar, M., Buchanan, S.K., and Deisenhofer, J. (2000). Crystal structure of the catalytic portion of human HMG-CoA reductase: insights into regulation of activity and catalysis. EMBO J. 19(5), 819-830.

166. Jackman, R.W., and Kandarian, S.C. (2004). The molecular basis of skeletal muscle atrophy. Am.J. Cell Physiol. 287, C834-C843.

167. Jagoe, R.T., Lecker, S.H., Gomes, M., and Goldberg, A.L. (2002). Patterns of gene expression in atrophying skeletal muscles: response to food deprivation. FASEB J. 16(13), 1697-1712.

168. Jaworska-Wilczynska, M., Wilczynski, G.M., Engel, W.K., Strickland, D.K., Weisgraber, K.H., and Askanas, V. (2002). Three lipoprotein receptors and cholesterol in inclusion-body myositis muscle. Neurology. 58, 438-445.

169. Johnson, P., Harris, C.I., and Perry, S.V. (1967). 3-Methylhistidine in actin and other muscle proteins. Biochem. J. 105(1), 361-370.

170. Johnson, P., and Perry, S.V. (1970). Biological activity and the 3-methylhistidine content of actin and myosin. Biochem. J. 119(2), 293-298.

171. Johnson, T.E., Zhang, X., Bleicher, K.B., Dysart, G., Louglin, A.F., Schaefer, W.H., and Umbenhauer, D.R. (2004). Statins induced apoptosis in rat and human myotube cultures by inhibiting geranylgeranylation but not ubiquinone. Toxicol. Appl. Pharmacol. 200(3), 237-250.

172. Kang, P.B., Kho., A.T., Sanoudou, D., Haslett, J.N., Dow, C.P., Han, M., Blasko., J.M., Lidov, H.G.W., Beggs, A.H., and Kunkel, L.M. (2005). Variations in gene expression among different types of human skeletal muscle. Muscle Nerve, 32(4), 483-491.

173. Kashani, A., Phillips, C.O., Foody, J.M., Wang, Y., Mangalmurti, S., Ko, D., and Krumholz, H.M. (2006). Risks associated with statin therapy: a systematic overview of randomized clinical trials. Circulation. 114(25), 2788-2797.

174. Kaspera, R., Naraharisetti, S.B., Tamraz, B., Sahele, T., Cheesman, M.J., Kwok, P.Y., Marciante, K., Heckbert, S.R., Psaty, B.M., and Totah, R.A. (2010). Cerivastatin in vitro metabolism by CYP2C8 variants found in patients experiencing rhabdomyolysis. Pharmacogenet. Genomics. 20(10), 619-629.

175. Kaufman, P. Torok, M., Zahno, A., Waldhauser, K.M., Brecht, K., and Krahenbuhl, S. (2006). Toxicity of statins on rat skeletal muscle mitochondria. Cell. Mol. Life Sci. 63(19-20), 2415-2425.

176. Keys, A. (1997). Coronary heart disease in seven countries. 1970. Nutrition. 13(3), 250-252.

177. Kidd, J. (2006). Life after statin patent expires. Nat. Rev. Drug Discov. 5(10), 813-814.

178. Kimura, N., Kumamoto, T., Oniki, T., Nomura, M., Nakamura, K., Abe, Y., Hazama, Y., and Ueyama, H. (2009). Role of ubiquitin-proteasome proteolysis in muscle fiber destruction in experimental chloroquine-induced myopathy. Muscle Nerve. 39(4), 521-528.

179. Kivisto, K.T., and Niemi, M. (2007). Influence of drug transporter polymorphisms on pravastatin pharmacokinetics in humans. Pharm. Res. 24(2), 239-247.

180. Knopp, R.H., Zhu, X., and Bonet, B. (1994). Effects of estrogens on lipoprotein metabolism and cardiovascular disease in women. Atherosclerosis. 110, Suppl, S83-S91.

181. Koerker, D.J., Sweet, I.R., and Baskin, D.G. (1990). Insulin binding to individual rat skeletal muscles. Am. J. Physiol. 259(4 Pt 1), E517-E523.

182. Komamura, K., Shirotani-Ikejima, H., Tatsumi,R., Tsujita-Kuroda, Y., Kitakaze, M., Miyatake, K., Sunagawa, K., and Miyata, T. (2003). Differntial gene expression in the rat skeletal and heart musscle in glucocoriticoid-induced myopathy: Analysis by microarray Cardiovasc. Drugs Ther. 17(4), 303-310.

183. Kuhl, D.A., Mouser, J.F., Methvin, J.T., Hak, E.B., Hak, L.J., and Dickerson, R.N. (1998). Alterations in N-acetylation of 3-methylhistidine in endotoxemic parenterally fed rats. Nutrition. 14(9), 678-682.

184. Kuhn, D.E., and Logan, D.M., (1990). Cholesterol metabolism in dystrophic mice. II. Altered enzyme activities. Biochim. Biophys. Acta. 1046(3), 322-325.

185. Kumagai, M., Kondo, T., Ohta, Y., and Ishihara, T. (2001). Size and composition changes in diaphragmatic fibers in rats exposed to chronic hypercapnia. Chest. 119(2), 565-571.

186. Kumar, R., and Sharma, S. (2009). Lipid profile changes in mouse gastrocnemius muscle after denervation and beta-adrenoreceptor stimulation. Indian J. Exp. Biol. 47(5), 314-319.

187. Laaksonen R., Jokelainen K., Sahi T., Tikkanen M.J., and Himberg J.J. (1995). Decreases in serum ubiquinone concentrations do not result in reduced levels in muscle tissue during short-term simvastatin treatment in humans. Clin. Pharmacol. Ther. 57(1), 62-66.

188. Laaksonen, R., Katajamaa, M., Paiva, H., Sysi-Aho, M., Saarinen, L., Junni, P., Lutjohann, D., Smet, J., Van Coster, R., Seppanen-Laasko, T., Lehtimaki, T., Soini, J., and Oresic, M. (2006). A systems biology strategy reveals biological pathways and plasma biomarker candidates for potentially toxic statin-induced changes in muscle. Plos One. 1(1), e97.

189. Law, M., and Rudnicka, A.R. (2006). Statin safety: a systematic review. Am. J. Cardiol. 97(8A), 52C-60C.

190. Lebherz, H.G., and Rutter, W.J. (1969). Distribution of fructose diphosphate aldolase variants in biological systems. Biochemistry, 8(1), 109-121.

191. Lecker, S.H., Goldberg, A.L., and Mitch, W.E. (2006). Protein degradation by the ubiquitin-proteasome pathway in normal and disease states. J. Am. Soc. Nephrol. 17(7), 1807-1819.

192. Lecker, S.H., Jagoe, R.T., Gilbert, A., Gomes, M., Baracos, V., Bailey, J., Price, S.R., Mitch, W.E., and Goldberg, A.L. (2004). Multiple types of skeletal muscle atrophy involve a common program of changes in gene expression. FASEB J. 18(1), 39-51.

193. Lee, D.S., and Vasan, R.S. (2005). Novel markers for heart failure diagnosis and prognosis. Curr. Opin. Cardiol. 20(3), 201-2110.

194. Lee, M.C., Wee, G.R., and Kim, J.H. (2005). Apoptosis of skeletal muscle on steroid-induced myopathy in rats. J. Nutr. 135(7), 1806S-1808S.

195. Lee, S-J. (2004). Regulation of muscle mass by myostatin. Annu. Rev. Cell Dev. Biol. 20, 61-86.

196. Lennernas, H. (2003). Clinical pharmacokinetics of atorvastatin. Clin. Pharmacokinet. 6(6), 1399-1406.

197. Leung, K.F., Baron, R., and Seabra, M.C. (2006). Thematic review series: lipid posttranslational modifications. geranylgeranylation of Rab GTPases. J. Lipid Res. 47(3), 467-475.

198. Levy, H.B., and Kohlhaas, H.K. (2006). Considerations for supplementing with coenzyme Q10 during statin therapy. Ann. Pharmacother. 40(2), 290-294.

199. Lexell, J. (1995). Human agining, muscle mass, and fiber type composition J. Gerontol. A. Biol. Sci. Med. Sci. 50A, (spec no:11-6).

200. Li, J.B., and Wassner, S.J. (1981). Muscle degradation in uremia: 3-methylhistidine release in fed and fasted rats. Kidney Int. 20(3), 321-325.

201. Liantonio, A., Giannuzi, V., Cippone, V., Camerino, G.M., Pierno, S., and Camerino, D.C. (2007). Fluvastatin and atorvastatin affect calcium homeostasis of rat skeletal muscle fibers in vivo and in vitro by impairing the sarcoplasmic reticulum/mitochondrial $Ca2^{+}$-release system. J. PHARMACOL. EXP. THER.. 321(2), 626-634.

202. Lin, J., Wu, H., Tarr, P.T., Zhang, C.Y., Wu, Z., Boss, O., Michael, L.F., Puigserver, P., Isotani, E., Olson, E.N., Lowell, B.B., Bassel-Duby, R., and Spiegelman, B.M. (2002). Transcriptional co-activator PGC-1 alpha drives the formation of slow-twitch muscle fibers. Nature. 418(6899), 797-801.

203. Lin, S., Yang, Z., Liu, H., and Cai, Z. (2011). Metabolomic analysis of liver and skeletal muscle tissues in C57BL/6J and DBA mice exposed to 2,3,7,8-tetrachlorodibenzo-p-dioxin. Mol. Biosyst. 7(6), 1956-1965.

204. Livingstone, C., and Collinson, M. (2002). Sex steroids and insulin resistance. Clin. Sci. (Lond). 102(2), 151-166.

205. Loeb, W.F., (1999). The rat. Quimby, F.W. (Eds.), The clinical chemistry of laboratory animals. Taylor and Francis, 33-48.

206. London, S.F., Gross, K.F., and Ringel, S.P. (1991). Cholesterol-lowering agent myopathy (CLAM). Neurology. 41(7), 1159-1160.

207. Long, C.L., Haverberg, L.N., Young, V.R., Kinney, J.M., Munro, H.N., and Geiger, J.W. (1975). Metabolism of 3-methylhistidine in man. Metabolism. 24(8), 929-935.

208. Lowell, B.B., Ruderman, N.B., Goodman, M.N. (1986). Regulation of myofibrillar protein degradation in rat skeletal muscle during brief and prolonged starvation. Metabolism. 35(12), 1121-1127.

209. Maher, A.C., Fu, M.H., Isofort, R.J., Varbanov, A.R., Qu, X.A., and Tarnopolsky, M.A. (2009). Sex differences in global mRNA content of human skeletal muscle. PloS One. 4(7), e6335, 1-14.

210. Mahoney, D.J., Parise, G., Melov, S., Safdar, A., and Tarnopolsky, M.A. (2005). Analysis of global mRNA expression in human skeletal muscle during recovery from endurance exercise. FASEB J. 19(11), 1498-1500.

211. Mahoney, D.J., Safdar, A., Parise, G., Melov, S., Minghua, F., MacNeil, L., Kaczor, L., Payne, E.T., and Tarnopolsky, M.A. (2008). Gene expression profiling in human skeletal muscle during recovery from eccentric exercise. Am. J. Regul. Integr. Comp. Physiol. 294(6), R1901-R1910.

212. Mallinson, J.E., Constantin-Teodosiu, D., Sidaway, J., Westwood, F.R., and Greenhaff, P.L. (2009). Blunted Akt/FOXO signaling and activation of genes controlling atrophy and fuel use in statin myopathy. J. Physiol. 587(Pt 1), 219-230.

213. Marcoff, L., and Thompson, P.D. (2007). The role of coenzyme Q10 in statin-associated myopathy: a systematic review. J. Am. Coll. Cardiol. 49(23), 2231-2237.

214. Marieb, E., N. (2000). Essentials of Human Anatomy and Physiology. Benjamin-Cummings Publishing Company (Pearson Eduction, Inc.), 5th edition.

215. Marotta, M., Ruiz-Roig, C., Sarria, Y., Peiro, J.L., Nunez, F., Ceron, J., Munell, F., and Roig-Quillis, M. (2009). Muscle genonme-wide expression profiling during disease evolution in mdx mice. Physiol. Genommics. 37(2), 119-132.

216. Martini, C., Trapani, L., Narciso, L., Marino, M., Trentalance, A. and Pallottini, V. (2009). 3-hydroxy-3-methylglutaryl coenzyme A reductase increase is essential for rat muscle differentiation. J. Cell. Physiol. 220(2), 524-530.

217. Masiero, E., and Sandri, M. (2010). Autophagy inhibition induces atrophy and myopathy in adult skeletal muscles. Autophay, 6(2), 307-309.

218. Masters, B.A., Palmoski, M.J., Flint, O.P., Gregg, R.E., Wangiverson, D., and Durham, S.K. (1995). In vitro myotoxicity of the 3-hydroxy-3-methylglutaryl coenzyme a reductase inhibitors, pravastatin, lovastatin, and simvastatin, using neonatal rat skeletal myocytes. Toxicol. Appl. Pharmacol. 131(1), 163-174.

219. Matzno, S., Yasuda, S., Juman, S., Yamamoto, Y., Nagareya-Ishida, N., Tazuya-Murayama, K., Nakabayashi, T., and Matsuyama, K. (2005). Statin-induced apoptosis linked with membrane farnesylated Ras small G protein depletion, rather than geranylated Rho protein. J. Pharm. Pharmacol. 57(11), 1475-1484.

220. McCormick, K.M., and Thomas, D.P. (1992). Exercise-induced satellite cell activation in sensescent soleus muscle. J. Appl. Physiol. 72(3), 888-892.

221. McManus, I.R., and Benson, M.S. (1967). Studies on the formation of carnosine and anserine in pectoral muscle of the developing chick. Arch. Biochem. Biophys. 119(1), 444-53.

222. McTaggart, S.J. (2006). Isoprenylated proteins. Cell. Mol. Life Sci. 63, 255-267.

223. Mermelstein, C.S., Portilho, D.M., Mendes, F.A., Costa, M.L., and Abreu, J.G. (2007). Wnt/beta-catenin pathway activation and myogenic differentiation are induced by cholesterol depletion. Differentiation. 75(3), 184-192.

224. Mikura, M., Yamaoka, I., Doi, M., Kawano, Y., Nakayama, M., Nakao, R., Hirasaka, K., Okumura, Y., and Nikawa, T. (2008). Glucose infusion suppresses surgery-induced muscle protein breakdown by inhibiting ubiquitin-proteasome pathway in rats. Anesthesiology. 110(1), 81-88.

225. Milatovic, D., Gupta, R.C., Dekundy, A., Montine, T.J., and Dettbarn, W.D. (2005). Carbofuran-induced oxidative stress in slow and fast skeletal muscles: prevention by memantine and atropine. Toxicology. 208(1), 13-24.

226. Mitch, W.E., and Goldberg, A.L. (1996). Mechanisms of muscle wasting. The role of the ubiquitin-proteasome pathway. N. Engl. J. Med. 335(25), 1897-1905.

227. Morikawa, S., Murakami, T., Yamazaki, H., Izumi, A., Saito, Y., Hamakubo, T., and Kodama, T. (2005). Analysis of the global RNA expression profiles of skeletal muscle cells treated with statins. J. Atheroscler. Thromb. 12(3), 121-131.

228. Moser, H. (1984). Duchenne muscular dystrophy: pathogenic aspects and genetic prevention. Hum. Genet. 66(1), 17-40.

229. Motojima, K. (2002). A metabolic switching hypothesis for the first step in the hypolipidimic effects of fibrates. Biol. Pharm. Bull. 25(11), 1509-1511.

230. Motojima, K., and Seto, K. (2003). Fibrates and statins rapidly and synergistically induce pyruvate dehydrogenase kinase 4 mRNA in the liver and muscles of mice. Biol. Pharm. Bull. 26(7), 954-958.

231. Mullen, A.J., and Barton, P.J. (2000). Sturctural characterization of the human fast skeletal muscle troponin I gene (TNNI2). Gene 242(1-2), 313-320.

232. Mullen, P.J., Luscher, B., Scharnagl, H., Krahenbuhl, S., and Brecht, K. (2010). Effect of simvastatin on cholesterol metabolism in C2C12 myotubes and HepG2 cells, and consequences for statin-induced myopathy. Biochem. Pharmacol. 79(8), 1200-1209.

233. Munoz, K.A., Satarug, S., and Tischler, M.E. (1994). Time course of the response of myofibrillar and sarcoplasmic protein metabolism to unweighting of the soleus muscle. Metabolism. 42(8), 1006-1012.

234. Murton, A.J., Constantin, D., and Greenhaff, P.L. (2008). The involvement of the ubiquitin proteasome system in human skeletal muscle remodeling and atrophy. Biochim. Biophys. Acta. 1782(12), 730-743.

235. Nakagawa, H., Mutoh, T., Kumano, T., and Kuriyama, M. (1998). HMG-CoA reductase inhibitor-induced L6 myoblast cell death: involvement of the phosphatidylinositol 3-kinase pathway. FEBS Letters. 438(3), 289-292.

236. Nakahara, K., Kuriyama, M., Sonoda, Y., Yoshidome, H., Nakagawa, H., Fujiyama, J., Higuchi, I., and Osame, M. (1998). Myopathy induced by HMG-CoA reductase inhibitors in rabbits: a pathological, electrophysiological, and biochemical study. Toxicol. Appl. Pharmacol. 152(1), 99-106.

237. Nakashima, K., and Yakabe, Y. (2007). AMPK activation stimulates myofibrillar protein degradation and expression of atrophy-related ubiquitin ligases by increasing FOXO transcription factors in C2C12 myotubes. Biosci. Biotechnol. Biochem. 71(7), 1650-1656.

238. Narici, M.V., and Maffulli, N. (2010). Sarocpenia: characteristics, mechanisms and functional significance. Br. Med. Bull. 95, 139-159.

239. Needham, D.M. (1926). Red and white muscle. Physiol. Rev. 6, 1-27.

240. Needham, M., and Mastaglia, F.L. (2008). Sporadic inclusion body myositis: a continuing puzzle. Neuromuscul. Disord. 18(1), 6-16.

241. Newlands S., Levitt, L.K., Robinson, C.S., Karpf, A.B., Hodgson, V.R., Wade R.P., and Hardeman, E.C. (1998). Transcription occurs in pulses in muscle fibers. Genes Dev. 12(17), 2748-2758.

242. Ng, Y., Goldspink, D.F., Burniston, J.G., Clark, W.A., Colyer, J., and Tan, L. (2002). Characterization of isoprenaline myotoxicity on slow-twitch skeletal versus cardiac muscle. Int. J. Cardiol. 86(2-3), 299-309.

243. Nicholson, J.K., Connelly, J., Lindon, J.C., and Holmes, E. (2002). Metabonomics: a platform for studying drug toxicity and gene function. Nat. Rev. Drug Discov. 1(2), 153-161.

244. Nikolaidis, M.G., Petridou, A., and Mougios, P.V. (2006). Comparison of the phospholipid and triacylglycerol fatty acid profile of rat serum, skeletal muscle and heart. Physiol. Res. 55(3), 259-265.

245. Nilsson, O., Fredman, P., Klinghardt, G.W., Dreyfus, H., and Svennerholm, L. (1981). Chloroquine-induced accumulation of gangliosides and phospholipids in skeletal muscles. Quantitiative determination and characterization of stored lipids. Eur. J. Biochem. 116(3), 565-571.

246. Nishida, K., Kyoi, S., Yamaguchi, O., Sadoshima, J., and Otsu, K. (2009). The role of autophagy in the heart. Cell Death. Differ. 16(1), 31-38.

247. Nishimoto, T., Tozawa, R., Amano, Y., Wada, T., Imura, Y., and Sugiyama, Y. (2003). Comparing myotoxic effects of squalene synthase inhibitor, T-01485, and 3-hydroxy-3-methylglutaryl coenzyme A (HMG-CoA) reductase inhibitors in human myocytes. Biochem. Pharmacol. 66(11), 2133-2139.

248. Noe, J., Portmann, R., Brun, M.E., and Funk, C. (2007). Substrate-dependent drug-drug interactions between gemfibrozil, fluvastatin and other organic anion-transporting peptide (OATP) substrates on OATP1B1, OATP2B1, and OATP1B3. Drug Metab. Dispos. 35(8), 1308-1314.

249. Obayashi, H., Nezu, Y., Yokota, H., Kiyosawa, N., Mori, K., Maeda, N., Tani, Y., Manabe, S., and Sanbuissho, A. (2011). Cerivastatin induces type-1 fiber-, not type-II fiber, predominant muscular toxicity in the young male rat. The Journal of Toxicol. Sci. 36(4), 445-452.

250. Okumura, N., Hashida-Okumura, A., Kita, K., Matsubae, M., Matsubara, T., Takao, T., and Nagai, K. (2005). Proteomic analysis of slow- and fast-twitch skeletal muscles. Proteomics. 5(11), 2896-2906.

251. Orrenius, S., Nicotera, P., and Zhivotovsky, B. (2011). Cell death and their implications in toxicology. Toxicol. Sci. 119(1), 3-19.

252. Ostrowski, S.M., Wilkinson, B.L., Golde, T.E., and Landreth, G. (2007). Statins reduce amyloid-β production through inhibition of protein isoprenylation. J. Biol. Chem. 282(37), 26832-26844.

253. Otto, A., and Patel, K. (2010). Signalling and the control of skeletal muscle size. Exp. Cell Res. 316(18), 3059-3066.

254. Owczarek, J., Jasinska, M., and Orszulak-Michalek, D.O. (2005). Drug-induced myopathies. An overview of the possible mechanisms. Pharmacol. Rep. 57(1). 23-34.

255. Owens, K., and Hughes, B.P. (1970). Lipids of dystrophic and normal mouse muscle: whole tissue and particulate fractions. J. Lipid Res. 11(5), 486-495.

256. Paiva, H., Thelen, K.M., Van Coster, R., Smet, J., Paepe, B.E., Mattila, K.M., Laakso, J., Lehtimaki, T., Bergmann, K.V., Lutjohann, D., and Laaksonen, R. (2005). High-dose statins and skeletal muscle metabolism in humans: A randomized controlled trial. Clin. Pharmacol. Ther. 78(1), 60-68.

257. Pearen, M.A., Ryall, J.G., Lynch, G.S., and Muscat, G.E.O. (2009). Expression profiling of skeletal muscle following acute and chronic β2-adrenergic stimulation: implications for hypertrophy, metabolism and circadian rhythm. BMC Genomics. 10(448), 1-20.

258. Pekkanen, J., Linn, S., Heiss, G., Suchindran, C.M., Leon, A., Rifkind, B.M., and Tyroler, H.A., (1990). Ten-year mortality from cardiovascular disease in relation to cholesterol level among men with and without preexisting cardiovascular disease. N. Engl. J. Med. 322(24), 1700-1707.

259. Penafiel, R., Ruzafa, C, Monserrat, F., and Cremades, A. (2004). Gender-related differences in carnosine, anserine and lysine content of murine skeletal muscles. Amino acids. 26(1), 53-58.

260. Pette, D., Peuker, H., and Staron, R.S. (1999). The impact of biochemical methods for singl muscle fibre analysis. Acta. Physiol. Scand. 166(4), 261-277.

261. Pette, D., and Staron, R.S. (1997). Mammalian skeletal muscle fiber type transitions. Int. Rev. Cytol. 170, 143-223.

262. Phillips, P.S., Ciaraldi, T.P., Kim, D.L., Verity, M.A., Wolfson, T., and Henry, R.R. (2009). Myotoxic reactions to lipid-lowering therapy are associated with altered oxidation of fatty acids. Endocrine. 35(1), 38-46.

263. Phillips, P.S., Haas, R.H., Bannykh, S., Hathaway, S., Gray, N.L., Kimura, B.J., Vladutiu, G.D., and England, J.D.F. (2002). Statin-associated myopathy with normal creatine kinase levels. Ann. Intern. Med. 137(7), 581-585.

264. Phillips, P.S., and Haas, R.H. (2008). Statin myopathy as a metabolic muscle disease. Expert Rev. Cardiovasc. Ther. 6(7), 971-978.

265. Phillips, P.S., Verity, M.A., Schick, B.A., Vladutiu, G.D., Laaksonen, R., Oresic, M., Hohl, R.J., Ciaraldi, T.P., Sukhatme, V.P., Lecker, S.H., Cote, H.C.F., Powell, H., Davidson, W., and Wlfson, T. (2010). Survey of muscle characteristics after statin-induced rhabdomyolysis. Clin. Lipidol. 5(1), 17-27.

266. Philp, A., Perez-Schindler, J., Green, C., Hamilton, D.L., Baar, K. (2010). Pyruvate suppresses PGC1alpha expression and substrate utilization despite increased respiratory chain content in C2C12 myotubes. Am. J. Physiol. Cell Physiol. 299(2), C240-2550.

267. Pierno, S., Liantonio, A., Camerino, G.M., De Bellis, M., Cannone, M., Gramegna, G., Scaramuzzi, A., Simonetti, S., Paola Nicchia, G., Basco, D., Svelto, M., Desaphy, J-F., and Camerino, D.C. (2011). Potential benefits of taurine in the prevention of skeletal muscle impairment induced by disuse in the hindlimb-unloaded rat. Amino Acids. Published ahead of print.

268. Pilegaard, H., and Neufer, P.D. (2004). Transcriptional regulation of pyruvate dehydrogenase kinase 4 in skeletal muscle during and after exercise. Proc. Nutr. Soc. 63(2), 221-226.

269. Pires-Oliveira, M., Leticia, A.,Maragno, G.C., Parreiras-e-Silva, L.T., Chiavegatti, T., Gomes, M., and Godinho, R.O. (2010). Testosterone represses ubiquitin ligases atrogin-1 and murf-1 expression in an androgen-sensitive rat skeletal muscle in vivo. J. Appl. Physiol. 108(2), 266-273.

270. Preedy, V.R., Paice, A., Mantle, D., Dhillon, A.S., Palmer, T.N., and Peters, T.J. (2001). Alcoholic myopathy: biochemical mechanisms. Drug Alcohol Depend. 63(3), 199-205.

271. Preiss, D, and Sattar, N. (2012). Statins and new-onset diabetes: a review of recent evidence. Curr. Opin. Lipidol. 22(6), 460-466.

272. Pritt, M.L., Hall, D.G., Recknor, J., Credille, K.M., Brown, D.D., Yumibe, N.P., Schultze, A.E., and Watson, D.E. (2008). Fabp3 as a biomarker of skeletal muscle toxicity in the rat: comparison with conventional biomarkers. Toxicol. Sci. 103(2), 382-396.

273. Pruznak, A.M., Hong-Brown, L., Lantry, R., She, P., Frost, R.A., Vary, T.C., and Lang, C.H. (2008). Skeletal and cardiac myopathy in HIV-1 transgenic rats. Am. J. Physiol. Endocriol. Metab. 295(4), E964-E973.

274. Rabinowitz, J.D., and White, E. (2010). Autophagy and metabolism. Science 330(609), 1344-1348.

275. Radcliffe, K.A., and Campbell, W.W. (2008). Statin myopathy. Curr. Neurol. Neurosci. Rep. 8(1), 66-72.

276. Ranvier, L. (1873). Proprietes et structures differentes des muscles rouges et des muscles blanc, chez les lapins et chaez les raises. CR Hebd. Acad. Sci. (Paris). 77, 1030-1043.

277. Ravenscroft, G., Nowak, K.J., Jackaman, C., Clement, S., Lyons, M.A., Gallagher, S., Bakker, A.J., and Laing, N.G. (2007). Dissociated flexor digitorum brevis myofiber culture system. Cell Motil. Cytoskeleton. 64(10), 727-738.

278. Rathmacher, J.A., Link, G.A., Flakoll, P.J., and Nissen, S.L. (1992). Gas chromatographic/mass spectrometric analysis of stable isotopes of 3-methylhistidine in biological fluids: application to plasma kinetics in vivo. Biol. Mass Spectrom. 21(11), 560-566.

279. Reinoso, R.F., Sanchez Navarro, A., Garcia, M.J., and Prous, J.R. (2002). Preclinical pharmacokinetics of statins. Methods Find Exp. Clin. Pharmacol. 24(9), 593-613.

280. Repko, E.M., and Maltese, W.A. (1989). Post-translational isoprenylation of cellular proteins is altered in response to mevalonate availability. J. Biol. Chem. 264(17), 9945-9952.

281. Ridgway, N.D., Byers, D.M., Cook, H.W., and Storey, M.K. (1999). Integration of phospholipid and sterol metabolism in mammalian cells. Prog. Lipid Res. 38(4), 337-360.

282. Riechman, S.E., Lee, C.W., Chikani, G., Chen, V.C.W., and Lee, T.V. (2009). Cholesterol and skeletal muscle health. World Rev. Nutr. Diet. 100, 71-79.

283. Rizzi, D., Basile, C., Di Maggio, A., Sebastio, A., Introna, F., Rizz, R., Scatizzi, A., De Marco, S., and Smialek, J.E. (1991). Clinical spectrum of accidental hemlock poisoning: Neurotoxic manifestations, rhabdomyolysis and acute tubular necrosis. Nephrol. Dial. Transplant. 6(12), 939-943.

284. Robertson, D.G., Ruepp, S.U., Stryker, S.A., Hnatyshyn, S.Y., Shipkova, P.A., Aranibar, N., Mcnaney, C.A., Fiehn, O., and Reily, M.D. (2011). Metabolomic and transcriptomic changes induced by overnight (16 h) fasting in male and female sprague-dawley rats. Chem. Res. Toxicol. 24(4), 481-487.

285. Rodenburg, J., Vissers, M.N., Wiegman, A., van Trotsenburg, A.S. P., van der Graaf, A., de Groot, E., Wijburg, F.A., Kastelein, J.J.P., and Hutten , B.A. (2007). Statin treatment in children with familial hypercholesterolemia: The younger, the better. Circulation. 116(6), 664-668.

286. Rodino-Klapac, L.R., Haidet, A.M., Kota, J., Handy, C., Kaspar, B.K., and Mendell, J.R. (2009). Inhibition of myostatin with emphasis on follistatin as a therapy for muscle disease. Muscle Nerve. 39(3), 283-296.

287. Ropero, A.B., Alonso-Magdalena, P., Quesada, I., and Nadal, A. (2008). The role of estrogen receptors in the control of energy and glucose homeostasis. Steroids. 73(9-10), 874-879.

288. Rosenson, R.S. (2004). Current overview of statin-induced myopathy. Am. J. Med. 116(6), 408-416.

289. Roth, S.M., Ferrell, R.E., Peters, D.G., Metter, E.J., and Hurley, B.F. (2002). Influence of age, sex, and strength training on human muscle gene expression determined by microarray. Physiol. Genomics. 10(3), 181-190.

290. Rutecki, G.W., Ognibene, A.J., and Geib, J.D. (1998). Rhabdomyolysis in antiquity: From ancient descriptions to scientific explanation. Pharos Alpha Omega Alpha Honor Med Soc. 61(2), 18-22.

291. Sacheck, J.M., Ohtsuka, A., McLary, C., and Goldberg, A.L. (2004). IGF-1 stimulates muscle growth by suppressing protein breakdown and expression of atrophy-related ubiquitin ligases, atrogin-1 and MuRF1. Am. J. Physiol. Endocrinol. Metab. 287(4), E591-E601.

292. Sacher, J., Weigl, L., Werner, M., Szegedi, and Hohenneger, M. (2005). Delineation of myotoxicity induced by 3-hydroxy-3-methylglutaryl CoA reductase inhibitors in human skeletal muscle cells. J. Pharmacol. Exp. Ther. 314(3), 1032-1041.

293. Sakamoto, K., Honda, T., Yokoya, S., Waguri, S., and Kimura, J. (2007). Rab-small GTPases are involved in flubastatin and pravastatin-induced vacuolation in rat skeletal myofibers. FASEB J. 21(14), 4087-4094.

294. Sakamato, K., Mikami, H., and Kimura, J. (2008). Involvement of organic anion transporting polypeptides in the toxicity of hydrophilic pravastatin and lipophilic fluvastatin in rat skeletal myofibers. Br. J. Pharmacol. 154(7), 1482-1490.

295. Sakamoto, K., Wada, I., and Kimura, J. (2011). Inhibition of Rab1 GTPase and endoplasmic reticulum-to-golgi trafficking underlies statins's toxicity in rat skeletal myofibers. J. Pharmacol. Exp. Ther. 338(1), 62-69.

296. Salehian, B., Mahabadi, V., Bilas, J., Taylor, W.E., and Ma, K. (2006). The effect of glutamine on prevention of glucocorticoid-induced skeletal muscle atrophy is associated with myostatin suppression. Metabolism. 55(9), 1239-1247.

297. Salehzadeh, F., Rune, A., Osler, M., and Al-Khalili. (2011). Testosterone or 17β-estradiol exposure reveals sex-specific effects on glucose and lipid metabolism in human myotubes. J. Endocrinol. 210(2), 219-229.

298. Sandri, M. (2010) Autophagy in health and disease. 3. Involvement of autophagy in muscle atrophy. Am. J. Physiol. Cell Physiol. 298(6), C1291-C1297.

299. Sanoudou, D., Haslett, J.N., Kho, A.T., Guo, S., Gazda, H.T., Greenberg, S.A., Lidov, H.G., Kohane, I.S., Kunkel, L.M., and Beggs, A.H. (2003). Expression profiling reveals altered satellite cell numbers and glycolytic enzyme transcription in nemaline myopathy muscle. Proc. Natl. Acad. Sci. USA. 100(8), 4666-4471.

300. Sardao, V.A., Pereira, S.L., and Oliveira, P.J. (2008). Drug-induced mitochondrial dysfunction in cardiac and skeletal muscle injury. Expert Opin. Drug. Saf. 7(2), 129-146.

301. Sato, K., Iemitsu, M., Aizawa, K., and Ajisaka, R. (2008). Testosterone and DHEA activate the glucose metabolism-related signaling pathway in skeletal muscle. Am. J. Physiol. Endocrinol. Metab. 294(5), E961-E968.

302. Sauret, J.M., Marinides, G., and Wang, G.K. (2002). Rhabdomyolysis. Am. Fam. Physician. 65(5), 907-912.

303. Scandinavian Simvastatin Survival Study Group. (1994). Randomised controlled trial of cholesterol lowering in 4444 patients with coronary heart disease: the Scandinavian Simvastatin Survival Study (4S). Lancet. 344(8934), 1383-1389.

304. Scatena, R., Martorana, G.E., Bottoni, P., and Giardina, B., (2004) Mitochondrial dysfunction by synthetic ligands of peroxisome proliferator activated receptors (PPARs). IUBMB Life. 56(8), 477.

305. Schaars, C.F., and Stalenhoef, A.F. (2008). Effects of ubiquinone (coenzyme Q10) on myopathy in statin users. Curr. Opin. Lipidol. 19(6), 553-557.

306. Schaefer, W.H., Lawrence, J.W., Loughlin, A.F., Stoffregen, D.A., Mixson, L.A., Dean, D.C., Raab, C.E., Yu, N.X., Lankas, G.R., and Frederick, C.B. (2004). Evaluation of ubiquinone concentration and mitochondrial function relative to cerivastatin-induced skeletal myopahty in rats. Toxicol. Appl. Pharmacol. 194(1), 10-23.

307. Schiaffino, S., and Reggiani, C. (1996). Molecular diversity of myofibrillar proteins: gene regulation and functional significance. Physiol. Rev. 76(2), 371-423.

308. Schmitt, T.L., and Pette, D. (1991). Fiber type-specific distribution of paravalbumin in rabbit skeletal. A quantitative microbiochemical and immunohistochemical study. Histochemistry. 96(6), 459-465.

309. Stevens, W., Stevens, J., Binder-Macleod, S.A. (2001). Human skeletal muscle fiber type classifications. Phys. Ther. 81(11), 1810-1816.

310. Seachrist, J.L., Loi, C.M., Evans, M.G., Criswell, K.A., and Rothwell, C.E. (2005). Roles of exercise and pharmacokinetics in cerivastatin-induced skeletal muscle toxicity. Toxicol. Sci. 88(2), 551-561.

311. Segaud, F., Combaret, L., Neveux, N, Attaix, D., Cynober, L., and Moinard, C. (2007). Effects of ornithine alpha-ketoglutarate on protein metabolism in Yoshida sarcoma-bearing rats. Clin. Nutr. 26(5) 624-30.

312. Sever, N., Yang, T., Brown, M.S., Goldstein, J.L., and DeBose-Boyd, R.A. (2003). Accelerated degradation of HMG CoA reductase mediated by binding of Insig-1 to its sterol-sensing domain. Mol. Cell. 11(1), 25-33.

313. Sharma, U., Atri, S., Sharma, M.C., Sarkar, C., and Jagannathan, N.R. (2003a). Skeletal muscle metabolism in Duchenne muscular dystrophy (DMD): an in vitro proton NMR spectroscopy study. Magn. Reson. Imaging. 21(2), 145-153.

314. Sharma, U., Atri, S., Sharma, M.C., Sarkar, C., and Jagannathan, N.R. (2003b). Biochemical characterization of muscle tissue of limb girdle muscular dystrophy: an ^{1}H and ^{13}C NMR study. NMR Biomed. 16(4), 213-223.

315. Shefer, G., and Yablonka-Reuveni, Z. (2005). Isolation and culture of skeletal muscle myofibers as a means to analyze satellite cells. Methods Mol. Biol. 290. 281-304.

316. Sheffield-Moore, M., and Urban, R.J. (2004). An overview of the endocrinology of skeletal muscle. Trends Endocrinol. Metab. 15(3), 110-115.

317. Shepherd, J., Cobbe, S.M., Ford, I, Isles, C.G., Lorimer, A.R., MacFarlane, P.W. McKillop, J.H., and Packard, C.J. (1995). Prevention of coronary heart disease with pravastatin in men with hypercholesterolaemia. N. Engl. J. Med. 333(20), 1301-1307.

318. Sher, R.B., Aoyama, C., Huebsch, K.A., Ji, S., Kerner, J., Yang, Y., Frankel, W.N., Hoppel, C.L., Wood, P.A., Vance, D.E., and Cox, G.A. (2006). A rostrocaudal muscular dystrophy caused by a defect in choline kinase beta, the first enzyme in phosphatidylcholine biosynthesis. J. Biol. Chem. 281(8), 4938-4948.

319. Shewmon, D.A., and Craig, J.M. (2010). Creatine supplementation prevents statin-induced toxicity. Ann. Intern. Med. 153(10), 690-692.

320. Shitara, Y., and Sugiyama, Y. (2006). Pharmacokinetic and pharmacodynamic alterations of 3-hydroxy-3-methylglutaryl coenzyme A (HMG-CoA) reductase inhibitors: Drug-drug interactions and interindividual differences in transporter and metabolic enzyme functions. Pharmacol. Ther. 112(1), 71-105.

321. Sidaway, J.E., Mallinson, J.E., Glaves, P.D., Martin, E.A., Davies, W.J., Westwood, F.R., Constantin-Teodosiu, D., and Greenhaff, P.L. (2010) Dichloroacetate prevents simvastatin-induced muscle damage in the rat, suggesting that impaired mitochondrial glucose oxidation is responsible for statin induced myopathy. The Toxicologist (Toxicol. Sci. Supplement), 114(1), 1673.

322. Sidway, J., Wang, Y., Marsden, A.M., Orton, T.C., Westwood, F.R., Azuma, C.T., and Scott, R.C. (2009). Statin-induced myopathy in the rat: relationship between systemic exposure, muscle exposure and myopathy. Xenobiotica. 39(1), 90-98.

323. Simpson, J.A., Labugger, R., Collier, C., Brison, R.J., Iscoe, S., and Van Eyk, J.E. (2005). Fast and slow skeletal troponin I in serum from patients with various skeletal muscle disorders: A pilot study. Clin. Chem. 51(6), 966-972.

324. Singh, D., Chander, V. and Chopra, K. (2005) Rhabdomyolysis. Methods Find. Exp. Clin. Pharmacol. 27(1), 39-48.

325. Sinha-Hikim, I., Artaza, J., Woodhouse, L., Gonzalez-Cadavid, N.G., Singh, A.B., Lee, M.I., Storer, T.W., Casaburi, R., Shen, R., and Bhasin, S. (2002). Testosterone-induced increase in muscle size in healthy young men is associated with muscle fiber hypertrophy. Am. J. Physiol. Endocrinol. Metab. 283(1), E154-E164.

326. Sinha-Hikim, I., Cornford, M., Gaytan, H., Lee, M.L., and Bhasin, S. (2006). Effects of testosterone supplementation on skeletal muscle fiber hypertrophy and satellite cells in community-dwelling older men. J. Clin. Endocrinol. Metab. 91(8), 3024-3033.

327. Sirtori, C.R., (1993). Tissue selectivity of hydroxymethylglutaryl coenzyme A (HMG CoA) reductase inhibitors. Pharmacol. Ther. 60(3), 431-459.

328. Sirvent, P., Mercier, J., and Lacampagne, A. (2008). New insights into mechanisms of statin-associated myotoxicity. Curr. Opin. Pharmacol. 8(3), 333-338.

329. Sjolin, J., Hjort, G., Friman, G., and Hambraeus, L. (1987). Urinary excretion of 1-methylhistidine: A qualitative indicator of exogenous 3-methylhistidine and intake of meats from various sources, Metabolism 36(12), 1175-1184.

330. Slade, J.M., Delano, M.C., and Meyer, R.A. (2006). Elevated skeletal muscle phosphodiesters in adults using statin medications. Muscle Nerve. 34(6), 782-784.

331. Smith, P.F., Eydelloth, R.S., Grossman, S.J., Stubbs, R.J., Schwartz, M.S., Germershausen, J.I., Vyas, K.p., Kari, P.H., and Macdonald, J.S. (1991). HMG-CoA reductase inhibitor-induced myopathy in the rat: cyclosporine A interaction and mechanism studies. J. Pharmacol. Exp. Ther. 257(3), 1225-1235.

332. Solomon, V., and Goldberg, A.L. (1996). Importantce of the ATP-ubiqutin-proteasome pathway in the degradation of soluble and myofibrillar proteins in rabbit muscle extracts. J. Biol. Chem. 271(43), 26690-26697.

333. Sorichter, S., Puschendorf, B., and Mair, J. (1999). Skeletal muscle injury induced by eccentric muscle action: muscle proteins as markers of muscle fiber injury. Exerc. Immunol. Rev. 5, 5-21.

334. Spady, D.K., and Dietschy, J.M. (1983). Sterol synthesis in vivo in 18 tissues of the squirrel, monkey, guinea pig, rabbit, hamster and rat. J. Lipid Res. 24(3), 303-315.

335. Sprott, H., Rzanny, R., Reichenbach, J.R., Kaiser, W.A., Hein, G., and Stein, G. (2000). ^{31}P magnetic resonance spectroscopy in fibromyalgic muscle. Rheumatology (Oxford). 39(10), 1121-1125.

336. Spurlock, D.M., McDaneld, T.G., and McIntyre, L.M. (2006). Changes in skeletal muscle gene expression following clenbuterol administration. BMC Genomics. 7(320), 1-15.

337. Srivastava, N.K., Pradhan, S., Mittal, B., and Gowda, G.A.N. (2010). High resolution NMR based analysis of serum lipids in Duchene muscular dystrophy patients and its possible diagnostic significance. NMR Biomed. 23(1), 13-22.

338. Stamler, J., Wentworth, D., and Neaton, J.D. (1986). Is relationship between serum cholesterol and risk of premature death from coronary heart disease continuous and graded? Findings in 356,222 primary screenees of Multiple Risk Factor Intervention Trial (MRFIT). JAMA. 256, 2823-2828.

339. Stange, E., and Dietschy, J.M. (1984). Age-related decreases in tissue sterol acquisition are mediated by changes in cholesterol synthesis and not low density lipoprotein uptake in the rat. J. Lipid Res. 25(7), 703-13.

340. Stefanyk, L.E., Coverdale, N., Roy, B.D., Peters, S.J., and LeBlanc, P.J. (2010). Skeletal muscle type comparison of subsarcolemmal mitochondrial membrane phospholipid fatty acid composition in rat. J. Membrane. Biol. 234(3), 207-215.

341. Steinke, W., Yamashita, S., Tabei, M., Ahr, H.J., Beckermann, B., Domdey-Bette, A., Goller, G., Schwarz, T., and Siefert, H.M. (1996). Cerivastatin, a new inhibitor of hmg-coa reductase. Jpn. Pharmacol. Ther. 24, 7-27.

342. Stevenson, E.J., Giresi, P.G., Koncarevic, A., and Kandarian, S.C. (2003). Global analysis of gene expression patterns during disuse atrophy of skeletal muscle. J. Physiol. 551(1), 33-48.

343. Straadt, I.K., Young, J.F., Bross, P., Gregersen, N., Oksbjerg, N., Theil, P.K., and Bertram, H.C. (2010a). NMR-based metabonomic investigation of heat stress in myotubes reveals a time-dependent change in the metabolites. J. Agric. Food Chem. 58(10), 6376-6386.

344. Straadt, I.K., Young, J.F., Petersen, B.O., Duus, J.O., Gregersen, N., Bross, P., Oksbjerg, N., and Bertram, H.C. (2010b). Metabolic profiling of heat or anoxic stress in mouse C2C12 myotubes using multnuclear magnetic resonance spectroscopy. Metabolism. 59(6), 814-823.

345. Sugatani, J., Sadamitsu, S., Kurosawa, M., Ikushiro, S., Sakaki, T., Ikari, A., and Miwa, M. (2010). Nutritional status affects fluvastatin-induced hepatotoxicity and myopathy in rats. Drug Metab. Dispos. 38(10), 1655-1664.

346. Sugden, M.C. (2003). PDK4: a factor in fatness. Obes. Res. 11(2). 167-169.

347. Taillandier, D., Combaret, L., Pouch, M-N., Samuels, S.E., Bechet, D., and Attaix, D. (2004). The role of ubiquitin-proteasome-dependent proteolysis in the remodelling of skeletal muscle. Proc. Nutr. Soc. 63(2), 357-361.

348. Tamaki, N., Morioka, S. Ikeda, T., Harada, M., and Hama, T. (1980). Biosynthesis and degradation of carnosine and turnover rate of its constituent amino acids in rats. J. Nutr. Sci. Vitaminol. (Tokyo). 26(2), 127-139.

349. Tanaka, S., Sakamoto, K., Yamamoto, M., Mizuno, A., Ono, T., Waguri, S., and Kimura, J. (2010). Mechanism of statin-induced contractile dysfunction in rat cultured skeletal myofibers. J. Pharmacol. Sci. 114(4), 454-463.

350. Tarnopolsky, M.A. (2011). Creatine as a therapeutic strategy for myopathies. Amino Acids. 40(5), 1397-1407.

351. Tews, D.S. (2005). Muscle-fiber apoptosis in neuromuscular diseases. Muscle Nerve. 32(4), 443-458.

352. The Search Collaborative Group. (2008). SLC01B1 variants and statin-induced myopathy – a genome wide study. N. Engl. J. Med. 359(8), 789-799.

353. Thompson, P.D., Clarkson, P., and Karas, R.H. (2003). Statin-associated myopathy. JAMA. 289(13), 1681-1690.

354. Tidball, J.G., and Villalta, S.A. (2010). Regulatory interactions between muscle and the immune system during muscle regeneration. Am. J. Physiol. Regul. Integr. Comp. Physiol. 298(5), R1173-R1187.

355. Tiidus, P.M. (2008). Skeletal muscle damage and repair. Human Kinetics. 1st edition.

356. Tobert, J.A. (1987). New developments in lipid-lowering theraphy: the role of inhibitors of hydroxymethylglutaryl-coenzyme A reductase. Circulation. 76(3), 534-538.

357. Tobert, J.A. (2003). Lovastatin and beyond: the history of the HMG-CoA reductase inhibitors. Nat. Rev. Drug Discov. 2(7), 517-526.

358. Tomas, F.M., Munro, H.N., and Young, V.R. (1979). Effect of glucocorticoid administration on the rate of muscle protein breakdown in vivo in rats, as measured by urinary excretion of N tau-methylhistidine. Biochem. J. 178(1), 139-146.

359. Tomaszewski, M., Stepien, K.M., Tomaszewska, J., and Czuczwar, S.J. (2011). Statin-induced myopathies. Pharmacol. Rep. 63(4), 859-866.

360. Tomlinson, B.E., and Irving, D. (1977). The numbers of limb motor neurons in the human lumbosacral cord throughout life. J. Neurol. Sci. 34(2), 213-219.

361. Tonomura, Y., Mori, Y., Torii, M., and Uehara, T. (2009). Evaluation of the usefulness of biomarkers of cardiac and skeletal myotoxicity in rats. Toxicology 266(1-3), 48-54.

362. Totsuka, T., and Watanabe, K. (1982). Elevated free cholesterol content in hindleg muscle of the dystrohic mouse during a postnatal period from 2.1 to 30 weeks. Jikken Dobutsu. 31(2), 139-142.

363. Trapani, L., Martini, C., Trentalance, A., and Pallottini, V. (2010). Mechanism underlying long-term regulation of 3-hydroxy-3-methylglutaryl coenzyme A reductase during L6 myoblast differentiation. J. Cell. Biochem. 110(2), 392-398.

364. Trapani, L., Melli, L., Segatto, M., Trezza, V., Campolongo, P., Jozwiak, A., Swiezewska, E., Pucillo, L.P., Moreno, S., Fanelli, F., Linari, M., and Pallottini, V. (2011). Effects of myosin heavy chain (MHC) plasticity induced by hmgcoa-reductase inhibition on skeletal muscle functions. FASEB J. 25(11), 4037-4047.

365. Tuckow, A.P., Jefferson, S.J., Kimball, S.R., and Jefferson, L.S. (2011). Simvastatin represses protein synthesis in muscle-derived C2C12 cell line with concomitant reduction in eukaryotic initiation factor 2B expression. Am. J. Physiol. Endocrinol. Metab. 300(3), E564-E570.

366. Turley, S.D., Andersen, J.M., and Dietschy, J.M. (1981). Rates of sterol synthesis and uptake in the major organs of the rat in vivo. J. Lipid Res. 22(4), 551-569.

367. Urso, M.L., Clarkson, P.M., Hittel, D., Hoffman, E.P., and Thompson, P.D. (2005). Changes in ubiquitin proteasome pathway gene expression in skeletal muscle with exercise and statins. Arterioscler. Thromb. Vasc. Biol 25(12), 2560-2455.

368. Ustunel, I., Akkoyunlu, G., and Demir, R. (2003). The effect of testosterone on gastrocnemius muscle fibres in growing and adult male and female rats: a histochemical, morphometric and ultrastructural study. Anat. Histol. Embryol. 32(2), 70-79.

369. Vaklavas, C., Chatzizisis, Y.S., Ziakas, A., Zamboulis, C., and Giannoglou, G.D. (2009). Molecular basis of statin-associated myopathy. Atherosclerosis. 202(1), 18-28.

370. Vanholder, R., Sever, M.S., Erek, E., and Lameire, N. (2000). Rhabdomyolysis. J. Am. Soc. Nephrol. 11(8), 1553-1561.

371. Vary, T.C., Frost, R.A., and Lang, C.H. (2008). Acute alcohol intoxication increases atrogin-1 and MuRF1 mRNA without increasing proteolysis in skeletal muscle. Am. J. Physiol. Regul. Integr. Comp. Physiol. 294(6), R1777-R1789.

372. Vassallo, J.D., Janovitz, E.B., Wescott, D.M., Chadwick, C., Lowe-Krentz, L.J., and Lehman-McKeeman, L.D. (2009). Biomarkers of drug-induced skeletal muscle injury in the rat: troponin I and myoglobin. Toxicol. Sci. 111(2), 402-412.

373. Vassallo, J.D., Rathmacher, J.A., Janovitz, E.B., Stryker, S., Robertson, D., Lowe-Krentz, L.J., and Lehman-McKeeman, L.D. (2011). Cerivastatin induces the muscle atrophy program in a time- and fiber-dependent manner with an increase in biomarkers of myopathy. The Toxicologist (Toxicol. Sci. Supplement), 120(2), 1451.

374. Vega, G.L. and Grundy, S.M. (1998). Effect of statins on metabolism of apo-B-containing lipoproteins in hypertriglyceridemic men. Am. J. Cardiol. 81(4A), 36B-42B.

375. Veillard, N.R., and Mach, F. (2002). Statins: The new aspirin? Cell Mol. Life Sci. 59(11), 1771-1786.

376. Vejux, A., Malvitte, L., and Lizard, G. (2008). Side effects of oxysterols: cytotoxicity, oxidation, inflammation, and phospholipidosis. Braz. J. Med. Biol. Res. 41(7), 545-556.

377. Velasco, E., Finol, H.J., and Marquez, A. (1995). Toxic and neurogenic factors in chloroquine myopathy fibre selectivity. J. Submicrosc. Cytol. Pathol. 27(4), 451-457.

378. Vinagre, C.G.C., Ficker, E.S., Finazzo, C., Alves, M.J.N., Angelis, K.D., Irigoyen, M.C., Negrao, C.E., and Maranhao, R.C. (2007). Enhanced removal from the plasma of LDL-like nanoemulsion cholesteryl ester in trained men compared with sedentary healthy men. J. Appl. Physiol. 103(4), 1166-1171.

379. Voet, D., and Voet. J.G. (2004). Biochemistry, biomolecules, mechanisms of enzyme action, and metabolism. John Wiley and Sons, Inc. 3rd Edition.

380. Waclawik, A.J., Lindal, S., and Engel, A.G. (1993). Experimental lovastatin myopathy. J. Neuropathol. Exp. Neurol. 52(5), 542-549.

381. Warner, G.J., Stoudt, G., Bamberger, M., Johnson, W.J., and Rothblat, G.H. (1995). Cell toxicity induced by inhibition of acyl coenzyme A: cholesterol

acyltransferase and accumulation of unesterified cholesterol. J. Biol. Chem. 270(11), 5772-5778.

382. Warren, M.P., and Fried, J.L. (2001). Temporomandibular disorders and hormones in women. Cells Tissues Organs. 169(3), 187-192.

383. Wassner, S.J., Orloff, S., and Holliday, M.A., (1977). Protein degradation in muscle: response to feeding and fasting in growing rats. Am. J. Physiol. 233(2), E119-123.

384. Waterfield, C.J., Jairath, M., Asker, D.S., and Timbrell, J.A. (1995). The biochemical effects of clenbuterol: with particular reference to taurine and muscle damage. Eur. J. Pharmacol. 293(2), 141-149.

385. Weber, M.A., Kinscherf, R., Krakowski-Roosen, H., Aulman, M., Renk, H., Kunkele, A., Adler, L., Kauczor, H.U., and Hildebrandt, W. (2007). Myoglobin plasma level related to muscle mass and fiber composition: a clinical marker of muscle wasting? J. Mol. Med. 85(8), 887-896.

386. Welle, S., Tawil, R., and Thornton, C.A. (2008). Sex-related differences in gene expression in human skeletal muscle. PloS ONE. 3, e1385.

387. Wende, A.R., Huss, J.M., Schaeffer, P.J., Giguere, V., and Kelly, D.P. (2005). PGC-1α coactivates PDK4 expression via orphan nuclear receptor ERRα: a mechanism for transcriptional control of muscle glucose metabolism. Mol. Cell Biol. 25(24), 10684-10694.

388. Westwood, F.R., Bigley, A., Randall, K., Marsden, A.M., and Scott, R.C. (2005). Statin-induced muscle necrosis in the rat: distribution, development, and fibre selectivity. Toxicol. Pathol. 33(2), 246-257.

389. Williams, K.D., and Smith, D.O. (1989). Cholesterol conservation in skeletal muscle associated with age- and denervation-related atrophy. Brain Res. 493(1), 14-22.

390. Wilkinson, J.M., and Grand, J.A. (1978). Comparison of amino acid sequence of troponin I from different striated muscles. Nature. 271(5640), 31-35.

391. Willis, R.A., Folkers, K., Tucker, J.L., Ye, C.Q., Xia, L.J., and Tamagawa, H. (1990). Lovastatin decreases coenzyme Q levels in rats. Proc. Natl. Acad. Sci. USA. 87(22), 8928-2930.

392. Wong, J., Quinn, C.M., Gelissen, I.C., Jessup, W., and Brown, A.J. (2008). The effect of statins on ABCA1 and ABCG1 expression in human macrophages is influenced by cellular cholesterol levels and extent of differentiation. Atherosclerosis. 196(1), 180-189.

393. Wu, J.S., Buettner, C., Smithline, H., Ngo, L.H., and Greenman, R.L. (2011). Evaluation of skeletal muscle during calf exercise by 31-phosphorous magnetic resonance spectroscopy in patients on statin medications. Muscle Nerve. 43(1), 76-81.

394. Xu, C., Bailly-Maitre, B., and Reed, J.C. (2005). Endoplasmic reticulum stress: cell life and death decisions. J. Clin. Invest. 115(10), 2656-2664.

395. Xu, L., and Simoni, R.D. (2003). The inhibition of degradation of 3-hydroxy-3-methylglutaryl coenzyme A (HMG-CoA) reductase by sterol regulatory element binding protein cleavage-activating protein requires four phenylalanine residues in span 6 of HMG-CoA reductase transmembrane domain. Arch. Biochem. Biophys. 414(2), 232-243.

396. Xu, Q., Vu, H., Liu, L., Want, T-C., and Schaefer, W.H. (2011). Metabolic profiles show specific mitochondrial toxicities in vitro in myotube cells. J. Biomol. NMR. 49(3-4), 207-219.

397. Yablonka-Reuveni, Z., Day, K., Vine, A., and Shefer, G. (2008). Defining the transcriptional signature of skeletal muscle stem cells. J. Anim. Sci. 86(E. Suppl.) E207-E216.

398. Yamazaki, H., Suzuki, M., Aoki, T., Morikawa, S., Maejima, T., Sato, F., Sawanobori, K., Kitahara, M., Kodama, T., and Saito, Y. (2006). Influence of 3-hydroxy-3-methylglutaryl coenzyme a reductase inhibitors on ubiquinone levels in rat skeletal muscle and heart: Relationship to cytotoxicity and inhibitory activity for cholesterol synthesis in human skeletal muscle cells. J. Atheroscler. Thromb. 13(6), 295-307.

399. Yan, Z., Choi, S., Liu, X., Zhang, M., Schageman, J.J., Lee, S,Y., Hart, R., Lin, L., Thurmond, F.A., and Williams, R.S. (2003). Highly coordinated gene regulation in mouse skeletal muscle regeneration. J. Biol. Chem. 278(10), 8826-8836.

400. Yang, T., Espenshade, P.J., Wright, M.E., Yabe, D., Gong, Y., Aebersold, R., Goldstein, J.L., and Brown, M.S. (2002). Crucial step in cholesterol homeostasis: Sterols promote binding of SCAP to INSIG-1, a membrane protein that facilitates retention of SREBPs in ER. Cell. 110(4), 489-500.

401. Yokoyama, M., Seo, T., Park, T., Yagyu, H., Hu, Y., Huiping Son, N., Augustus, A.S., Vikramadithyan, R.K., Ramakrishnan, R., Pulawa, L.K., Eckel, R.H., and Goldberg, I.J. (2007). Effects of lipoprotein lipase and statins on cholesterol uptake into heart and skeletal muscle. J. Lipid Res. 48(3), 646-655.

402. Yoshioka, M., Boivin, A., Bolduc, C., and St-Amand, J. (2007). Gender difference of androgen actions on skeletal muscle transcriptome. J. Mol. Endocrinol. 39(2), 119-133.

403. Yoshioka, M., Boivin, A., Ye, P., Labrie, F., and St-Amand, J. (2006). Effects of dihydrotestosterone on skeletal muscle transcriptome in mice measured by serial analysis of gene expression. J. Mol. Endocrinol. 36(2), 247-259.

404. Yoshioka, Y., Masuda, T., Nakano, H., Miura, H., Nakaya, S., Itazawa, S-I., and Kubokawa, M. (2002). In vitro ^{1}H-NMR spectroscopic analysis of metabolites in fast- and slow-twitch muscles of young rats. Magn. Reson. Med. Sci. 1(1), 7-13.

405. Young, V.R., Alexis, S.D., Baliga, B.S., and Munro, H.N. (1972). Metabolism of administered 3-methylhistidine. Lack of muscle transfer ribonucleic acid charging and quantitative excretion as 3-methylhistidine and its N-acetyl derivative. J. Biol. Chem. 247(11), 3592-3600.

406. Young, V.R., Havenberg, L.N., Bilmazes, C., and Munro, H.N. (1973). Potential use of 3-methylhistidine excretion as an index of progressive reduction in muscle protein catabolism during starvation. Metabolism. 23(2), 1429-36.

407. Young, V.R., and Munro, H.N. (1978). Ntau-methylhistidine (3-methylhistidine) and muscle protein turnover: an overview. Fed. Proc. 37(9), 2291-3000.

408. Yu, J-G., Sewright, K., Hubal, M.J., Liu, J-X., Schwartz, L.M., Hoffman, E.P., and Clarkson, P.M. (2009) Investigation of gene expression in C2C12 myotubes following simvastatin application and mechanical strain. J. Atheroscler. Thromb. 16(1), 21-29.

409. Xu, E.Y., Schaefer, W.H., and Xu, Q. (2009). Metabolomics in pharmaceutical research and development: Metabolites, mechanisms and pathways. Curr. Opin. Drug Discov. Devel. 12(1), 40-52.

410. Xu, Q., Vu, H., Liu, L., Wang, T-C., and Schaefer, W.H. (2011). Metabolomic profiles show specific mitochondrial toxicities in vitro in myotube cells. J. Biomol. NMR. 49(3-4), 207-219.

411. Zammit, P.S., Partridge, T.A., and Yablonka-Reuveni, Z. (2006). The skeletal muscle satellite cell: the stem cell that came in from the cold. J. Histochem. Cytochem. 54(11), 1177-1191.

412. Zhang, Y., Ma, K., Sadana, P., Chowdhury, F., Gaillard, S., Wang, F., McDonnell, D.P., Unterman, T.G., Elam, M.B., and Park, E.A. (2006). Estrogen-related receptors stimulate pyruvate dehydrogenase kinase isoform 4 gene expression. J. Biol. Chem. 281(52), 39897-39906.

413. Zhang, Y.W., Shi, J., Li, Y., J., and Wei, L. (2009). Cardiomyocyte death in doxorubucin-induced cardiotoxicity. Arch. Immunol. Ther. Exp. (Warsz.), 57(6), 435-445.

414. Zhao, J., Brault, J.J., Schild, A., and Goldberg, A.L. (2008a). Coordinate activation of autophagy and the proteasome pathway by FoxO transcription factor. Autophagy. 4(3), 378-380.

415. Zhao, Y., and Bruemmer, D. (2010). NR4A orphan nuclear receptors. Transcriptional regulators of gene expression in metabolism in vascular biology. Arterioscler. Thromb. Vasc. Biol. 30(8), 1535-1541.

416. Zhao, W., Pan, J., Wang, X., Wu, Y., Bauman, W.A., and Cardozo, C.P. (2008b). Expression of the muscle atrophy factor muscle atrophy F-box is suppressed by testosterone. Endocrinology. 149(11), 5449-5460.

417. Zierath, J.R., and Hawley, J.A. (2004). Skeletal muscle fiber type: influence on contractile and metabolic properties. PLoS Biology. 2(10), 1523-1527.

418. Zong, W.X., and Thompson, C.B. (2006). Necrotic death as a cell fate. Genes Dev. 20(1), 1-15.

Jeffrey D. Vassallo

Discovery Toxicology, Bristol-Myers Squibb
Route 206 and Province Line Road
Princeton, NJ 08540
513-478-8342 (cell), 609-252-7112 (work)
jeff.vassallo@bms.com

EDUCATION

Ph.D., Molecular Biology, Lehigh University, Bethlehem, PA, May 2012
Dissertation: Integration of transcriptomic and metabolomic profiling to identify mechanisms and biomarkers of statin-induced myopathy
Advisors: Dr. Lois D. Lehman-McKeeman and Dr. Linda J. Lowe-Krentz

M.S., Molecular Biology, Lehigh University, Bethlehem, PA, January 2008
Thesis: Biomarkers of skeletal muscle toxicity in the rat: troponin I and myoglobin
Advisors: Dr. Lois D. Lehman-McKeeman and Dr. Linda J. Lowe-Krentz

B.S., Biology, University of Cincinnati, Cincinnati, OH, June 1993

RESEARCH EXPERIENCE

9/05 – Present **Research Scientist / Senior Research Scientist**
Bristol-Myers Squibb, Discovery Toxicology
Princeton, New Jersey

- Responsible for research directed towards understanding mechanisms of preclinical toxicity and relevance to human risk assessment.

- Responsible for applying metabolomics, transcriptomics and other standard molecular and biochemical methods to advance understanding of mechanisms of toxicity, biomarker identification and human risk assessment with emphasis on preclinical drug-induced myotoxicity.

- Investigated mechanisms of 2-bromoethanamine-induced renal toxicity in collaboration with researchers from academia and industry as part of the Consortium on Metabonomics in Toxicology.

- Identified and qualified biomarkers of drug-induced myotoxicity in collaboration with the myopathy working group as part of the FDA's Critical Path Initiative.

4/98 – 8/05 **Senior Researcher / Principal Researcher**
Procter and Gamble, Central Product Safety
Cincinnati, Ohio

- Responsible for technical conduct of research programs applied broadly to determine the role of metabolism in toxicity and specifically to investigate the mechanism of coumarin-induced lung and liver toxicity in mice and rats, respectively and relevance to human risk assessment.

- Investigated mechanisms of reproductive toxicity reported for parabens and decamethylcyclopentasiloxane and determined the human relevance of these findings.

- Developed in vitro assays to predict the skin sensitization potential of a compound as a strong, moderate, weak or non-sensitizer.

3/95 – 3/98 **Researcher**
Procter and Gamble, OTC Health Care Product Development
Cincinnati, Ohio

- Supported product development of Helidac® and ThermaCare® which required development and validation of analytical methods including x-ray fluorescence, ion chromatography, infrared spectroscopy, HPLC, GC, atomic absorption spectroscopy, UV/VIS spectroscopy, dissolution and infrared thermography.

- Worked with the FDA to address various analytical method issues in support of the NDA for Helidac®.

- Responsible for the technical conduct of a clinical trial using infrared thermography to evaluate heat transfer and skin safety of ThermaCare®.

- Established an analytical quality control laboratory in support of the ThermaCare® test market which included writing all methods and standard operating procedures, setting up equipment, training analysts, and record keeping according to good manufacturing practices.

9/94 – 2/95 **Research Assistant**
Cincinnati Children's Hospital Medical Center
Cincinnati, Ohio

- Designed and conducted experiments using S1 nuclease, polymerase and gyrase to study the mechanism of DNA hairpin extrusion through modification of superhelical tension. Implemented cloning strategies to clone and isolate highly mutable regions of C1 inhibitor for determining secondary structure and performing mutation analysis.

6/93 – 8/94 **Temporary Research Position**
Lab Support
Cincinnati, Ohio

- Developed bioanalytical methods and conducted routine analysis using existing methods while working for Meridian Diagnostics, Procter and Gamble and WR Grace Davison Chemical Company.

10/91 – 5/93 **Student Laboratory Assistant**
University of Cincinnati
Cincinnati, Ohio

- Maintained cell cultures of various cell lines and investigated the mechanism of heat shock-induced HSV II reactivation.

MEMBERSHIP IN PROFESSIONAL SOCIETIES

2010 – 2011	Graduate Student Councilor, Mechanisms Specialty Section, Society of Toxicology
2005 – Present	Society of Toxicology (Full Member)
	Society of Toxicology, Drug Discovery Toxicology Specialty Section
	Society of Toxicology, Mechanisms Specialty Section
	Society of Toxicology, Molecular Biology Specialty Section

JOURNAL REVIEWER

2005 – Present	Toxicological Sciences
2009 – Present	Drug Metabolism and Disposition

FULL LENGTH MANUSCRIPTS

1. **Vassallo, J.D**. Aranibar, N., Shipkova, P., Lowe-Krentz, L.J., and Lehman-McKeeman, L.D. Cerivastatin-induced myopathy is associated with alterations in cholesterol homeostasis and upregulation of the 25-hydroxycholesterol pathway. *In preparation.*

2. **Vassallo, J.D**., Rathmacher, J.A., Janovitz, E.B., Robertson, D., Lowe-Krentz, L.J., and Lehman-McKeeman, L.D. Utility of 3-methylhistidine as a preclinical biomarker of drug-induced myopathy. *In preparation.*

3. **Vassallo, J.D**., Aranibar, N., Frerman, F.E., Cantor, G.H., Stryker, S., Coen, M., Lindon, J.C., Nicholson, J.K., and Lehman-McKeeman, L.D. The role of glutaric aciduria in 2-bromoethanamine-induced renal papillary necrosis. *In preparation.*

4. Aranibar, N., **Vassallo, J.D**., Rathmacher, J.A., Janovitz, E.B., Dai, J., Zhang, Y., Reily, M., Robertson, D., Lowe-Krentz, L.J., and Lehman-McKeeman, L.D. (2011). Identification of 1- and 3-methylhistidine as biomarkers of skeletal muscle toxicity by nuclear magnetic resonance-based metabolic profiling. Analytical Biochemistry, 410(1): 84-91.

5. Shipkova, P., **Vassallo, J.D**., Aranibar, N., Hnatyshyn, Zhang, H., Clayton, T. A., Coen, M., Campbell, A., Cantor, G.H., Sanders, M., Lindon, J.C., Nicholson, J.K., Lehman-McKeeman, L. (2011). Urinary metabolites of 2-bromoethanamine identified by stable isotope labeling: evidence for carbamoylation and glutathione conjugation. Xenobiotica, 41(2): 144-154.

6. **Vassallo, J.D**., Kaetzel, R.S., Born, S.L., Lewis, C.L., Lehman-McKeeman, L.D., and Reed, D.J. (2010). γ-Glutamyl transpeptidase null mice fail to develop tolerance to coumarin-induced Clara cell toxicity. Food and Chemical Toxicology, 46(8): 1612-1618.

7. Aranibar, N., Bhaskaran, V., Ott, K.H., **Vassallo, J.D**., Nelson, D., Lecureux, L., Gong, L., Stryker, S., and Lehman-McKeeman, L.D. (2009). Modulation of ascorbic acid metabolism by cytochrome P450 induction revealed by metabonomics and transcriptional profiling. Magnetic Resonance in Chemistry, 47(1): S12-S19.

8. Gerberick, G.F., Troutman, J.A., Foertsch, L.M., **Vassallo, J.D**., Quijano, M., Dobson, R.L., Goebel, C., Lepoittevin, J-P. (2009). Investigation of peptide reactivity of pro-hapten skin sensitizers using a peroxidase peroxide oxidation system. Toxicological Sciences, 112(1): 167-174.

9. **Vassallo, J.D**., Wescott, D.M., Janovitz, E.B., Lowe-Krentz, L.J., and Lehman-McKeeman, L.D. (2009). Biomarkers of drug-induced skeletal muscle injury in the rat: troponin I and myoglobin. Toxicological Sciences, 111(2): 402-412.

10. Watson, L., **Vassallo, J.D**., Cantor, G., Lehman-McKeeman, L.D. (2008). Lectin Histochemistry: An alternative to immunohistochemistry for identifying specific structures in rat renal papillary necrosis. Histologic, XLI(2): 28-31.

11. Gerberick, G.F., **Vassallo, J.D**., Foertsch, L.M., Price, B.B., Chaney, J.G., and Lepoittevin, J.P. (2007). Quantification of chemical peptide reactivity for screening contact allergens: a classification tree model approach. Toxicological Sciences, 97(2): 417-27.

12. Felter, S.P., **Vassallo, J.D**., Carlton, B.D., and Daston, G.P. (2006). A safety assessment of coumarin taking into account species-specificity of toxicokinetics. Food and Chemical Toxicology, 44(4): 462-475.

13. Pease, C.K.S., Divkovic, M., Payne, O., **Vassallo, J.D**., Coulter, E., Naisbitt, D.J., Park, B.K., Panico, M., Dell, A., Morris, H., Alvarez Sanchez, R., Gimenez-Arnau, E., Lepoittevin, J.P., Gerberick, G.F., and Basketter, D.A. (2005). Development of in vitro haptenation assays for skin sensitization through chemical and metabolic understanding. Toxicology Letters, 158: S222-S223.

14. **Vassallo, J.D**., Hicks, S.M., Born, S.L., and Daston, G.P. (2004). Roles for epoxidation and detoxification of coumarin in determining species differences in Clara cell toxicity. Toxicological Sciences, 82(1): 26-33.

15. Gerberick, G.F., **Vassallo, J.D**., Bailey, R.E., Chaney, J.G., Morrall, S.W., and Lepoittevin, J.P. (2004). Development of a peptide reactivity assay for screening contact allergens. Toxicological Sciences, 81(2): 332-343.

16. **Vassallo, J.D**., Hicks, S.H., Daston, G.P., and Lehman-McKeeman, L.D. (2004). Metabolic detoxification determines species differences in coumarin-induced hepatotoxicity. Toxicological Sciences, 80(2): 249-257.

17. Hicks, SM., **Vassallo, J.D**., Dieter, M.Z., Lewis, C.L., Whiteley, L.O., Fix, A.S., Lehman-McKeeman, L.D. (2003). Immunohistochemical analysis of Clara cell secretory protein expression in a transgenic model of mouse lung carcinogenesis. Toxicology, 187: 217-228.

18. **Vassallo, J.D**., Morrall, S.W., Fliter, K.L., Curry, S.M., Daston, G.P., and Lehman-McKeeman, L.D. (2003). Liquid chromatographic determination of the glutathione conjugate and ring-opened metabolites formed from coumarin epoxidation. Journal of Chromatography B, 794: 257-271.

19. Lehman-McKeeman, L.D., Gamsky, E.A., Hicks, S.M., **Vassallo, J.D**., Mar, M.H., Zeisel, S.H. (2002). Diethanolamine induces hepatic choline deficiency in mice. Toxicological Sciences, 67(1): 38-45.

20. Lehman-McKeeman, L.D., Caudill, D., **Vassallo, J.D.,** Pearce, R.E., Madan, A., Parkinson, A. (1999). Effects of musk xylene and musk ketone on rat hepatic cytochrome P450 enzymes. Toxicology Letters, 111: 105-115.

PRESENTATIONS

1. **Vassallo, J.D**., Rathmacher, J.A., Janovitz, E.B., Lowe-Krentz, L.J., and Lehman-McKeeman, L.D. (2011). Cerivastatin induces the muscle atrophy program in a time- and fiber-dependent manner with an increase in biomarkers of myopathy. Presented at the annual Society of Toxicology meeting

2. Robertson, D., Stryker, S., **Vassallo, J.D**., Mandal, R., and Wishart, D. (2011). Metabolomic assessment of temporal changes induced during the course of a typical overnight fast in the SD Rat. Presented at the annual Society of Toxicology meeting.

3. **Vassallo, J.D.** (2010). Statin-induced skeletal muscle toxicity: mechanism of injury revealed by transcriptomic and metabolomic profiling. Presented at Lehigh University, Department of Biological Sciences.

4. **Vassallo, J.D**., Aranibar, N., Rathmacher, J.A., Janovitz, E.B., Stryker, S., DiPiero, J., Wescott, D.M., Robertson, D., Lowe-Krentz, L.J., Lehman-McKeeman, L.D. (2010). Evaluation of 1- and 3-methylhistidine as preclinical urine biomarkers of drug-induced skeletal muscle toxicity in rats. Presented at the annual Society of Toxicology meeting. The Toxicologist, 114, 1315.

5. **Vassallo, J.D**., Aranibar, N., Campbell, A.J., Coen, M., Onorato, J.M., Shipkova, P., Lehman-McKeeman, L.D., Lindon, J.C., Nicholson, J.K. Investigating the mechanism of 2-bromoethanamine-induced glutaric aciduria. (2009). Presented at the annual Society of Toxicology meeting. The Toxicologist, 108, 1018.

6. Campbell A.J., Coen, M., Cantor, G., Aranibar, N., Pearce, J., Want, E.J., Sanders, M., **Vassallo, J.D**., Lehman-McKeeman, L., Holmes, E., Lindon, J.C., Nicholson, J.K. (2008). A metabonomic investigation into the diuretic effects of bromoethanamine. Presented at the annual Society of Toxicology meeting. The Toxicologist, 102, 472.

7. **Vassallo, J.D**., Wescott, D.M., Janovitz, E.B., Chadwick, C., Lehman-McKeeman, L.D. (2008). Evaluation of serum troponin I and urinary myoglobin as preclinical biomarkers of skeletal muscle toxicity in rats. Presented at the annual Society of Toxicology meeting. The Toxicologist, 102, 390.

8. Shipkova, P., Sanders, M., Hnatyshyn, S., Zhang, H., Warack, B., Aranibar, N., **Vassallo, J.D**., Lehman-McKeeman, L (2008). Utility of stable labels for metabonomics: metabolites of bromoethylamine, a potent nephrotoxicant. Presented at the 56th ASMS Conference on Mass Spectrometry.

9. **Vassallo, J.D.**, Rohde, CM, Robertson, DG, Coen, M, Keun, HC, Lindon, JC, Holmes, EC, Baker, V, Amberg, A, Walther, B, Goldfain-Blanc, F, Nicholson, JK. (2007). Use of metabonomics to define mechanisms of toxicity: Consortium for Metabonomic Toxicology-2 (COMET-2) Project. Presented at the annual Society of Toxicology meeting. The Toxicologist, 96, 244.

10. Pearce, J.T., Coen, M., Keun, H.C., Ebbels, T.D., Holmes, E.C., Lindon, J.C., Nicholson, J.K., **Vassallo, J.D**., Cantor, G.H., Lehman-McKeeman, L.D. (2007). Metabonomic evaluation of renal papillary necrosis: comparison of three chemically-diverse agents. Presented at the annual Society of Toxicology meeting. The Toxicologist, 96, 458.

11. **Vassallo, J.D**. (2006). Bromoethylamine-induced renal papillary necrosis: hypothesized mechanism of action. Presented at the Consortium on Metabonomics in Toxicology.

12. **Vassallo, J.D**., Gerberick, G.F., Riley, P., Quijano, M., Dobson, R.L., Lepoittevin, J.P. (2006). Development of a metabolism-based peptide reactivity assay for screening the skin sensitization potential of prohaptens. Presented at the annual Society of Toxicology meeting. The Toxicologist, 90, 1590.

13. **Vassallo, J.D.** (2005). Development of a peptide reactivity model for screening the skin sensitization potential of contact allergens. 19th Meeting of the European Research Group on Experimental Contact Dermatitis. Invited presentation.

14. **Vassallo, J.D**., Chaney, J.G., Bailey, R.E., Morrall, S.W., Price, B.B., Lepoittevin, J.P., and Gerberick, G.F. (2005). Development of a peptide reactivity model for screening the skin sensitization potential of contact allergens. Presented at the annual Society of Toxicology meeting. The Toxicologist. 84, 1197.

15. **Vassallo, J.D**., and Daston, G.P. (2004). Epoxidation of coumarin is the major determinant of coumarin-induced Clara cell toxicity in the mouse. Presented at the annual Society of Toxicology meeting. The Toxicologist, 78, 1448.

16. **Vassallo, J.D**., Daston, G.P., and Lehman-McKeeman, L.D. (2003). o-Hydroxyphenylacetaldehyde detoxification is a major determinant of coumarin-induced hepatotoxicity. Presented at the annual Society of Toxicology meeting. The Toxicologist, 72, 967.

17. Hicks, S.M., Lewis, C.L., **Vassallo, J.D**., Whiteley, L.O., Fix, A.S. and Lehman-McKeeman, L.D. (2002). Histopathologic evaluation of Clara cell-derived lung tumor progression in a transgenic mouse model. Presented at the annual Society of Toxicology meeting. The Toxicologist, 66, 1518.

18. **Vassallo, J.D**., Curry, S.M., Flitter, K.L., Morrall, S.W., Eads, C.D., and Lehman-McKeeman, L.D. (2002). Hepatic glutathione conjugation of coumarin 3,4-epoxide in mice, rats and humans. Presented at the annual Society of Toxicology meeting. The Toxicologist, 66, 1121.

19. **Vassallo, J.D**., R. Kaetzel, R.S., Lewis, C.L., Fix, A.S., Reed, D.J., and Lehman-McKeeman, L.D. (2001). Clara cell tolerance does not develop in γ-glutamyl transpeptidase knockout mice. Presented at the annual Society of Toxicology meeting. The Toxicologist, 60, 1000.

20. **Vassallo, J.D**., Curry, S., Purdon, M., Lewis, C., Fix, A., and Lehman-McKeeman, L.D. (2000). Elevated glutathione pools and γ-glutamyl transpeptidase activity in coumarin-induced Clara cell tolerance. Presented at the annual Society of Toxicology meeting. The Toxicologist, 54, 127.

21. Lehman-McKeeman, L.D., Caudill, D., **Vassallo J.D**., and Fix, A.S. (1999). Increased spontaneous liver tumor susceptibility in cytochrome P450 2B1 (CYP2B1) transgenic mice. Presented at the annual Society of Toxicology meeting. The Toxicologist, 48, 253.